SUITABILITY OF DEMS DERIVED FROM SAR INTERFEROMETRY AND ASTER STEREOSCOPY FOR HYDROLOGICAL APPLICATIONS USING GIS

A CASE STUDY OF Al-JAFER BASIN, JORDAN

Thesis submitted for the degree of
Doctor of Philosophy
at the University of Leicester

by

Sultan Duham Al Harbi
Department of Geography
University of Leicester

June 2009

Suitability of DEMs derived from SAR interferometry and ASTER stereoscopy for hydrological applications using GIS

A case study of Al-Jafer basin, Jordan

Sultan Al-Harbi

Abstract

Digital elevation models (DEMs) provide an essential quantitative environmental variable for a vast amount of the research published in remote sensing, GIS and physical geography. Traditionally, DEMs have been derived from ground surveys and photogrammetric techniques, and from topographic maps using contour data and spot heights. Satellite remote sensing now provides the most accurate digital elevation datasets with worldwide coverage by means of optical, radar or laser sensors. The aim of this study is to evaluate the accuracy and reliability of DEMs generated from InSAR (ERS-1/2) and ASTER data over a sparsely vegetated drainage system in central Jordan. DEMs of the study area were generated by each of these systems and an accuracy assessment was carried out through verification of the DEM based on the characteristics of the terrain against a number of independent check points collected using differential GPS data and references to generate a DEM from a topographic map (scale 1:50,000). The accuracy of independent check points used in this study is less than 1 m, which is more accurate than remote sensing techniques. The accuracy of the DEMs derived from InSAR and ASTER are represented by their RMSE, which were ± 6.95 m and 13.28 m respectively. The increase in errors in high elevation areas for ASTER DEM was higher than in InSAR DEM. The effect of these errors is investigated using stochastic conditional simulation to generate multiple equal likelihood representations of an actual terrain surface. The propagation of data uncertainty to the elevation derivatives, and the impact on the extracted surface flow are assessed. The results suggest that an elevation error propagates to flow accumulation especially in low slope areas. The effects of DEM resolution on a set of topographic parameters, including slope, accumulated flow area, flow length and catchment area, are examined.

Acknowledgments

First of all, I would like to express my deep gratitude to my supervisor, Dr. Kevin Tansey, for his trust, decisive guidance, and constant encouragement throughout this research.

Secondly, I would like to thank the staffs at Geography department have shown me their kindness and friendship and their generosity in transferring their knowledge.

Although my father passed away when I was child, and my brother Abdulrahman passed away when I was studying in this department, I dedicate this thesis to them. I never ever forget you.

Special thanks go to my mother and also dedicate this thesis to her, as her love and care for me are my main source of strength in overcoming any difficulties in life, and to my brothers and my sister for their love and patience.

Last, but not least, I would like to thank my wife, my son Faisal, my daughter Rema and my little boy Abdulrahman for their love and patience during my study.

Table of Contents

List of Figures

Chapter 5

Chapter 6

List of Tables

Chapter 3

Chapter 4

Chapter 5

Chapter 6

Chapter 1: Introduction

1.1 Research Context

The Earth's surface is a continuous phenomenon. Digital Elevation Model (DEM) is the most common form of digital representation of topography of the Earth's surface (Toutin, 2008). The study presented here is concerned with DEMs because it is the type of surface model most commonly used for spatial modelling applications and for environmental modelling in particular. DEMs provide essential quantitative environmental variables used in many research studies in remote sensing and geographical information science (GIS). They are essential for a wide range of applications, in hydrology, climatology, geomorphology and ecology. They are also important for many applications in civil and military agencies and in industrial applications, such as telecommunications, navigation, disaster management (prevention, relief, and assessment), transportation and infrastructure planning (Maune, 2001; Li *et al.,* 2005). The relevance of the source data used to derive DEMs and its impact on morphometric variables can help at the time of choosing a source for modelling and provides an idea of the accuracy level of models that could be achieved to meet the requirements in these applications.

With an increasing use of and demand for elevation data for a wide range of applications in GIS and other scientific applications, it is necessary to analyse the advantages and potential problems of methodologies for generating DEMs. Furthermore, it is important that the user has an idea of the accuracy of each method that is going to be used for a particular application and the level of accuracy that can reasonably be expected. Different sources, sensors, and formats with different characteristics like cost, accuracy or spatial resolution, have been developed to satisfy this rising demand for elevation data. These sources have included digitizing topographic maps, ground surveys, and the use of photogrammetric techniques. A DEM can be produced from contour lines digitized from topographic maps using

interpolation methods, from irregularly spaced three-dimensional points collected from field surveys, from photogrammetric techniques using stereoscopic methods, or from aerial photographs or satellite images.

Remote sensing from spaceborne sensors now provides an excellent source of efficient, economical and accurate generation of DEM data for worldwide coverage. Nowadays, satellite remote sensing provides continuous surface information by means of optical, radar or laser sensors. This involves the use of optical satellite sensors, such as IKONOS, SPOT, Quickbird and The Advanced Spaceborne Thermal Emission and Reflection Radiometer (ASTER), radar remote sensing sensors, such as data from ERS-SAR, JERS-SAR, RADARSAT and SRTM. The particular method used will depend on factors such as the size of the area to be surveyed, required accuracy, the type of information that will be extracted from the DEM, the type of terrain and weather conditions as well as other factors specific to an application (Kennie and Petrie, 1990; Aronoff, 1989). Slope and type of land cover can affect and limit the accuracy and density of elevation data that can be achieved by spaceborne techniques. A number of the authors are studying the relationship between errors and terrain. Bolstad and Stowe (1994) evaluate the accuracy of elevation values for two DEMs. They found that the largest elevation errors tended to occur in the highest and the lowest parts of the study area. Ehlshlaeger and Shortridge (1997) reported that empirical studies have shown DEM error to be related to slope values. Kyriakidis et al (1999) found that DEM error is correlated with terrain ruggedness. Guth (1992) found DEM error to be highly correlated with slope and image reflectance value.

The generation of DEMs from ground surveys is time- and effort-consuming in addition to being costly and requiring professional surveyors; a further issue is that the area that could be covered in this way is potentially very small. Thus, this method is rarely used, although it can provide the most accurate results. It is suitable for terrain modelling in engineering applications particularly for small areas (Kennie and Petrie, 1991). Aerial photogrammetry is accurate, but can be limited sometimes because of weather conditions and, in most cases; the aerial image covers only a small area. Aerial laser scanning is detailed and accurate, but relatively expensive (Li *et al.*, 2005;

Ravibabu and Jain, 2008). Satellite photogrammetry is also weather dependent, is still quite expensive and as the very high resolution satellites operate mainly in a single image mode; stereo pairs are usually collected on demand. Radar interferometry is weather independent and is quite accurate (3-20 for most areas), except tropical forest or regions with significant vegetation or moisture variability (Toutin and Gary, 2000), but the theory of the technique is often perceived to be difficult to process and is time consuming. The production of DEMs in most countries is by digitizing topographic maps at continental and national levels, but, again, there is no guarantee that the level of accuracy will be satisfactory in any country, especially in some developing countries.

During the past few decades, efforts have been made to collect global elevation datasets. In 1986, Spot was the first satellite using the stereoscopic technique, which allowed the extraction of DEMs over large areas of the Earth's surface. In the past 10 years, automatic DEM generation has become an important part of international research as a result of the existence of many satellite sensors that can provide stereo pairs, such as SPOT images. More recently, along-track stereo data acquisition was adopted on the ASTER. Using ASTER stereoscopy for the generation of DEMs has the advantage of reducing the radiometric image variations, such as refractive effects, sun illumination, and temporal changes, which leads to an increase in the correlation success rate in any image matching (Nikolakopoulos *et al.*, 2006). A commonly used method for extracting relative or absolute elevation information is radar interferometry. The main advantages of radar systems and of digital image processing, which include all-weather, night and day operation, and automated or semi-automated processing, and can cover large areas (Nikolakopoulos *et al.*, 2006). In terms of accuracy, it is acceptable in many applications. It is the most effective methods of extracting information, particularly in countries with limited financial resources. With InSAR data, the ability to distinguish and analyse the physical character of the Earth's surface has been greatly expanded as the InSAR permits a very fast and nearly automatic generation of DEMs. The InSAR images can be collected either by the same antenna during two different passes with Earth Resources Satellites 1 and 2 (ERS-1/2),

or by two antennas during the same pass with Shuttle Radar Topography Mission (SRTM).

As part of this study, the potential of ASTER and InSAR datasets in the derivation of DEMs to support mapping applications is investigated. Experimental testing of the accuracy of DEMs derived from these sources has been carried out using highly accurate reference data collected during the field survey. Another part of the accuracy assessment has been done by comparing the accuracy of these DEMs with the DEM created from 1:50,000 topographic maps. Issues that influence the accuracy of derived DEMs, the significance of the processing parameters that affect the accuracy of DEMs, such as baseline estimation methods for InSAR DEM and ground control points (GCPs), and issues that are specific to the study area are identified and discussed. Furthermore, the study considers the effect of spatial resolution on the accuracy of derived DEM derivatives. This study takes DEMs derived from topographic maps and tested using differential global positioning system (DGPS) as a base to compare with InSAR and ASTER DEMs. An evaluation of InSAR and ASTER derived DEMs includes a comparison of stream networks derived from InSAR and ASTER DEMs. Water hydrology is of great concern to the people of Jordan. Current modelling techniques are limited to the use of coarse resolution DEMs, such as those from the SRTM mission at 90 m resolution. Given the nature and form of the landscape in Jordan, it is proposed that improving the quality of elevation models will lead to improvements in the modelling of surface flow and accumulation area. This study has relevance for generating suitable DEMs to use in the modelling of water hydrology in semi-arid regions such as Jordan. The production of a DEM in this study will contribute to a topographic database for GIS data being established within the country. This research will develop the knowledge and understanding of the hydrological processes that contribute to the form of the Jafer Basin, a closed basin system in central Jordan. The DEM generated is also available to any researcher wanting to study the hydrology, geomorphology, soil, and geology of the Jafer area.

1.2 Aim and Objectives

1.1.1 1.2.1 Main aim

The overall aim of this research is to understand accuracies and uncertainties associated with digital elevation models derived from spaceborne remotely-sensed data and the implications of their use to understanding hydrological processes in a closed basin system in central Jordan.

1.1.2 1.2.2 Specific objectives

To address the aim stated above, the specific objectives of this research are to:

1. Evaluate the suitability of DEMs derived from interferometric synthetic aperture radar (InSAR) data from ERS-1/2 and ASTER in a semi arid region.

2. Evaluate the accuracy of DEMs derived from interferometric synthetic aperture radar (InSAR) data from ERS-1/2 and an ASTER of stereoimage using differential global positioning system (DGPS) measurements.

3. Evaluate the accuracy of DEMs derived from interferometric synthetic aperture radar (InSAR) data from ERS-1 and ERS-2 SAR and ASTER of stereoimage using a DEM generated from topographic maps.

4. Understanding of error and resolution implications of DEM in surface flow modelling.

1.3 The Importance and Need for DEMs

The digital description of the three-dimensional surface is important for several applications. Geographical information technology and remote sensing has become a rapidly expanding field in recent years with particular significance for the treatment of geographic information for scientific, commercial and operational applications. For most applications in these three domains, digital elevation models (DEMs) are an

important, integral part. In the following sections, the various application areas of DEMs are described in more detail.

1.1.3 1.3.1 Mapping applications

The development of methods for collecting DEM data together with the advances in graphics hardware and software technology has provided an extremely powerful set of tools to map relief quickly and effectively (Lo and Albert, 2007). The DEM is a standard data structure in digital cartography. DEMs have drastically changed the ways land surveyors and photogrammetrists collect elevation data for the production of contour maps. With the aid of DEMs, high quality contour maps can now be produced more quickly and economically. Errors that occur during the data acquisition and map production processes can also be detected more easily when the data are examined visually in three dimensions. In mapping for commercial sectors, DEMs are used by the recreation, real estate, banking, mortgage and insurance industries for a variety of purposes. The recreation industry uses DEMs to help with the conservation of natural land for beaches, state parks and national forests that are useful for sports. For the real estate, banking, mortgage, and insurance industries, accurate DEMs are important in the determination of flood-prone areas and to assess the levels of risk in different areas for a range of commercial applications. The quality needed for these applications is not high, and their assessment methods will depend on how accurate the application needs to be (Kyaruzi, 2005).

1.1.4 1.3.2 Engineering applications

Planning and construction is one of the fields where DEMs are widely applied to different aspects, such as reconnaissance, design, construction and the maintenance of roads, railroads, airports, harbours, canals, dams, water reservoirs, pipe lines, power transmission lines and many others. Each of these applications could have different quality requirements, each requiring different assessments of products. Some of the products derived from DEMs for engineering work are longitudinal profiles and cross sections, volume, and cut and fill maps. Assessment methods for these products depend on the accuracy level of the product itself and the accuracy requirements of the

particular application. For example, the user may require a relatively low accuracy DEM for road reconnaissance, compared to the DEM that would be needed for road design (Sulebak, 2000). Also, the communication field needs DEMs for the planning of cellular radio transmissions, locating signal transmitter stations and all kinds of communication planning and design. DEMs are needed in this case to show all kinds of visibility from one area to another. The quality required for communication purposes might not be very high, because in most cases, such DEMs will include all surface features that allow terrain obstacles to be determined. Visual methods of quality assessment might be suitable for these kinds of products (Kyaruzi, 2005).

1.1.5 1.3.3 Natural resource management applications

DEMs play a significant role in natural resource planning and management. Many biophysical processes that occur in the natural landscape are sensitive to topographic characteristics, for example, slope and aspect. Therefore, DEMs are central to climatic and biological modelling (Lo and Albert, 2007). In agriculture, DEMs are mainly applicable in the design of irrigation networks, water flow management, and surface modulation and in determining suitable areas for cultivation and agricultural land use management. Slope maps can be extracted from DEMs to show suitable areas for various crops and cultivation schemes. Also, in precise farming, DEMs enable the implementation of the best management practices to occur through the careful control of the quantity of water and fertilizer and the management of pesticides on different areas of land, depending upon soil type and condition, slope, and other factors (Kyaruzi, 2005). DEMs have special relevance because slopes determine the direction in which runoff will flow, and could adversely affect other areas. For these reasons, the agriculture industry needs accurate DEMs (Kyaruzi, 2005). Exploration experts are possibly the most experienced users of remote sensing data and DEMs. By analysing optical radar images, they determine promising regions of potential mineral deposits around the world. The estimation of solar radiation, moisture and nutrient regimes are other applications of DEM that are highly dependent on the topographic attributes of elevation, slope and aspect.

1.1.6 1.3.4 Military applications

DEMs are used in many military applications, including intervisibility for the optimal positioning of communications and weapons, cruise missile guidance, cover and concealment planning, and simulation for mission planning and rehearsal. New computer and military engineering technologies have greatly expanded the scope of DEM applications to include a wide variety of application areas ranging from relatively simple battlefield management to sophisticated missile guidance (Griffin, 1991). Regarding the improvements of operational safety and quality, aircraft staffs are required to handle increasingly complex situations. The use of simulated topography provides additional information and improves safety, particularly in critical situations, such as darkness and bad weather conditions. The detailed simulation of the landscape based on accurate DEMs is important for training purposes, and even more so for guiding the aircraft when approaching an unsupported airstrip, be it in times of military action or during an attempt to reach an undeveloped area affected by natural hazards or other catastrophic events. Only if the integrated terrain data are reliable can they be introduced safely to such critical applications. DEMs with high accuracy and high resolution are very important, particularly in this application. Quality needs may also differ depending on the accuracy level needed; for example, visibility and accessibility might need DEMs with a few metres' accuracy, while for aircraft and missile guidance, higher quality DEMs will be appropriate (Lo and Albert, 2007).

1.4 Role of GIS and Remote Sensing in Topographical Modelling

Information about the Earth's surface is of vital importance in all geosciences. Hydrology requires knowledge about the catchment topography to model the movement of water, glaciers and sediment. A DEM is now considered a crucial data input to generate and analyse hydrological model. An excellent review of typical examples of topographically based hydrological and geomorphologic models can be found in Moore *et al.* (1991). One of the important tasks in hydrological analysis is to delineate drainage basins and stream networks. With the advent of GIS, DEMs have been used to delineate drainage networks and watershed boundaries, to calculate slope characteristics, to enhance distributed hydrologic models and to produce flow paths of

surface runoff (Moore *et al.*, 1991; Quinn *et al.*, 1991; Tarboton *et al.*, 1997; Wiche *et al.*, 1992; Hogg *et al.*, 1993; Garrote and Bras, 1995; Moussa, 1997).

A DEM is a spatial data set, which describes the elevation of the land surface (Moore *et al.*, 1991, Stocks and Heywood, 1994, Weibel and Heller, 1991). The role of a GIS in modelling is to provide an environment for integration of spatial data at multi scale collected from multi sources such as ground, air and space borne sensors to create spatial data of catchment characteristics. These data can be used to derive spatial input parameters for distributed and dynamic modelling. A GIS with spatial data management and analysis tools in addition to other standard functionality provides an excellent environment to create database of input parameters at a particular scale or resolution (Burrough and McDonnell, 1998). GIS can be used to represent the landscape by means of locationally referenced data describing the character and shape of geographic features (Holmes *et al.*, 2000). A DEM is a fundamental necessity for many GIS applications due to the impact of elevation and topographic parameters derived from a DEM such as slope and aspect on many environmental phenomena and processes (Ravibabu and Jain, 2008). DEMs are often processed by GIS packages to define the configuration of the channel network, location of drainage divides, channel length and slope, and sub catchment properties. The automated derivation of such information from DEMs is faster, less subjective and provides more reproducible measurements than traditional manual evaluation of maps (Martz and Garbrecht, 1999).

Collection of large amounts of spatial data through traditional methods is expensive and time consuming and has been a deterrent in the application of these models. Remote sensing technologies can be exploited as cost effective and timely spatial data collection tools to improve the availability of spatial information on physiographic characteristics of a catchment, which can further be used for the model parameterisation. Image data is considered a primary source of natural resource information, which is utilized in various hydrological and geomorphologic studies. However, one of the greatest advantages of using remote sensing data for topographic modelling is its ability to generate information in spatial and temporal domains, which is crucial for successful model analysis, prediction and validation.

1.5 Structure of the Thesis

Chapter 2 provides an overview of DEMs. This begins with the definitions, structure and applications of DEMs. A discussion on the quality of DEMs and how the quality is quantified in terms of precision, accuracy and reliability are also presented in this chapter. In addition to a discussion of sources and types of error, potential terms in DEM accuracy measurements are identified. The chapter finishes with a discussion of topographic parameters, which are commonly extracted from DEMs.

Chapter 3 reviews methods of DEM generation from different data sources. It also describes the methods of elevation data collection used in this study. In addition, the use of interferometric synthetic aperture radar (InSAR) for DEM generation is described in Section 3.3 and the generation of DEMs using the photogrammetry technique from ASTER data is described in Section 3.4. The chapter finishes with a comparative discussion of methods of DEM generation.

Chapter 4 gives the methods and materials used in this study, including a description of the study area and data sets. It also describes the global positioning system (GPS) field measurements carried out to establish the test field in the Jafer area including GPS theory and techniques followed by the selection of the control points. Furthermore, the generation of DEM steps from three data sources, that is, InSAR, ASTER and topographic maps, are presented.

Chapter 5 presents the steps of extraction of InSAR and ASTER DEMs and the results of this process. The effects of processing parameters on the accuracy of InSAR and ASTER DEMs are addressed. The chapter finished with validation of DEM extracted from digitizing topographic maps against independent check points.

Chapter 6 provides the results of an accuracy assessment and a comparison of different of models. Analysis of the spatial distribution of the elevation error in order to understand the error present in generated DEMs is also discussed. Furthermore, the

effect of propagation of error and the effect of different resolution DEM on derivatives are addressed. The chapter summarises a general discussion about the suitability of the DEMs created to determine and map topographic structure.

Chapter 7 presents the main conclusion of this study. Some suggestions for further research are recommended at the end of this chapter.

Chapter 2: Digital Elevation Model

2.1 Definition and concept

Three types of terrain model are commonly used: digital elevation models (DEM), digital terrain models (DTM) and Digital Surface Models (DSM). There are many definitions for digital elevation models. O'Callaghan and Mark (1984) define a DEM as any numeric or digital representation of the elevations of all or part of a planetary surface. Meanwhile, Burrough (1986) defined the DEM as any digital representation of the continuous variation of relief over space. Also, a DEM is defined as a mathematical model of the Earth's surface that, at present, are the most powerful method of representing relief (Stocks and Heywood, 1994). However, Burrough and McDonnell (1998:30) defined a DEM as "a quantitative model of part of the earth's surface in digital form". A DEM provides a method for subdividing a landscape in an attempt to represent the local topography. More recently, a DEM definition was given by Fisher and Tate (2006:468). They defined a DEM as "a set of elevation values which are recorded on a regular grid, most commonly in a square form, less frequently in a triangular or rectangular form".

Aronoff (1989) argued that a DEM is a set of elevation measurements for locations distributed over the land surface and that this method carries different names, including digital elevation model (DEM), digital terrain model (DTM) and digital terrain data. The first definition for a DTM was presented by Miller and La Flamme (1958). They define a DTM as a statistical representation of a continuous surface of ground by a large number of selected points with known x, y, and z coordinate fields. Wood (1996) defines a DTM as a surface model that includes explicit representation of surface form by means of ridgelines, valley lines, form lines and spot heights. However, Schmid-McGobbon and Eyton (1996) defined a DTM as any digital data set that describes some attribute of the terrain surface, such as elevation, slope gradient or slope aspect. Wood (1996) defines a DEM as a specific form of terrain model, namely

a raster data set, representing the elevation of the terrain surface as a two dimensional array or matrix of height values. The DEM matrix is visualized by colouring each element of the matrix, or cell, according to its elevation value from a palette of graded colours or grey levels.

Meijerink *et al.* (1994) made a distinction between DEMs and DTMs. They define a digital terrain model as a spatial distribution of terrain attributes, a topographic map in digital format, which consists not only of the DEM but also slope, aspect, the types of land use, settlements, and types of drainage lines, and so on. Maune (2001) stated that DTM may be similar to DEM, but they may also incorporate the elevation of significant topographic features on the land, plus mass points and break lines that are irregularly spaced, so as to better characterize the true shape of the bare earth terrain. Therefore, contours generated from a DTM more closely approximate the real shape of the terrain. The use of the DTM term is often used because 'terrain' often implies attributes of a landscape more than the altitude of the land surface. Although DEMs were originally developed for modelling relief, they can of course be used to model the continuous variation of any other attributes over a two-dimensional surface.

A DEM represents a reconstruction of the height of the surface but when objects of a selected region are included it is called a DSM (Digital Surface Model). Such surfaces may also be of urban and forested areas, where the tops of buildings or trees are represented. The term DSM has been defined by various authors. DSM is sometime used as a synonym for Digital Building Model (DBM); the more logical definition is to use DSM for the representation of the entire surface of the observed region. A DSM is generated over a regular grid of equidistant points, where the corresponding height is a measure of the average height within the cell (Poidomani *et al.*, 2000). On the other hand, ComputaMaps (2001) defined DSM as "a model of terrain and all significant above-ground features (such as buildings and vegetation) represented in digital form by an elevation grid or list of three-dimensional coordinates". DSM is similar to a DEM or DTM, except that a DSM represents the elevations of the top of surface features on the bare earth, which can be building, trees, towers, and other features (Maune, 2001).

2.2 Elevation Data Structure

A continuous surface, such as that of the earth, has an infinite number of points. Obviously, it is impossible to record every point, and consequently a sampling method must be used to extract representative points. These discrete points can then be used to build a surface model that approximates the actual surface. These types of representation of elevation can be line models (contours lines), grid/raster models, or triangular irregular networks (TIN). In GIS environment, DEMs are commonly modelled by grid/raster models, or triangular irregular networks (TIN) (Burrough and McDonnell, 1998). Each of these types of DEM format has advantages and disadvantages; also, their respective applicability is mainly dependent on the methods by which the source data were collected.

2.2.1 Contour lines

Contour lines are defined as a set of lines that connect points of the same elevation value (Figure 2.1a). Each contour line contains an infinite number of potential sample points, which are connected together to draw a continuous line following the contour across the surface. They are an excellent representation of the heights and variations of a surface for a two-dimensional printed map because with topographic maps, it is easy to interpret the contours since anyone can look at contour lines on a map, can recognize peaks, ridges, valleys, relative slope, aspect, stream direction, and other characteristics that cannot all be easily interpreted from a TIN or grid (Maune, 2001). Contour accuracy depends upon whether the lines have been generated from primary or derived data. When contours have been captured directly from aerial photographs as primary data using a stereoplotter, the contours are highly accurate. If the contours have been generated from point data, the location of the contours must be interpolated between known values.

One major drawback of contours is that they only indicate surface values along the lines while the change of the surface between contour intervals cannot be represented. Once the surface has been represented as contours, interpolation can be used to derive an elevation for locations between contours (El-Sheimy *et al.,* 2005). Contours have

most often been used by cartographers to represent relief. Due to their crude topological structure, they are not particularly suitable for automated spatial analysis of ground morphology. Even the derivation of slope or shaded relief maps from contours are rather cumbersome operations (Carrara *et al.*, 1997).

2.2.2 Raster or grid structure

The most commonly used digital elevation model form is a raster or a regular grid of spot heights (Maune, 2001). A grid is a rectangular array of cells, each of which stores the elevation value for the cell (Figure 2.1b). Grids have a matrix structure that implicitly record topological relation between data points (El-Sheimy *et al.*, 2005). The size of a grid cell is determined by resolution required for application and the level of detail of the input data used to create the grid. The cell must be small enough to capture the required detail, but large enough so that computer storage and analysis can be performed efficiently (Maune, 2001). Gridded terrain models are appropriate for small scale mapping applications where absolute positional accuracy is not paramount and where surface features do not need to be characterised exactly.

Although the grid format is a fast and efficient data structure for analysis algorithms, and is a useful DEM structure to calculate contours, slope, aspects, hill shading and automatic catchment area delineation, in addition to having a lower storage requirements, it is not without disadvantages. The disadvantages of the grid representation are that surface discontinuities such as ridges and stream centrelines are not well represented, and precise locations for features such as peaks are lost in the sampling of the grid (Maune, 2001). For these same reasons, grids are not good for representing man-made objects such as road cuts, buildings, etc., but are good for bare earth terrain models. Grids can be an inefficient storage method in cases where there is little change in value over an area (Maune, 2001).

Burrough and McDonnell (1998:124) identified a further three disadvantages: (1) the large amount of redundancy in areas of uniform terrain; (2) the inability to adapt to areas of differing relief complexity without changing the grid size; and (3) the exaggerated emphasis along the axes of the grid for certain kinds of computation such

as line of sight calculation. Moore *et al.* (1991) also stated that grid DEMs have several disadvantages: (1) they cannot easily handle discontinuities in elevation; (2) the resolution affects the results and computational efficiency; (3) grid spacing needs to be based on the roughest terrain in the catchment, resulting in redundancy in smoother areas; and (4) the computed flow paths tend to zigzag, not following the drainage lines, and are hence systematically too long.

2.2.3 Triangular irregular network

The triangular irregular network (TIN) model is a significant alternative to the regular raster of a DEM and has been adopted by numerous GIS and automated mapping and computer packages (El-Sheimy *et al.*, 2005). This model is based on point, line and triangular structures. A TIN model approximates a topographic surface by connecting a set of irregularly spaced elevation vertices into triangular facets. The triangles share edges and vertices to exhaust the space as if they were a triangular mosaic (Figure 2.1c). Peuker *et al.* (1978) designed a triangular irregular network (TIN) for digital elevation modelling that avoid the redundancies of the grid format and was more efficient for many types of surface calculation, such as slope. They defined the TIN as a digital terrain model that was based on an irregular array, which forms a sheet of non-overlapping contiguous triangular facets. The points used to construct a TIN come from individually sampled locations or from the vertices of linear features. Ideally, these represent a set of critical locations on the surface, which defines breaks in slope such as peaks, pits, ridges, valleys, and passes (Maune, 2001).

The accuracy of a TIN is consistent with the degree of variation in the terrain. TINs may contain many more surface-specific points in high relief areas, such as peaks, pits, saddle points, and points along streams and ridges (Wang and Lo, 1999). Unlike the grid, the TIN allows for extra information to be gathered from areas of simple relief that leads to the data capture process for a TIN being able to specifically follow ridges, stream lines, and other important topological features that can be digitized for the accuracy required (Burrough and McDonnell, 1998). As the terrain becomes more complex, the resolution of the TIN should increase accordingly. This occurs because more points are sampled and included in the TIN model in areas of high complexity

(Weibel and Heller, 1991). The simplest interpretation of the model, in terms of defining a continuous surface, is a linear approach and is based on the principle that a flat plane can be fitted to any three non-collinear points (Carter, 1988). Thus, areas of consistent slope and aspect are represented in the TIN by individual triangles. Areas can be considered uniform if changes in slope or aspect are within a given tolerance level. A tolerance allowing for high levels of error will result in a generalized model of the surface. Slope and aspect can be computed rapidly because only individual triangles need to be examined, rather than the relationships between them (Maune, 2001).

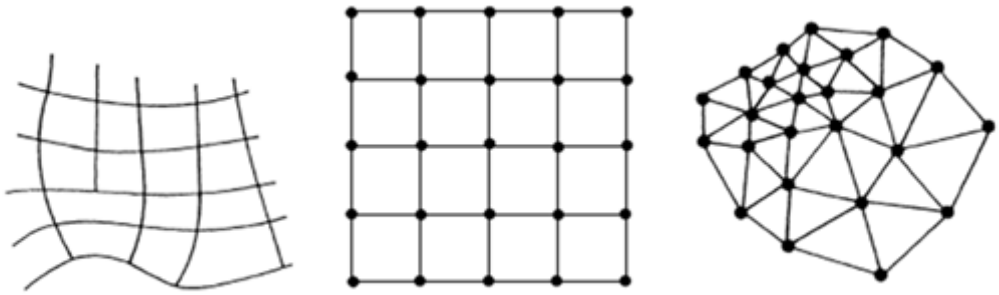

(a) (b) (c)

Figure 2.1: Examples of structuring an elevation data: (a) contour lines (b) raster or grid structure (c) triangular irregular network (TIN). Source: Wilson and Gallant (2000:470).

2.3 DEM Quality Issues

2.3.1 Definition of DEM quality

The quality of a DEM refers to horizontal and vertical accuracies. Data quality assessment has become a core practice in fields such as GIS (Zhang and Goodchild, 2002) and remote sensing (Lunetta and Lyon, 2004). The quality of spatial data means how well these data represent reality and fulfils the user requirements (Ehlschlaeger and Goodchild, 1994). The quality of a DEM is dependent upon a number of interrelated factors, including the methods of data acquisition, the nature of the input

data, and the methods employed in generating the DEMs (Shearer, 1990, Gong *et al.* 2000). Of all these factors, data acquisition is the most critical. Previous studies on DEM data acquisition have focused either on the examination of generation methods, or on case studies of accuracy testing (Ackermann, 1978; Ebner and Reiss, 1984; Torlegard *et al.*, 1987). Cooper and Cross (1988) stated that aspects of data quality included reliability, accuracy, and precision, which are related to three types of error.

Reliability refers to error blunders: internal reliability indicates how easy it is to detect a blunder, and external reliability measures the effect of an undetected blunder on results. In the context of terrain modelling, the term 'accuracy' is used to refer to systematic errors (Cooper, 1998). The accuracy of a DEM is considered critical when the DEM data are used for environmental modelling and for the prediction of the spatial distribution of hydrological, geomorphological, and biological properties (Thompson *et al.*, 2001). The term 'precision' is used to describe random errors (Cooper and Cross, 1988; Wise, 2000). The difference between accuracy and precision is often not understood. Accuracy refers to the closeness of measured values, observations or estimates to the real or true value (Chrisman, 1991). Precision can be divided into two main types: statistical precision is the closeness with which repeated observations conform to themselves and numerical precision is the number of significant digits in which an observation is recorded.

Other authors categorize spatial data quality as a function of three primary components: accuracy, precision and uncertainty (Chrisman, 1991; Aspinall and Pearson, 1993; Burrough, 1993). Accuracy and precision are important when generating precise data sets, such as those utilized in civil engineering, while uncertainty must be included in natural resources data analysis (Davis and Keller, 1997).

2.3.2 DEM accuracy: sources and types of errors

Error is defined as the difference between a model value and the true value (Fisher and Tate, 2006). Sources of DEM error are closely related to DEM production methods

(USGS, 1997). These methods include ground survey, photogrammetry, digitizing or scanning contour maps, and remote sensing data. Each of these methods provides data or has a varying degree of accuracy depending on the processing steps taken to construct the DEM (Wechsler, 2007). Fisher and Tate (2006) concluded that sources of error in the DEM can usually be identified to originate from three main sources. First, errors can result from the source of the data because the use of different methods for collection data can lead to differences in the 'accuracy, density and distribution' (Li and Chen, 1999) of the measured source data. Second, errors can result from the processing steps and interpolation techniques used to derive the DEM from the source data. Finally, errors can result from variability within the terrain surface. Terrain characteristics have effects on error magnitude and distribution within DEM, which leading to different level of accuracy based on the slope values. The largest errors in slope gradient were found on the steepest slopes while the smallest errors were in the more level areas (Sasowski et al., 1992; Bolstad and Stowe, 1994). Wood (1993, 1996) shows how accuracy of a DEM can be related to gradient and aspect. He produced a regreaaion model to predict accuracy from known gradient and aspect measurements. Zhou and Liu (2004a) distinguished sources of errors as those in data, inherent in data structure and created by algorithms. They further analysed components of errors caused by data and data processing in derived slope and aspect by employing a mathematical model to delineate error components, contributed by data and algorithm errors, in derived slope and aspect from a grid-based DEM. They also analysed the influence of DEM data properties, such as precision, resolution and orientation, on the resulting topographic parameters (Zhou and Liu, 2004b).

The widespread use of DEMs in a range of applications and the increasing range of digital elevation data products have given rise to a large body of work on DEM error (Arrell *et al.*, 2008). DEM errors are generally categorized as either systematic, blunder or random errors. Systematic errors result from the procedures used in the DEM generation process and follow fixed patterns that can cause bias or artefacts in the final DEM product. These errors are not easily detectable, but when the error is identified, systematic error can be reduced or even eliminated (Wechsler, 2007). Blunders are vertical errors associated with the data collection process and are

generally identified and removed through carful procedures and subsequent quality control checking (Wechsler, 2007). Random errors result from accidental or unknown combinations of problems. Random errors remain in the data after blunders and systematic errors are removed (USGS, 1997).

The extraction of a DEM from contour maps is affected by the source data used to create the map. Error in the source map data generally comes from the process of collection, recording, and generalization inherent in the cartographic process (Fisher and Tate, 2006). The contour interval of topographic maps used to collect elevation data may affect the density and the distribution of data. The elevations can be derived by manually digitizing the contour lines from paper maps or from scanned maps. In both techniques, errors can occur during the digitizing/scanning process or in automatically identified contour lines. In addition, the degree of DEM error can vary depending on the suitability of the interpolation method for a certain relief. Wood and Fisher (1993) applied visualization techniques to identify DEM interpolation errors. Desmet (1997) investigated the effect of interpolation on precision (accuracy of the predicted heights) and shape reliability (degree of fidelity in the spatial pattern of topography) expressed by derived topographic parameters. For this study, he selected the calculation of slope gradients, aspect directions, profile curvatures and upslope areas.

DEMs produced from photogrammetric techniques are affected by both human errors and instrumental errors (Hunter and Goodchild, 1995). Fisher and Tate (2006) stated that the production of DEMs from photogrammetry introduces both random and systematic errors. Random errors may accrue through the lack of precision in the identification of target points on a photograph as part of the process of aerial triangulation, and systematic errors may accure from changes in the film media, instrument errors and from human errors. The data collected by active systems may require not only interpolation, but also considerable processing to obtain the resultant DEM. For example, Gens (1999) observes that the errors introduced into InSAR-derived DEMs may come from the registration processes of radar images or from the

phase unwrapping process. Figure 2.4 shows an example of a simple occurrence of errors (Fisher and Tate, 2006).

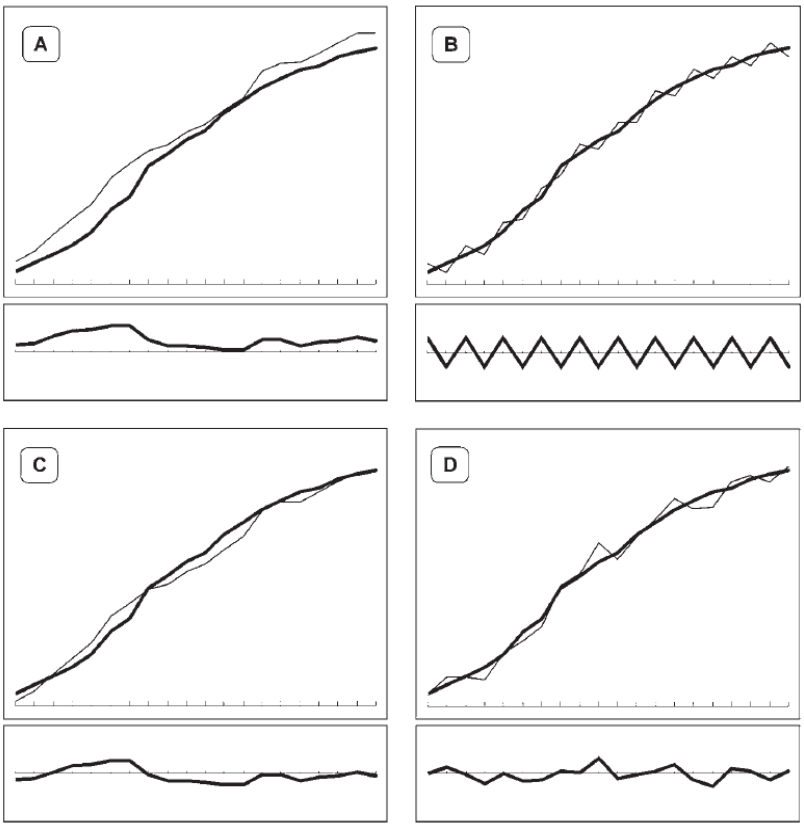

Figure 2.2: Comparisons of a profile through a DEM and the occurrence of error. (A) The occurrence of error with bias; (B) the occurrence of systematic error; (C) the occurrence of spatially autocorrelated error (the normal situation); (D) the occurrence of random error (no spatial autocorrelation). In each instance the upper diagram shows the ground surface as a thick line and the ground surface with the error as a thin line, and in the lower diagram the error alone. Source: Fisher and Tate (2006:470).

2.3.3 DEM resolution for representing topography

The quality of a DEM refers to more than just its vertical accuracy. The spatial resolution is also a very important aspect that affect on the DEM accuracy and its derivatives. Raster or regular grid DEM record elevations at a constant interval known as resolution. Li (1992) stated that DEM accuracy decreases with coarser resolutions due to the averaging of elevations. Smaller grid cell sizes can capture more detail and smaller variations in topography. They also increase the volume of the data to be

stored and might result in data redundancy (Gao, 1997). The accuracy of DEM-derived variables is affected by DEM resolution. Chang and Tsai (1991) examined how spatial resolution affects the accuracy of slope and aspect. Comparison of the results from resolutions of 20 m, 40 m, 60 m and 80 m with those at 8m revealed that the two parameters are less accurate if generated from a DEM of a coarser resolution.

Hodgson (1995) suggested that, the slope and aspect are most commonly associated with cell sizes approximately two times the initial DEM grid resolution. The solution is to select a resolution that is as coarse as possible while still meeting a defined accuracy required for the specific purpose (Gao, 1997). The impact of spatial resolution on the accuracy of hydrologic derivative has been shown in the following applications: topographic index (Quinn *et al.*, 1991; Valeo and Moin, 2000), drainage properties such as channel networks and flow extracted from DEMs (Garbrecht and Martz, 1994; Wang and Yin, 1998; Tang *et al.*, 2001; Lacroix *et al.*, 2002), the spatial prediction of soil attributes (Thompson *et al.*, 2001), computation of geomorphic measures such as area-slope relationships, cumulative area distribution and Strahler stream orders (Hancock, 2005), modelling processing of erosion and sedimentation (Schoorl *et al.*, 2000).

2.3.4 Measures of DEM accuracy

Accuracy can be defined as the degree of closeness an observation or estimated value to the true value (Wolf and Dewitt, 2000). A value which is very close to the true value has high accuracy and a value that is far from true has low accuracy. Assessment of DEM accuracy typically can be made by comparing a DEM with a set of ground truths that have a higher degree of accuracy than that of the data being investigated (Wise, 1998). The accuracy of a DEM depends on (i) the source of the elevation data, including the techniques for measuring elevation either on the ground or remotely, the locations of samples, and the density of samples; (ii) the methods used to create the DEM from this elevation data, (iii) the data model, or structure of the elevation data (grid, contour, triangular irregular network), (iv) the horizontal resolution and vertical precision at which the elevation data is represented, (v) the topographic complexity of

the landscape being represented, and (vi) the algorithms used to calculate different terrain attributes (Thompson *et al.*, 2001). A few descriptors are used for DEM accuracy assessment, namely, root mean square error (RMSE), standard deviation histogram analysis, and difference elevation (error).

The measurement of errors in DEMs is often impossible because the true value for every geographic feature or phenomenon represented in a geographic data set is rarely determinable (Garbrecht and Martz, 1999). Uncertainty, instead of error, should be used to describe the quality of a DEM. Quantifying uncertainty in DEMs requires a comparison to be made between the high accurate elevations, for example elevations collected using differential global positioning systems (DGPS) with the elevations in a DEM surface model. Such a comparison results in height differences (or residuals) at the tested points. The most important consideration should be taken into account when check points used in accuracy assessment of DEM. Check points should be independent, representative of the population and truthful. As a result of the high variability of data it can be said that it is very difficult to determine the minimum number of checkpoints needed to guarantee a reliable assessment of DEM accuracy (Aguilar *et al.*, 2007). In most cases, a sample size employed is at least 30 checkpoints (Griffith, 1996). The widely quoted National Standards for Spatial Data Accuracy (NSSDA), given by the Federal Geographic Data Committee (FGDC, 1998), recommend the use of a minimum of 20 checkpoints to reflect geographical area of interest and the error distribution in the dataset. Such standards assume a normal distribution of residuals.

The statistical measures such as the root mean square error, standard deviation, and mean are the conventional ways to analyse the deviation between two sets of elevation data. Probably the most widely used measure for reporting accuracy is the root mean squared error (RMSE). It is used, for example, by both the USGS (USGS, 1998) and the Ordnance Survey (Ordnance Survey, 1993). It measures the dispersion of the frequency distribution of deviations between the original elevation data and the DEM data, and is mathematically expressed as follows:

$$\boldsymbol{RMSE} = \sqrt{\frac{\sum(\boldsymbol{Z_{DEM} - Z_{Ref}})^2}{\boldsymbol{n}}} \tag{2.1}$$

Where Z_{DEM} is the i^{th} elevation value measured on the DEM surface, Z_{Ref} is the corresponding original elevation, and n is the number of elevation points checked. The main attraction of the RMSE lies in its easy computation and straightforward concept. However, this measure is essentially a single global measure of deviations, and thus is incapable of accounting for the spatial variation of errors over the interpolated surface (Wood, 1996). The RMSE is not necessarily a good description of the statistical distribution of the error.

Some studies (Sansosti *et al.,* 1999; Gamba *et al.,* 2003; Doucette and Beard, 2000; Fisher and Tate, 2006) have suggested the use of a more complete statistical description of errors by reporting the mean error (ME). This statistical measure determines the extent to which the DEM is free from systematic errors or bias. The residual will tend to zero if there is any similarity in the magnitudes of the positive and negative values. If the significant positive or negative values were determined, then this would give an indication or evidence about systematic error. The mean error is computed as follows:

$$\boldsymbol{ME} = \frac{\sum(\boldsymbol{Z_{DEM} - Z_{Ref}})}{\boldsymbol{n}} \tag{2.2}$$

ME can be either negative or positive, and records systematic under or overestimation of the elevations in the DEM.

The standard deviation (S) is a common statistical expression that is used to measure the spread of the data about the mean value. It is a measure precision and is similar in representation to the RMSE; both are based on squared residuals and hence provide information concerning the distribution of residuals either side of a mean value.

$$S = \sqrt{\frac{\Sigma[(Z_{DEM} - Z_{Ref}) - ME]^2}{n-1}} \quad (2.3)$$

2.4 DEM-based Topographic Parameters

A DEM is a primary source of topographic parameters that are used to describe the geometric properties of the Earth's surface (Oksanen and Sarjakoski, 2005). Topographic parameters may be divided into primary topographic parameters, such as slope, aspect, surface curvature, or catchment area, and secondary parameters, such as the topographic wetness index, or stream-power index (Wilson and Gallant, 2000). The primary attributes are calculated directly from the elevation data or from one of its derivatives, whereas the secondary attributes are calculated from two or more primary attributes (Oksanen and Sarjakoski, 2005). Wilson and Gallant (2000) provide a detailed review of the DEM-derived primary and secondary topographic attributes. Topographic parameters derived from DEMs are sensitive to both the quality of the DEMs from which they are generated (Bolstad and Stowe, 1994; Wise, 2000) and the algorithms that are used to produce them. Numerous algorithms exist for calculating topographic parameters. For example, slope is calculated for the centre cell of a 3×3 matrix from values in the surrounding eight cells. Algorithms differ in the way the surrounding values are selected to compute change in elevation (Skidmore, 1989; Carter, 1990; Guth, 1995; Dunn and Hickey, 1998; Hickey, 2001).

2.4.1 Slope and aspect

Slope and aspect are essential topographic parameters derived from DEMs which are widely used in the environmental sciences applications. These parameters describe the magnitude and direction of the vector tangent to the downhill in the Earth surface (Raaflaub and Collins, 2006). Slope is the rate of elevation change in the direction of the steepest descent, and aspect is the direction of the steepest slope. Since the shape of the downhill surface is used to determine the spatial routing of water over terrain, one such application is distributed hydrological modelling. Hydrologically, slope is an indication of the amount of gravitational energy available to drive water flow; hence, it influences the rate of water flow. Aspect, which defines the slope direction, can be

used to determine the direction of water flow, which is the information required to determine other hydrologically significant variables, such as the upslope area (Raaflaub and Collins, 2006).

The calculation of slope and aspect is not straightforward. Difficulties arise as specific elements from the terrain surface are calculated from a different model of the terrain surface. Many algorithms have been developed to derive slope and aspect from DEMs (Raaflaub and Collins, 2006). Different algorithms produce different results for the same derived parameter, and their suitability in representing the parameters in varied terrain types may differ. Skidmore (1989) found large differences between the results when he compared a number of algorithms for calculating slope and aspect. When the estimated slope value was used as a parameter in a soil erosion model, the differences were seen to be magnified (Srinivasan and Engel, 1991). Calculating the slope and aspect for a cell is based on neighbourhood operations using the values of the cells that are spatially adjacent in the grid. The methods differ in their suitability for representing the parameters in different terrain types, and for specific applications. The slope algorithm currently implemented in ESRI GIS products was developed by Horn (1981) and is considered to be better suited for rough surfaces (Horn, 1981; Burrough and McDonnell, 1998), while the slope algorithm implemented in the IDRISI GIS package, and developed by Zevenbergen and Thorne (1987) is thought to perform better in representing slope on smoother surfaces (Eastman, 1992).

In terms of a topographic surface, the numerical derivative is calculated from two quantities: the elevation difference and the ground distance (Eyton, 1991). Together, the slope in the x direction and the slope in the y direction (the partial derivatives of z with respect to the x and y directions), define the gradient vector of the surface. The maximum slope can be determined by the following equation,

$$\boldsymbol{Slope} = \sqrt{\left(\frac{dz}{dx}\right)^2 + \left(\frac{dz}{dy}\right)^2} \qquad (2.4)$$

The aspect, which is the direction of the maximum slope, is the angle between the slope defined in *x* and the slope defined in *y*, which is given by the relationship,

$$\boldsymbol{Aspect} = \tan^{-1}\left(\frac{dz/dx}{dz/dy}\right) \tag{2.5}$$

2.4.2 Flow direction

A flow direction raster shows the direction of water flow out of each cell of a DEM. There are numerous algorithms to calculate flow direction known as D8, multiple flow direction (MFD), 2D-Lea, 2D-Jensen, and D-Infinity. D8 algorithm was reported by O'Callaghan and Mark in 1984. 3×3 local window of a DEM is used to calculate the direction of surface water flow by the D8 algorithm, in which the flow direction is defined as the direction of maximum drop from the centre point to one of its eight neighbours (Oksanen and Sarjakoski, 2005). Therefore, if the cell size is 1, the distance between two orthogonal cells is 1, and the distance between two diagonal cells is $\sqrt{2}$. The algorithm is the most popular one, particularly in commercial GIS software, because of its simple and efficient computation, and strong capability in dealing with local depressions and at areas (Tarboton 1997). One major disadvantage of the D8 algorithm is that although the centre cell can receive upstream flow from several sources, the downstream flow can only be in one direction. Thus it is not suitable for areas where divergent flow occurs, such as convex slopes and ridges (Costa-Cabral and Burges 1994, Moore 1996, Wilson and Gallant 2000).

The random eight-node (Rho8) algorithm developed by Fairfield and Leymarie (1991) introduced a degree of randomness into the flow direction computations to break up the parallel flow paths that D8 produces (Wilson and Gallant 2000). This algorithm starts by identifying all the down slope neighbouring cells, then calculating the slope gradients in each of these directions, and finally choosing a number from a table of random numbers to direct the flow to one of these candidate cells. In multiple flow direction (MFD) algorithm, the flow direction from the centre cell does not necessarily point to a single neighbouring cell, but rather, it may flow into all or part of

downstream neighbours. Based on this principle, a number of algorithms have been developed with various ways of distributing flow proportionally. Quinn *et al.* (1991) and Freeman (1991) reported different implementation of the MFD algorithms, a common point of which is that they do not need to determine the flow direction for individual cell.

Lea (1992) develops an algorithm that uses the aspect associated with each pixel to identify flow directions. Flow is routed as a ball rolling on a plane released from the centre of each grid cell. A plane is fit to the elevations of pixel corners, these corner elevations being estimated by averaging the elevations of adjoining pixel centre elevations. This procedure has the advantage of identifying flow direction continuously (as an angle between 0 and 2π) and without dispersion. Costa-Cabral and Burges (1994) present an elaborate set of procedures named DEMON that extend the ideas of Lea (1992). This elaboration includes the assumption that grid elevation values are used as pixel corners, rather than block cantered, and a plane surface is fitted for each pixel. The final algorithm is D∞ that was proposed by Tarboton (1997) and incorporates several ideas from DEMON to assign multiple flow directions to selected cells. The flow direction is determined in the direction of the steepest descent and is represented as a continuous quantity between 0 and 2л (Tarboton 1997). Each down slope vector is drawn outward from the center and may be at an angle that lies within or outside the 45°. If the slope vector angle falls within the facet, it represents the steepest flow direction of that facet. If the slope vector angle lies outside the facet, the steepest flow occurs along the steepest edge.

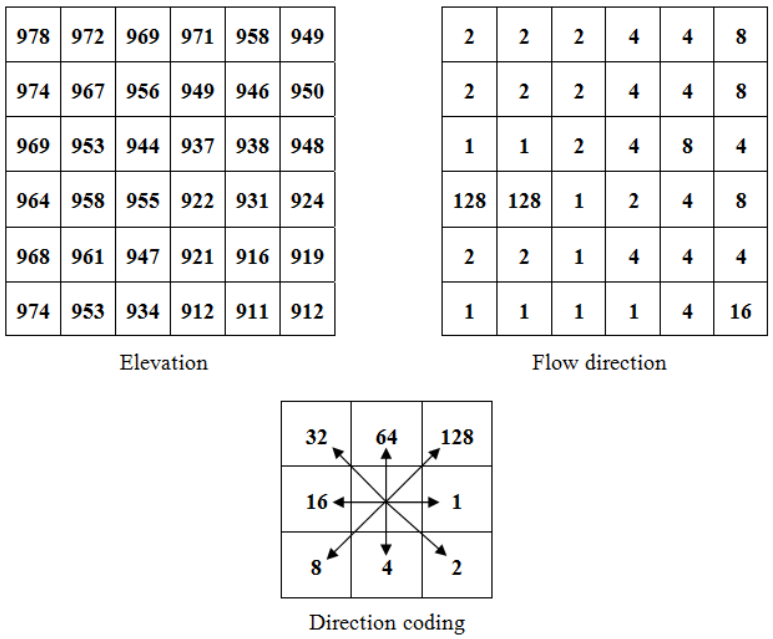

Figure 2.3: Extraction flow direction from DEM. Source: (ArcGIS documentations).

2.4.3 Flow accumulation

A flow accumulation for each cell represents the number of cells that will flow through it, recording how many upstream cells will contribute drainage to each cell (the cell itself is not counted) as shown in Figure 2.4. Flow accumulation is a power full GIS application because calculating it as a spatially distributed quantity allows determining drainage area not at just one point, but at any point within the domain of the original DEM field. The flow accumulation function calculates accumulated flow based on the flow direction. Flow accumulation can be interpreted in two ways. First, cells having high accumulation values generally correspond to stream channels, whereas cells having an accumulation value of zero generally correspond to ridge lines (Jenson and Domingue, 1988). Secondly, if multiplied by the cell size, the accumulation value at a cell represents a drainage area flowing through that point.

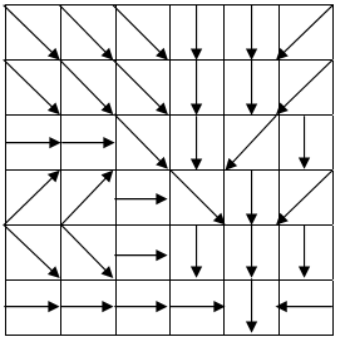

Flow direction

0	0	0	0	0	0
0	1	1	2	2	0
0	3	7	5	4	0
0	0	0	20	2	1
0	0	0	1	24	0
0	2	4	7	35	2

Flow accumulation

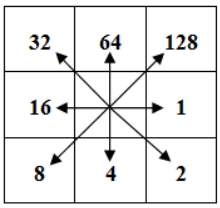

Direction coding

Figure2.4: Extraction flow accumulation from DEM. Source: (ArcGIS documentations).

2.5 Summary

This chapter has presented the terms and issues related to DEMs used in this study. These issues included the definition and structure of DEMs. The issues of accuracy, error DEM and topographic parameters derived from DEM also were presented in this chapter. The methods of generating of DEM and their issues are reviewed in Chapter 3.

Chapter 3: Techniques for the Acquisition of DEM Source Data

3.1 Introduction

There are different methods to manage and analyse topographic information to obtain the greatest benefit. Two factors play a very important role in determining which method can be used: the purpose of the data and the cost of the method. There are different kinds of DEM generation methods as discussed in previous chapters, such as photogrammetry and ground surveys and from digitizing topographic maps. Also, the new technologies of LiDAR (Light Detection and Ranging) and interferometric Synthetic Aperture Radar (InSAR) can be used to generate DEMs. In this chapter, a critical review of the techniques for acquiring a DEM will be outlined before details are given of the Synthetic Aperture Radar interferometry (InSAR) and the ASTER stereoscopy techniques, which are the subject of this research project, and issues surrounding the use of these techniques are discussed. A comparison of all these techniques is also given at the end of the chapter.

3.2 DEM Generation Methods

3.2.1 Ground surveys

The generation of DEMs from ground surveys is one of the most expensive methods; it is rarely used, although it can provide the most accurate results. In this method, the surveyors can collect extremely accurate elevation data using theodolites and computerized total stations or a global positioning systems instruments (GPS). This surveying technique determines the coordinates of a point through the measurement of distances and angles. A ground survey can provide the most accurate measurement of terrain information with accuracy of up to ±1cm (Ravibabu and Jain, 2008). It is a more efficient method due to the development of total station, GPS, and field data recording techniques for small areas,

applications include those within civil engineering and mining (Kennie and Petrie, 1991). Ground survey is time consuming and expensive and need professional surveyors.

3.2.2 Digitizing topographic maps

Most of the DEM data currently available have been extracted from digitizing topographic maps. The usual process followed to derive DEMs from such data sources involves the digitizing of contour lines from the maps, and the interpolation of elevation values for every pixel in the surface, as a function of the values of neighbouring contours cells. Cartographic digitization techniques can be divided into vector-based line following and raster-based scanning (Li *et al.*, 2005). The most widely used method is manual line following. After the map is carefully put onto the digitizer table, a cursor with cross hairs is used to trace the contour lines by hand and to record the coordinates. Digitizing the contour lines can be done in stream or point mode. In point mode digitization, the x, y coordinates of the cursor's position are recorded each time the operator presses a button, and a decision is made by the operator on which point is to be recorded. In point mode manual digitization, the operator has control over the selection of points to reduce data volume. On the other hand, in stream mode the tracing/measurement process is carried out dynamically and can be less accurate (Li *et al.*, 2005).

Scanning is considered to be an effective means of automating DEM data generation from contour maps (El-Sheimy *et al.*, 2005). In the raster scanning process, a map is converted into raster (digital) format. This is followed by vectorisation, which can be either manual or automated. In manual vectorisation, the scanned map is displayed on a screen and line following digitization is carried out on screen. Algorithms are used in automated vectorisation. Scanning usually produces more accurate digital contours after editing than manual digitizing, as many of the errors introduced by human intervention are eliminated. The accuracy of a DEM created in this way depends on the level of detail of the source and the grid spacing used to sample that source. The main factor that affects the level of detail of the source is the scale. The level of content that may be extracted from a given source during digitisation is dependent on the proper selection of grid spacing.

3.2.3 Photogrammetry

Photogrammetry is the "*art, science and technology of obtaining reliable information about physical objects and the environment through the process of recording, measuring and interpreting photographic images and patterns of electromagnetic radiant imagery and other phenomena*" (American Society of Photogrammetry, 1980). Photogrammetry has passed through three main stages of development, that is, analogue photogrammetry and analytical photogrammetry, and now digital photogrammetry. In analogue photogrammetry, optical or mechanical instruments were used to reconstruct three-dimensional geometry from two overlapping photographs. The main product from this stage was topographic maps. In analytical photogrammetry, the computer replaces some expensive optical and mechanical components. The main developments in this stage were analytical aerotriangulation, analytical plotters, and orthophoto projectors. Outputs of analytical photogrammetry can be topographic maps, which can also be digital products, such as digital maps and DEMs (Cheng, 2000**).**

Digital photogrammetry is photogrammetry applied to digital images that are stored and processed on a computer. Digital images can be scanned from photographs or can be directly captured by digital cameras. The output products are in digital form, such as digital maps, DEMs, and digital orthophotos. The main purpose of photogrammetry, whether analogue, analytical or digital, is to obtain precise three-dimensional measurements by using the overlapping images to recreate the original stereo geometry of each adjacent pair of images (Shears and Allan, 1996). The standard procedures to generate DEMs are based on two fundamental steps, which consist of internal orientation and external orientation. The internal orientation is performed to define the frame position inside the camera, using the camera calibration certificate (provided by the factory) to correct distortion and to assign known coordinate values at specific points. The external orientation is obtained by two subsequent steps: relative and absolute orientation. In the first case, the aim is to create the stereoscopic model in an arbitrary relative system using points common to both images (tie points). The absolute orientation is the transformation of the generated stereoscopic model into an external reference frame (for instance, UTM) defined by the coordinates of several ground control points recognized on the images.

The production of DEMs from remote sensing imagery has become a vital area of research and development over the past two decades, beginning with the launch of the first civilian remote-sensing satellite. Recently launched high-resolution imaging satellites, such as SPOT-5, IKONOS, and QUICKBIRD, form an excellent source for the efficient, economic, and accurate generation of DEM data. These images are all obtained by passive systems, where the sensors record the electronic radiations reflected by the terrain surface and objects on the terrain surfaces (Li and Gold, 2005). Stereo image viewing has been the most common method for elevation modelling used by photogrammetry, and remote sensing communities. Two methods are possible to obtain stereo images from satellite scanners: across-track stereo images from two adjacent orbits, and along-track stereo images from the same orbit, using fore and aft images. Landsat was the first dataset used with a cross-track approach from two adjacent orbits in 1980, then with SPOT, and finally with IRS-1C/D (Cheng and Chaaple, 2006). A long-track stereoscopy technique is used in a large number of satellites, including JERS, ASTER, IKONOS, QuickBird, OrbView, SPOT-5, Formosat II, and CartoSat. Toutin (2008) addressed the objectives of the along-track stereo experiment during the six year mission into two objectives. The first was to acquire cloud free stereo coverage of 80% of the Earth's land surface between 82º N and 82º S, and the second was to produce, with commercial software, standard product DEMs at a rate of one per day.

SPOT images are widely used to produce geographic information. SPOT has always been popular with the photogrammetric community particularly for use in 3D topographic mapping. Al-Rousan (1998) has given a detailed review of published results on DEM generation and validation from earlier SPOT missions. SPOT data can be used to produce relatively high accuracy DEMs at large scales, for example, 1:50,000 (Sasowsky *et al.*, 1992; Bolstad and Stowe, 1994). SPOT 5, launched in May 2002, is the latest satellite of the SPOT family. This satellite ensures data continuity with the previous satellites, but also provides enhanced images (at 2.5 m resolution with its two HRG instruments), new stereoscopic capabilities with the HRS instrument, and images are taken in a short time difference which gives better accuracy for derived DEM. Much has been published about the SPOT 5 mission, discussing the image quality as well as DEM generation and validation procedures. Nonin and Piccard (2003) tested DEM accuracy of 10 stereopairs with the standard and super mode using different base to height (B/H) ratios ranging from 0.12 to 0.84 and time lags between

the two acquisitions. They used 81 ground control points (GCPs) and the RMSE of elevation 2.38 m using data from an airborne digital scanner with an accuracy of 0.8 m as reference data. For the DEM validation, the best result was obtained by a stereo pair with a smaller time lag (2 days) and a B/H ratio of 0.61; in this case (H: flying height above ground, B: the distance between the two exposures images), the RMSE was found to be 2.89 and 2.60 m in standard and super mode, respectively. Additionally, the authors noticed a strong correlation between the time lag and the quality of the DEM.

More recently, IKONOS became the first commercially owned satellite providing 1m resolution panchromatic image data and 4 m multispectral imagery. Applications range from national security and disaster assessment to urban planning and agricultural monitoring (Cheng *et al.*, 2008). DEMs can be created based on IKONOS stereo models available with high accuracy, which is in any case sufficient for the creation of orthoimages at the scale 1:10,000 (Jacobsen, 2002). Due to the high resolution of the IKONOS images and the possible geometric quality that can be achieved with few control points, IKONOS data can compete with aerial images, and the use of the different products is based only on cost. IKONOS stereo models are taken from the same orbit, which allows excellent image matching with sub-pixel accuracy (Büyüksalih *et al.*, 2004).

QuickBird is high resolution, multispectral commercial remote sensing satellite, offering imagery from 0.60 m resolution. Launched on 18 October, 2001, QuickBird collects multi-spectral and panchromatic imagery concurrently, and Pan-sharpened products in natural or infrared colours are offered. Strips up to 250 km long can be collected in a single pass. QuickBird provides the widest swathe, the largest on-board storage, and the highest resolution of any current commercial satellite (Masini and Lasaponara, 2007). QuickBird is designed to image large areas efficiently and accurately with industry-leading geolocational accuracy (Euroimage, 2002). QuickBird Imagery has quickly become a popular choice for large-scale mapping using high-resolution satellites. The satellite has panchromatic and multispectral sensors with resolutions of 0.61-0.72 m and 2.44-2.88 m, respectively. The sensor, therefore, has coverage of 16.5-19 km in the across-track direction. In addition, the along-track and across-track capabilities provide a good stereo geometry and a high revisit frequency of 1 to 3.5 days.

3.2.4 LiDAR (Light detection and Ranging)

Light Detection and Ranging is an active remote sensing sensor for the acquisition of high density and accurate elevation data (Lillesand, 2005). The laser scanner emits a light, which is reflected from the ground, and it records the time difference between the emission and the reflection. The return time for each pulse back to the sensor is processed to calculate the variable distances between the sensor and the various surfaces present on the ground. Combined with accurate information about the position and orientation of the aircraft or satellite during flight, the elevation of the scanned area can be determined. The use of LiDAR for the accurate determination of terrain elevations began in the late 1970s. Initial systems were profiling devices that obtained elevation data directly under the path of an aircraft. These initial laser terrain systems were complex and not necessarily suited for cost effective terrain data acquisition over large areas, so their utilization was limited. One of the more successful early applications of LiDAR was the determination of accurate water depths (Lillesand, 2005).

For the terrain mapping purpose, the LiDAR system consists of subsystems, including an inertial navigation system (INS), which monitors the pitch, roll, and altitude of the aircraft and thereby the directional orientation of the laser scanner, and a differential GPS receiving unit, which determines the location of the laser scanning system in three-dimensional space (Hodgson *et al.*, 2005, Barber and Shortrudge, 2004). Incorporating the technologies of INS and GPS into the LiDAR system results in the system being capable of determining the three-dimensional location of the sensor, the direction of the ranging laser, and the distance to a target (Barber and Shortrudge, 2004). With this information, target location in three-dimensional spaces can be determined at high accuracy.

The most important advantage of LiDAR over traditional methods is its very high vertical accuracy, which enables it to represent the Earth's surface with great accuracy (Ma, 2005). Density elevation data is another advantage of LiDAR that can be used for many topographic mapping applications. Water resource management and hydrological modelling require high quality DEMs (Garbrecht and Martz, 1999) because the accuracy of DEMs does affect the accuracy of hydrological predictions (Kenward *et al.*, 2000). Therefore, LiDAR data are applicable to water resource management and hydrological modelling. In addition, this

system offers the opportunity to collect terrain data about steep slopes and shadowed and inaccessible areas (Lillesand, 2005).

3.2.5 Synthetic Aperture Radar (SAR)

Synthetic Aperture Radar is an active microwave instrument, producing high-resolution imagery of the Earth's surface in all weathers condition. SAR data is imaged using a radar transmitting and receiving pulses perpendicular to its flight direction (side looking) at an angle of incidence on the ground (Small *et al.*, 1996). Each pixel in the radar image represents the radar backscatter (digital number) for that area on the ground: darker areas in the image represent low backscatter, brighter areas represent high backscatter. Bright features mean that a large fraction of the radar energy was reflected back to the radar, while dark features imply that very little energy was reflected. A large number of researchers around the world have investigated elevation modelling and the production of DEMs (Toutin and Gray, 2000). Discussions on different aspects of radar for radargrammetry and for cartography can be found in Leberl (1990) and Polidori (1997), respectively. There are four different types of methods to extract a DEM from SAR data, namely, clinometry, stereoscopy, interferometry (InSAR) and polarimetry (Toutin and Gray, 2000). In this research, the focus will be on InSAR. More details will be given in Section 3.3.

3.3 Synthetic Aperture Radar Interferometry (InSAR)

3.3.1 Historical review

Graham was the first to introduce synthetic aperture radar (SAR) for topographic mapping in 1974. He augmented a conventional airborne SAR system with an additional physical antenna displayed in the cross track plane from the conventional SAR antenna, forming an imaging interferometer. By mixing the signals from the two antennas, the Graham interferometer recorded amplitude variations that represented the beat pattern of the relative phase of the signals (Gens and Van, 1996). The first practical results of observations with a side looking airborne radar have been done by Zebker and Goldstein in 1986. They mounted two SAR antennas on an aircraft a distance of 11.1 m from each other. This distance between

the antennas was called the baseline. The signals transmitted from one antenna were received simultaneously by both antennas.

Li and Goldstein (1990) studied the effects caused by choosing different baseline separations to obtain topographic data. They used repeat pass data from the Cotonbal Basin in Death Valley which is a very arid area. Therefore, the imaged surface did not change during the observation. The spacing between fringes varies systematically with the baseline separation. Hagberg and Ulander (1993) investigated the altitude error caused by the radar system and by the topography, and simulated an interferometric measurement based on ERS-1 SAR parameters. They found that topography had a significant effect on the height error, which in many cases is more severe than baseline decorrelation.

Numerous papers have been published since the European Space Agency (ESA) launched the ERS-1 satellite with its C-band SAR in July 1991. Most of them deal with potential applications made to optimize the capabilities of future implementations. Most requirements for future InSAR missions concerning SAR interferometry have been based on the work carried out with ERS-1 data. Gens and Van Genderen (1996) reviewed the issues, techniques and applications of SAR interferometry. They described the geometric implementations, general processing techniques and an introduction to various phase unwrapping techniques. Also, the review focuses on parameters such as baseline, decorrelation and motion compensation which have a limiting influence on the quality of the data. After the launch of ERS-2 in 1995 and simultaneously operation in a tandem mission mode with a 24 hour time difference, the applications of spaceborne SAR interferometry were greatly expanded worldwide with availability of InSAR datasets.

Studies of Zebker *et al.* (1994) and Rufino *et al.* (1998) showed that the achievable accuracy for DEM generation is about 10 m and 5 m respectively in favourable situations. Herland (1997) generated DEMs of Finland from ERS tandem mission using 35 image pairs of ascending and descending pass with an elevation accuracy of about 10 m. Zebker *et al.* (1997) also stated that the atmospheric effect might deteriorate DEM accuracy as much as 100 m at an unfavourable baseline. Sansosti *et al.* (1999) showed how ascending and descending ERS-1/ERS-2 tandem data can be used to generate a precise digital elevation

model. The experiments showed that a DEM with a standard deviation of about 14 m can be obtained. The algorithm of ERS data used for generation a DEM in Taiwan by Rong and Hsu Chen (2001). The test results showed that a DEM using ERS data has an accuracy of about 23 m in urban area and about 5 m in bare areas without vegetation and buildings.

In recent years, studies have focused on evaluating the accuracy of DEMs from InSAR under different conditions. Rao *et al.* (2006) has studied applicability of repeat-pass SAR interferometry for generating DEMs over several Indian tests sits. Three test sites were selected for the analysis: one over Mumbai, which is a part with hilly terrain, lakes and forests; another is the Kolar area with gently undulating terrain with agricultural and forested lands; and the last was Bhuj, an arid plains region which is close to the Rajasthan desert. In the case of the Mumbai and Kolar study areas with two interferograms each, the atmospheric effects were almost negligible. In these cases, it is shown that it was also possible to estimate the height of buildings to an accuracy of 1–2 m. The method adopted for the accuracy assessment for InSAR derived DEMs consist of comparison with field measured differential (D) GPS elevations and comparison with SRTM (X-band) derived elevations.

3.3.2 Principles of the InSAR system

Interferometric synthetic aperture radar (InSAR) allows to the extraction of high resolution elevation based on the phase information derived from complex radar images (Zebker and Goldstein, 1986; Zebker *et al.*, 1994). There are several different approaches to collecting interferometric radar data. The simplest case is single pass interferometry. In this approach, two antennas are placed on a single aircraft or satellite platform. One antenna works as both a transmitter and receiver, while the second antenna works only as a receiver. In this case the baseline is the distance between the two antennas. An alternatively approach is repeat-pass interferometry. On this approach, an aircraft or satellite with only a single radar antenna makes two or more passes over the area of interest, the antenna working as both a transmitter and receiver on each pass. The baseline is then the distance between the two flight lines or orbital tracks. It is generally preferable to have the sensor pass as close as possible to its initial position, to keep this baseline small. For airborne repeat pass interferometry, the flight lines should generally be separated by no more than tens of metres, while for spaceborne

systems this distance can be as much as hundreds or thousands of meters. Another type of collection of interferometry data is differential interferometry. This approach works best for changes that affect spatially large areas opposed to changes that occur in a spatially disjointed manner, such as the growth of trees in a forest (Gens and Van Genderen, 1996).

The geometry of InSAR repeat passes is shown in Figure 3.1. Two radar antennas, which simultaneously view the same region from two positions *A1* and *A2* respectively, in single pass, or at different times by the same antenna (repeat pass). The distance between two antennas is referred to as the baseline, *B*. The range distance between *A1* and an illuminated point on the ground is ρ_1 while ρ_2 is the distance between *A2* and the same point. In this example, the radar wave is transmitted from antenna *A1* and *A2* after interaction with the terrain, the backscattered return is recorded. These signals are then processed to complex SAR images, and phases measured in each image are differenced on a pixel by pixel basis. The phase differences between the two returns signals in two passes are sensitive to viewing geometry, baseline orientation and the height of the illuminated point with respect to reference surface. For repeat pass interferometry SAR, as in the case with the satellite based tandem mission, since on each pass the antenna acts as both transmitter and receiver, the total path difference for each observation to an illuminated point on the ground is twice what would be expected in a single pass imaging geometry with two physical antennas. Therefore, the equations for repeat pass geometry are:

$$\emptyset_1 = \frac{4\pi}{\lambda}\rho_1 \tag{3.1}$$

$$\emptyset_2 = \frac{4\pi}{\lambda}\rho_2 \tag{3.2}$$

Where:

ρ_1, ρ_2 are the slant ranges from satellite positions *A1* and *A2* to the ground point P.

$\emptyset_1$, $\emptyset_2$ are the phases of the returned signals in two images.

λ is the radar wavelength.

The resulted interferometric phase is the phase difference $\emptyset_1 - \emptyset_2$ which can be calculated for each ground point using equation:

$$\emptyset_1 - \emptyset_2 = \frac{4\pi}{\lambda}(\rho_1 - \rho_2) = \frac{4\pi}{\lambda}\Delta\rho \qquad (3.3)$$

This leads to an ambiguity in determining the range, which must be solved by so-called 'phase unwrapping' techniques. Hence the phase information can be converted to an image, an interferogram, displaying variations in height, provided the viewing geometry is known to sufficient accuracy. The height (h) of the point *P* is given by the equation:

$$h = H - \rho\cos\theta \qquad (3.4)$$

Where *H* is the altitude of the radar antenna and ρ is the slant range distance from antenna to the target.

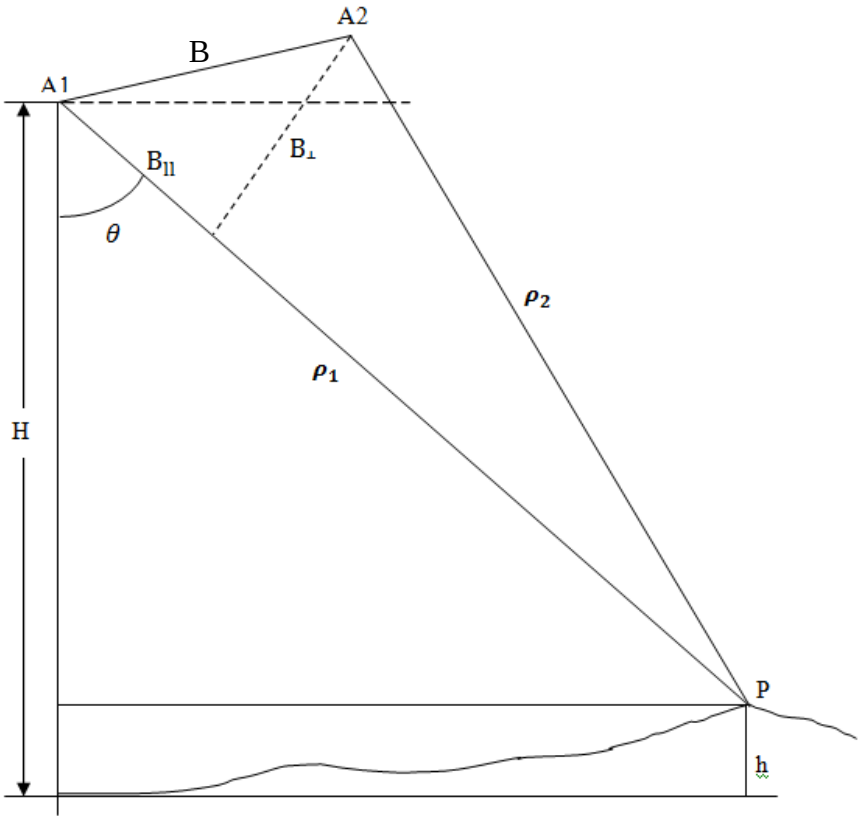

Figure 3.1: The geometry of repeat pass interferometry SAR, with ERS-1/2 tandem mission. Source: Li and Gold, (2005).

3.3.3 Factors affecting InSAR DEM accuracy

The accuracy of SAR data and their derived DEM is affected by many factors some of these factors shown in Table 3.1. Franceschetti and Lanari (1999) concluded that the main factors may affect the accuracy of InSAR DEM are misregistration decorrelation, spatial decorrelation, and temporal decorrelation. Misregistration error results in a decrease in the cross-correlation index amplitude which leads to increase the interferogram noise contribution and degradation of the DEM reconstruction accuracy. The length of the baseline is also considered a limiting factor for coherence. (Gen and Van Genderen, 1996). Orbital errors result in horizontal and vertical shift in an entire DEM as well as height distortions. These are more evident and significant with increasing swath width. The orbital errors of ERS satellites are in the order of tens of centimetres and introduce systematic elevation errors ranging from metres to tens of metres. The orbit errors are reduced by an optimisation approach to refine the baseline and orbital geometry using GCPs.

Phase noise originates at different stages of a DEM generation from acquisition to InSAR processing. Phase noise (Zebker et al, 1994; Huang et al, 1996) is mainly caused by radar thermal noise, quantisation noise, speckle noise, defocusing, baseline and temporal decorrelation, registration noise, unwrapping error, processing artefacts, resampling and interpolation noise. The high phase noise can lead to loss of some fringes completely in the interferogram. The geometric distortions in radar images depend on the characteristics of the sensor looking geometry and terrain type. The distortions in radar images result in forms of layover, shadow and foreshortening. Layover is caused by slopes steeper than the sensor incidence angle while shadow is caused by slopes less than sensor incidence angle. SAR images from ERS-1 and ERS-2 satellites contain almost no shadows due to 23 degree of incidence angle for earth observation (Eineder and Holzner, 2000), but they contain large amount of layover and foreshortening for mountainous region.

In repeat-pass interferometry, the position and orientation of objects on the surface may change substantially between passes, particularly if the passes are separated by an interval of days or weeks. This results in a situation known as temporal decorrelation, in which precise

phase matching between the two signals is degraded. For example, in a forested area, the individual leaf elements at the top of the canopy may change position due to wind action over the course of a single day. In more arid landscapes, where vegetation is sparse, temporal decorrelation will be less of a problem. Coherence can be considered as the correlation level between the images of the InSAR couple (Kervyn, 2001). The atmosphere is assumed to be one of the most limiting factors for the processing of InSAR data, particularly because of the effects of the troposphere and ionosphere (Gen and Genderen, 1996). Goldstein *et al.* (1988) pointed out that there are two types of errors can be occurred in the unwrapped processing step. Local error which results in a few points are corrupted by noise and global errors which the local error may be propagated through whole area.

Table 3.1: Factors influencing the accuracy of InSAR data. Source: (Gens and Van Genderen, 1996: 1809).

Major element	Factors
Satellite System	incidence angle spatial resolution internal clock drift approximate focusing image misregistration system noise
Orbit	determination of accuracy (precise range and range rate equipment) baseline (coherence, geometric decorrelation) repeat phase (temporal decorrelation) non-parallel orbits (range mis-registrations)
Signal	frequency polarization (backscattering behaviour) bandwidth (averaging) noise/speckle
Topography	phase difference (volume scattering) direction of slope (angle of phase gradient) surface characteristics (e.g. frozen soil)
Weather conditions	wind (backscattering behaviour) snow coverage (decorrelation)
Atmosphere	Repeat pass SAR interferometry is not independent of clouds.

3.4 DEM Generation from ASTER Stereo Images

3.4.1 Introduction

The Advanced Spaceborne Thermal Emission and Reflection Radiometer (ASTER) is a high spatial resolution, multispectral imager with along-track stereo capabilities, and was launched on the first NASA spacecraft of the Earth Observing System (Terra) in 1999 (Yamaguchi *et al.*, 1998). ASTER data is used to study a wide range of applications dealing with the surface of the Earth, including vegetation and ecosystem dynamics, hazard monitoring, geology and soils, land surface climatology, hydrology, and land cover change. To address the issues outlined above, ASTER provides observations in three spectral regions, as well as stereo observations, using three separate radiometers: the visible and near-infrared (VNIR) system has three spectral bands covering 0.52–0.86 μm at 15 m resolution; the short wavelength infrared (SWIR) subsystem has six spectral bands covering 1.60–2.45 μm at 30 m resolution; and the thermal infrared (TIR) subsystem has five spectral bands covering 8.125–11.65 μm at 90 m resolution (Abrams, 2000). The basic characteristics of these subsystems are given in table 3.2. The main objectives for the ASTER mission were to obtain free cloud high spatial resolution global, regional and local images of the Earth in fourteen spectral bands.

In addition, the stereo capability of ASTER can be used to generate a high-resolution DEM. Among the optical sensors, across-track stereoscopy has been widely used, for example, SPOT 1 to 4. The two images of a stereo pair are acquired by pointing the sensor at the same area, with different incidence angles, in different orbits. Along-track stereoscopic image acquisition requires two sensors with different inclinations, and acquisition images at the same time. SPOT-5, the most recent satellite of the SPOT programme. That is also the case in ASTER, which requires two sensors, both sensible in the range of 0.78-0.86μm, one pointing in the nadir direction and the other pointing backwards, with an offset angle of 26°. There is an approximately 55 second interval between the time the nadir sensor passes over a ground location and the time the after sensor records the same location on the ground track of the satellite (Al-Harbi and Tansey, 2008). Images generated from the nadir and after sensors yield a B/H ratio of 0.6, which is close to ideal for generating DEMs by automated techniques for a variety of terrain conditions (Hirano *et al.,* 2003).

Table 3.2: General characteristic of the three ASTER subsystems. Source: (Lang and Welch, 1999).

Characteristics	Band number	Spectral range (μm)	Spatial resolution (m)
VNIR	1	0.52 - 0.60	15
	2	0.63 - 0.69	
	3N	0.76 - 0.86	
	3B	0.76 - 0.86	
SWIR	4	1.600 - 1.700	30
	5	2.145 - 2.185	
	6	2.185 - 2.225	
	7	2.235 - 2.285	
	8	2.235 - 2.285	
	9	2.360 - 2.430	
TIR	10	8.125 - 8.475	90
	11	8.475 - 8.825	
	12	8.925 - 9.275	
	13	10.25 - 10.95	
	14	10.95 - 11.65	

3.4.2 Stereoscopy system

In modern photogrammetry, stereoscopy is the science that uses a pair of images to produce a 3D visual model, which then is applied with aerial and satellite photogrammetry to compute the terrain elevation from the measured parallaxes between the two images (Toutin, 2008). Stereoscopy can be collected either from same date along-track stereo pairs acquired from the same orbit, or from multi date across-track stereo pairs acquired from two different orbits (Toutin, 2008). The along-track stereo pairs acquisition gives a strong advantage in terms of

radiometric variations compared to across-track stereo because they are acquired every few seconds (rather than days) apart under uniform environmental and lighting conditions, resulting in stereo pairs of consistent quality that are well suited for DEM generation by automated stereocorrelation techniques (Toutin, 2008).

The ASTER stereo subsystem is, in fact, an implementation of the Stereosat-Mapsat concept to acquire global stereo coverage of the land using along-track digital sensors in order to produce global DEMs with the principles of photogrammetry (Toutin, 2008). The stereo image acquisition of ASTER is done using the VNIR subsystem. The VNIR subsystem consists of two independent sensors, namely, the backward and the nadir looking sensors. They are used for along-track stereo-imaging with a 27.7º intersection angle and a 0.6 base-to-height (B/H) ratio (Yamaguchi *et al.*, 1998). ASTER VNIR data at 15 m resolution is currently the best resolution multispectral satellite data available commercially with the exception of the 4 m resolution from Ikonos data. Comparison with the 10 m resolution from the SPOT panchromatic band shows that it has a much better resolution than the ASTER data while a comparison with the Panchromatic 15 m band from the Landsat7 ETM+ shows that the ASTER data are better both spectrally and spatially. The characteristics of the VNIR subsystem are shown in Table 3.3.

Table 3.3: Characteristics of the VNIR subsystem.

Parameter	**VNIR subsystem**
Sensors	Nadir and Backward
Spectral range	Green, Red, NIR for Nadir; NIR for Backward
Resolution	15 m
Along-track B/H ratio	0.6
Cross-track pointing	±24 (degree)
Coverage	60×60 km
Quantization	8 bits

The process for generating DEMs using the stereoscopy technique starts with registering two images of the same ground area taken from slightly different places in space. In the stereo pair, any positional differences parallel to the direction of satellite travel (parallax differences) are attributed to displacements caused by relief. Relative ground elevations are determined by measuring parallax differences in the registered images. The parallax differences were converted to absolute elevations using GCPs. The parallax differences are computed from stereocorrelation procedure.

The stereocorrelation procedure is statistical and is utilized to automatically derive a DEM from a stereopair of registered images (Welch *et al.*, 1998; Lang and Welch, 1999). Referring to Figure 3.2, the ASTER aft image (3B) can be registered to the nadir (3N) reference image by establishing transformation equations for conjugate image locations. The result of the transformation computation is a set of coefficients that define the relationship between both images of the stereo pair. After transformation coefficients have been calculated, the band 3B and the band 3N full-scene images must be matched to establish parallax difference ($\Delta\rho$) values (Lang and Welch, 1999). More details about digital image matching will be illustrated

in the following sections. The difference in pixel location (in the conjugate images) parallel to the direction of satellite motion is the $\Delta\rho$ value, and it is proportional to the terrain elevation relative to the vertical datum.

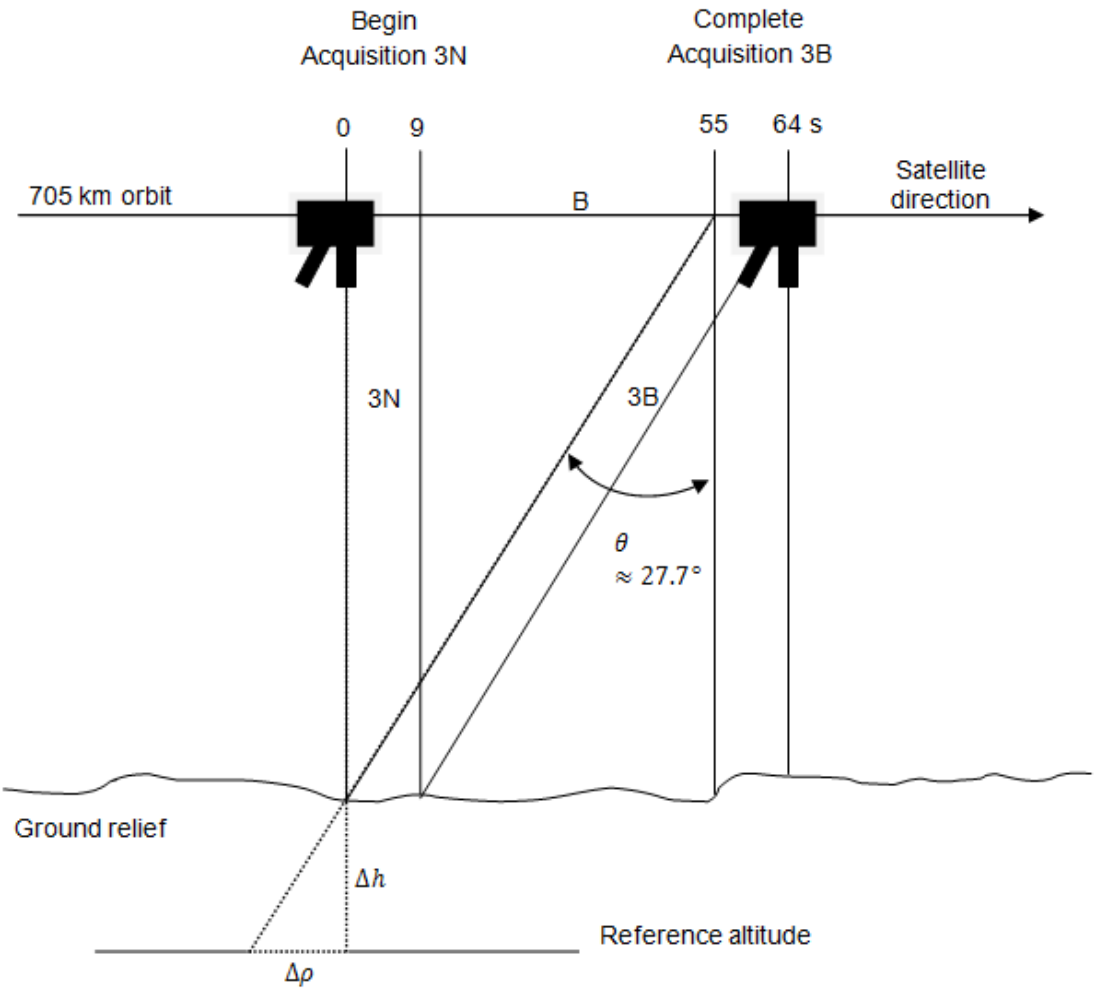

Figure 3.2: Geometry and timing of the nadir-band 3N and the after-band 3B for ASTER a long-track stereo. Source: Modified from Toutin (2008:1858).

3.4.3 Digital image matching

Image matching is a fundamental task used in digital photogrammetry to finds the conjugate points on both the left and right images which correspond to the same ground feature. Generally the quality of DEM generated from stereo pairs depends essentially on how accurate corresponding points are determined (Silveira *et al.*, 2008). Digital image matching techniques fall into three general categories: area-based, feature-based, and hybrid methods.

Area-based methods perform the image matching by a numerical comparison of digital numbers in small target window from each image. While, feature-based perform the image match by comparison based on feature characteristics such as size and shape. Hybrid methods involve some combination of the two approaches (Wolf and Dewitt, 2000). The simplest area-based digital image matching method is a technique known as cross correlation. The image matching technique illustration in this section will focus on the cross correlation approach, since this is the technique used by ENVI® software used in this study.

In cross correlation technique, a statistical comparison is computed from a digital number taken from same size subarrays in the left and right images. Since the exact position of the image in the right image is not initially known, a search window is selected with dimension much larger than those of the target window. A moving window approach is then used, comparing the candidate target window from left image with all possible window locations within the search window from the right image, as illustrated in Figure 3.3. At each moving window location in a search window, the correlation coefficient is computed. A correlation coefficient is computed by the following equation, using digital numbers from subarrays *A* and *B* (Wolf and Dewitt, 2000).

$$C = \frac{\sum_{i=1}^{m}\sum_{j=1}^{n}\left[(Aij-\overline{A})[(Bij-\overline{B})]\right]}{\sqrt{\left[\sum_{i=1}^{m}\sum_{j=1}^{n}(Aij-\overline{A})^2\right]\left[\sum_{i=1}^{m}\sum_{j=1}^{n}(Bij-\overline{B})^2\right]}} \qquad (3.5)$$

Where: *C* is the correlation coefficient;

m and *n* are the number of rows and columns, respectively, in moving window;

Aij is the digital number from moving window *A* at row i, column j;

$\overline{A}$ is the average of all digital numbers in moving windows *A*;

Bij is the digital number from moving window B at row i, column j;

$\overline{B}$ is the average of all digital numbers in moving windows *A*;

The correlation coefficient can range from -1 to +1, +1 indicates perfect correlation (an exact match), and -1 indicates negative correlation. Correlation coefficient values near zero indicate a non match. Due to factors such as image noise, perfect (+1) correlation is extremely rare.

Generally a threshold value, such as 0.7 is chosen and if the correlation coefficient exceeds that value, the moving windows assumed to match.

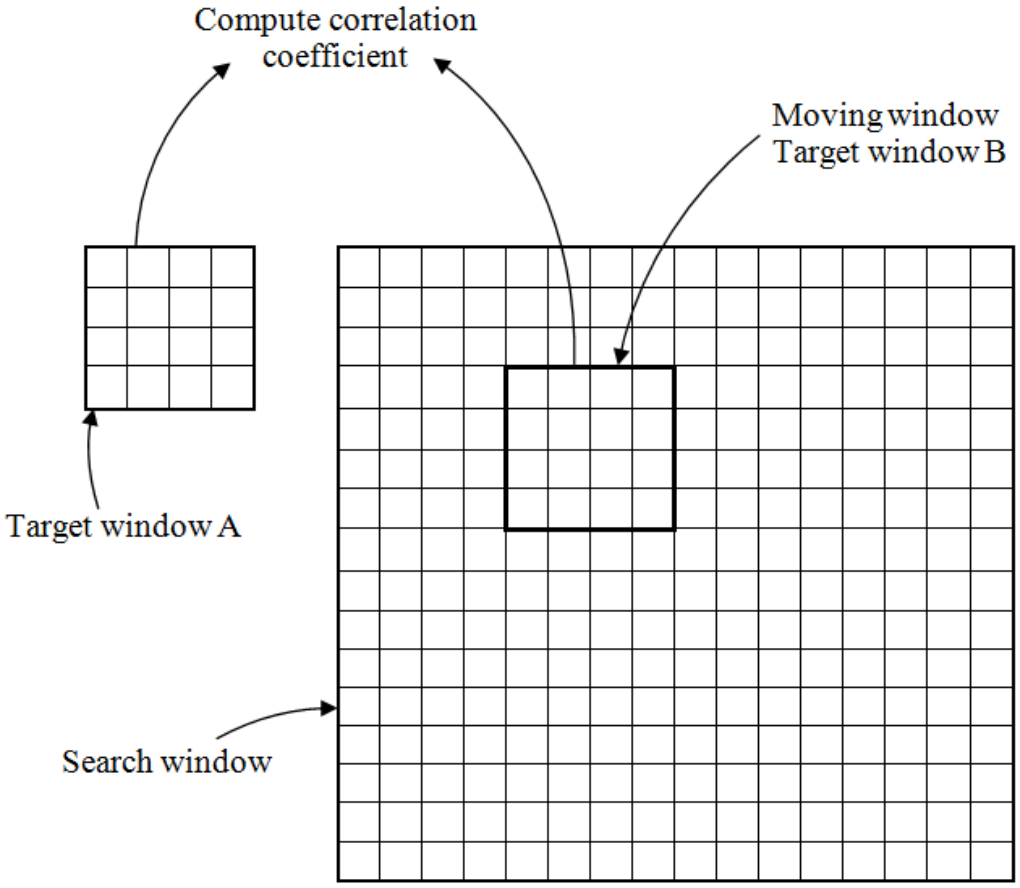

Figure 3.3: Computing correlation coefficient using a moving window within search window. Modified from Wolf and Dewitt (2000:337).

3.4.4 Accuracy of the DEM from ASTER data

DEM generation from ASTER stereo images is based on the principle of automatic stereo correlation techniques. The accuracy to which absolute elevation can be obtained using those photogrammetric techniques is governed by 1) the B/H ratio, 2) the reliability of the correlation procedure, and 3) the accuracy and density of ground control points. Height differences (Δh) or relative elevations of objects are closely approximated by the following equation as was seen in Figure 3.2:

$$\Delta h = \Delta\rho/\tan\theta \approx \Delta\rho/(B/H) \quad (3.6)$$

Where θ is the angle between the vertical axis from the nadir camera (3N) at observation station 1 and the intersecting ray from the aft pointing camera (3B) at observation 2. This angle yields a *B/H* ratio of 0.6 for ASTER stereo image. The difference in parallax ($\Delta\rho$) is computed from the stereocorrelation procedure as previously described. These relative height measurements can be transformed to absolute elevations tied to a vertical datum by employing an adequate number and distribution of GCPs.

Accuracy is the most important factor to be considered in the production of DEMs because if the accuracy of a DEM does not meet the requirements, then the whole project needs to be repeated and thus the economy and efficiency will ultimately be affected (Li *et al.,* 2005). An ASTER DEM can be generated either with or without GCPs. An absolute DEM is created with GCPs that is supplied with an absolute horizontal and vertical accuracy of up to 7 m with appropriate GCPs. However, a relative DEM can be generated without GCPs with horizontal and vertical accuracy of up to 10 m. Altmaier and Kany (2002) stated that DEM accuracy depends mainly on sensor model, image deformations, and resolution. Also, the availability of accurate GCPs will allow the production of absolute DEMs with accuracies depending on the number, quality and distribution of the GCPs as can be seen in Table 3.4.

Table 3.4: DEM accuracies as a function of GCPs. Source: Lang and Welch (1999).

Product Name	No. of GCPs (Minimum)	GCPs Accuracy ($RMSE_{xyz}$)	DEM Accuracy ($RMSE_{xyz}$)
Relative DEM	0	N/A	10-30 m
Absolute DEM	1	15-30 m	15-50 m
Absolute DEM	4	5-15 m	7-30

In the past few years, DEM generation from ASTER stereo data has become a target for studies due to its accuracy, availability and applicability for geoscience applications. Hirano *et al.,* (2003) validated and assessed ASTER DEM accuracy with considerations of the suitability of the ASTER DEM for various mapping applications. A comparison of the

ASTER DEM elevations against two types of independent check points collected from topographic maps produced an RMSE of elevation ±10.1, ±26.3 and ±15.8m using maps 1:24,000, 1:25,000 and 1:50,000 respectively. These results indicate that RMSE elevation values can be within expectation when adequate ground control is used. San and Suzen (2005) checked the best effort of 15m spatial resolution DEM generation from ASTER L1A data by collecting different numbers of ground control points (30, 45, and 60) and tie points. These results showed that the accuracy of the DEM increases when the number of GCPs is increased.

Cuartero *et al.* (2005) studied the accuracy and reliability of DEMs generated from two different satellite sources, namely, ASTER and SPOT stereoscopic images, using three different photogrammetric software products. A set of 91 DEMs were generated from SPOT data and 55 DEMs from ASTER data. Error control was performed with 315 check points determined by differential global positioning systems. The results of ASTER DEMs show that the elevation root mean square error (RMSE) equals 13.0 m. The corresponding RMSE value for SPOT DEM is 7.3 m. In both cases, the error is less than the pixel size. It is satisfactory for many cartographic and analytical applications comparable to that of conventional topographical maps which could be used for updating maps from large scale 1:25000 to medium scale 1:50000.

Another study assessing the accuracy of generating DEMs from ASTER data was conducted by Eceret *et al.,* (2005). In this study, the accuracy was tested by comparing the DEMs to three reference models: a highly accurate surface model generated with airborne InSAR data, the DHM25 (an elevation model based on the digitized contour lines of national 1:25,000 topographical maps), and an interferometric DSM (Digital Surface Model) calculated from ERS SAR data. The results show that the DEMs were very accurate in nearly flat regions and on smooth slopes, errors were generally within ±10 m in those cases. It was noticed that larger errors (approximately reaching a few hundred meters) appear in forested, snow covered or shady areas and at steep cliffs and deep valleys.

Comparison between ASTER and SRTM (90 m data) derived DEMs was made for a qualitative assessment of the horizontal and vertical component of the error, while statistical measures were used to estimate their vertical accuracy. The elevation difference between SRTM and ASTER products was evaluated using the root mean square error (RMSE), which was found to be less than 5 m (Nikolakopoulos *et al.*, 2006). Toutin (2008) has reviewed the basic characteristics of stereoscopy and its application to the ASTER system for DEM generation, which concentrates on the methods, algorithms and commercial software to extract an absolute or relative elevation and an assessment of their performance using the results from various research and commercial organizations.

3.4.5 Factors affecting ASTER DEM accuracy

It can be concluded that the quality of the ASTER DEM data can be affected by a number of factors, including the cloud cover present in the data, terrain variation across the scene, and spectral contrast across the kernel used during correlation calculation (Stevens *et al.*, 2004). Furthermore, the number, accuracy and distribution of the GCPs are important factors that affect DEM accuracy (Abrams, 2000). Areas covered by cloud will be obscured in the visible and near-infrared wavelengths, leading to gaps in the data. Also, DEM accuracy decreases consistently as slopes increase with larger errors in the steeper slopes. Spectral contrast is an issue because in relatively homogeneous regions of spectral reflectance, there are few or no features to match from one scene to the other, as is demonstrated by the correlation distributions for land cover types over the ASTER images. Areas in relief, shadow or with excessively high and low albedo like snow, salt lakes and some types of forest may also become problematic during the stereo matching process. The correlation in this case is a measure of how well the offsets are determined in the ASTER stereo pair. Lower relief areas with a reasonable amount of spatial heterogeneity between neighbouring pixels should yield the highest correlation (Kervyn *et al.*, 2008)

3.5 Comparison of DEM Extraction Methods

Various aspects should be taken into account when choosing a DEM generation method, such as the purpose or application for which the DEM will be used and the level of accuracy required for this application, the availability of source materials, the efficiency and the cost

(see Table 3.5). In terms of accuracy, the most accurate measurements are generally collected by ground survey and photogrammetry. A millimetre level can be reached using ground survey and a centimetre level using photogrammetry, while a metre level can be achieved using digitization from maps (Li *et al.*, 2005). The accuracy of photogrammetry is based on the resolution of the images used. The accuracy could be very high in the case of air photogrammetry images and varied in the case of space photogrammetry depending on the resolution. For example, if SPOT images with 10 m resolution are used, then the accuracy will be from 5 m to 10 m, while IKONOS with a 4 m resolution gives an accuracy range of between 1 and 2 m. Ground survey and photogrammetry tend to be more labour intensive, slower, and more costly than InSAR and Lidar. InSAR offers all weather capability, more rapid collection, and lower cost per unit area. Lidar surveys require clear flying weather and are flown at lower altitudes than InSAR. GPS data collection is quite fast but sometimes is not possible to use in some difficult topography area for example high mountains.

In terms of availability, in all developed and most developing countries, contours maps are available. Such maps are the major source for digital elevation modelling. In many countries, the national DEMs have been generated from existing contour maps. The accuracy of DEMs generated using this method is based on the scale of the maps. In terms of efficiency, ground surveying is more labour intensive and therefore is suitable only for modelling a small area when high accuracy is required Li *et al.* (2005). Therefore, data acquisition is more efficient. Indeed, the photogrammetric technique is suitable for medium and large-sized areas. For cartographic digitization, the raster scanning process can easily be automated, but the raster and vector conversions need to be performed by human workers. The cost associated with the various methods of generating DEMs, refers to how labour intensive they are and the equipment used in the processes. Cost is one of the most important factors when deciding on which method to use (see Table 3.5). In general, ground surveying is most suitable for applications that cover small areas, such as engineering and mining applications. Photogrammetric methods using airborne or satellite images are suitable for modelling covering large geographic areas. However, as a vast amount of terrain data already exist in topographic maps, many national mapping agencies tend to acquire DEMs by digitizing existing maps. DEMs obtained in this way are usually of a small scale and have a national or regional coverage.

Table 3.5: Comparison of the accuracy of DEM data obtained by different techniques. Source: Li *et al.* (2005:62).

Methods of data acquisition	**Accuracy of data**	**Speed of data acquisition**	**Cost of data acquisition**	**Applications Domain**
Traditional surveying	High (cm-m)	Very slow	Very high	Small areas
GPS survey	Relatively high (cm-m)	Slow	Relatively high	Small areas
Photogrammetry	Medium to high (cm-m)	Fast	Relatively low	Medium to large areas
Space photogrammetry	Low to medium	Very fast	Low	Large areas
SAR interferometry	Low (m)	Very fast	Low	Large areas
Radargrammetry	Very low (10 m)	Very fast	Low	Large areas
LIDAR	High (cm)	Fast	High	Medium to large areas
Map Digitization	Relatively low (m)	Slow	High	Any sized area
Map scanning	Relatively low (m)	Fast	Low	Any sized area

3.6 Summary

This chapter reviews the elevation mapping technologies and includes details on spaceborne radar interferometry and digital photogrammetry. Whilst there have been a number of studies evaluating the accuracy of DEMs (Sasowsky *et al.,* 1992; Zebker *et al.,* 1994; Welch *et al.,* 1998; Hirano *et al.,* 2003; Noguchi *et al.,* 2004; Büyüksalih *et al.,* 2005; Eckert *et al.,* 2005; San and Züzen, 2005; Rao *et al.,* 2006; Ludwig and Schneider, 2006; Gorokhovich and Voustianiouk, 2006; Weydahl *et al.,* 2007) and also making comparisons of DEMs (Gelautz *et al.,* 2003; Hodgsona *et al.,* 2003; Cuartero *et al.,* 2005; Saraf *et al.,* 2005; Nikolakopoulos *et al.,* 2006; Kervyn *et al.,* 2008), this study has evaluated DEMs from two different acquisition technologies using data captured at approximately the same scale and also with

topographic data from contour maps. These issues are explicitly addressed and the implications for hydrological parameter retrieval are further presented. The next chapter will describe the materials and methods that are used in this study.

Chapter 4: Materials and Methods

4.1 Introduction

A methodology is a standard framework describing the way in which a certain analysis is carried out. The methodology in this study was completed in four steps, including data preparation, extraction digital elevation model from different sources, accuracy assessment and comparison of the results. This chapter presents the methodology used to achieve the main aim of this study, as stated in Chapter 1, including a description of the data used and their preparation and the software used.

4.2 The Study Area

The study area is located in the central of Jordan and lies between 36º to 37º E and 30º to 31º N (Figure 4.1). The Al-Jafer Basin is a closed depression, with a catchment area of 12,200 km², most of which is classified as an arid desert. It is a flat area bordering the highlands in the west and in some areas there is medium relief. Ground elevation ranges from about 850 m.a.m.s.l. in the Jafer Basin to about 1,750 m.a.m.s.l. in the western highlands. The minimum slope is 0º and the maximum slope is reach to 26º. The centre of the basin contains a large qa`, or dry playa, that covers an area of ~240 km2. The landscape surrounding the qa` consists mainly of Quaternary sheetwash deposits blanketed by a desert pavement, or hamada, of chert clasts. The mean annual rainfall over the basin ranges from the highs of about 200 mm/year in the western highlands to less than 25 mm/year in its eastern parts, averaging over the whole basin to about 40 mm/year. Climate in the AL-Jafer Basin varies widely between day and night, and between summer and winter. Daytime summer temperatures can exceed 40°C, while winter nights can be very cold, dry and windy. The potential evaporation ranges from 3,300 mm/year in the western parts of the catchment to 4,000 mm/year in the centre of the depression. The average discharge is approximately 0.10 MCM/year. Perennial vegetation is sparse, and mostly limited to within intermittent streambeds. Agriculture has been developed along the foothills of the mountains in the west by

extracting groundwater. Al-Jafr Basin is crossed by a number of broad, sparsely-vegetated wadis. South of al-Jafer and east of the Rum Desert, Al-Mudawwara Desert is characterized by isolated hills and low rocky mountains separated by broad, sandy wadis. The main sub-catchments of Jafer Basin are wadi Jurdaneh, wadi Wheida, wadi Huseinan, wadi Shidiya and wadi Ghubeya. The mean annual rainfall over the basin ranges from the highs of about 200 mm/year in the western highlands to less than 25 mm/year in its eastern parts, averaging over the whole basin to about 40 mm/year. The catchment area is very sparsely populated, with Ma'an and Shoubak as major urban centers. About 90% of Jordan is in the arid to semi arid region that faces water scarcity (Al- Zubi and Al-Kharabsheh, 2004). The study region is selected for hydrological modeling because there is no vegetation that may affect the result of DEM generation particulary for InSAR data. The shortage of water is associated with growing demand on water due to population growth, industrial development, urbanization and the improving of standard of living in addition to limited surface water resources. The use of water in Jordan is divided into three categories included 75% in agriculture, 22% in domestic and 3% in industry.

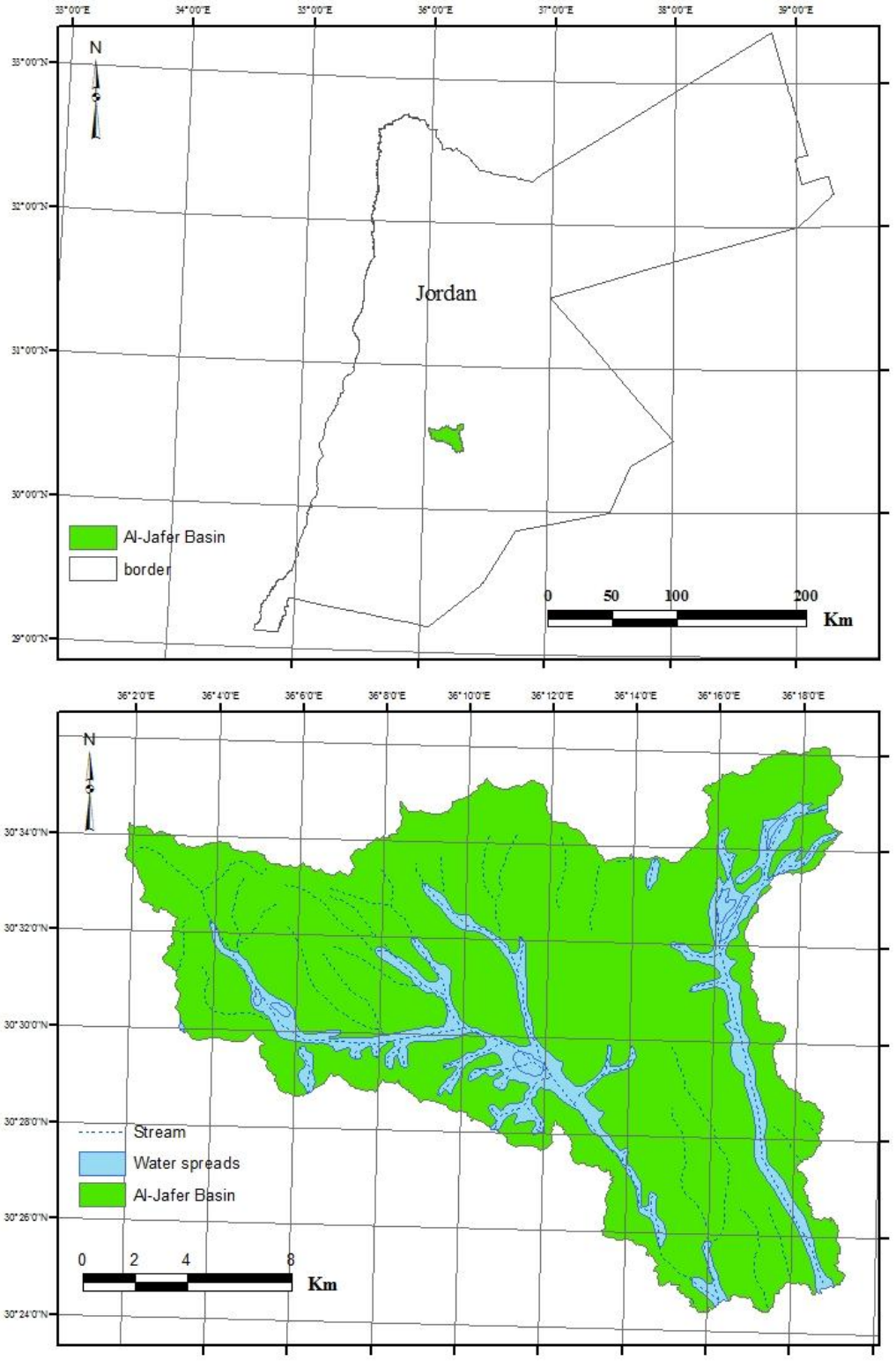

Figure 4.1: The location of Al-Jafer basin in central of Jordan.

4.3 Description of Data

4.3.1 InSAR data

The tandem operation of European remote sensing ERS-1 and ERS-2 satellites is the first SAR interferometric space mission which aimed to collect data at global scale and with a short temporal baseline. In the tandem operation, the two satellites are flying in the same orbital at the same altitude and the orbit phasing is adjusted to make ERS-2's ground track be simultaneously with that of ERS-1 24 hour earlier. Thus, any point on the ground can be revisited after one day and re-observed. The technical specification of the ERS-1/2 SAR instrument is shown in Table 4.1. The availability of tandem data certainly gives a great interest for global topographic mapping. The images used in this study include the tandem mission data (ERS1/2) acquired from European Space Agency (ESA) on May 1, 2 1996 (Figure 4.2). Each image covered 100x100 km² with a spatial resolution of 24m.

Table 4.1: Technical specification of the ERS-1/2 SAR instrument. Source: Franceschetti and Lanari (1999).

Incidence angle – near range	20.1º
Incidence angle – mid range	23º
Incidence angle – far range	25.9º
Frequency	5.3 GHz (C-band)
Bandwidth	15.55 ± 0.1 MHz
Swath width	102.5km (telemetered) 80.4km (full performance)
Swath stand – off	244.5km to the right of the orbital track
Polarisation	Linear Vertical
Antennae size	10m long, 1m wide
Spatial resolution – azimuth range	≤ 30 m ≤ 26.3 m
Temporal resolution (during this phase)	One day
Radiometric resolution	2.5 dB at sigma-nought = -18 dB

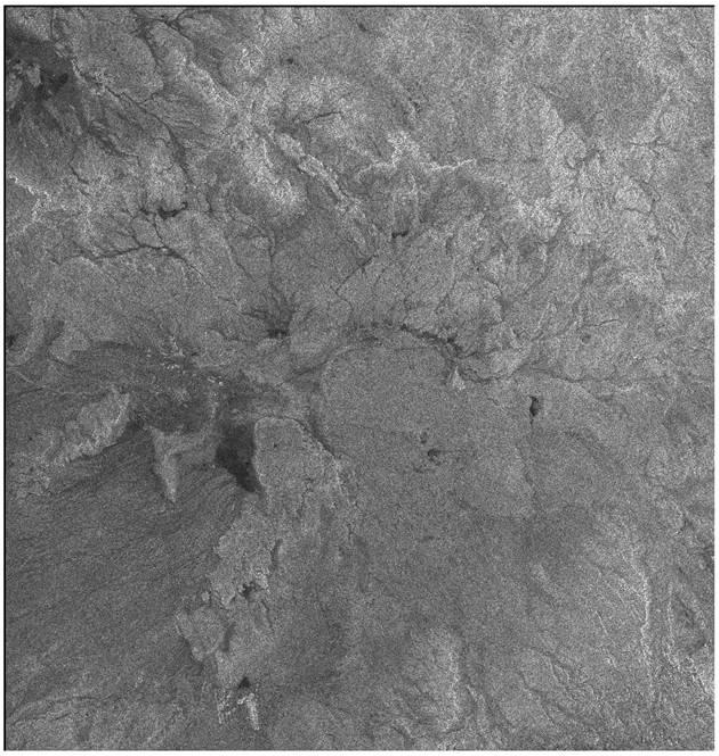

(a)

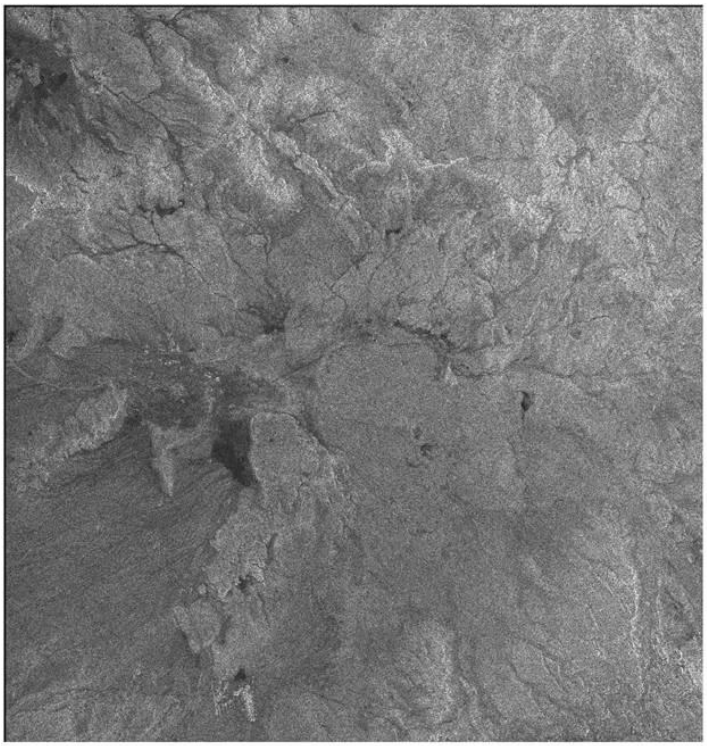

(b)

Figure 4.2: (a) ERS-1 intensity image in slant range (100X100 km) relative to the 1 May 1996 acquisition and (b) ERS-2 image relative the 2 May 1996 acquisition.

4.3.2 ASTER data

The ASTER stereo images used in this study were acquired on 19 June 2001, over the region of Al-Jafer, Jordan. The ASTER stereo images consist of two scenes, backward and nadir directions with a time difference of 55 seconds. Both scenes were in level 1A raw data format. Figure 4.3 shows the ASTER image. The Terra platform is on a sun-synchronous near-polar quasi-circular orbit with a mean attitude of around 705 km, an orbital inclination of 98.2±0.15u at the equator, an equatorial crossing time at 10: 30±15 min, and an orbit period of 98.9 min with a repeat cycle of 16 days, resulting in 233 revolutions in 16 days with a distance between adjacent orbits of 172 km at the equator. With its 8 min/orbit duty cycle, ASTER can acquire a maximum of around 770 stereo pairs per day, and will thus be capable of acquiring the 45 000 cloud free digital stereo pairs required to cover the land surface of the Earth below 82º N and 82º S during the 6 year mission (Lang and Welch 1999).

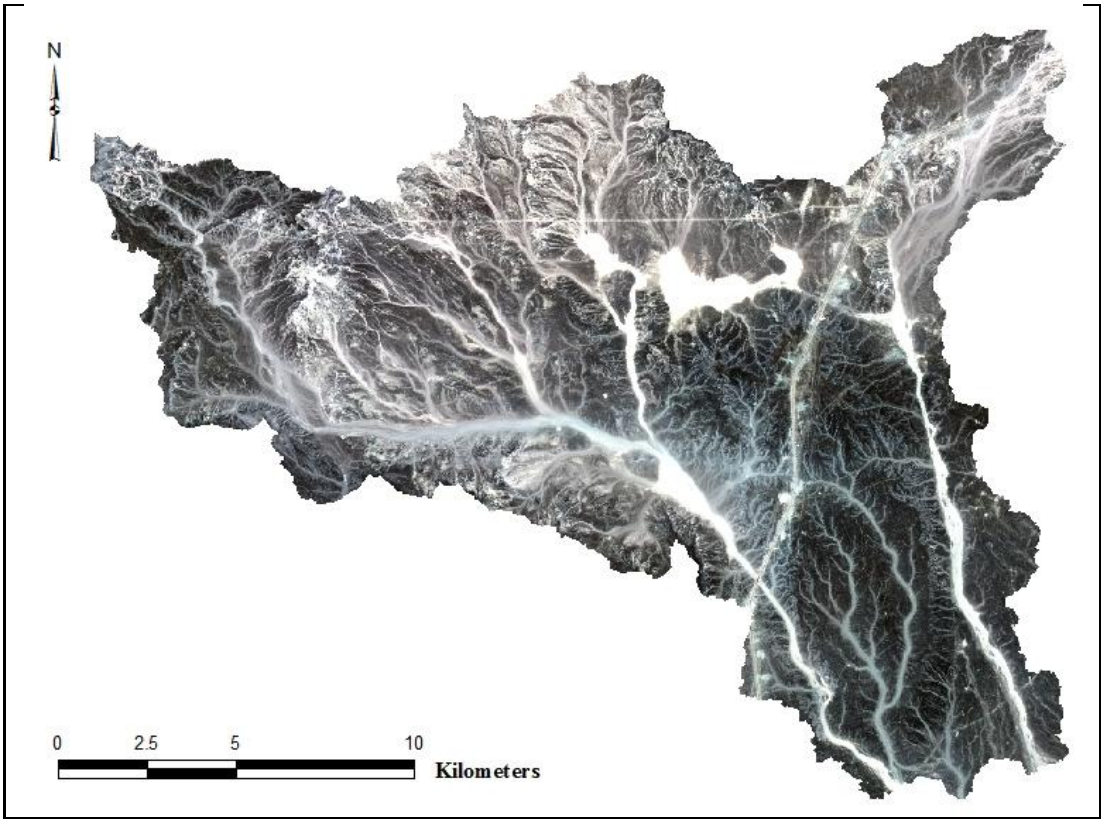

Figure 4.3: ASTER image which covers Al-Jafer basin.

4.3.3 Topographic map data

The topographic maps of the study area used in this study were published in 1997 by Royal Jordan Geographic Centre, the national mapping agency. The maps were at a scale of 1:50,000 with a contour interval of 20m. These maps were scanned and georeferenced to be available for this study. Figure 4.4 shows a topographical map extract over the study area.

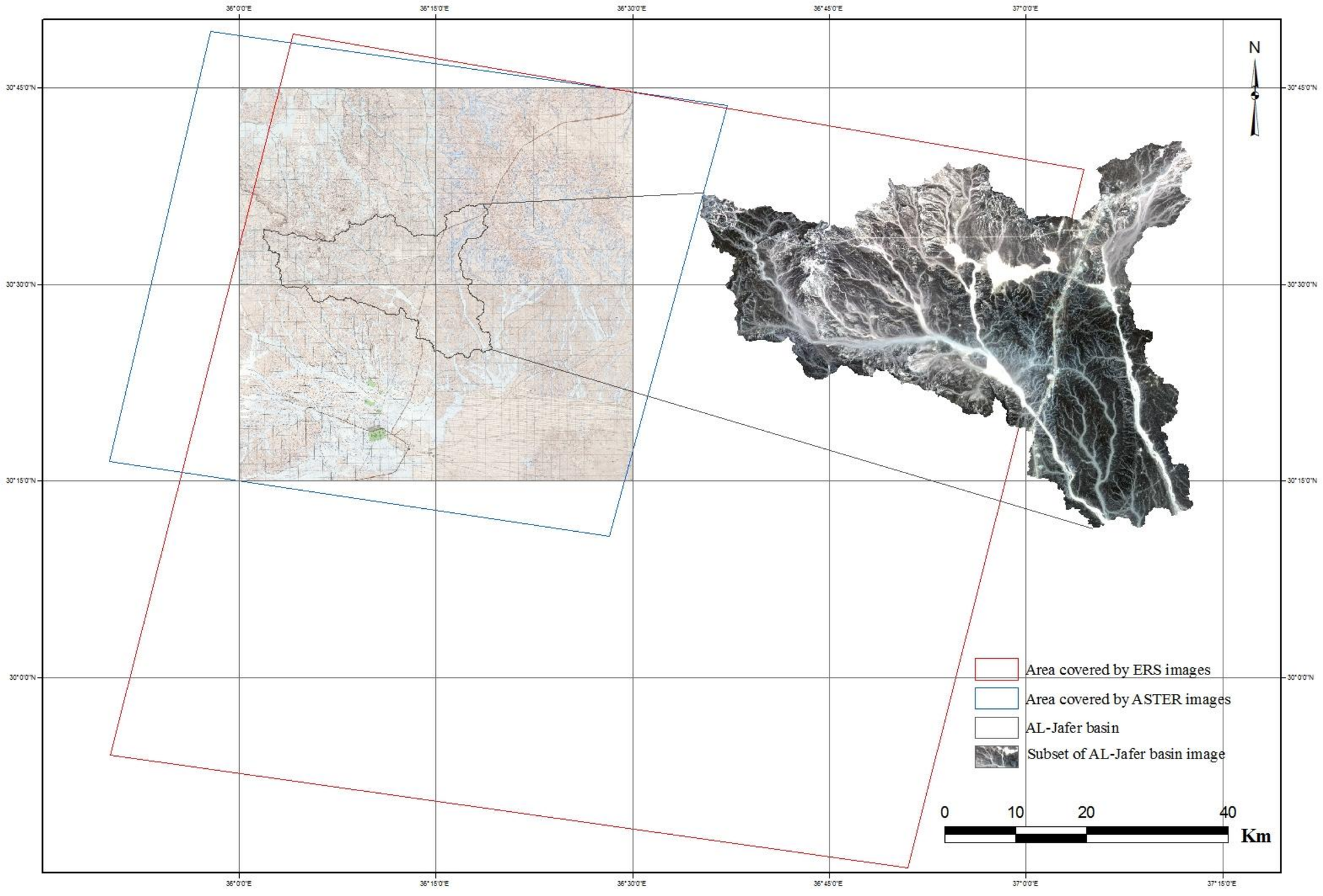

Figure 4.4: Maps and images (ERS 1-2 and ASTER) covered study area.

4.4 GPS observations

4.4.1 Introduction

Global positioning system (GPS) consists of 24 satellites orbiting the globe at an altitude of approximately 20 km to give an accurate location on the ground. Four satellites together form an elliptical orbit that has an angle with the horizon equal to 55º degrees. Therefore, there are six orbital planes spaced equally from each other around the earth. GPS can accurately determine the speed and direction, time and location coordinates around the clock, in all weather conditions and at any place on the globe (Leica, 2006). This system was developed by the US Department of Defence in 1970s. It was designed originally for military use at any time and any place on the Earth's surface. Shortly after, it became clear that civilians could also use it, and now it has a dual system that can be used by the military and civilians. The first two main civilian applications were navigation and marine surveying (El-Rabbany, 2002).

If the distance from a point on the earth (GPS receiver) to the location of three satellites is known, the location of this point can be determined simply by applying the concept of the resection. Each GPS satellite constantly transmits a microwave radio signal consisting of two carriers: the location of the satellite and the signal time travel to GPS receivers. When a GPS receiver is switched on, it will pick up the GPS satellite signal through the receiver's antenna and process it to determine the distance from receiver to satellite (El-Rabbany, 2002). The process of identifying a location using GPS can be concluded in several steps: Figure 4.5 shows the location of the receiver (A), which is located at a distance of D1 miles from satellite 1. Therefore, it can be said that the receiver is located on the circle that has at its centre the satellite, and that has a radius D1. Also, Figure 4.5 shows that the receiver (A) is located at a distance D2 from satellite 2 and at a distance D3 from satellite 3. Therefore, it can be said that the location of the receiver is intersection points between the satellites' circles.

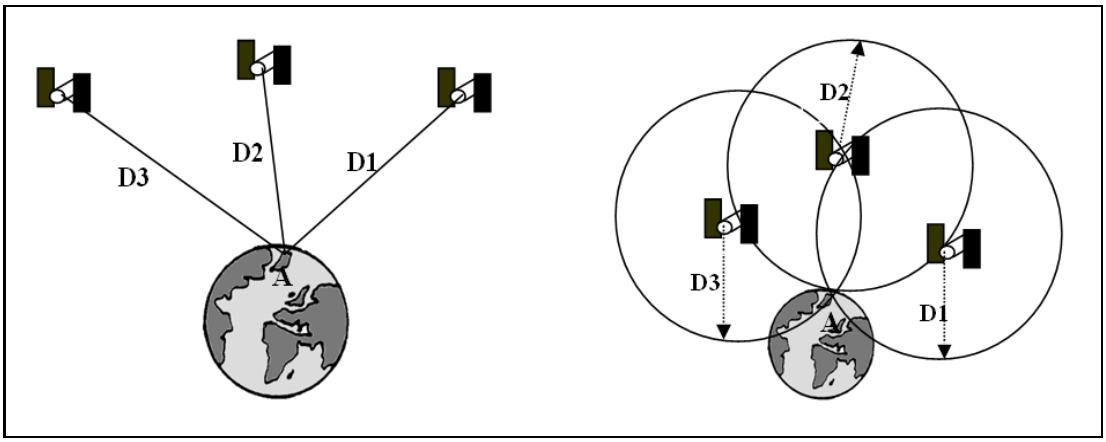

Figure 4.5: Basic idea of positioning. Source: Al-Rabbany (2002).

4.4.2 GPS positioning techniques

Static surveying was the first method to be developed for GPS surveying. It is a relative positioning technique that employs two or more stationary receivers simultaneously tracking the same satellites. One receiver is placed on a point, the Reference receiver, whose coordinates are accurately known. The other receiver is placed on the other end of the baseline and is known as the Rover. The Reference receiver can support any number of Rover receivers, as long as a minimum of four common satellites is visible at both the Reference and Rover sites (El-Rabbany, 2002). Data are then recorded at both stations simultaneously. The observation time varies from 20 minutes to a few hours based on the distance between the reference base and the rover receivers, the number of satellites observed and the satellite geometry (Leica, 2006).

The kinematic technique is typically used for detailed surveying, and for recording trajectories. The technique involves a moving Rover, whose position can be calculated relative to the Reference. It employs two or more stationary receivers simultaneously tracking the same satellites. One receiver is placed on a point, the Reference receiver, whose coordinates are accurately known. The other receiver is placed on the other end of the baseline and is known as the Rover. The Reference and Rover are switched on and remain absolutely stationary for 5-20 minutes, collecting data. The actual time

depends on the baseline length from the Reference and the number of satellites observed. After this period, the Rover may then move freely. The user can record positions at a predefined recording rate, can record distinct positions, or record a combination of the two (Leica, 2006).

Real time kinematic (RTK) is a kinematic on the fly survey carried out in real time (Leica, 2006). The Reference station has a radio link attached and this rebroadcasts the data it receives from the satellites. The Rover also has a radio link and receives the signal that is broadcasted from the Reference. The Rover also receives satellite data directly from the satellites using its own GPS antenna. These two sets of data can be processed together at the Rover to resolve the ambiguity and therefore obtain a very accurate position relative to the Reference receiver. This is similar to the initialization performed in a post-processed kinematic survey, the main difference being that it is carried out in real-time. RTK is quickly becoming the most common method of carrying out high precision, high accuracy GPS surveys in small areas and can be used for similar applications as a conventional total station.

Differential Phase GPS is used mainly in surveying and related industries to achieve relative positioning accuracies of typically 0.5-5 cm. The technique used differs from previously described techniques and involves a lot of statistical analysis. It is a differential technique, which means that a minimum of two GPS receivers are always used simultaneously. As before, the Reference receiver is always positioned at a point with fixed or known coordinates. The other receiver(s) are free to rove around. Thus they are known as Rover receivers. The baselines between the Reference and Rover receivers are calculated. DGPS survey was the method used in this study.

4.4.3 Field survey

A field survey was conducted in September 2007 for the purpose of ground truth point's acquisition. Differential GPS measurements were provided by two Leica SR20 GPS receivers. The SR20 GPS receiver can be used as a high accuracy land surveying device, a powerful GIS data collector, or even a Reference Station. Leica Geo Office® software was used to post-process the data. In this measurement, ground truth points

were divided into two set of points, the first used as ground control points to calibrate DEMs generation during processing steps and the second set of points is independent check points for accuracy assessment of DEM after finished processing steps. These points spread among study area and the most of points collected from the roads. Selecting the ground control points is the first step in fieldwork and establishes the approximate location and number of points that should be selected. A hardcopy of the ASTER images was used to achieve this purpose. This gave a view of interesting points that could be suitable as ground control points. In addition, roads could be viewed using these images to access those points easily. It was decided to use a kinematic technique to collect ground control points. This technique allows many points to be observed along different types of roads over the study area. Each of these points could be used as a ground control point.

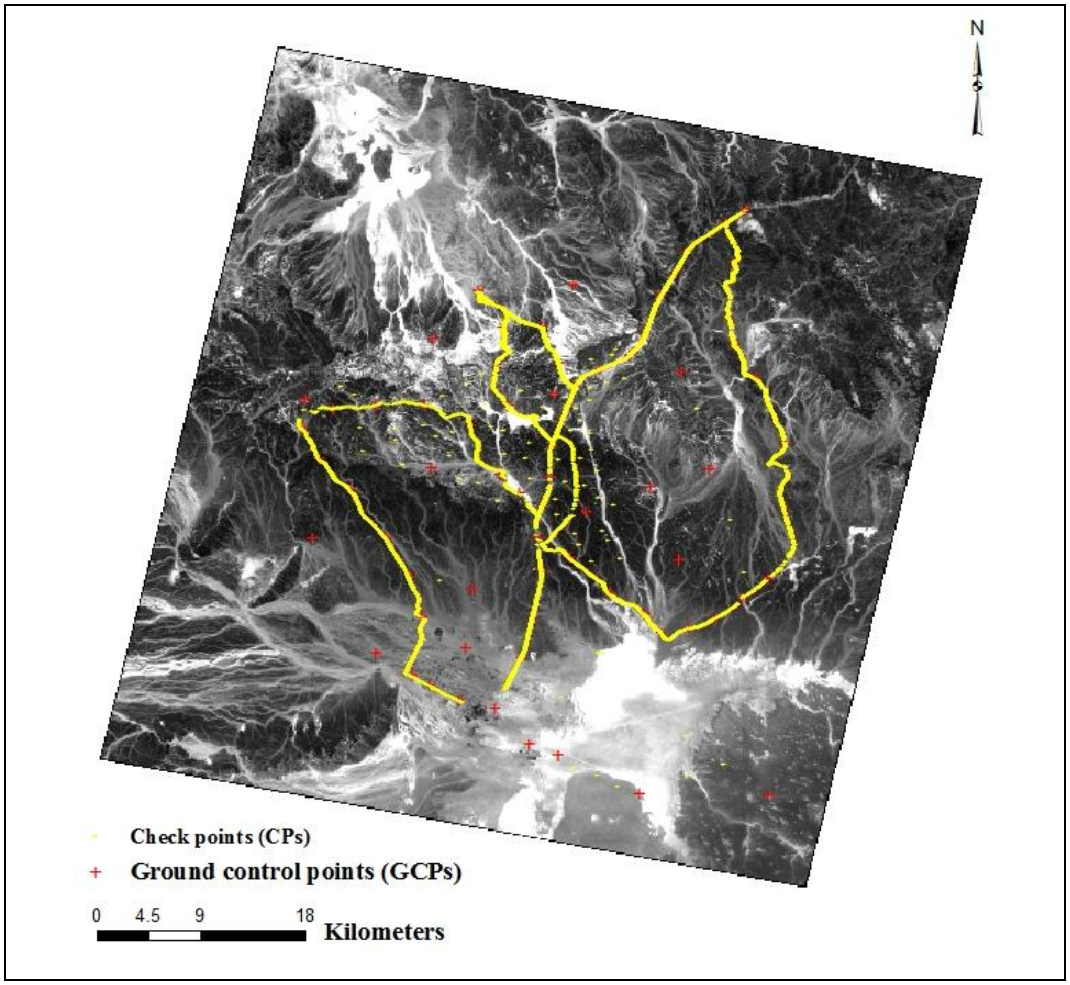

Figure 4.6: Distribution of the GCPs and CPs through the ASTER image.

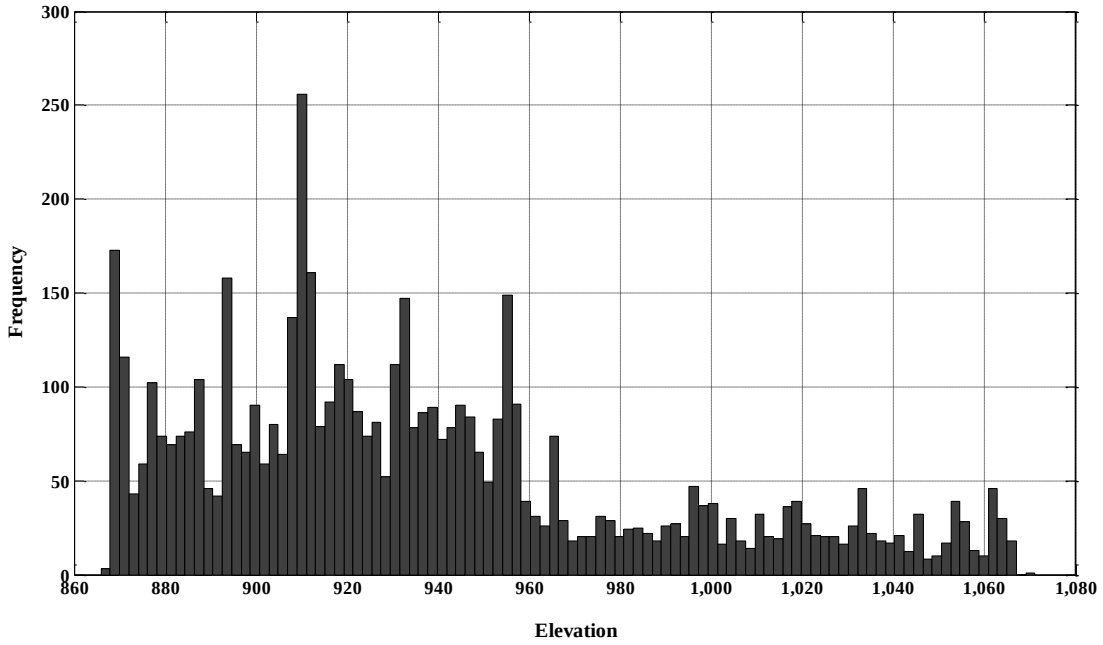

Figure 4.7: DGPS data elevation range.

4.4.4 GPS processing and adjustment

The post-processing software is used to process the observations taken by the receiver in order to compute baselines and coordinates. After that, data need to transfer from the GPS to a PC to running the GPS post-processing software. The software computes a baseline using simultaneous measurement data from two or more GPS receivers. The baselines represent a three-dimensional line drawn between the two points occupied by each pair of GPS antennas. The post-processed measurements allow more precise positioning, because most GPS errors affect each receiver nearly equally, and therefore can be cancelled out in the calculations.

4.5 DEM Generation from InSAR Data

InSAR is a technique in which two SAR images of the same area of the earth taken from slightly different satellite positions are used to generate an interferogram, which represents the phase difference between the return signals in the two images. The phase difference results from the topography and the changes in the line of sight distance (range) due to displacement of the surface or change in the propagation path

length. InSAR systems provide images that represent the topographic surface in all weather conditions, in daylight or at night (Rosen *et al.*, 2000). The generation of DEMs from InSAR data, particularly ERS-1/2, is not straightforward; it includes several steps. Figure 4.8 shows the overview of the processing steps in the generation of DEMs from the InSAR technique. First, InSAR pair images are selected and the SAR signal data are processed to produce the single look complex (SLC) step. Then, the InSAR images must registered into a common geometry before interferogram generation. After that, calculation of the baseline between two defined orbits is required, followed by interferogram generation, which includes flattening and filtering. Phase unwrapping is the next step after interferogram generation. Height model generation and geocoding are the final step. The following sections will explain these steps in more detail.

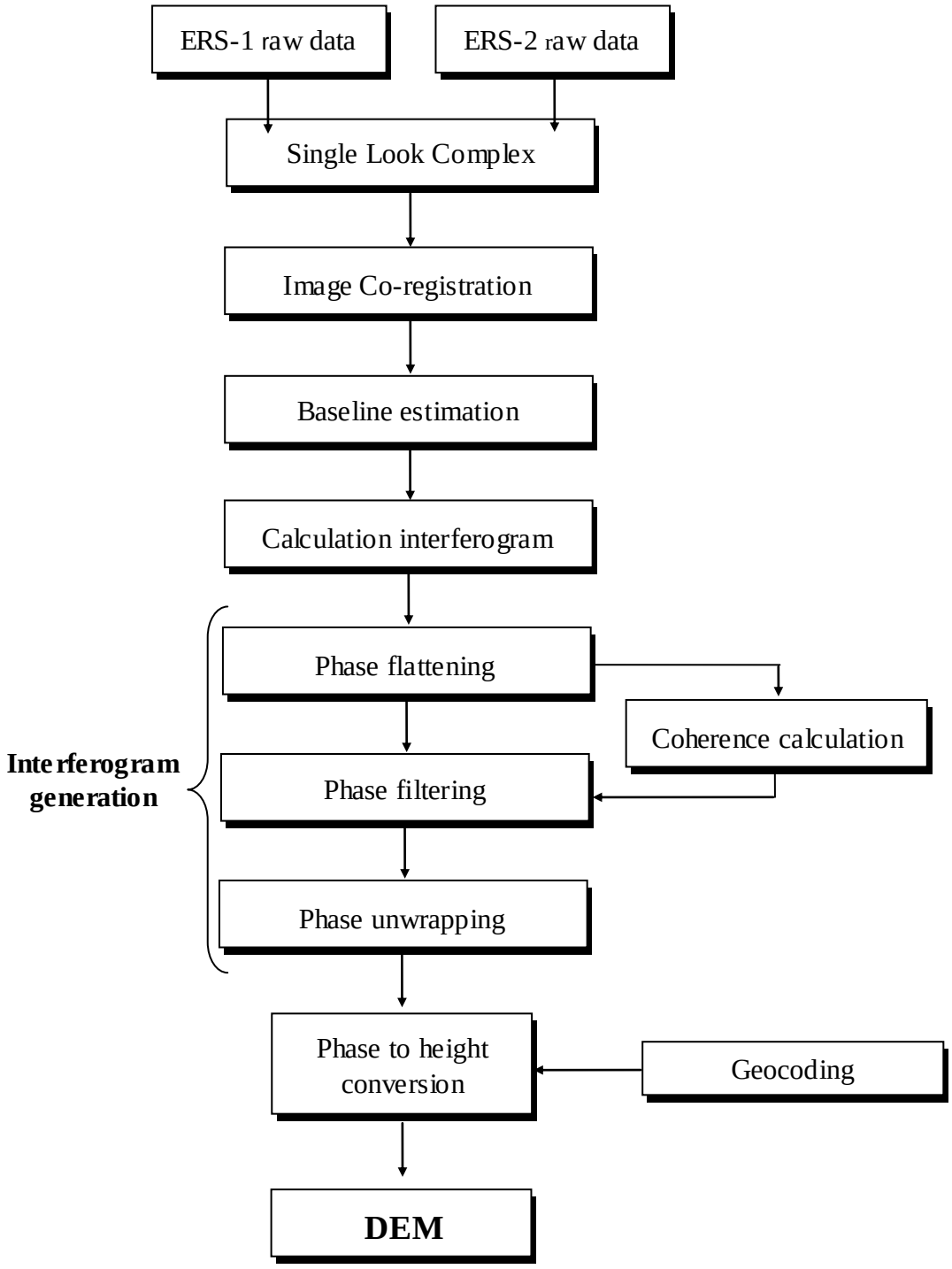

Figure 4.8: Processing steps of InSAR data for generation of digital elevation model.

4.5.1 Co-registration

The InSAR DEM generation is based on the processing of at least two complex SAR images covering the same area and acquired from slightly different points of view. The interferogram is calculated through a complex conjugate multiple of the slave image with the complex conjugate of a master image. Master and slave (SLC) images are acquired by the two spatially separated antennae for repeat-pass satellite data. Because an interferogram represents the phase difference between two SLC images at the same location, in repeat-pass InSAR processing, a pair of SLC images not covering exactly the same area need to be registered. Registration offsets are modelled as bilinear functions in range and azimuth. The cross-correlation co-registration method (Zebker *et al.,* 1994) is applied between two real-valued intensity images. Co-registration offsets are estimated by locating the peak of the cross-correlation between small subsets of image pairs. This procedure is repeated throughout the image to determine the offsets as functions of azimuth and range coordinates. One image is then resampled to be co-registered with respect to the other image, based on the offset functions.

4.5.2 Interferogram flattening and filtering

Before the phase-unwrapping stage, the interferogram must be flattened to decrease the density of the fringes in the interferogram or the phase unwrapping process may fail. The spherical Earth phase must be added to the phase in the interferogram to get the full interferometric phase. Flattening of the interferogram consists of removing the phase component due to the variation of the range distance across the image. Removal of this phase term flattens the interferogram leaving fringes only related to changes in elevation. The operation is called flattening because, in the case of a flat surface, this would be the only component of the interferometric phase, under the assumption that the other components are null. Flattening is performed by computation of the fringe rate across the image in order to take into account the variations of slant range distance, incidence angle and perpendicular component of the baseline. This operation assumes the surface of the earth to be curved (ellipsoid) and without topographical features. For the practical application of InSAR, if the interferogram is not flattened well, the residual phase due to the Earth will be considered to be the phase due to the

topography or the deformation. After that, the flattened interferogram is filtered to improve the phase signal-to-noise ratio on the cost of spatial resolution. Filtering an interferogram has the objective of reducing phase noise, thereby reducing the number of residues. A residue is a point in the interferogram where the sum of the phase differences between pixels around a closed path is not 0. Generally, thermal noise causes the generation of pairs of residues that are close together. The ultimate objective of filtering is to reduce the phase noise and therefore make the phase unwrapping simpler, more robust, and more efficient.

4.5.3 Baseline estimation

Baseline is a very important parameter in InSAR processing and applications. It influences the generation and quality of DEMs from interferogram (Ren *et al.,* 2003). In the InSAR processing, accurate knowledge of the baseline separation and orientation is important for mapping accuracy (Li and Goldstein, 1990). Interferograms with normal baseline values (higher than ~450 m) are usually almost impossible to unwrap if the topography of the area is not very smooth. Large baselines reduce the effects of phase noise and atmospheric artefacts but at the same time, large baseline interferograms have many tightly packed fringes and are usually very noisy and difficult to unwrap (ESA, 2008). The optimum perpendicular baseline for ERS-1/2 is in the range between 150 and 300 metres (ESA, 2008). The initial baseline estimation derived from satellite orbit data is not accurate enough to achieve acceptable results. Therefore, GCPs points are needed to calculate precise baseline length. The GAMMA software allows the estimation of the baseline separation through a number of methods. ERS baseline estimates are published by ESA (www.gamma-rs.ch).

To obtain a precise baseline estimate, the equation linking topographic phase, ϕ, and elevation of a point, Z, can be used:

$$\emptyset = \frac{4\pi\beta}{\lambda R \sin\theta} Z \qquad (4.1)$$

where ß is the baseline, λ represents the wavelength, R the slant range distance to the point and θ the local incidence angle.

Knowing the height and unwrapped InSAR phase of at least one point on the ground allows the baseline to be obtained:

$$\beta = \frac{\lambda R \sin \theta}{4\pi Z} \phi \tag{4.2}$$

4.5.4 Phase unwrapping

The phase obtained in the interferogram is a wrapped phase and this needs to be unwrapped before it can be used to estimate height. Phase unwrapping is a technique that permits retrieval of the unwrapped phase from the wrapped phase, which for the InSAR, is a necessary step for the generation of DEMs (Fornaro *et al.*, 1996). Since the interferometric phase is wrapped modulo 2π, an integer number of 2π has to be added to the interferometric phase for each pixel in order to obtain sequential phase values across the entire image. This works well when phase change between two consecutive pixels is less than π. This does not happen with an SAR image in reality due to layover and noise, both of which are properties of SAR images.

In an interferogram, points where phase change is more than π are known as points with phase discontinuities and they are called residues. Points with positive discontinuity are known as positive residues and points with negative discontinuity are known as negative residues. In addition, these discontinuities propagate phase errors globally across the scene and corrupt phase information at other places in the image. In order to avoid the above problem, first, residues are identified in the interferogram and then residues with opposite signs are joined by the shortest distance (Goldstein *et al.*, 1988). A residue that cannot be joined with other residues is connected to the nearest boundary of the scene with an assumption that a corresponding residue is lying in the adjacent scene. Phase integration is performed in such a way that the integration path

does not encircle any residue, or encircled residues are such that their net effect is zero. Coherence information is also used to check the quality of phase.

The phase unwrapping algorithm used in this study is branch cut. It starts at one residue and searches around it within a window of 3x3 for another residue. If a residue of a different sign is found, the branch cut is applied and the algorithm continues to the next residue. If the residue has the same sign, the search continues from this new position, and is repeated until all plus and minus residues are unloaded, thus spanning a tree (Franceschetti and Lanari, 1999).

4.6 DEM Generation from ASTER data

Automated stereocorrelation has become a standard method of generating DEMs from digital stereo images. Although approaches may vary according to the software employed, the procedures normally include the collection of GCPs, defining tie points, and determination of parallax values per pixel using automatic image matching techniques (Hirano *et al*. 2003) as can be seen in Figure 4.9. ITT Environment for Visualizing Images software (ENVI®) software was used to generate the DEMs. The DEM was directly produced from along-track stereoscopic images, which came from ASTER 3N and 3B channels, and which were read from the distribution file (HDF format) by the software. The DEM extraction process begins with the input of a stereo image pair. For this demonstration, a DEM is extracted from an ASTER L1A product using the visible near infrared (VNIR) telescope's nadir (3N) and backward (3B) viewing bands for along-track stereoscopic observation. Ground control points (GCPs), are collected in a field survey using the differential global positioning system (DGPS), the result of which would be an absolute DEM. An absolute DEM uses ground control and has horizontal and vertical reference systems tied to these geodetic coordinates. If DEM extraction was done without GCPs, the result would be a relative DEM, that is, a DEM with possible differences in position, scale and rotation from geodetic coordinates on the ground and mean sea level. For optimal results, the GCPs should be regularly distributed all over the scene and collected at different elevations (Eckert *et al.*, 2005).

The tie points are used to define the epipolar geometry and to create epipolar images, which are used to extract the DEM (ENVI, 2008). Tie points are used to join the images in a project so that they are positioned correctly relative to one another. Traditionally, tie points have been collected manually, two images at a time. With the advent of new, sophisticated, and automated techniques, tie points are now also can collect automatically. Digital image matching techniques are used to automatically identify and measure tie points in stereo images. Tie points should be visually well-defined in all images. Ideally, they should show good contrast, like the corner of a building or a road intersection. Tie points should also be well distributed over the study area. This operation computes a photogrammetric model using the orbital and sensor ephemeris information plus the GCPs and tie points, so that images were located relative to each other and to the ground.

After that, image matching used to calculate parallax differences from the ASTER stereo pair has to be calculated. The core of stereocorrelation is automatic image matching. To accomplish this, a correlation window of specified size (e.g., 9 by 9 pixels), defined prior to initiating the correlation procedure, is automatically centred over a 15 m pixel in the band 3N image. The area on the band 3B image within which the conjugate pixel is located is defined by a search window sized to account for the maximum possible image displacements due to terrain relief. The correlation window or moving window is then moved pixel-by-pixel across the search window, and the correlation coefficient is computed at every pixel location (Figure 3.3). The pixel location at which the correlation coefficient reaches a maximum is considered to be the match point (Lang and Welch, 1999). This procedure is systematically repeated across image space.

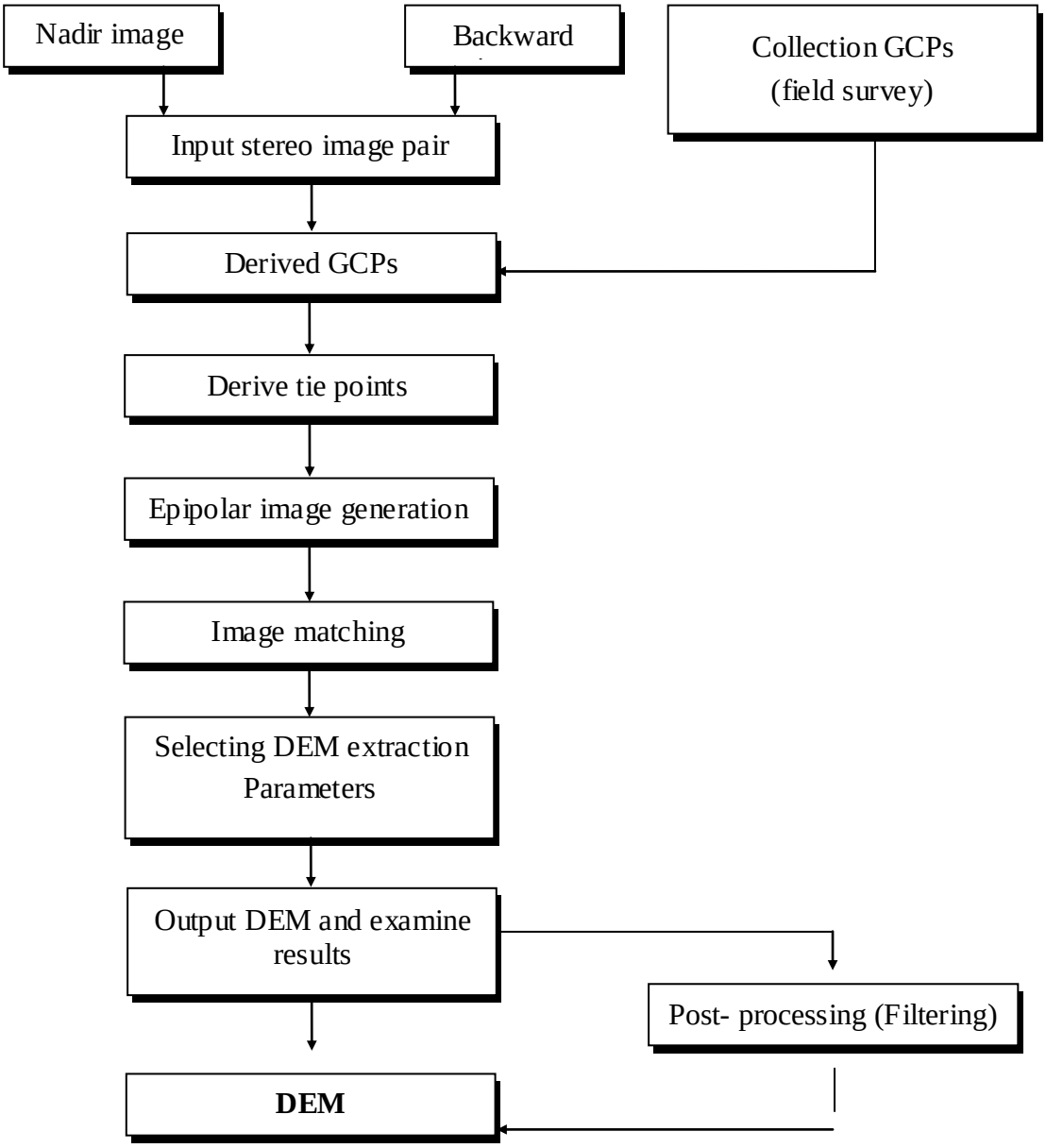

Figure 4.9: Processing steps of generation of digital elevation model from ASTER data.

4.7 Generation of a DEM from Topographic Maps

4.7.1 Introduction

To produce a DEM from digitizing points, interpolation is performed. The interpolation was done using ArcGIS®. Generation of DEM from topographic maps is the most common method used, especially in developing countries. In many countries, the only elevation data available are in the form of topographic paper maps at different scales. This type of DEM is used by many others as reference data to validate DEMs created from different methods such as optical source data (SPOT, ASTER, IKONOS, Quickbird) or interferometric synthetic aperture radar (InSAR). The accuracy of DEMs created from topographic maps depends on the map scale, quality of scanner and interpolation method.

4.7.2 Collection of elevations from maps

A topographic map of the study area is available at a 1:50,000 scale and the contours are shown at a contour interval of 20 m. There are two options for collecting elevations from topographic maps. The first one is using a digitizing table. The map is carefully put onto the digitizer table. A cursor with cross hairs is used to trace the contour lines by hand and to record the coordinates. The second option is to use digitizing on the computer screen. In this option, maps are scanned by an automatic scanner and displayed on the computer screen using ArcGIS; then, elevation can be collected from contour lines and spot heights. In this study, the second option was used because in this option, maps can be maximized on the screen to increase the accuracy of identification of elevation from contour lines. The recording of elevation points from contour lines is called point mode. With point mode digitization, each time the operator presses a button, the x, y coordinates of the cursor's position are recorded. The main advantage of point mode manual digitization is that the operator controls the selection of points to reduce data volume. With each contour line, hundreds or thousands of points were recorded; then, elevations were added using the attributes table in ArcView®.

Interpolation is the process of estimating unknown values that fall between known values. It can also be defined as a procedure used to predict the values for cells in a raster from a limited number of sample data points. The primary assumption of interpolation is based on the First Law of Geography by Waldo Tobler. This states that "everything is related to everything else, but near things are more closely related than are distant things". This means that points near each other are more alike than are those farther away; therefore, any location's values should be estimated based on the values of points nearby. Different types of interpolation can be used to create DEMs from topographic maps. These include inverse distance weighted, kriging, spline and natural neighbour. There are two approaches that allow control of the number of sample points used to estimate cell values: selecting points by defining a search radius that will use only the samples contained within it, or selecting the number of points that are closest to the estimated cell value. In this study, the second approach was used to control the number of sample points.

Several DEM interpolation methods are available in most mapping software. In environmental applications, the issue is more about the relative rather than the absolute accuracy. Relative accuracy refers to reproduction of terrain shape (Wise, 2000). Therefore, the appropriate DEM interpolation method should reproduce as close as possible the terrain shape. In our case the input data is 1:50,000 topographic maps with a 20m contour interval. This means that we have no elevation values between contours, although we know elevation values change between contours. Therefore the first step in choosing an appropriate DEM interpolation method from contours is to discard those methods that do not extrapolate elevation beyond contours.

4.8 Methods of Accuracy Assessment of DEMs

Accuracy is the most important factor to be considered in the production of DEMs because, if the accuracy of a DEM does not meet the requirements, then the whole project needs to be repeated and thus the economy and efficiency will ultimately be affected (Li and Gold, 2005). An accuracy assessment of a DEM requires the comparison of elevation values from another DEM created from an extremely accurate method, such as the photogrammetric method, or from check points observed by

DGPS or read from topographic maps with corresponding grid cell values in the DEM surface. The difference in elevation between two sets of elevation data was calculated to give an elevation error. A positive error value indicates that the DEM provides an overestimate of elevation at the point location, while a negative error indicates an underestimate. The method adopted to evaluate InSAR and ASTER derived DEMs consists of three approaches:

(1) Comparison with differential GPS elevations. In this comparison, a DEM accuracy assessment was performed using a set of independent checkpoints (ICPs), which were collected using a differential GPS. The elevation of checkpoints was compared with the elevation of interpolated from DEM at the same location of these points. The elevation difference yields an estimate of DEM error. These characteristics (locational accuracy, number and spatial distribution) of these points affect the accuracy of the DEMs to some extent. Two issues have to be taken into account when using ground truth points to assess DEM accuracy. The first is how those points should be selected. The second is how many points are needed to obtain an acceptable result.

(2) Comparison with the DEM derived from a digitized contour map. This approach of quality assessment is called absolute accuracy assessment and is based on a reference DEM since it provides the possibility of comparing both DEMs on every grid cell basis. In this study, accuracy assessment of a DEM was done by using a reference DEM created from existing topographic maps over a relatively small area. This type of DEM is used by many others as reference data to validate DEMs created from different methods such as optical source data (SPOT, ASTER, IKONOS, Quickbird, InSAR).

(3) Comparison of stream networks. The stream networks derived from the InSAR and ASTER DEMs were assessed against the reference stream network drawn and digitized from 1:50,000 topographic maps. Map stream networks were constructed from maps which scanned and display in ArcGIS® for digitizing.

Table 4.2 describes the statistical comparisons that were calculated to give a comprehensive quantitative assessment of DEM error, which includes a summary description of the size of error values and the statistical quality of error distribution.

Table 4.2: Statistical properties for accuracy assessment of DEMs.

Statistical parameter	Equation
Minimum and maximum elevation error (Min, Max): The minimum and maximum elevation difference between DEM and reference data.	Elevation difference = $Z_{DEM} - Z_{Ref}$
Mean elevation error (ME): The sum of the elevation difference for all the points or pixels divided by the total number of points.	$ME = \frac{\sum (Z_{DEM} - Z_{Ref})}{n}$
Mean absolute elevation error (MAE): the sum of the absolute elevation difference for all the points or pixels divided by the total number of points.	$MAE = \frac{\sum \lvert (Z_{DEM} - Z_{Ref}) \rvert}{n}$
Standard deviation of elevation error (SDE):	$SDE = \sqrt{\frac{\sum [(Z_{DEM} - Z_{Ref}) - ME]^2}{n-1}}$
Root Mean Square Error (RMSE): The global indicator of the quality of output DEM, which measures the dispersion of the frequency distribution of deviations between the original elevation data and the DEM data	$RMSE = \sqrt{\frac{\sum (Z_{DEM} - Z_{Ref})^2}{n}}$

4.9 Summary

In this chapter both InSAR and ASTER data and topographic map data have been described. A field campaign to collect both ground control and independent check points was conducted and included a description of the nature of the test site. A discussion of the methods used and the experience gained during the reconnaissance, observation and fixing of the ground control points and independent check points were presented. In addition, this chapter described the methodology used to generate DEMs from InSAR, ASTER and topographic maps. The methods of accuracy assessment were explained. The next chapter will focus on the results of the DEM generation and The factors that affect the results during the processing steps.

Chapter 5: Results

5.1 Introduction

This chapter presents the results of DEM generation from three different data sources. The first part shows the results of DEM generation using InSAR data and parts illustraters of aspects that may affect the generated DEM results which included identification of GCPs and effect of baseline estimation methods. The second part shows results of DEM generation from ASTER data. This included the results of examined of different parameters used in generation of DEM using photogrammetric techniques. These extraction parameters are minimum correlation, search windows size and terrain detail. Also, this part show post processing result that has been done to remove noisy pixels and smooth DEM. Validation of the topographic map DEM is presented in the final section.

5.2 Results of InSAR DEM Production

5.2.1 Pre-processing: The coherence image

The estimate of coherence is given by the complex correlation between two co-registered single-look complex interferometric SAR image pairs, that is, how much two SAR images are correlated with each other. It represents the similarity of two complex SAR images and is defined as the magnitude of the complex correlation coefficient (Stebler *et al.*, 2002):

$$\gamma = \frac{\sum_{n=1}^{N} S_1 S_2}{\sqrt{\sum_{n=1}^{N} |S_1|^2 \cdot \sum_{n=1}^{N} |S_2|^2}} \qquad 0 \le \gamma \le 1 \qquad (5.1)$$

Coherence may change depending on the backscatter properties from the ground surface, which can be roughness, moisture, or thawing conditions (Eldhuset, 2003). In this study, the coherence for each pixel in the InSAR images was estimated using a window size of 32 by 32 pixels in slant range and azimuth respectively (with an average

of 1024 pixels). However, the influence of the strong backscatter dominates its surroundings in the computation of the coherency. Sometimes, the results of the coherence calculation are affected by the size of window used. If the window size is increased, the estimation bias and the estimation uncertainty decrease while the spatial resolution of the coherence image decreases. To compromise between accurate estimation and high spatial resolution, the estimation algorithm can implement an adaptive window size depending on an initial estimate of the coherence. In areas of low coherence, larger estimation windows are used (Wegmuller *et al.*, 1998). Coherence is typically computed using a sliding window. For each pixel, the coherence is obtained by applying Equation 5.1, the window sliding from pixel to pixel. To decrease the effect of resolution loss due to the windowing operation, weighting functions (for example, linear or Gaussian) can be applied within the window. In this way, pixels further away from the centre of the window have less weight on the estimate. The type of weight to be applied depends on the nature of the objects in the scene. If the scene includes distributed targets, weighting plays a minor role.

On the contrary, if the scene is populated with small-size point targets, use of small windows and strong weighting functions is recommended to preserve the coherence of each of the point targets. The value of interferometric coherence ranges from 0 to 1; the value 0 indicates noisy, complete incoherence with no useful information in the interferogram and the value 1 indicates no noise in the interferogram. Both extremes are rarely seen and most interferometric image combinations lie somewhere in between. As a rule of thumb, values of 0.7 – 1.0 indicate excellent coherence, 0.5 – 0.7 good coherence, and 0.3 – 0.5 noisy but usable coherence (Massom and Lubin, 2006). A high coherence yields a better DEM. Low coherence results on bad phase quality and can cause many problems for the phase unwrapping. The coherence image given below in Figure 5.1 is very high for almost the whole area since the study area is a semi-arid region that had stable weather conditions. The maximum and minimum values for coherence were 0.93 and 0.46 respectively, while the mean value of coherence was 0.83. Figure 5.2 shows the histogram of coherence that was followed. As can be seen from the histogram, most of the area had a coherence value of between 0.80 and 0.90, as few pixels take a value between 0 and 0.70. In the middle left part of

the image and in the upper-left corner, the coherence is low in some locations because these locations are agricultural areas, which usually have low coherence. If we exclude the aspect of random noise, the changes with time of the scattering properties of a target determine its coherence. Motion and change in vegetation also affect coherence. L*oss* of coherence is usually caused by the leaf motion, but this does not imply that areas of vegetation will always appear with zero coherence: radiation will often penetrate the foliage, at least partially, and can be backscattered by the terrain underneath or by the trunk and branches of the trees, which are mechanically much more stable and will therefore contribute to its coherence. In general, deciduous trees will show high coherence during winter when there are no leaves and less coherence in summer due to foliage effects. Similarly, different types of vegetation will show different one-day coherence values, depending on the height of the plant and on the lengths of the leaves: short leaves could be practically transparent to the C-band radiation of ERS satellites.

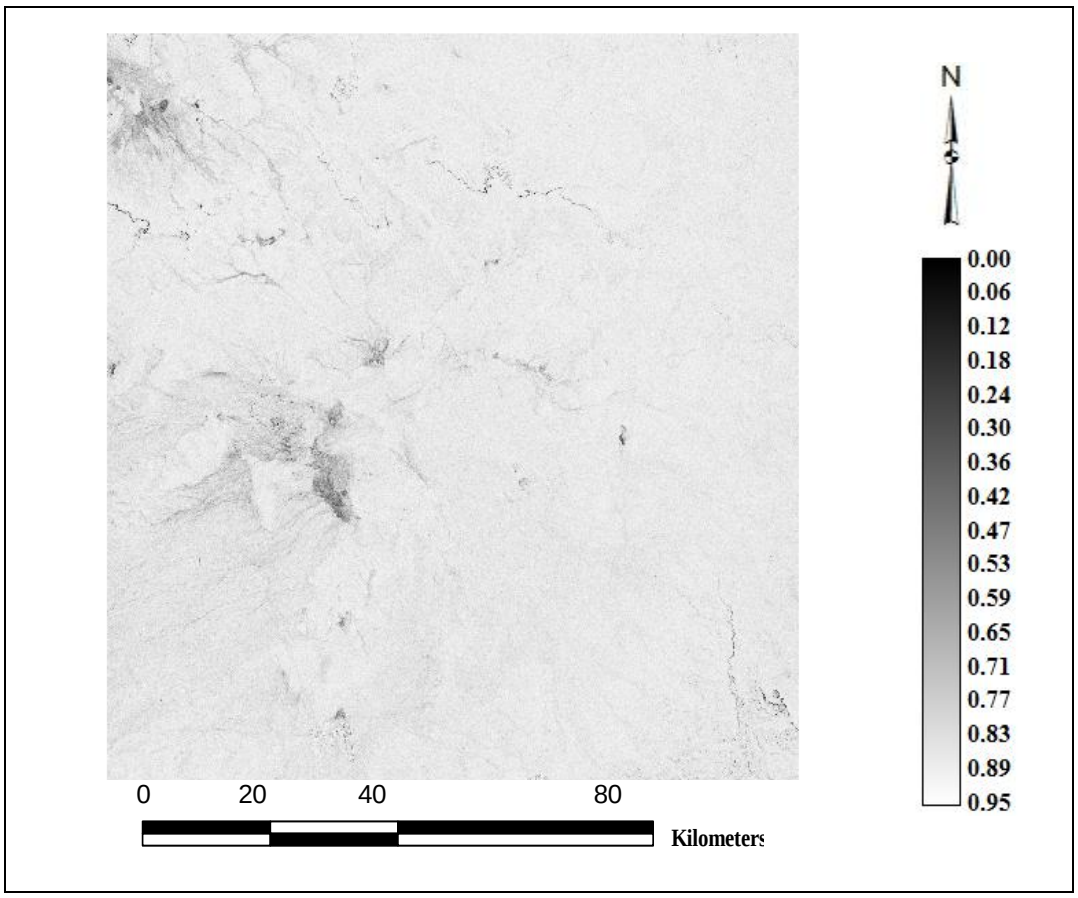

Figure 5.1: Coherence image derived from ERS-1/2 tandem pair acquired 1/2 May 1996.

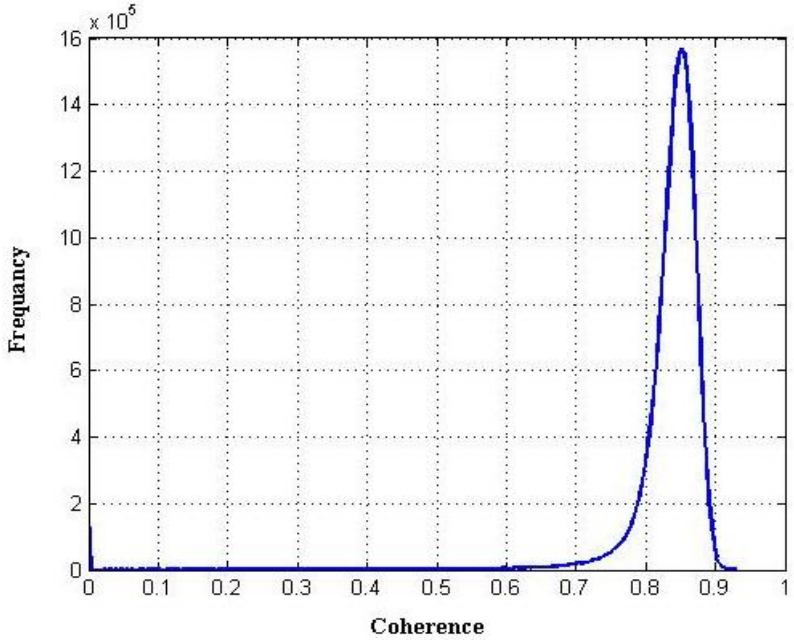

Figure 5.2: Histogram of coherence from ERS-1/2 tandem images acquired on dates 1/2 May 1996.

5.2.2 Multilook processing

Multilook processing after generation of an interferogram is the best option to filter out the phase noise and to preserve the fringe pattern of the interferogram as well (Hanssen, 2001). By this process, the values of phase of neighbouring pixels within window of fixed dimensions are averaged. Multi-looking results not only in an improved signal noise ratio but also increased computational efficiency by creating more manageable datasets. This is an important step, given the size of SAR datasets acquired at a high resolution. The major disadvantage of multi-looking is that it results in degraded spatial resolution. Another limitation related to possible under-sampling in cases where relatively high phase gradients are present. The interferogram was multilinked with a single look in range direction and five looks in azimuth direction, and the resultant slant range pixel size of a multilinked interferogram is estimated to be around 24 m (Table 5.1).

Table 5.1: Effect of multilooking on pixel sizes of the interferogram.

Interferogram range looks	1
Interferogram azimuth looks	5
Interferogram range pixel spacing	7.904
Interferogram azimuth pixel spacing	19.922
Resampled range pixel spacing	20
Resampled azimuth pixel spacing	20
Final ground resolution pixel size	24

5.2.3 Interferogram products maps

Figure 5.3 to 5.6 show various stages in the processing of interferogram generation. Figure 5.3 shows interferometric phase of the ERS-1/2 tandem image pair before flattening (raw interferogram). In interferogram, each complex element of the image matrix is represented by a pixel within which the phase is represented in colour map and the magnitude is mapped to a gray scale shade. Because phase depends on

topography, phase images tend to have colored bands called fringes where one complete fringe cycle represents a 2π phase shift. A fringe can be thought of as a collection of contours where each unique grey level within and along the fringe corresponds to a constant phase difference. The constant phase difference within a fringe is directly related to constant path difference. In turn, path difference is a function of ground elevation as this affects the distance to the satellite. Therefore, constant path difference can be related to constant elevation. i.e. the phase difference contours within the fringe are indeed height contours. Figure 5.4 shows interferometric phase after flattening and then after filtering (Figure 5.5). The fringes in an interferogram are not only a result of the surface topography but also of the Earth's curvature. An interferogram is said to have been "flattened" when the fringe and phase effects due to the shape of the Earth's ellipsoid have been eliminated and only fringes due to topography remain. The phase value or angle (and hence phase differences in an interferogram) is not known absolutely, but is given in the range 0-360 degrees, i.e. the phase is wrapped onto a fixed range of angle of 0-360 degrees. In order to compute terrain heights and generate a DEM, the interferogram fringes have to be unwrapped, i.e. the correct multiple of 360 degrees must be added to the phase difference at each pixel. If the ground were flat, unwrapping the above interferogram would produce an image of constant grey level. Figure 5.6 shows the unwrapped phases. The colour in the image represents the difference in the phase of the radar signal obtained on the two flights images that combined to make the interferogram.

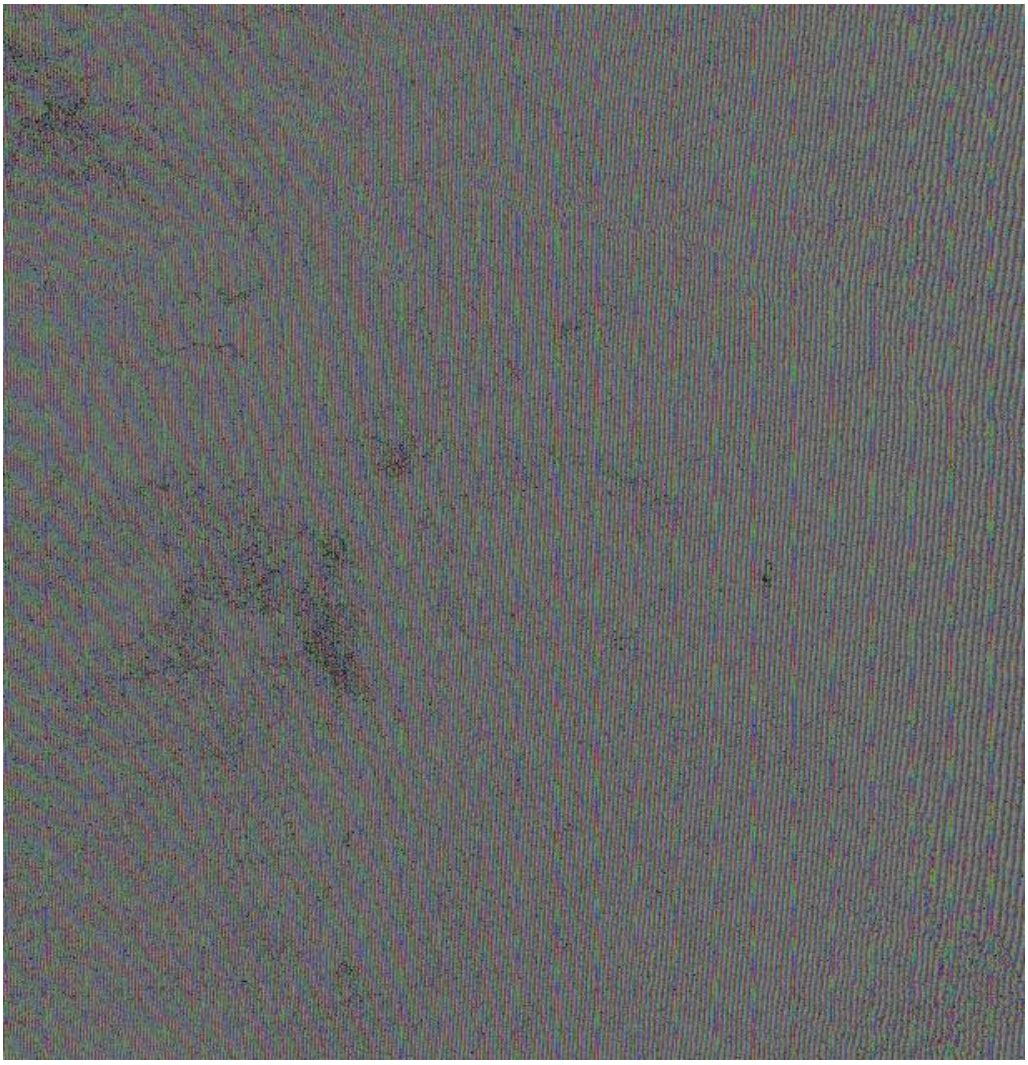

Figure 5.3: Interferometric phase of the ERS-1/2 tandem image pair before flattening.

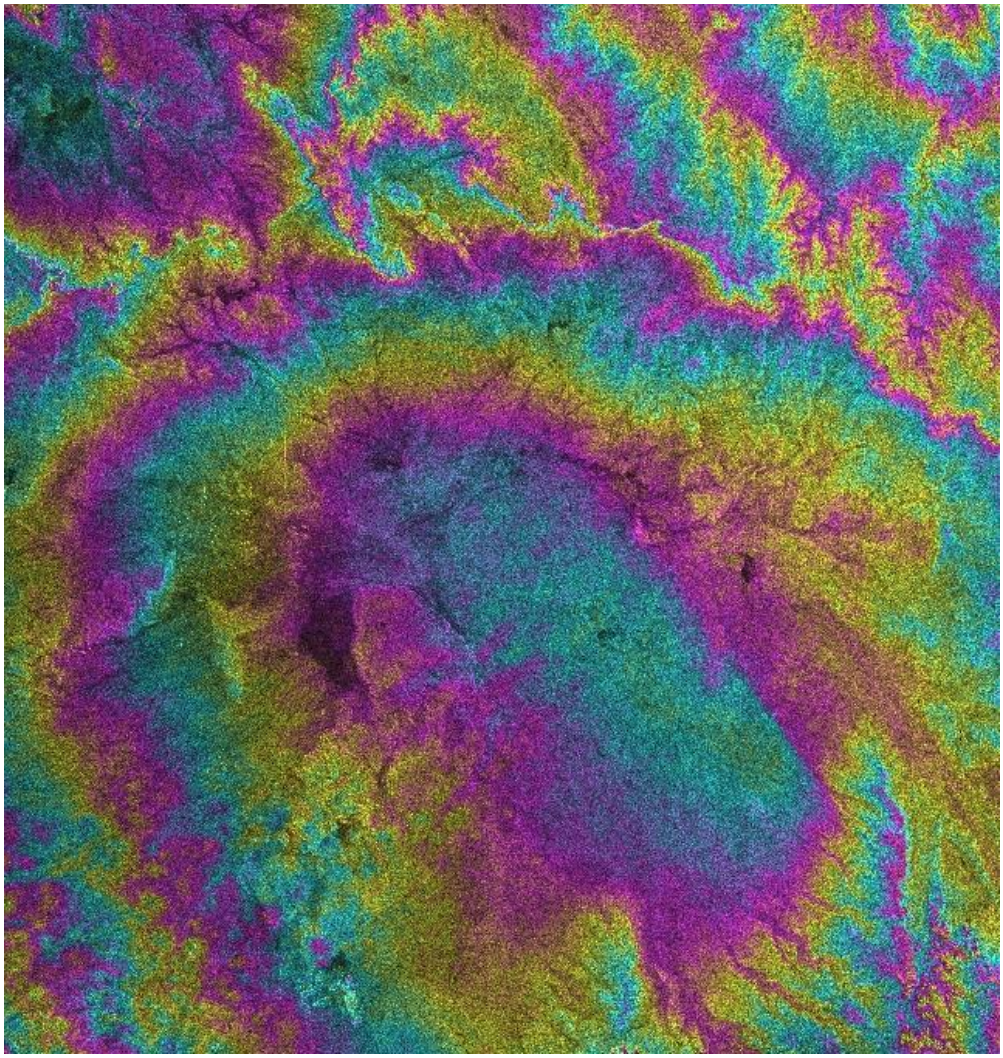

Figure 5.4: Flattened interferometric phase and image for the ERS-1/2 tandem image pair.

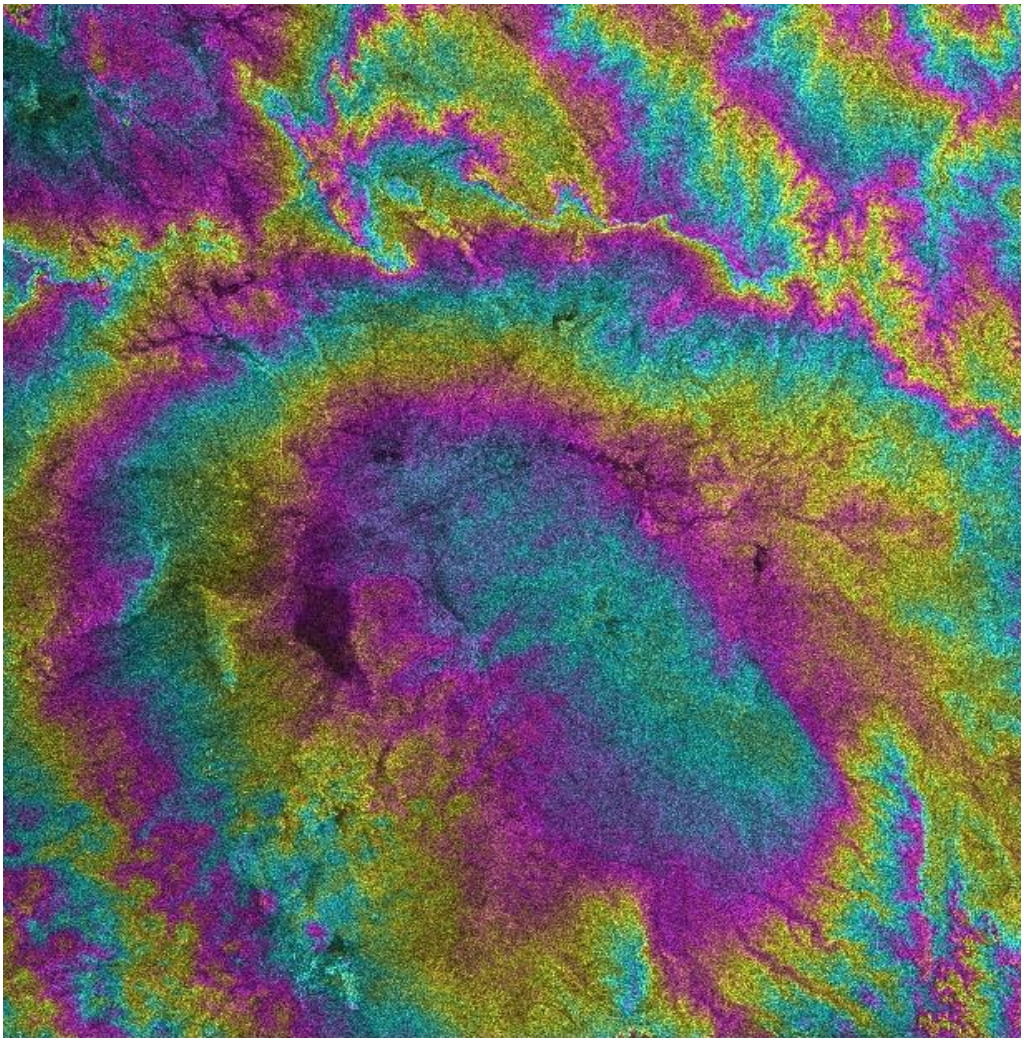

Figure 5.5: Flattened and filtered interferometric phase and intensity for the ERS-1/2 tandem image pair.

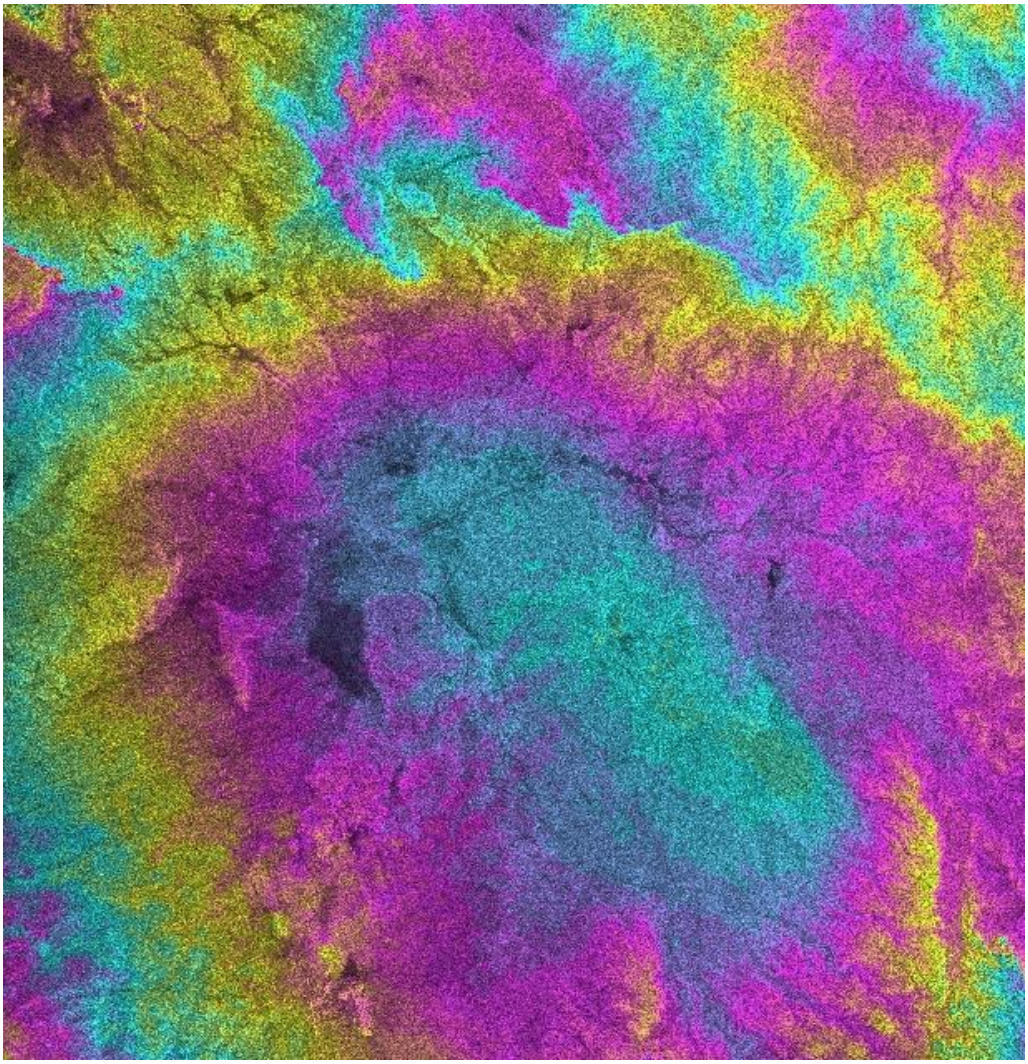

Figure 5.6: Unwrapped phase for the ERS-1/2 tandem image pair.

5.2.4 Height model generation and geocoding

The height values are calculated from the unwrapped phase values. These values are still in slant range coordinates. This is done by employing the theoretical phase relationship between phase and height. This relationship strongly depends on the imaging geometry. Therefore, a precise baseline estimation is required if an absolute height estimation is to be obtained. If this is not possible, then a number of GCPs must be known to improve the accuracy of the orbit data. The GCPs used for calibration of the unwrapped phase to ground height are shown in Table 5.1. Height error contributed by each GCP is displayed during the InSAR processing, and this information can be used

to decide if a GCP is to be accepted or deleted. In this study, all GCPs available were used. With repeated the GCPs input step several times, it can be get the acceptable result. After height estimation, the DEM remains in the slant range coordinate system. Since this geometry is different for each SAR image, and not related to any georeference frame, a geocoding has to be performed on the data to provide a comparable height map. This process is known as geocoding. This included: the translation of the image position of a pixel to the corresponding position on the reference system on the earth with the knowledge of the satellite position and velocity, conversion of earth location to geographic coordinates and conversion of geographic coordinates to map grid coordinates. Map projection used in this study is WG84. The final result of DEM is shown in Figure 5.7. The black parts in this Figure represent interferogram pixels that cannot be unwrapped. Such pixels do not contribute to the generation of DEM and result in holes in the DEM.

Table 5.2: List of GCPs used during generation of DEM from InSAR data for calibration of the unwrapped phase to ground height.

GCPs No	X (pixel)	Y (pixel)	Z (m)
1	3511	2065	904.8984
2	3574	1762	927.1336
3	3547	1220	937.0461
4	3247	748	1022.9103
5	2969	326	1043.8424
6	2774	1032	957.785
7	2717	2083	876.0617
8	2901	2137	870.464
9	3195	3007	865.7556
10	3733	2638	881.8892
11	4030	2368	893.9702
12	4189	2540	898.9741
13	4461	1895	968.0492
14	3822	1391	933.5357
15	4179	1455	972.2831
16	3967	1039	921.8189
17	4092	934	895.4687
18	3512	2419	883.8175

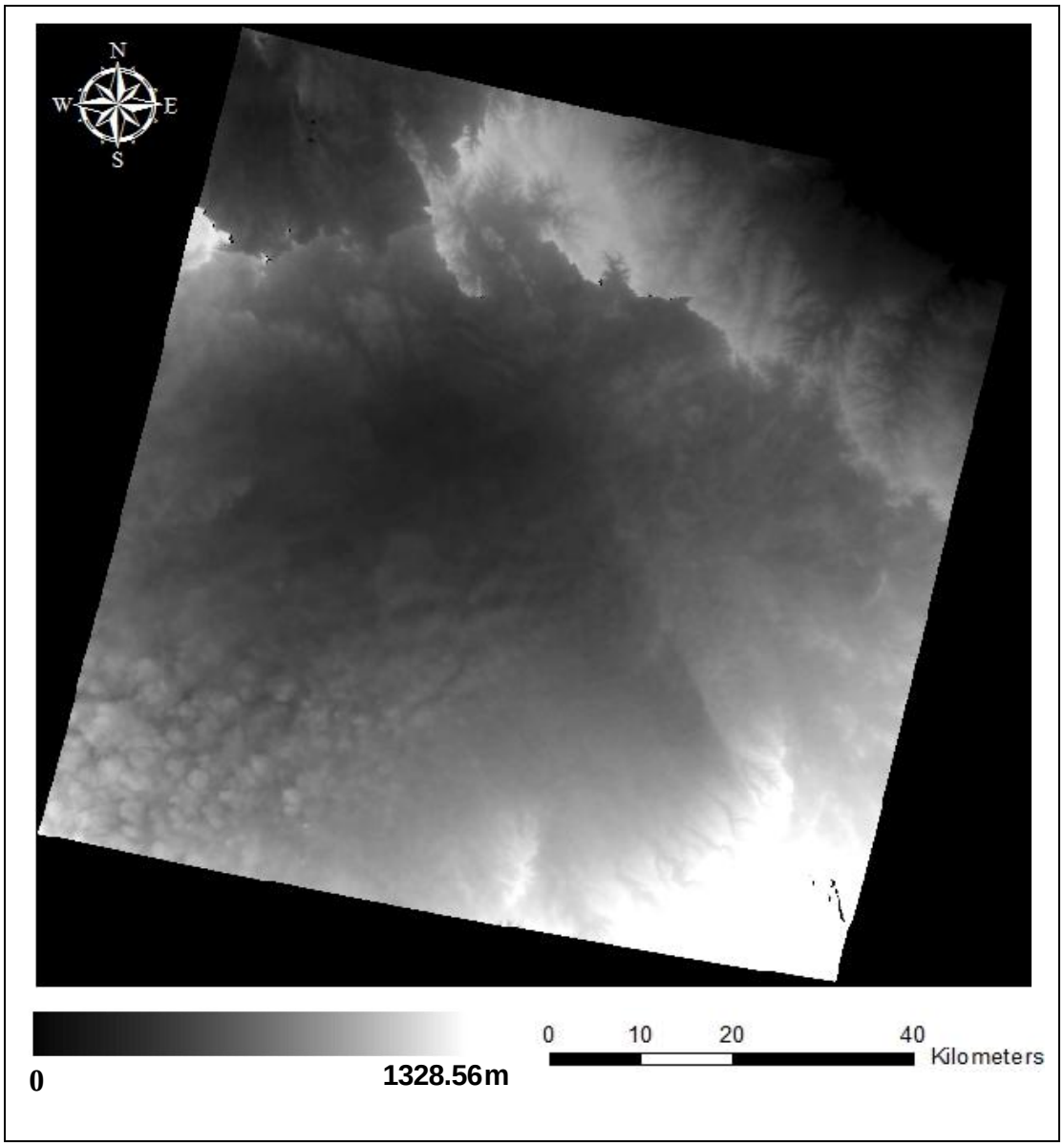

Figure 5.7: InSAR DEM displayed in units of metres.

5.2.5 Accuracy of GCP location experiment

Ground control points (GCPs) have a strong effect on the accuracy and reliability of DEMs**.** The number, accuracy and location of GCPs are the most important issues that have to be taken into account in the extraction of the DEM process. The number of GCPs required depends on the order of polynomial to be used. The user should be aware that while the higher order polynomial will result in a more accurate fit in the surrounding area of the GCPs, it may introduce new, significant errors in those parts of

the image that are further away from the GCPs. For InSAR data, the GCPs were studied related to the difficulty of identification of GCPs in InSAR images and the effect of the number of GCPs on the results. However, for ASTER data, the assessment of the effect of GCPs on the ASTER DEM is done related to the effect of the number of GCPs on the result because the identification of these points on ASTER stereo images is not as difficult as in InSAR images. This identification is a difficult task because of the large amount of noise in the image, and these points can be shifted from their rightful place by a cell or two cells or more.

To test identification of GCPs on InSAR DEM accuracy, three types of windows have been used 3x3, 5x5 and 7x7, for each GCP as shown in Figure 5.8. This test was applied on two subsets covering 24 km X 24 km which were chosen depending on the level of slope and value of elevation. In low relief areas (Min=852.37, Max=946.70, Mean=879.23 m), the terrain is almost flat (Min≈ 0 , Max=3.45, Mean=0.44º), while in high relief areas (Min=875.92, Max=1072.94, Mean=971.47 m), the slopes (Min≈ 0 , Max=22.36, Mean=1.44º) varied and the elevation is higher than other parts of the DEM. The GCPs are in the centre pixel of the window. The number of GCPs in low elevation sites was 12 points, while the number in high elevation sites was 6 points.

With each window, the GCP is moved randomly to any cell in the window. This step is repeated for all GCPs. Then, the steps of extraction of new DEM are completed as normal. Eighteen points were chosen to be ground control points in the extraction of a DEM from InSAR data. These new DEMs are named InSAR DEMs (3x3, 5x5 and 7x7). The results of the statistical properties shown in Table 5.3 indicate that the mean and the standard deviation of elevation of these DEMs have values close to the original and close to one another. The mean elevation differences were close to 1m and the standard deviation differences were less than 0.5 m which means that a slight displacement of the locations of GCPs from the true positions within three pixels around the original GCPs locations does not have a strong effect on the results of the DEM. This is more reasonable for the low relief areas or the areas that have low

variations of elevation. The number of GCPs in low elevation was sits 12 points, while in high elevation site was 6 points.

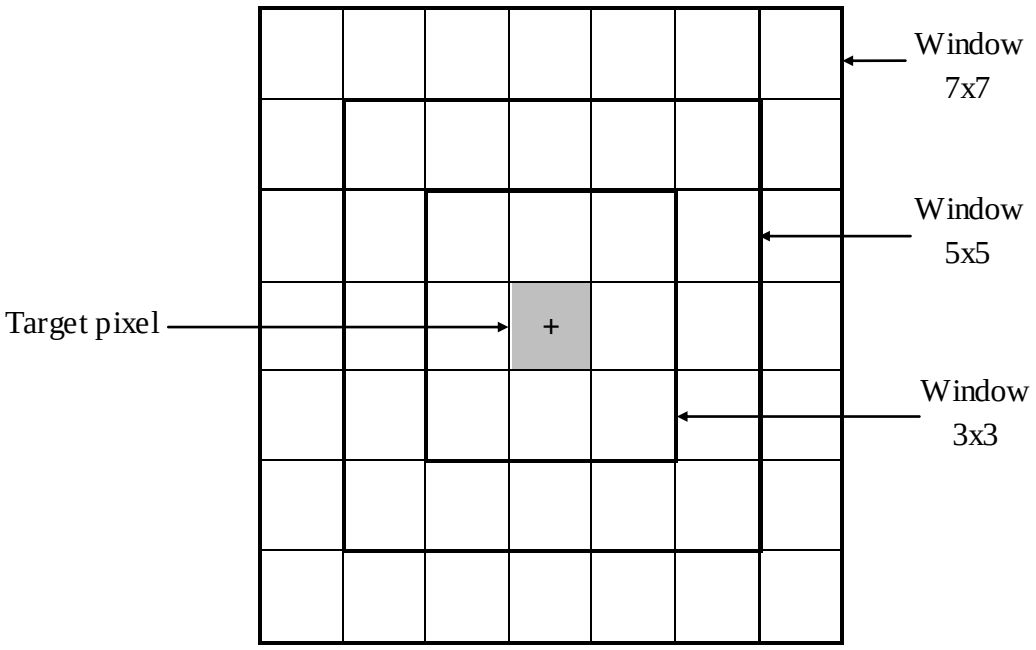

Figure 5.8: Window that used to test locating GCPs on InSAR image.

Table 5.3: Descriptive statistics of InSAR DEMs created to test locating GCPs on InSAR image.

Window type	Min (m)	Max (m)	Mean (m)	Std (m)
3X3	660.719	1325.800	963.944	79.772
5X5	665.046	1314.654	962.731	77.874
7X7	663.169	1326.368	965.030	79.788
Original DEM	659.268	1328.564	964.271	80.215

Also these DEMs were examined using image difference with original DEMs in two subset areas in low relief and high relief. From Figure 5.9 (a), it can be seen that the most elevation difference values in low relief site were zero in a DEM created with moving GCPs within 3x3 and 7x7 windows. However, the values given from elevation difference between original DEM and DEM created with moving GCPs within 5x5

were from 0 to +5 and the most of them equal to 2. From Figure 5.9 (b), it can be seen that the majority of the elevation difference values between the original DEM and the DEM in low relief sites were zero, with moving GCPs within 3x3 and 7x7 windows, and the rest of the values ranged between 0 and 2m. However, the elevation differences with moving GCPs within 5x5 were from 0 to +5 and the majority of them were equal to 2.

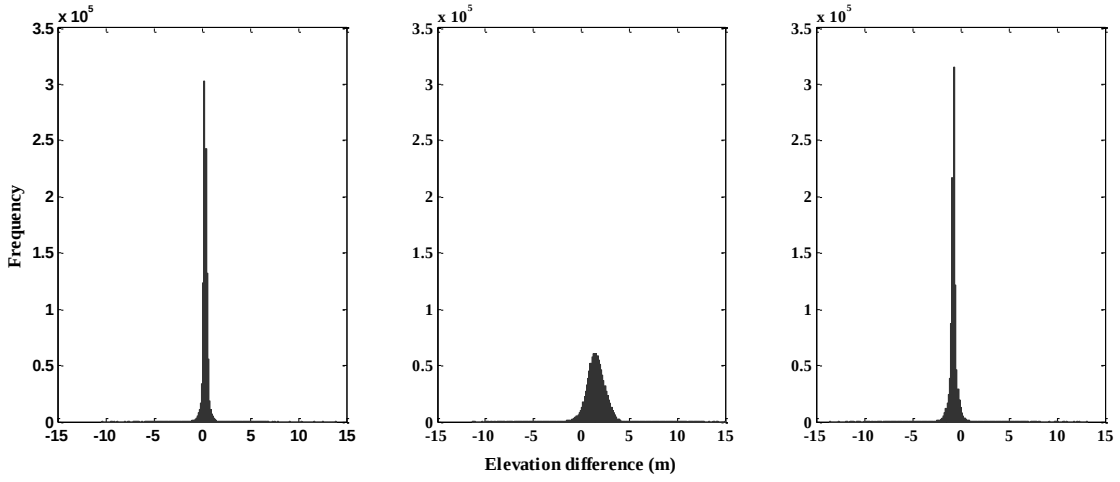

3X3 5X5 7X7

(a)

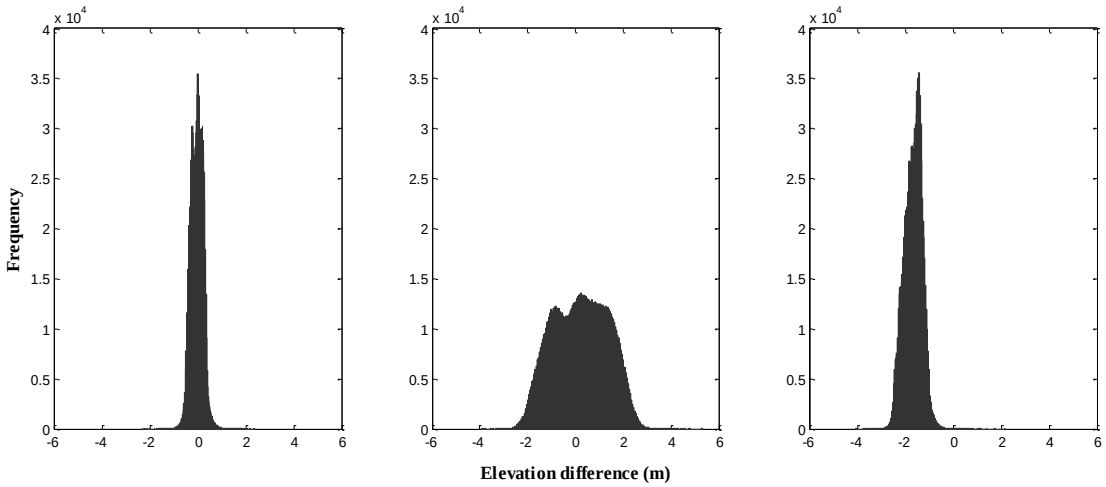

3X3 5X5 7X7

(b)

Figure 5.9: Histograms of variation between original created DEM and generated DEMs using different windows size around GCPs (a) area with medium relief (b) area with high relief.

5.2.6 Effect of baseline estimation methods on InSAR DEM accuracy

Estimation of baseline is one of the processing factors that seriously affects the accuracy of InSAR derived DEM. Baseline estimation based on ERS-1/2 pair orbital parameters. The parallel component of baseline is estimated based on the orbit parameters; the perpendicular component of baseline is estimated based on the interferogram fringe frequency. In order to achieve on one hand a high applicability and the other hand high quality estimates, several baseline estimation methods are included. The methods allow the user to estimate the interferometric baseline and the rate of change of the interferometric baseline from the orbit state vectors, the SLC registration offsets and the interferogram fringe rate. Orbit method is based on satellites tracks information, its accuracy depends on the quality of satellite ephemeris (Ren *et al.*, 1998). In the SLC registration offsets, the range image offset enables triangulation of the slant ranges to a point on a reference ellipsoid within the scene (Small *et al.*, 1996). Fringe rate method is based on frequency feature of interferogram. In practice it turns out that it is usually best to combine two of these methods. The first two methods give the better estimates for the parallel baseline component. The third method very often gives the better estimate for the perpendicular baseline component. Therefore, it is recommended to combine either one of the first two methods with the third method (Gamma, 2007). These methods are listed in the Table 5.4 below. These methods were used to assess the effect of baseline calculation on accuracy of derived DEM.

Table 5.4: Baseline estimation methods.

Method	**Parallel Baseline**	**Perpendicular Baseline**
1	From orbits	From orbits
2	From registration offsets	From registration offsets
3	From orbits	Fringe rate
4	From registration offsets	Fringe rate
5	Fringe rate	Fringe rate

From the descriptive statistics of InSAR DEM illustrated in Table 5.5, it can be noticed the difference between elevation values between method 1 and 3 are very small as well as between 2 and 4 while elevation values in method 5 were far away from other methods. From the statistical properties calculation for all five DEMs compared with the check point profiles that were collected using DGPS shown in Table 5.6, it is clear that the statistical results for methods 1 and 3 were similar. Also, methods 2 and 4 are similar but slightly more accurate than methods 1 and 3. However, method 4 gives the worst results of all methods; standard deviation and RMSE are 15.106 and 16.150 respectively.

Table 5.5: Descriptive statistics of InSAR DEM using different baseline estimation.

Baseline Methods	Method1	Method2	Method3	Method4	Method5
Bperp (m)	-110.70	-113.74	-110.69	-113.74	-93.81
Min (m)	658.87	719.97	659.26	719.12	301.35
Max (m)	1328.11	1398.32	1328.56	1399.16	1110.31
Mean (m)	964.32	982.712	964.27	982.49	859.93
Standard deviation (m)	80.33	88.54	80.21	88.46	124.69

Table 5.6: Accuracy of DEMs from DGPS check points using different baseline calculation methods from DGPS check points.

Baseline Methods	Method1	Method2	Method3	Method4	Method5
Bperp	-110.70	-113.74	-110.69	-113.74	-93.81
Min (m)	-25.068	-22.844	-25.064	-22.822	-65.651
Max (m)	28.618	27.822	28.794	28.116	31.897
Mean (m)	-0.023	0.970	-0.068	0.992	-5.712
Standard deviation (m)	7.705	8.828	7.704	8.803	15.106
RMSE (m)	7.705	8.810	7.704	8.858	16.150

5.3 Results of DEM Generation from ASTER Data

5.3.1 Automatic DEM extraction

Band 3N was selected as the left image and Band 3B was selected as the right image. If a data file contains an image obtained from a nadir-viewing direction while the other image is obtained from an off-nadir viewing angle, it is recommended to use the nadir-viewing image as the left image. The basis of this recommendation is that the left image is used as the base image during image matching, and it contains less geometric distortion. Also, the base-to-height (B/H) ratio of the two images should be close to 1, but not 0. This ensures the viewing angles provide enough parallax information to effectively compute elevations.

After the stereo image has been imported, the ENVI® program (DEM Extraction Wizard extension) was used to enter all the data related to the GCPs that are present on stereo image through the running "selecting GCPs step". This was done by inputting all the parameters including the zone, latitude, longitude, elevation and the projection and coordinate system that are being used for mapping of the area that has been covered by the stereo pair. In this research, the coordinate system that has been selected is UTM zone 37, WGS 84. 75 differential GCPs were used in this step which

collected from different types of terrain in study area to give the best representation of the surface (Figure 5.10). These points were most of points that can be identified on the image accurately. During the image matching, an area-based procedure is used based on the use of cross-correlation which determines the parallaxes resulting from the terrain relief. In cross correlation technique, a statistical comparison is computed from a digital number taken from same size subarrays in the left and right images. Since the exact position of the image in the right image is not initially known, a search window is selected with dimension much larger than those of the target window. A moving window approach is then used, comparing the candidate target window from left image with all possible window locations within the search window from the right image. At each moving window location in a search window, the correlation coefficient is computed. These are then converted to the differences in height from the given elevation values at the surrounding GCPs using a simple parallax formula to give the final DEM elevation values.

Automatic tie point generation requires four parameters to be specified. These parameters included determination the search windows size, and the moving window size. The search window is a defined subset of the image, within which the smaller moving window scans to find a topographic feature match for a tie point placement. The search window size can be any integer greater than or equal to 21, but it must be larger than the moving window size. The default is 81. However, the moving window scans the image subset area defined by the search window size, looking for matches to a topographic feature. The moving window size must be an odd integer. The smallest allowable value is 5. The default is 11. Using a larger value results in a more reliable tie point placement, but it takes longer processing time; conversely, a smaller value takes less processing time, but the tie points are less reliable. Determining a good moving window size largely depends upon the image resolution and terrain type. 25 of the points collected were used to build the epipolar images.

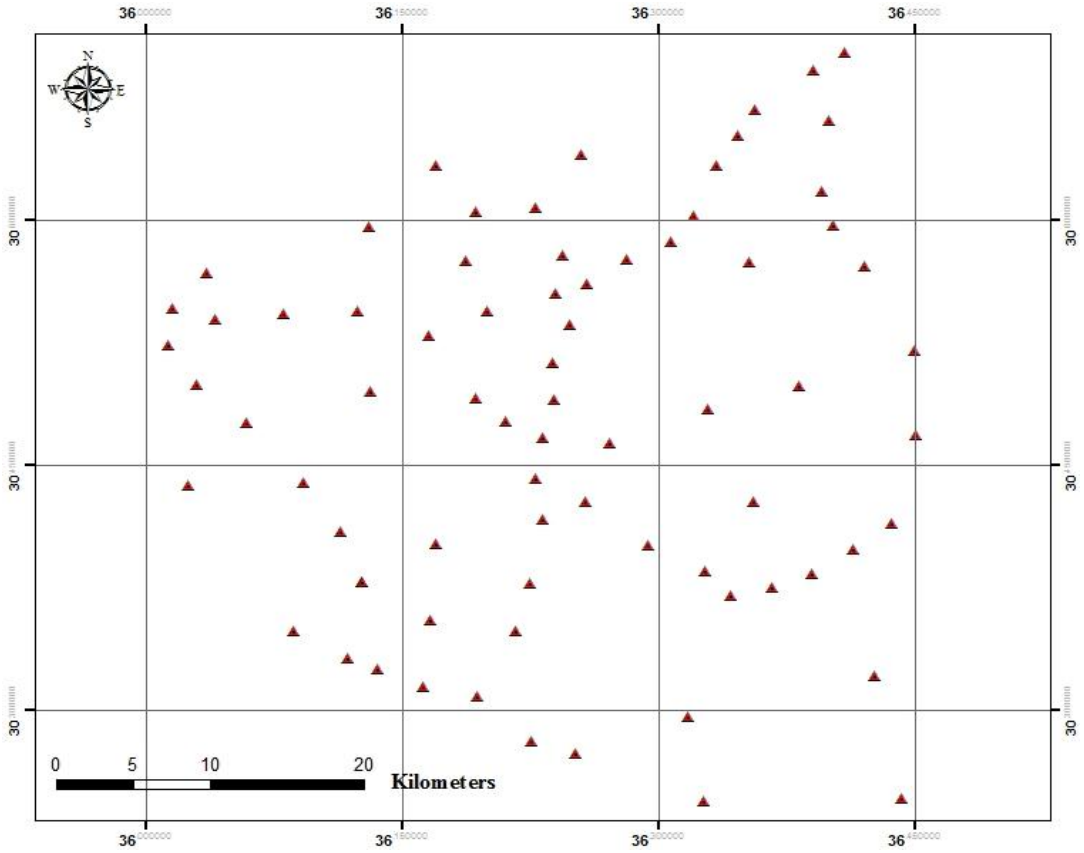

Figure 5.10: Distribution of the GCPs in the study area used to calibrate the ASTER DEM.

5.3.2 DEM extraction parameters

Generation of DEM using digital photogrammetric technique allows a degree of control of the search and quality characteristics of the algorithm during processing steps using a set of strategy parameters; hence the wrong choice of parameters can have a significant detrimental effect on the accuracy of DEM (Gooch and Chandler, 1999). This section describes the strategy parameters used in the ENVI® DEM extraction models and a set of tests used to define the optimum set of parameters for DEM generation in this study. The first step in the processing of tests was to create a DEM using the default parameters. Each parameter subsequently changed and keeping all other parameters at their default setting and DEM generated with 30 m grid resolution. Table 5.7 gives all the values of control parameters used in generated testing DEMs. And then, to analyze DEMs generated under the variation of individual parameter values and settings, using subset area from each new DEM was differenced

from the default DEM to produce a histogram of difference. A visual inspection was made of the histograms to identify the parameters which had the largest effect on the elevation estimates.

Table 5.7: Control parameters of DEM extraction using ENVI® software.

DEMs test	Control parameters change	
D	Default values : Minimum correlation = Search windows size: Terrain detail:	 0.7 5X5 Level 3
A1 A2 A3	Minimum correlation =	0.65 0.80 0.90
B1 B2 B3 B4 B5	Search windows size:	7X7 9X9 11X11 13X13 15X15
C1 C2 C4 C5	Terrain detail:	Level 1 Level 2 Level 5 Level 5

The parameters used in the testing are further described.

Minimum correlation – this is the threshold of a correlation coefficient used to determine whether two points are a good match or not. The two points are considered a good match, if a correlation coefficient is greater than this minimum. Using a smaller threshold value allows more matches, but it reduces the accuracy since some of the

matches will be false match points. A higher threshold value increases the accuracy, but it will result in fewer matches (ENVI, 2008).

As can be seen in Figure 5.11, the effect of minimum correlation is negligible because the difference between DEMs created with different minimum correlation values and that created using default values. Also, the results of a comparison of check points elevations with elevation interpolated from these DEMs are very similar (see Table 5.8). Therefore, the minimum correlation parameter is not consider and the best choice for user to leave it as default value.

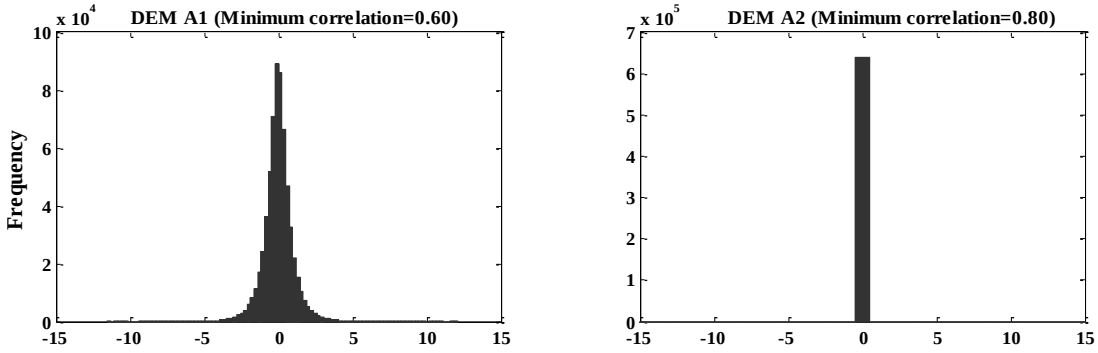

(A) (B)

Figure 5.11: Histograms of variation between default DEM and generated DEMs: A) DEM generated using a minimum correlation equal 0.60 and B) DEM generated using a minimum correlation equal 0.80.

Table 5.8: Summary of statistics comparison of ASTER derived DEMs using different minimum correlation against DGPS measured elevation.

DEMs	Mean (m)	Standard deviation (m)	RMSE (m)	Correlation
D	2.58	21.15	21.31	0.94
A1	2.58	21.14	21.30	0.94
A2	2.58	21.15	21.31	0.94
A3	2.58	21.14	21.30	0.94

Moving window size – this is the template window used for performing image matching. The moving window size defines the area in which the correlation coefficients between the two image templates are computed. A larger moving window size yields more reliable results. However, the results are less precise matching, and require more processing time to complete (ENVI, 2008).

Figure 5.12 shows that the differences between DEMs created with different moving window size and a DEM created with default size (5X5) is very similar. However, Table 5.9 gives summarises of comparisons between check points elevations and elevation extracted from DEM generated with different moving window size that shows a small improvement in accuracy with using the larger moving window size parameter than the default value. The means vary with a range of 0.41 m (2.58 to 2.17 m). The mean is greater with using small search window size while is a smaller with window 11x11 and tend to increase with large windows. The RMSE vary with a range 3.04 m (21.31 to 18.27 m). The RMSE values decrease with increasing search window sizes. The greater value is 21.31 m with 5x5 (Default size), while the smaller value is 18.27 with 15x15 (greater size).

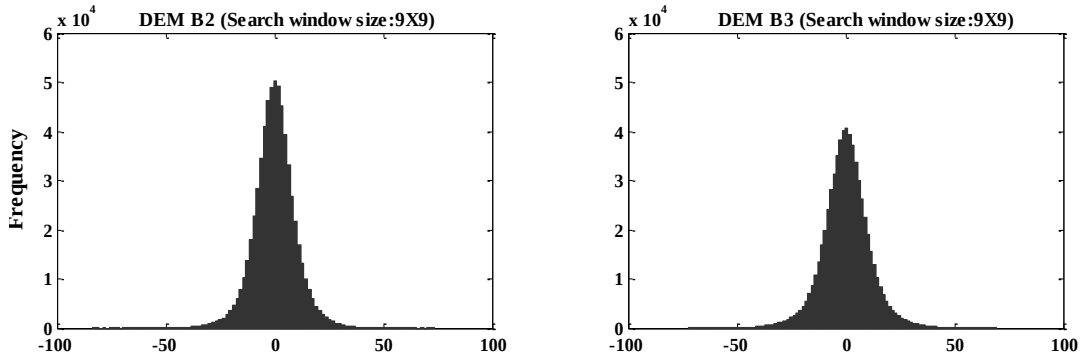

(A) (B)

Figure 5.12: Histograms of varitation between default DEM and generated DEMs: A) DEM generated using a moving window size 9x9 and B) DEM generated using a moving window size 11x11.

Table 5.9: Summary of statistics comparison of ASTER derived DEMs using different moving window size against DGPS measured elevation.

DEMs	Mean (m)	Standard deviation (m)	RMSE (m)	Correlation
D	2.58	21.15	21.31	0.94
B1	2.52	20.15	20.31	0.95
B2	2.23	19.47	19.59	0.95
B3	2.17	18.87	19.09	0.95
B4	2.29	18.38	18.53	0.96
B5	2.44	18.11	18.27	0.96

Terrain detail – The use of terrain detail determines how precisely is to be represented terrain in the DEM output by controlling the number of image pyramid levels used during the image matching. The levels range between 1 (minimum) and *N* (maximum), where *N* is determined by the epipolar image size. In Level 1, terrain the image matching stops after the coarsest level of image matching is finished. In Level *N* the image matching is performed at the epipolar image resolution, the highest image resolution possible. The processing time increases with level, but more terrain detail is represented in the output DEM (ENVI, 2008).

Figure 5.13 shows that the differences between DEMs created with different terrain detail level and DEM created with default level (level 3) is large. For example, the maximum and the minimum elevation difference between a DEM generated with default values and DEM generated with using level 2 as a choice for terrain detail parameter is between 115 and -98, while with using level 4 is between 50 and -50. Table 5.10 gives summarises of comparisons between check points elevations and elevations extracted from DEMs generated with different terrain detail level and shows that the big improvement in accuracy with using level 4 and level 5. Also, the processing time when using the higher level of terrain detail is longer than with lower

level. Therefore, terrain detail is a major controlling factor that determines the processing time needed to extract a DEM, as well as the accuracy of the output DEM.

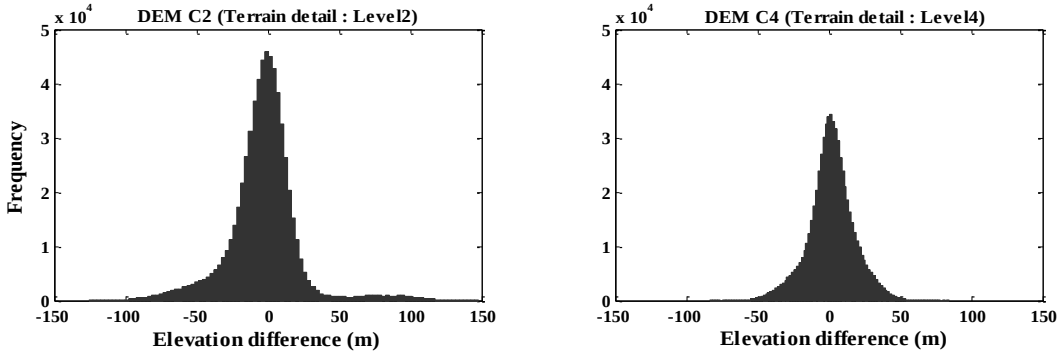

(A) (B)

Figure 5.13: Histograms of varitation between default DEM and generated DEMs: A) DEM generated using terrain detail Level2 and B) DEM generated using terrain detail Level4.

Table 5.10: Summary of statistics comparison of ASTER derived DEMs using different terrain detail level against DGPS measured elevation.

DEM	Mean (m)	Standard deviation (m)	RMSE (m)	Correlation
D	2.58	21.15	21.31	0.94
C1	4.41	50.27	50.46	0.39
C2	7.71	30.85	31.80	0.79
C4	0.32	14.55	14.56	0.97
C5	1.00	14.28	14.32	0.97

5.3.3 ASTER DEM post-processing

After automatic extraction of DEMs there is always a need for post-processing, since generated DEMs show blunders due to mismatching, missing data or cloud masking. Most software packages include standard procedures to edit generated DEMs, remove noisy pixels, and smooth the DEM (ENVI®, 2008). In this study, the post-processing

tools provided by the ENVI® software package were applied. The smooth method was applied to the DEM. Checking the quality of the resulting DEM, it appears that these post-processing procedures are sufficient. Table 5.11 gives summary statistics comparison of ASTER derived DEMs using different types of post processing (filtering) against DGPS measured elevation. Figure 5.15 a and b show histograms of ASTER DEM before and after post-processing. The final result of ASTER DEM is shown in Figure 5.16. The occurrence of underestimation is related to low image contrast inducing matching errors which increasing percentage of interpolation.

Table 5.11: Summary of statistics comparison of ASTER derived DEMs using different types of post processing (filtering) against DGPS measured elevation.

Type of processing	Mean	Standard deviation	RMSE	Correlation
Un processed	-2.82	14.10	14.38	0.9663
Smooth 3X3	-2.75	13.67	13.95	0.9686
Smooth 5X5	-2.70	13.42	13.69	0.9701
Smooth 7X7	-2.62	13.27	13.52	0.9709
Median 3X3	-2.80	13.83	14.11	0.9679
Median 5X5	-2.77	13.60	13.87	0.9693
Median 7X7	-2.69	13.41	13.68	0.9703

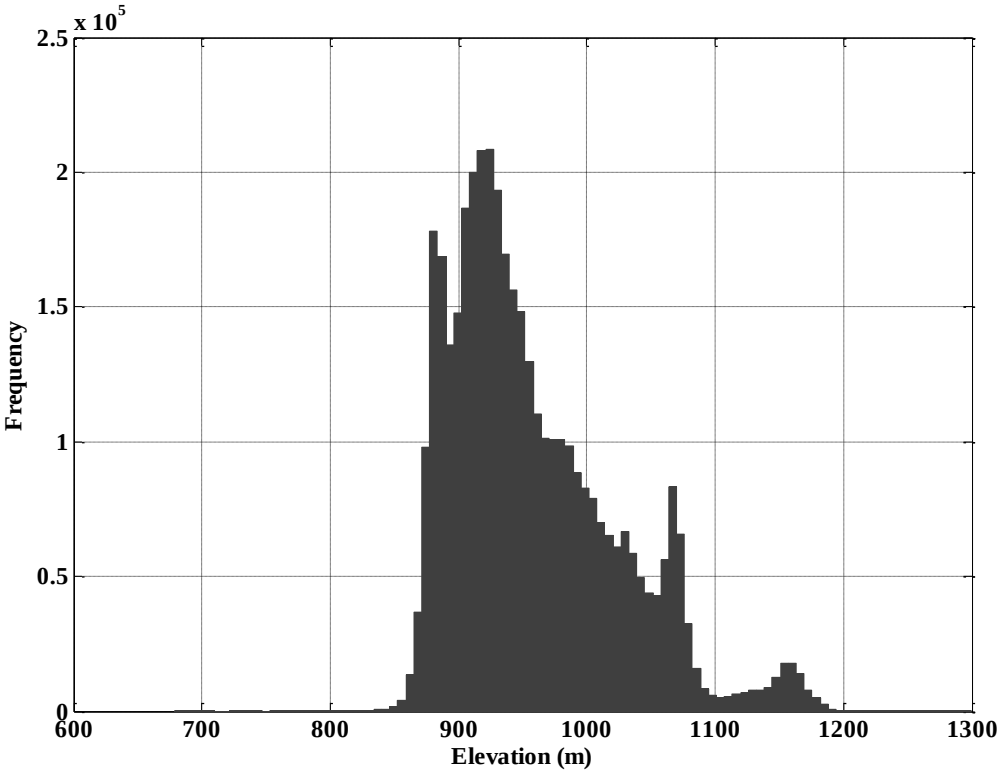

(a)

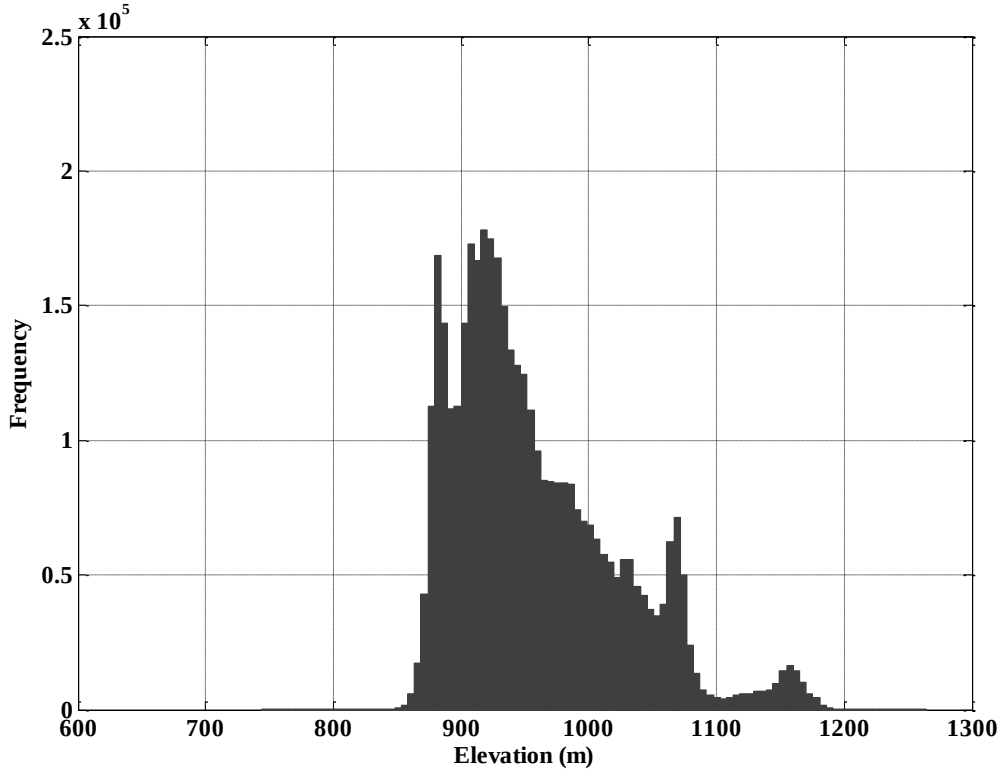

(b)

Figure 5.14: Histograms of ASTER DEM: (a) before post-processing, (b) after post-processing.

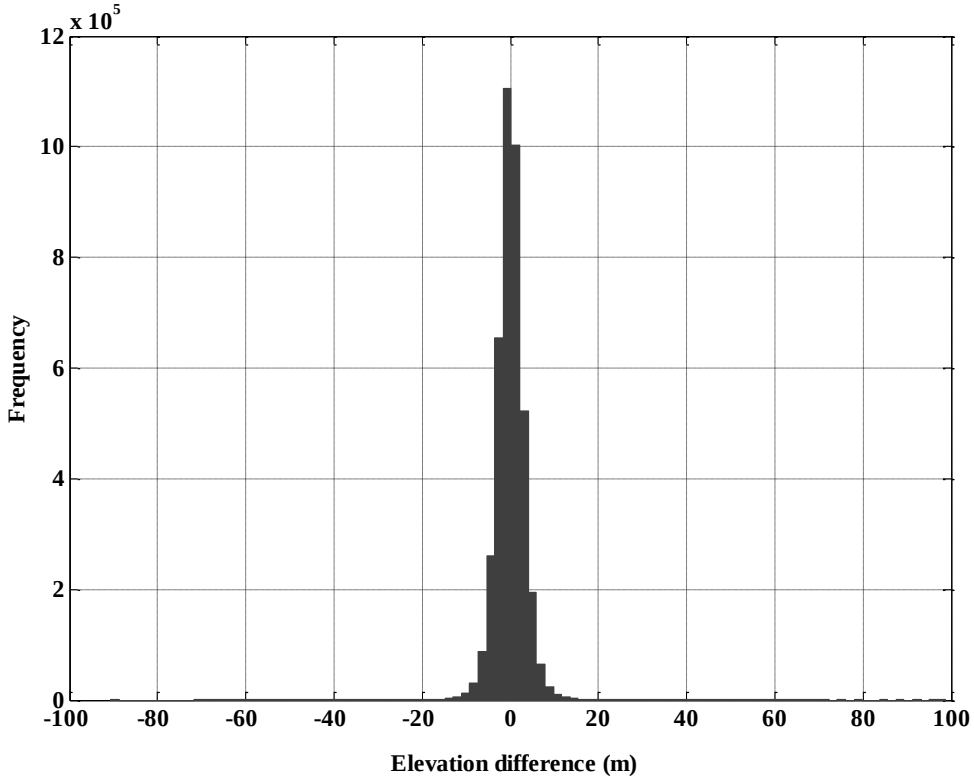

Figure 5.15: Histograms of elevation difference between ASTER DEM before and after post-processing.

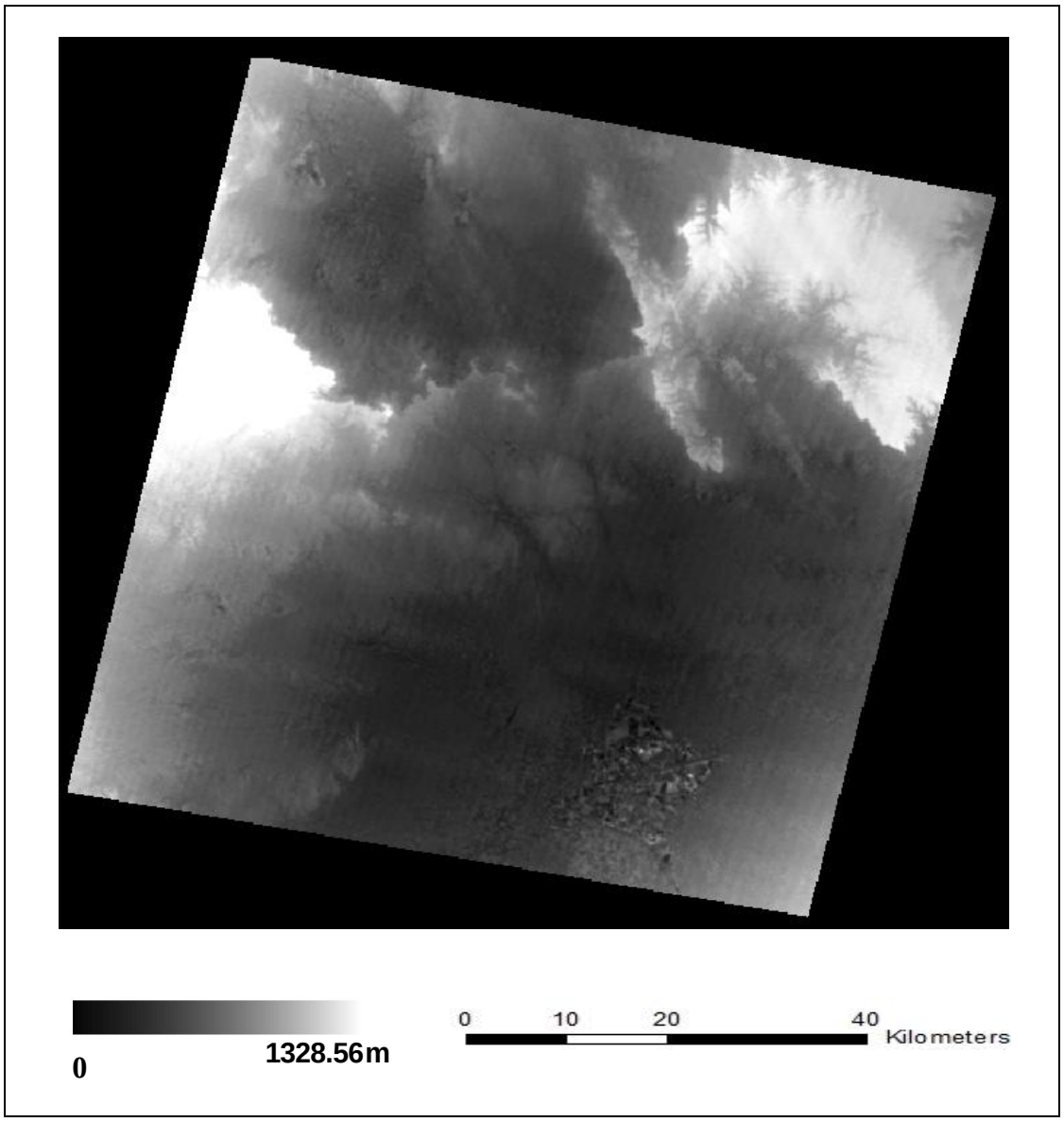

Figure 5.16: DEM derived from ASTER stereo image using ENVI® software.

5.4 Validation of the Topographic Map DEM

To investigate and validate the quality of the topographic map DEM, differential GPS (DGPS) techniques were adopted using a Leica GPS roving receiver with an external antenna attached and a Leica receiver as the base station. 28 DGPS points are used for this purpose (Table 5.12). The TopoMap elevations at the location of the DGPS points were extracted using ESRI ArcGIS® 9.2. The RMSE of the elevations extracted from the TopoMap DEM compared to the DGPS elevations is 10.08 m. The correlation computed shows a very high correlation of about 0.996 between the TopoMap DEM

elevation and DGPS elevation (Figure 5.17). However, it is noticed that a significant difference between both data sets can be seen with elevation collected on the main roads (points in red colour). The reason for that may be that the aircraft photo used to generate the topographic maps taken before the road built and the editing for these maps not take the elevation into account. Also, contour lines and spot heights give oversample elevation at certain heights, with no estimates of elevation between these heights. This means that there may be very little information about the terrain height in areas of low relief on which to base an interpolation. DEM derived using the interpolation techniques can smooth the surface more than the reality, for this reason the overall TopoMap DEM underestimated DGPS elevations.

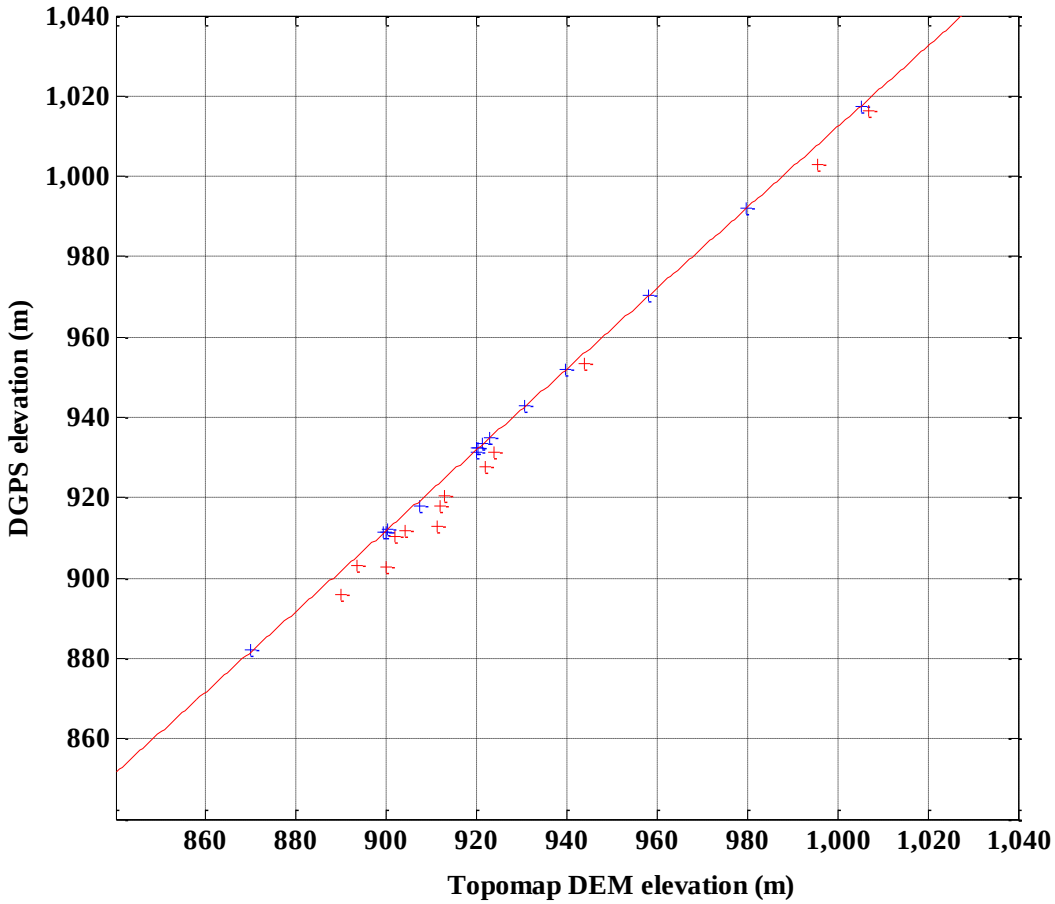

Figure 5.17: Correlation of elevations points from TopoMap DEM and DGPS.

Table 5.12: TopoMap DEM and DGPS statistical comparison.

No	DGPS elevation (m)	TopoMap DEM elevation (m)	Elevation difference (m)
1	1016.27	1006.90	-9.37
2	903.29	893.54	-9.75
3	895.78	889.84	-5.94
4	933.65	921.40	-12.25
5	912.31	900.27	-12.04
6	902.58	900.00	-2.58
7	917.77	907.32	-10.45
8	932.28	920.00	-12.28
9	991.95	979.65	-12.3
10	1017.46	1005.16	-12.30
11	1002.76	995.63	-7.13
12	970.39	958.07	-12.32
13	932.31	920.16	-12.15
14	920.37	912.86	-7.51
15	912.83	911.39	-1.44
16	882.27	870.00	-12.27
17	911.59	899.28	-12.31
18	931.49	923.99	-7.50
19	918.11	911.73	-6.38
20	911.62	904.07	-7.54
21	910.24	901.92	-8.32
22	927.63	921.97	-5.67
23	911.59	900.00	-11.59
24	953.39	943.83	-9.55
25	942.77	930.78	-11.99
26	934.80	922.79	-12.01
27	931.48	919.93	-11.55
28	951.96	939.63	-12.33
RMSE			**10.08**

5.5 Summary

This chapter showed the results of the generation of DEM from InSAR and ASTER data including details of each step of the process. Furthermore, it showed the result of validation of the TopoMap DEM against independent check points collected during the field survey using DGPS. System parameters that may affect the InSAR DEM result, such as baseline estimation methods and the accuracy of GCPs locations that were used in the calibration of the unwrapped phase, were addressed. ASTER DEM extraction parameters were examined to reach the best result.

Chapter 6: Accuracy Assessment and Comparison of DEMs

6.1 Introduction

In order to assess the accuracy of the DEMs derived from InSAR and ASTER data, reference data that represent the true height of surface are needed. Firstly, the accuracy of the DEMs was assessed against the DGPS elevation points collected during the field survey, which meant highly accurate data were available. Secondly, a comparison was made between these DEMs and DEMs derived from digitizing existing topographic maps. Visual analysis was used to assess the spatial distribution of the elevation difference resulting from this comparison. A third assessment was done using the stream network extracted from InSAR and ASTER DEMs against the stream network digitized from topographic maps. This comparison was needed to find how the difference in accuracy of different DEMs will affect the stream network results and will give the level of agreement between each other. In addition, the effect of DEM error on the surface flow and DEMs' resolution and error on topographic parameters was examined to evaluate the suitability of DEMs for hydrological modeling.

6.2 Accuracy Assessment of DEMs using Different Numbers of GCPs

Ground Control Points (GCPs) are used to establish an accurate relationship between a projected image, the sensor, and the ground. GCPs have a significant effect on the accuracy of the DEM extracted from InSAR data. Usually, the calibration step using GCPs results in a more accurate DEM when a greater number of GCPs are used. Selecting the location of these points is also important to obtain a good result. Poorly selected GCPs will seriously affect the accuracy of a DEM. Assessment of the accuracy of a DEM using a different number of GCPs was done against independent check points, as can be seen in Table 6.1. With increasing in GCPs used in the generation of the DEMs from 10 to 18 points, the difference between DEMs was the

largest difference. The RMSE for these DEMs was 8.39 and 6.95 m respectively. To assess the ASTER DEM accuracy regarding the number of GCPs used in DEM extraction processing, different numbers of GCPs (15, 30, 45, 60 and 75) and tie points (25) are used. The obtained results from both of the techniques show that the accuracy of the DEM can be increased by increasing the number of GCPs, as can be seen in Table 6.1. In addition, it can be seen that the number of GCPs used to create the ASTER DEM was more than the number of GCPs used to create the InSAR DEM this is due to the difficulty in locating GCPs in InSAR images as a result of noise and the lack of contrasting features.

Table 6.1: Summary of statistical parameters for elevation difference between DGPS checks points and InSAR and ASTER DEM elevations.

DEMs	InSAR DEM			ASTER DEM		
	No. of points	Mean error (m)	RMSE (m)	No. of points	Mean error (m)	RMSE (m)
1	10	-0.98	8.39	15	0.77	14.39
2	12	0.20	7.92	30	-2.39	14.25
3	14	1.15	8.06	45	0.65	14.22
4	16	1.03	7.94	60	-0.98	13.62
5	18	-0.93	6.95	75	-2.06	13.28

6.3 Accuracy Assessment of DEMs against GPS profiles

Accuracy assessments using different types of checkpoints were achieved using points that were collected using differential GPS (DGPS) techniques using Leica 500 GPS. This technique consists of the simultaneous operation of a fixed and a rover GPS station, the observations carried on a vehicle. The sampling rate is every 5 seconds, enabling the collection of large number of points along the track. This sampling rate allows a detailed description of the surface to be obtained, and is comparable with the pixel size of the DEMs produced from InSAR and ASTER data.

In this step of the accuracy assessment, a comparison was achieved by comparing the DGPS elevations profiles with the elevation data extracted from the DEMs. The elevation of each DGPS check point was compared with the elevation of the respective DEMs pixel. 5365 DGPS points spread over the study region with different elevations were used in this comparison. In ArcView, the DEM points were overlaid with the DGPS points, allowing the height difference of planimetrically similarly located points to be calculated. From the comparison between InSAR DEM elevation and kinematic profile check points, it can be noticed that about 95% of the elevation difference values were less than 15 m; 85% were less than 10 m; and more than 65% were less than 7 m. However, for the ASTER DEM, about 95% of the elevation difference values were less than 40 m; 75% were less than 25 m; and more than 50% were less than 15 m as can be seen in Figure 6.1. The maximum error was less than 61 m. This error in two set of data is consistent with results from previous studies (Hirano *et al.*, 2003; Cuartero *et al.*, 2005; Lee *et al.*, 2005; Kervyn *et al.*, 2008).

The absolute mean elevation difference (AMED) between the InSAR DEM elevation and DGPS elevations profiles was equal to 6.06 m with a standard deviation of 4.28 m, while the mean absolute value of the elevation difference between the ASTER DEM and the DGPS elevations profiles was equal to 17.11 m with a standard deviation of 12.09 m. The profiles show that the InSAR DEM is highly correlated with the DGPS survey data, while the profiles derived from the ASTER DEM have some variations. It is clear from these results that the DEM generated from InSAR images is more accurate than the DEM generated from ASTER images. In general, this assessment result reflected the relatively high accuracy of the height values contained in the DEMs at least in terms of the requirements of medium and small scale topographic maps (Al-Harbi and Tansey, 2008).

Table 6.2: Summary of statistical parameters for elevation difference between DGPS checks points and InSAR and ASTER DEMs elevations profile.

Statistical parameters	InSAR DEM	ASTER DEM
Minimum (m)	-20.46	-37.87
Maximum (m)	18.59	47.24
Mean error (m)	-1.12	-2.62
Standard deviation (m)	7.33	13.27
RMSE (m)	7.42	13.52
Correlation	0.99	0.97

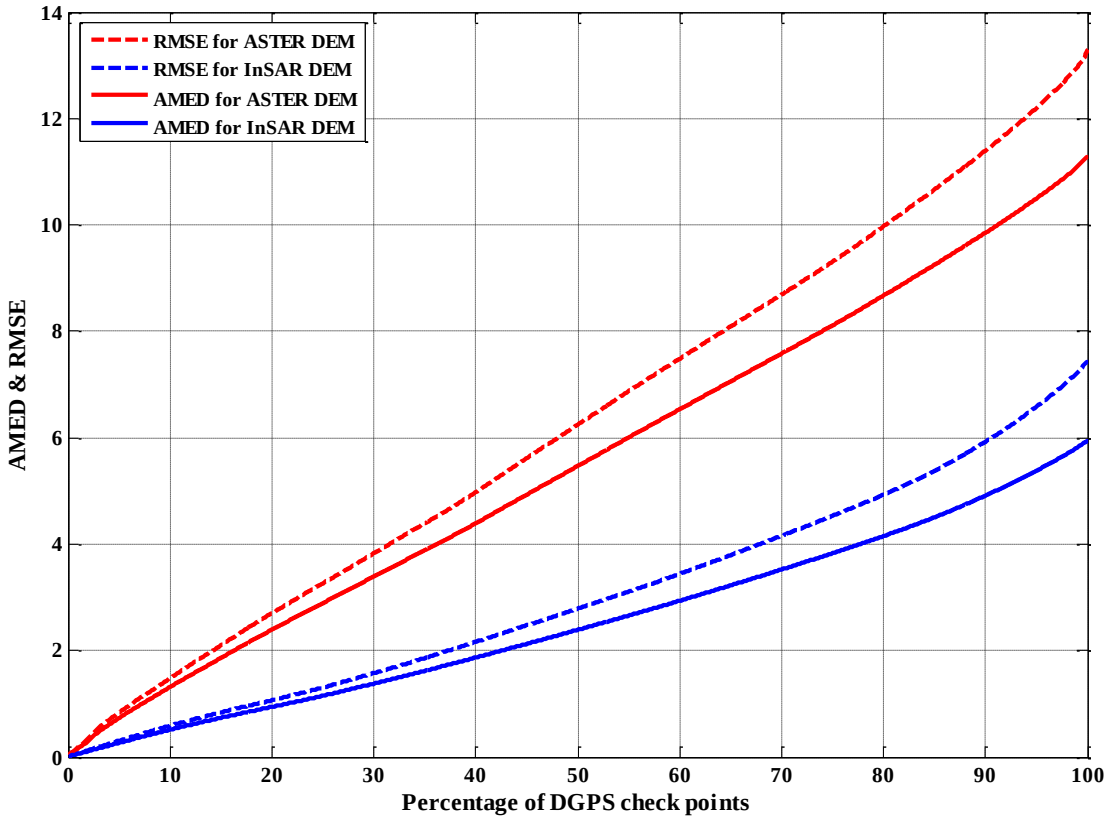

Figure 6.1: Cumulative RMSE and AMED values plotted against percentage of check points for both InSAR (blue) and ASTER (red) DEMs.

6.4 Accuracy Assessment using DEM Generated from Topographic Maps

6.4.1 Spatial correlation between DEMs

First, the descriptive statistics of both the DEM generated from InSAR and ASTER images and that generated from the topographic map (labelled as TopoMap DEM in the following images) were calculated. These statistics indicate that the closest results to the topographic map DEM were attained by the InSAR DEM (see Table 6.3) in statistical measures, such as the maximum and standard deviation, whereas the minimum, mean and median of ASTER DEM was slightly more successful. A probable reason for this difference could be the distribution of elevation values in the derived DEM. In order to find out the degree of relation between the TopoMap DEM and the two DEMs produced from the InSAR and ASTER data, spatial correlations were calculated. The correlation matrix computed shows a very high correlation of about 0.98 and 95% (Table 6.4) between the InSAR DEM, the ASTER DEM and the topographic map derived DEM respectively. Visual comparison between DEMs shown in Figure 6.2. Diagonal striping can be seen in the ASTER DEM. A revision of the processing steps of creating the DEM and the original image did not reveal the reason for this. Histograms of the ASTER and InSAR data show very different trends at 1050 m. This difference is due the error in the creation of the ASTER DEM, which was concentrated on a high elevation area. In addition, this result shows that the ASTER DEM is more sensitive than the InSAR DEM; this is because the spatial resolution of the ASTER image is higher than that of the InSAR image.

Table 6.3: Descriptive statistics of InSAR, ASTER and the TopoMap DEMs.

DEMS	Minimum (m)	Maximum (m)	Mean (m)	Median (m)	Standard deviation
InSAR DEM	864.95	1107.15	938.69	937.34	34.53
ASTER DEM	861.89	1162.70	933.34	926.32	43.00
TopoMap DEM	862.75	1078.30	929.49	927.07	30.81

Table 6.4: The correlation matrix computed for InSAR, ASTER and TopoMap DEMs.

DEMs	InSAR DEM	ASTER DEM	Topomap DEM
InSAR DEM	1	0.97	0.98
ASTER DEM	0.97	1	0.97
TopoMap DEM	0.98	0.95	1

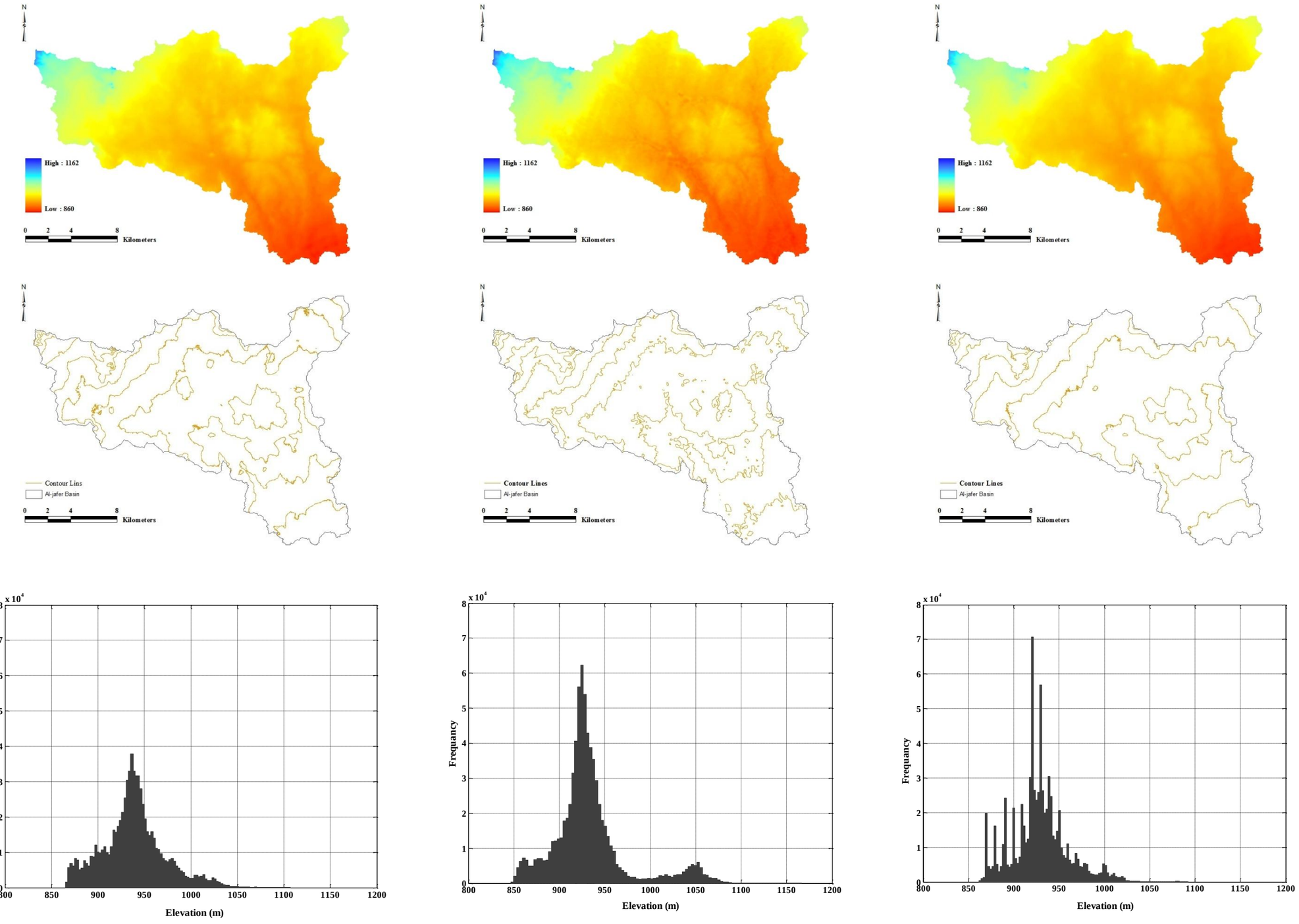

(a) (b) (c)

Figure 6.2:Visual comparison between (a) InSAR DEM, (b) ASTER DEM and (c) TopoMap DEM.

6.4.2 Difference images

Difference images are widely used to visualize the spatial distribution of error between a DEM and a particular reference. Elevation accuracy for TopoMap DEM is expected to be equal to one thirds of elevation differences between contour lines. Since the contour interval is 20 m in 1:50,000 scaled maps, the accuracy of the TopoMap DEM is assumed to be 7 m, which is acceptable using for the accuracy assessment of the elevations calculated from InSAR and ASTER stereo images. In this case, the InSAR and ASTER DEMs were compared with the topographic map DEM, pixel by pixel, by creating a difference image, which was derived by subtracting the reference DEM from the DEMs. The resulting values in the new raster indicate the difference in elevation at each pixel, which could be further analyzed statistically for minimum, maximum, and standard deviation and so on. But it should be taken into consideration that the TopoMap DEM used was generated by digitizing contours from topographic maps and interpolated to create a raster DEM. Therefore, the difference at each pixel refers to the error with the interpolated DEM and that may be an error with the topographic map derived elevations. For this reason, a comparison is made of height points collected using a differential global positioning system (DGPS) or from spot heights (on topographic maps) gives a more reliable picture at selected points. Also, the difference image is analyzed to obtain positive numbers for cases in which the DEM overestimates the elevation and negative numbers for those cases in which it underestimates the elevation:

$$\Delta Z = Z_{\text{InSAR / STER}} - Z_{\text{Reference}} \qquad (6.1)$$

where:

ΔZ is the elevation error,

$Z_{\text{InSAR / STER}}$ is the elevation of the InSAR DEM and

$Z_{\text{Reference}}$ is the elevation of the reference DEM at a particular location

Table 6.5 shows the basic statistics of the difference image with an absolute elevation difference of 9.20m and 3.76m and the relatively high Root Mean Square Error (RMSE) of 11.50m and 16.03m for InSAR and ASTER DEMs respectively. The images and histograms of the elevation difference are shown in Figure 6.3. From elevation difference images shown in Figure 6.4, it seems that the majority of the underestimation area is located in a low relief site while the overestimation area is located in a relatively high relief site. More than 90% of the test area is overestimated. The DEM generated from the topographic maps was smoother than the DEMs generated from the InSAR and ASTER data. This may be due to the absence of adequate samples to interpolate between contour lines, which lead to an overestimation in most areas for InSAR and ASTER DEMs. In addition, the TopoMap DEM was produced by digitizing the contour lines of 1:50,000 scale maps and represents the form of the surface without vegetation and buildings. Furthermore, it can be seen from the histograms for the InSAR and ASTER DEMs in Figure 6.3 that the deviation with the TopoMap DEM was within ±25 m except in small high elevation areas in the ASTER DEM, which caused significant errors. For this reason, the mean error of the image difference between the ASTER and the TopoMap DEMs is less than the mean error of the image difference between the InSAR and TopoMap DEMs.

Table 6.5: Descriptive statistics of InSAR and ASTER DEM relative to TopoMap DEM.

Statistical parameters	InSAR-TopoMap	ASTER-TopoMap
Minimum (m)	-12.05	-32.33
Maximum (m)	62.27	84.57
Mean error (m)	9.20	3.76
Standard deviation (m)	7.16	14.82
RMSE (m)	11.66	15.29

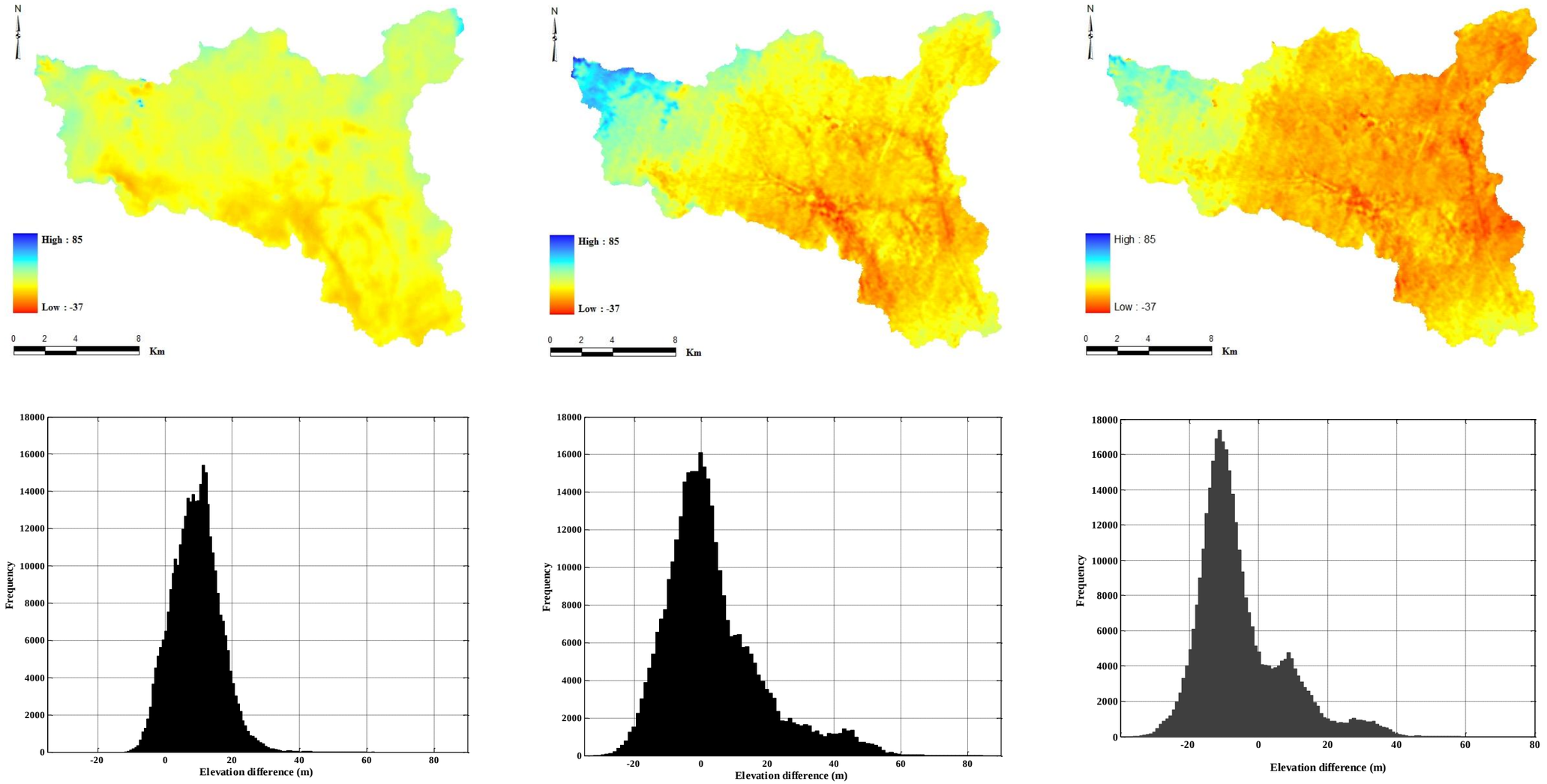

Figure 6.3: Image elevation difference and histograms between (a) InSAR DEM and TopoMap DEM, (b) ASTER DEM and TopoMap DEM, (c) InSAR DEM and ASTER DEM

The elevation differences obtained by subtracting the topographic map DEM from InSAR and ASTER DEMs can be classified depending on the value of the difference. This allows the study of the distribution of error, pixel by pixel, and helps in identifying the part of the test site with the greatest magnitude of error. From this, the factors causing the error can also be identified. From Figure 6.4, it can be seen that the RMSE is less than 10 m for approximately 90% of the InSAR and ASTER DEMs. Also from this figure, it can be said that about 95% of ASTER DEM pixels are more correlated to TopoMap DEM than pixels in InSAR DEM. In general, the RMSE for both DEMs increase gradually as the number of pixels increase. This indicates that the error is distributed uniformly throughout the area, which is clear in the InSAR DEM. In the ASTER DEM, the RMSE increases sharply from about 7 m to about 16 m in about 8% of the study area. Most of this is located in high relief areas and the rest, in very low areas, such as valleys.

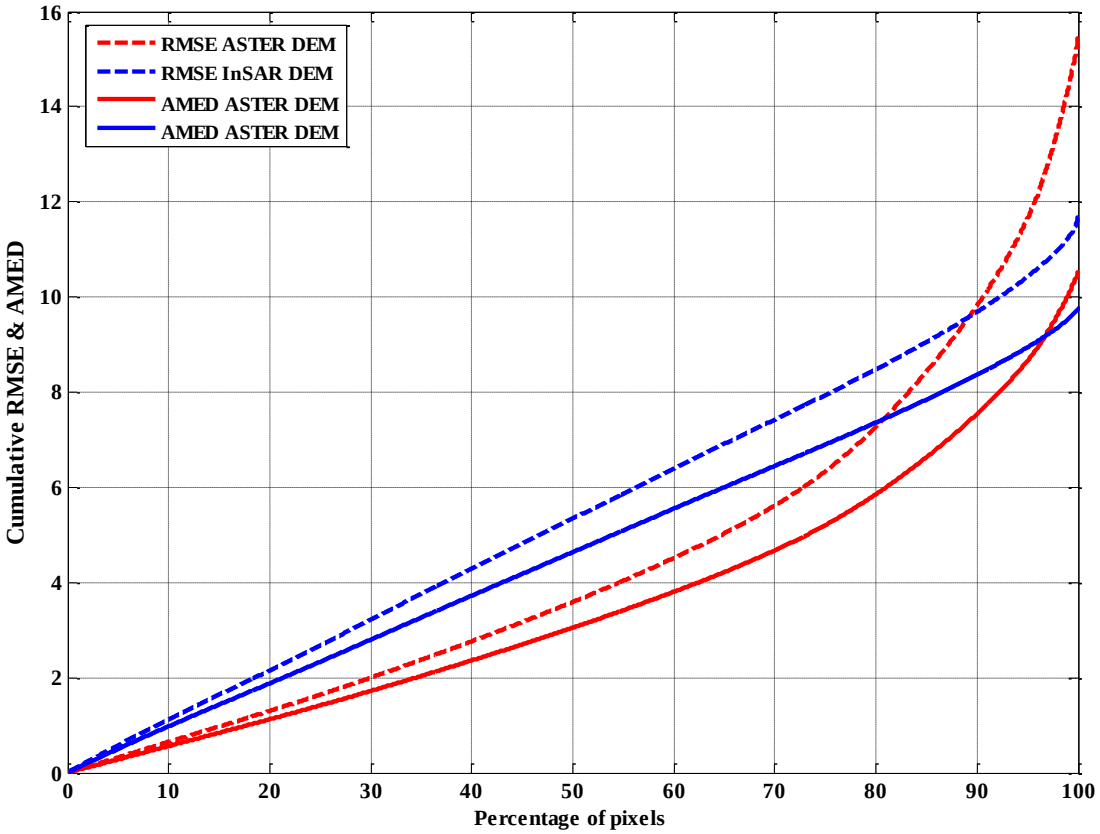

Figure 6.4: Cumulative RMSE and AMED values plotted against percentage of pixels.

Visual analysis can help to assess the spatial distribution of error in the DEM using the image of elevation difference. Elevation difference mapped in ArcGIS software was used to quantify spatial distribution in different parts of the test site. Elevation difference was divided into six classes as shown in Figures 6.5 and 6.6. As seen in Figure 6.5, for the InSAR DEM, most of the elevation difference in class 1 is located in low and medium relief parts of the test site. However, most of the pixels in class 6 which have high elevation differences are located in high relief parts of the test site and are few in number. The pixels in class 1 covered about 60% of the test site in both images. From Figure 10, elevation difference in class 5 and 6 for the ASTER DEM are located in highest elevation area in test site. Class 1 covers about 70% of the area.

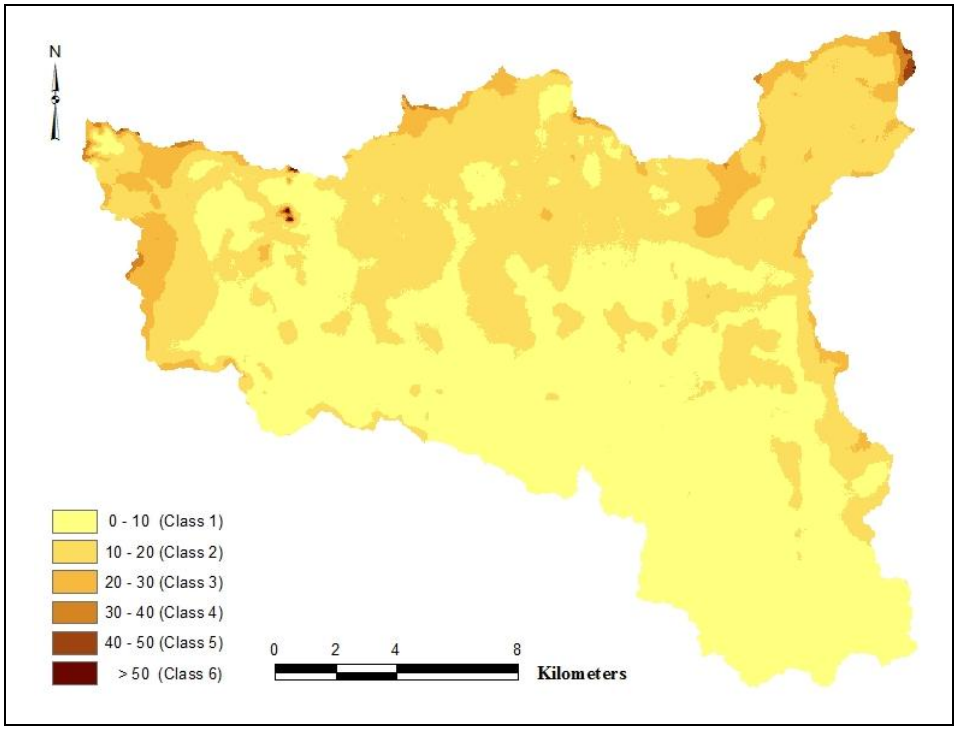

Figure 6.5: Spatial distribution of absolute elevation difference between InSAR DEM and DEM generated from topographic maps.

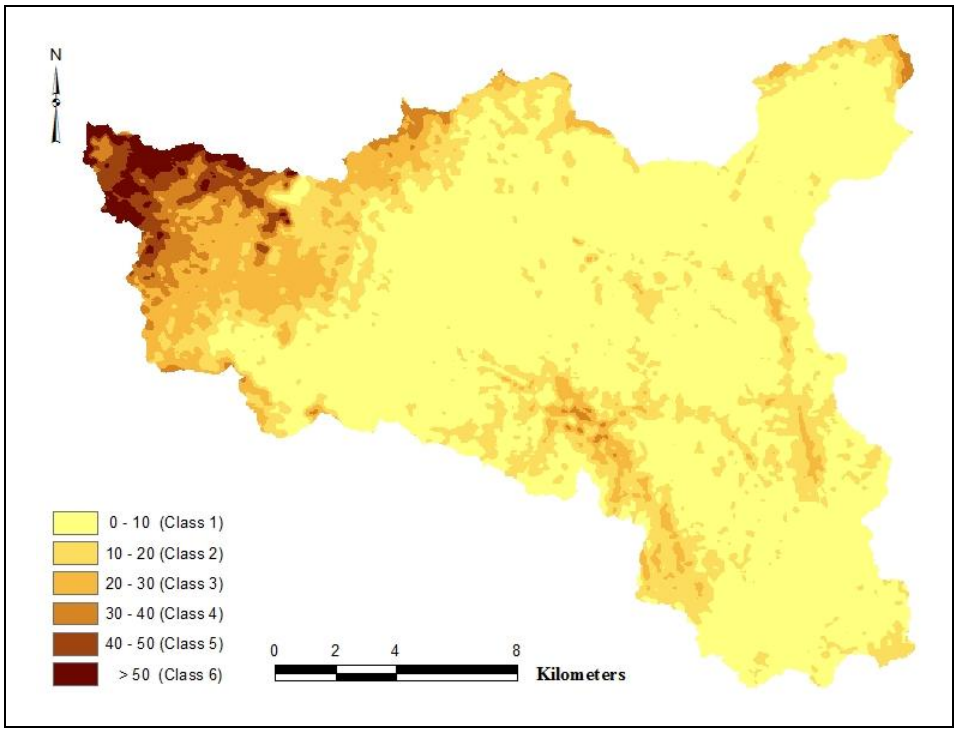

Figure 6.6: Spatial distribution of absolute elevation difference between ASTER DEM and DEM generated from topographic maps.

6.4.3 Spatial profiling of elevation

After the visual and statistical analysis, profiles were drawn for the InSAR, ASTER and TopoMap DEMs. Figure 6.7 shows the locations of a subset of an elevation profile along a west – east and north – south transect for the test site for all DEMs. From the image difference in the previous section, it was seen from a statistical comparison that the elevation difference between these DEMs was less than 20 m for approximately 95% of the study area and less than 30 m for approximately 99%. From comparing the profiles, both from north to south and from west to east, it is noted that the greatest elevation difference in profiles from north to south was more than that from west to east in a region with high elevation and medium elevation, while it was less in the region with low elevation. This demonstrates that the type of terrain plays a very important role in the accuracy of the DEMs. As can be seen in the profiles in Figures 6.8 and 6.9, small scale features that were located at 11 km in the figures were not visualized in profiles; this feature is represented in the map as a small circle of contour and its peak is represented as a spot height in the middle of circle. The interpolation process used to create the DEM from contour line and spot heights may cause smoothing that resulted in hiding the peak of this feature.

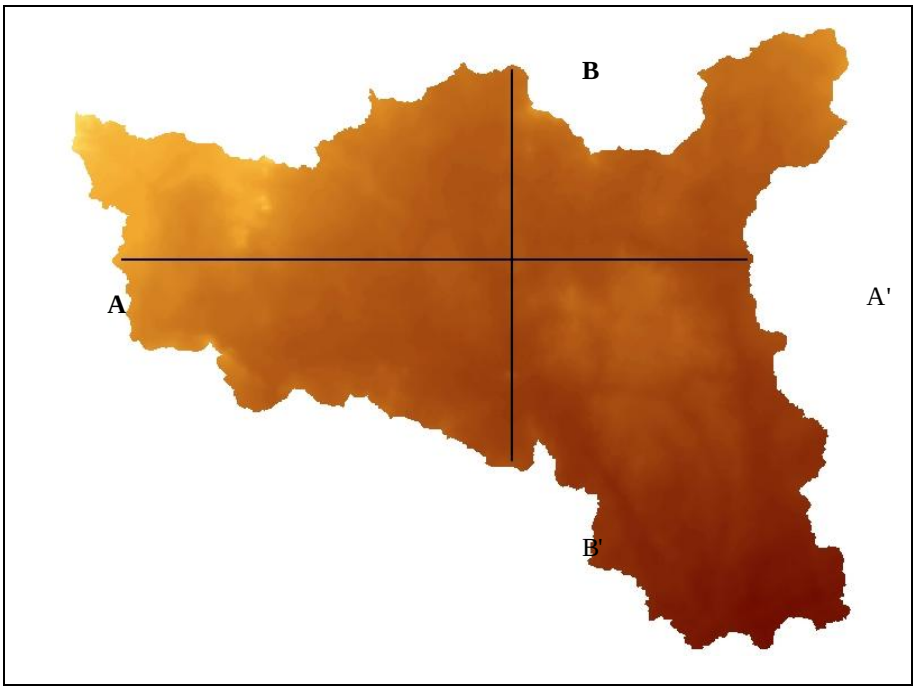

Figure 6.7: Elevation profiles in north-south and east-west directions.

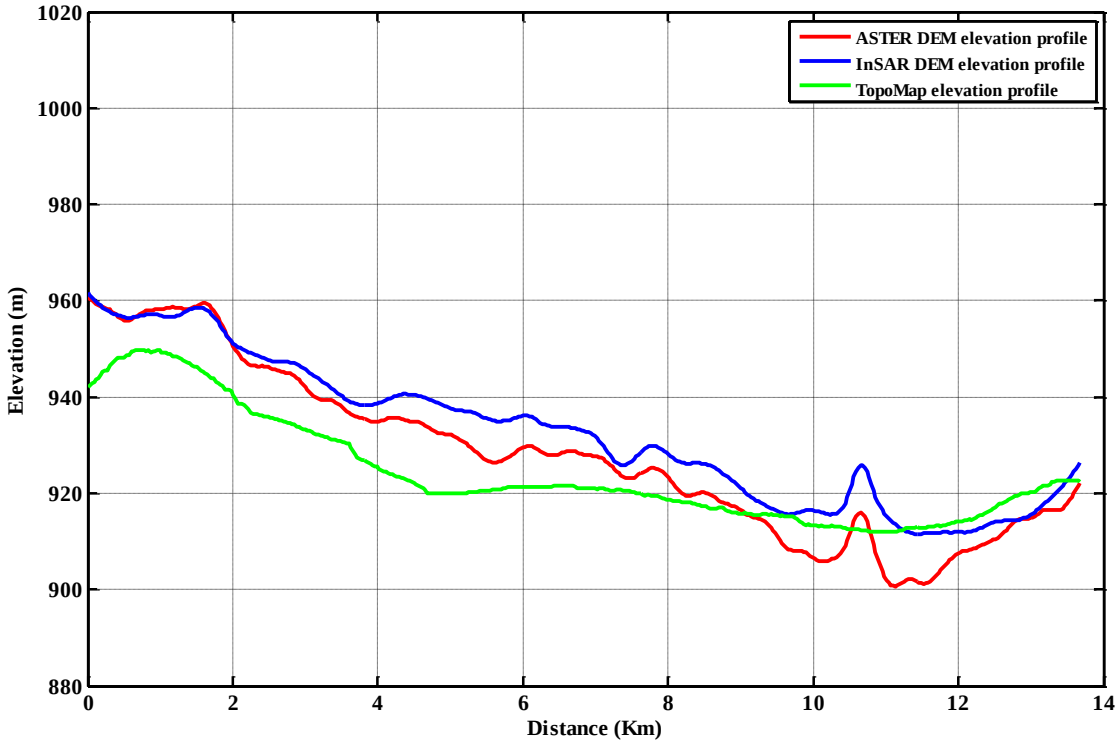

Figure 6.8: Elevation profiles in a north-south direction.

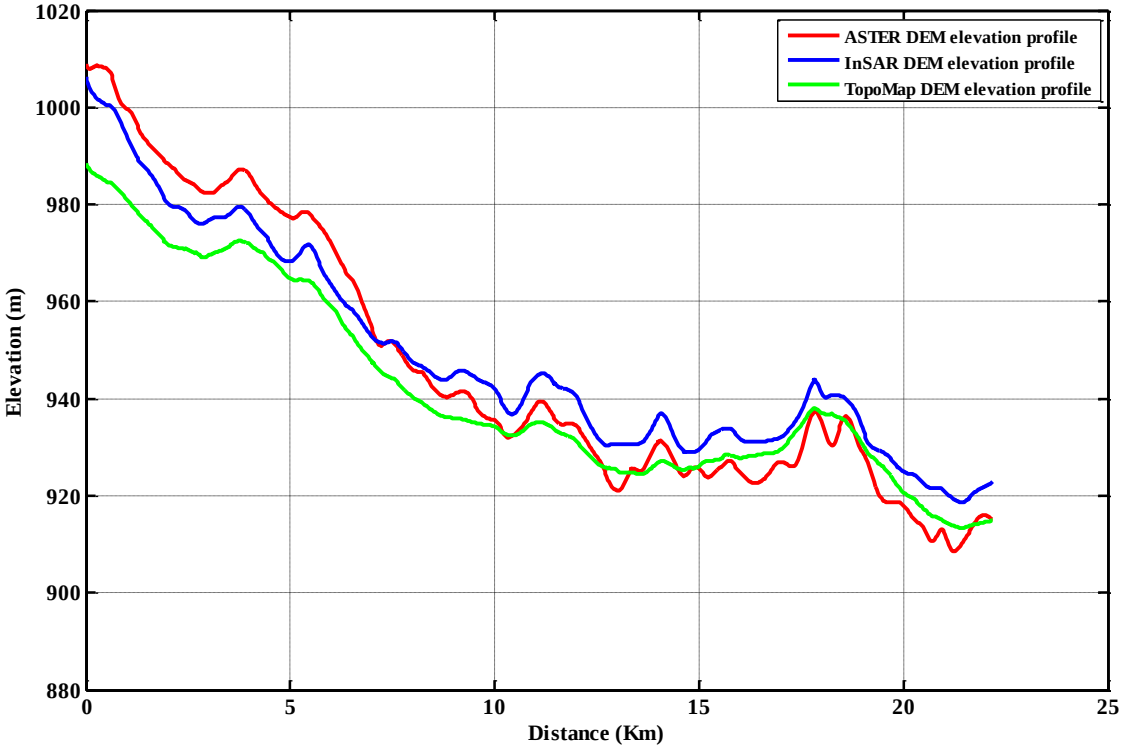

Figure 6.9: Elevation profiles in a west-east direction.

6.5 Comparison of Stream Networks

DEM error is often described in terms of the metric accuracy of elevation values. However, many applications of DEMs, such as generation of drainage networks using standard flow direction methods (Jenson and Domingue, 1991), rely on an accurate representation of surface shape rather than accurate elevation values, in such applications, it is more important for the slopes and valleys to be represented accurately, even if the error values are consistently lower or higher (Arrell *et al.*, 2008). Different methods have been developed to process raster DEMs to extract stream networks automatically (O'Callaghan and Mark, 1984; Band, 1986; Jenson and Domingue, 1988; Martz and Garbrecht, 1992, 1998, 1999). The most commonly used procedures for extracting stream networks from raster DEMs are based on O'Callaghan and Mark's (1984) algorithm for flow direction determination using a deterministic eight neighbours (D8) method on the basis of single flow within the different GIS softwares. In this section, the flow networks derived in ArcGIS and DIGEM versus the stream network digitized from the topographic maps.

The first step in extracting a stream network from DEM is filling in depressions or sinks. Sink-filling algorithms, which were used in this study, ensure that all DEM pixels route the flow of water towards a common outlet by filling anomalous elevation sinks. O'Callaghan and Mark (1984) observed that filling is seldom required on a sloping terrain, but is common in flat areas where the low signal-to-noise ratios generate sinks that frequently represent elevation errors. Sinks can be excluded from sink filling by setting the elevation limit. All sinks less than the elevation-limit and lower than their lowest adjacent neighbour filled to the height of their pour points. Then, flow direction was calculated using the filled DEM. After that, flow accumulation was calculated from the flow direction grid. Each pixel was assigned a value equal to the number of pixels drained through a given pixel in the flow accumulation. The stream network was extracted by considering the pixels greater than a threshold given. Threshold choice is an assumed constant value based on personal judgment or on a visual comparison of the networks generated with the streamlines identified or digitized from a topographic map (Jenson and Domingue, 1988; Li *et al.*, 2006). The stream threshold operation will identify all the cells in the flow

accumulation that are greater than the provided threshold. Higher thresholds will result in a less dense network and fewer internal subwatersheds, while lower thresholds will result in a denser network and more internal subwatersheds.

The stream networks derived from the InSAR DEM and ASTER DEM (Figure 6.10 and 6.11 using ArcGIS and Figure 6.12 and 6.13 using DIGEM) were assessed against the reference drainage network drawn and digitized from the 1:50,000 topographic maps (Figure 6.14) and against each other. The stream ordering (Strahler, 1964) was also computed for both networks. Quantitative comparisons were made between them, as can be seen in Table 6.6 and 6.7. These comparisons show that the total stream length derived from ASTER is more than the total length from InSAR and TopoMap by about 3% and 26% using ArcGIS and about 19% and 84% using DIGEM respectively. The large differences in the length of streams between those derived from DEMs and those digitized from topographic maps may result from the map scale or the level of detail about stream networks that can be digitized from maps.

In contrast, the catchment area in InSAR was larger than in ASTER by about 2% and 0.6% using ArcGIS and DIGEM respectively. In general, there are no large differences in the catchment areas extracted from DEMs and the catchment areas digitized from topographic areas for the Al-Jafer basin. Higher resolution DEM (15 m in the ASTER image) tends to generate a slightly smaller catchment area than a lower resolution DEM (25 m in InSAR image) (Usery *et al.*, 2004). The stream density in ASTER was greater than the stream density in InSAR and TopoMap. This may also be due to the resolution of the ASTER image. Checking the elevation of the disputed areas between two stream networks (Figure 6.15 and Figure 6.16) showed that they seemed to be very flat areas with small variations in slope, meaning that the error was most likely to be in this area. In addition, it is certain that the higher resolution of the ASTER DEM (15 m) will cause the stream network to be more irregular and thus longer. Also, the results of this set of comparisons shows that there are indeed some differences between the two softwares, DIGEM seems to be more computationally efficient in term of time processing. ArcGIS takes unacceptable time to fill the sinks, especially in the case of

high resolution DEM. In the other hand, DIGEM gives user more parameters to increase the ability to generate more accurate and smother stream networks.

Table 6.6: Quality assessment of DEMs on the basis of stream network.

DEMs	Total stream length, km	Max stream length, km	Catchment area, km²	Stream density, m/km²
Stream network derived using ArcGIS				
InSAR	257.43	7.25	305.35	843.07
ASTER	265.10	8.38	299.32	885.67
Stream network derived using DIGEM				
InSAR	304.26	13.39	302.56	1005.62
ASTER	361.03	12.47	300.76	1200.39
Stream network digitized from topographic maps				
TopoMap	196.45	-------	300.22	654.35

Table 6.7: Description of DEMs on the basis of total stream length.

DEMs	Stream order				Total stream length, km
	1(m)	2(m)	3(m)	4(m)	
Stream network derived using ArcGIS					
InSAR	142.81	64.25	42.36	8.01	257.43
ASTER	156.58	55.56	48.67	4.29	265.10
Stream network derived using DIGEM					
InSAR	186.86	57.54	46.16	13.70	304.26
ASTER	241.26	68.15	39.90	11.72	361.03

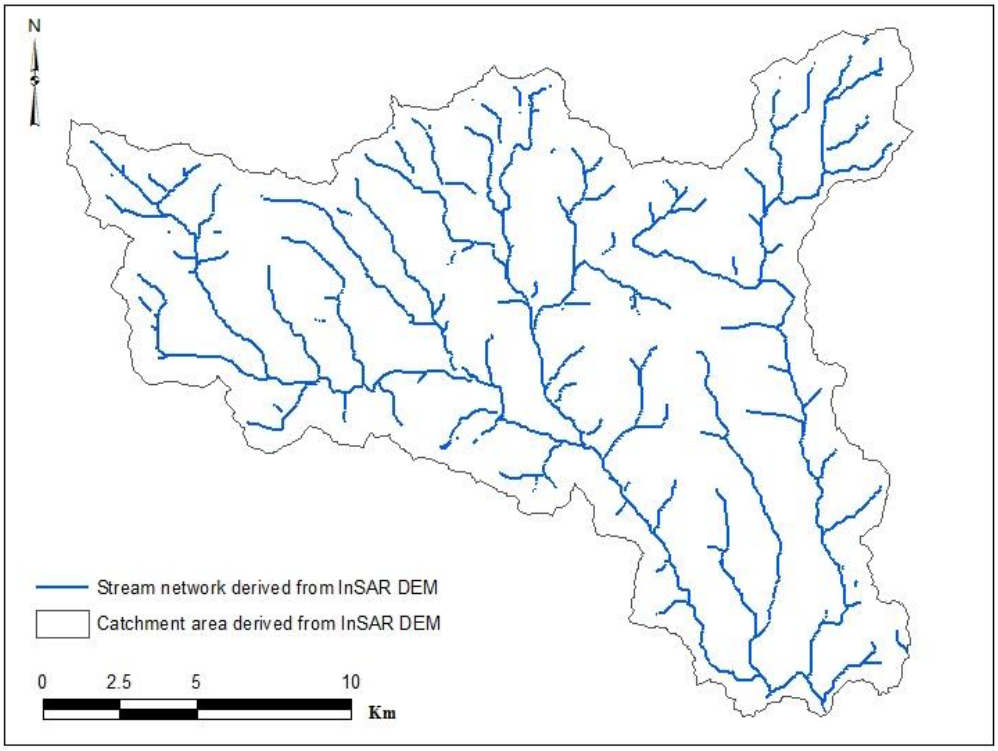

Figure 6.10: Accumulated stream network derived from InSAR DEM using ArcGIS.

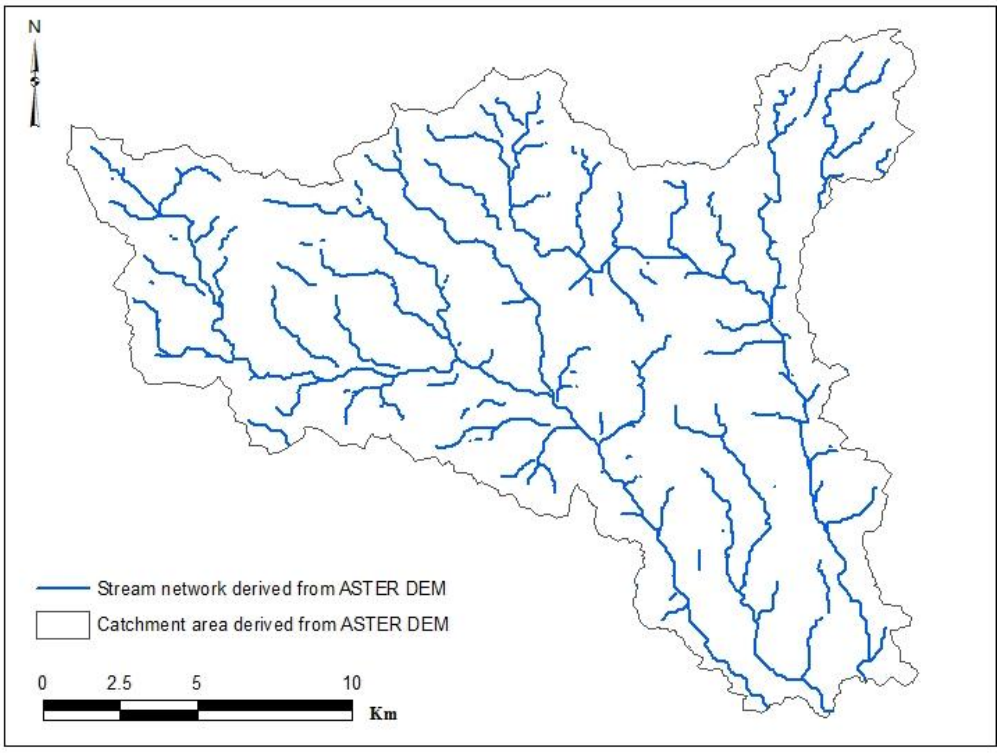

Figure 6.11: Accumulated stream network derived from ASTER DEM using ArcGIS.

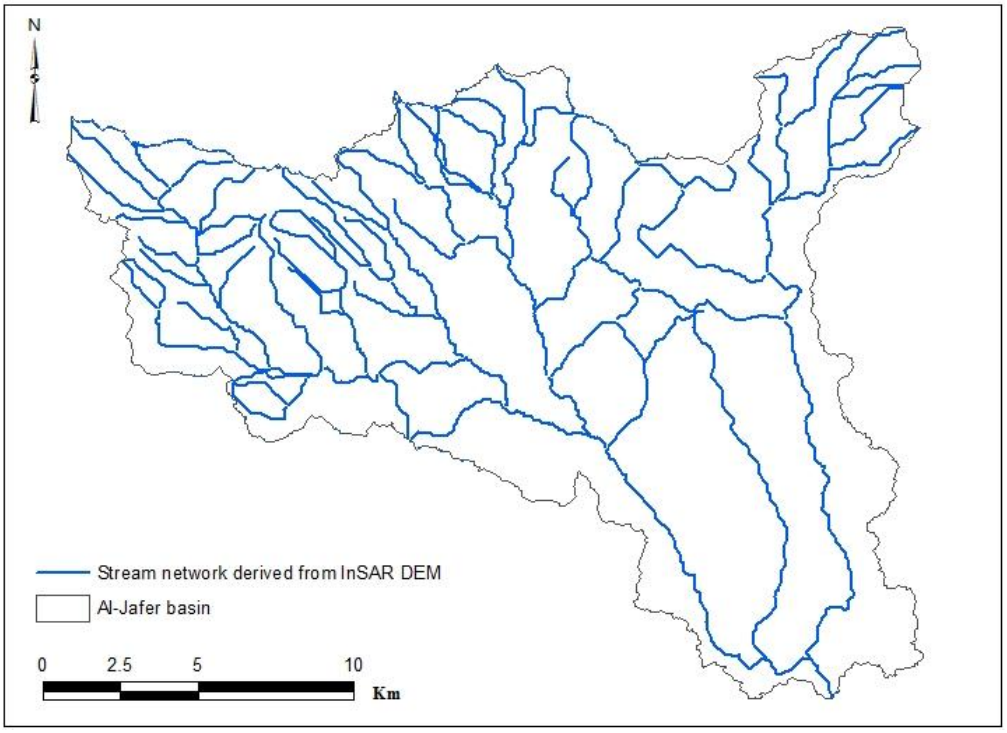

Figure 6.12: Accumulated stream network derived from InSAR DEM using DIGEM.

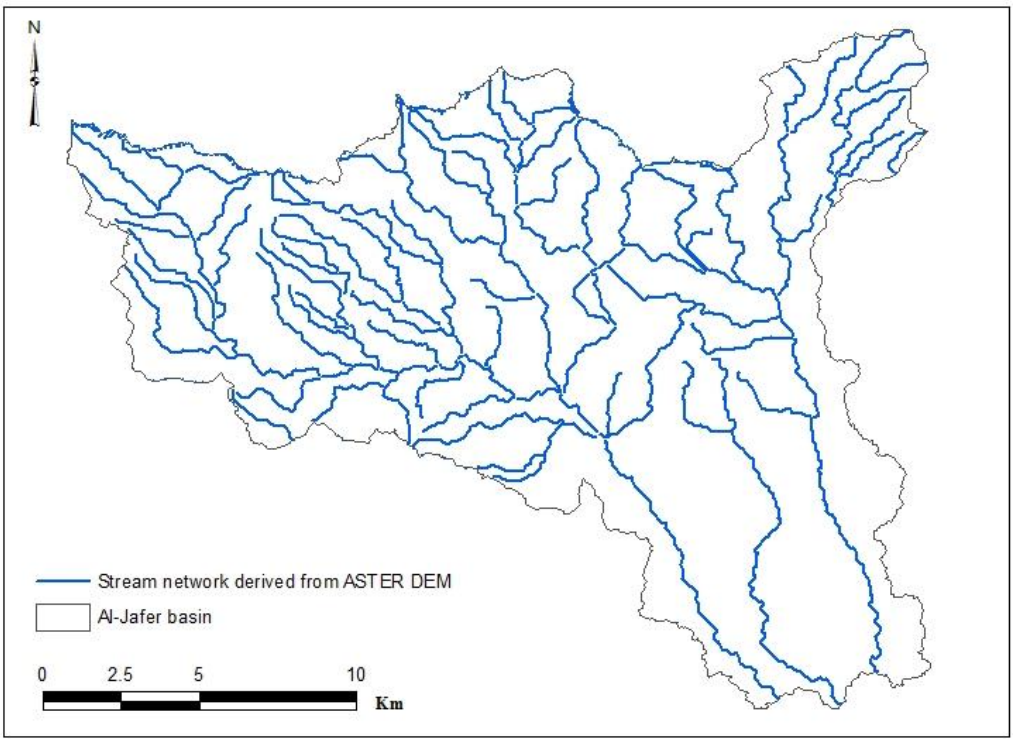

Figure 6.13: Accumulated stream network derived from ASTER DEM using DIGEM.

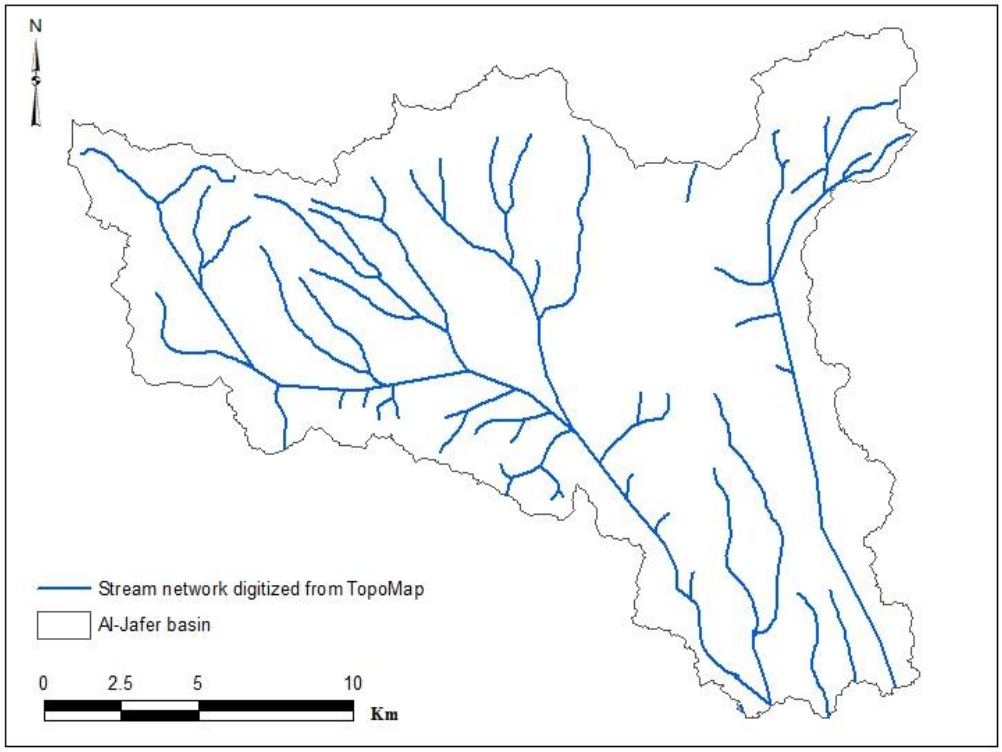

Figure 6.14: Accumulated stream network digitized from topographic maps.

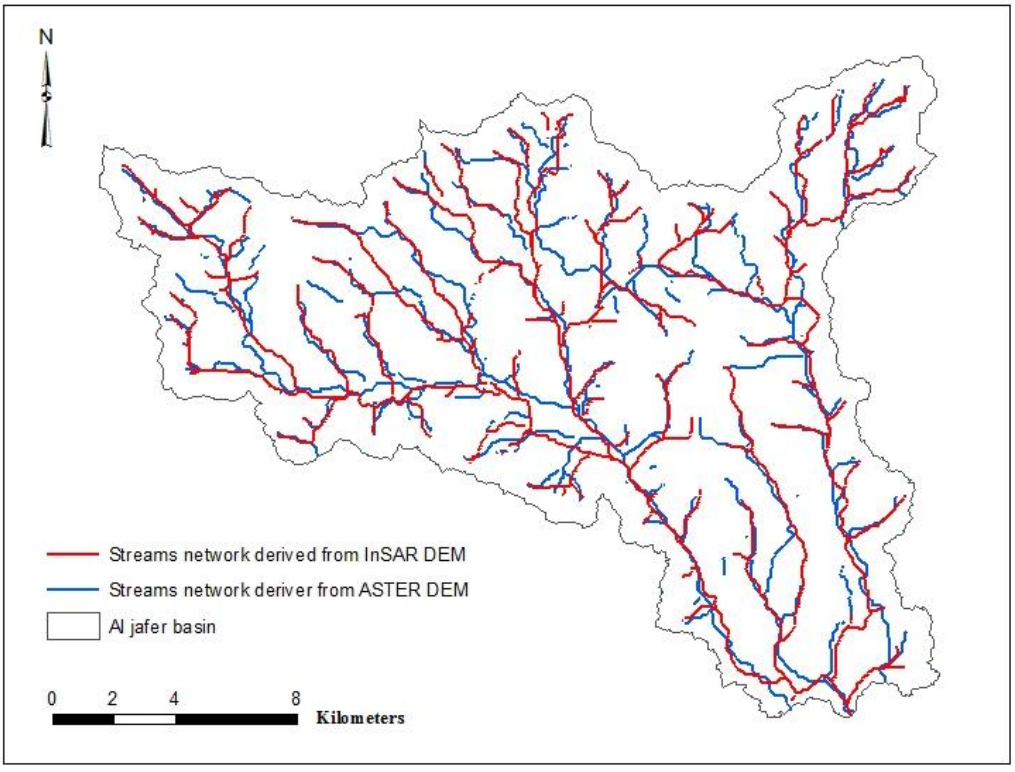

Figure 6.15: Accumulated stream network comparison from InSAR and ASTER sources using ArcGIS.

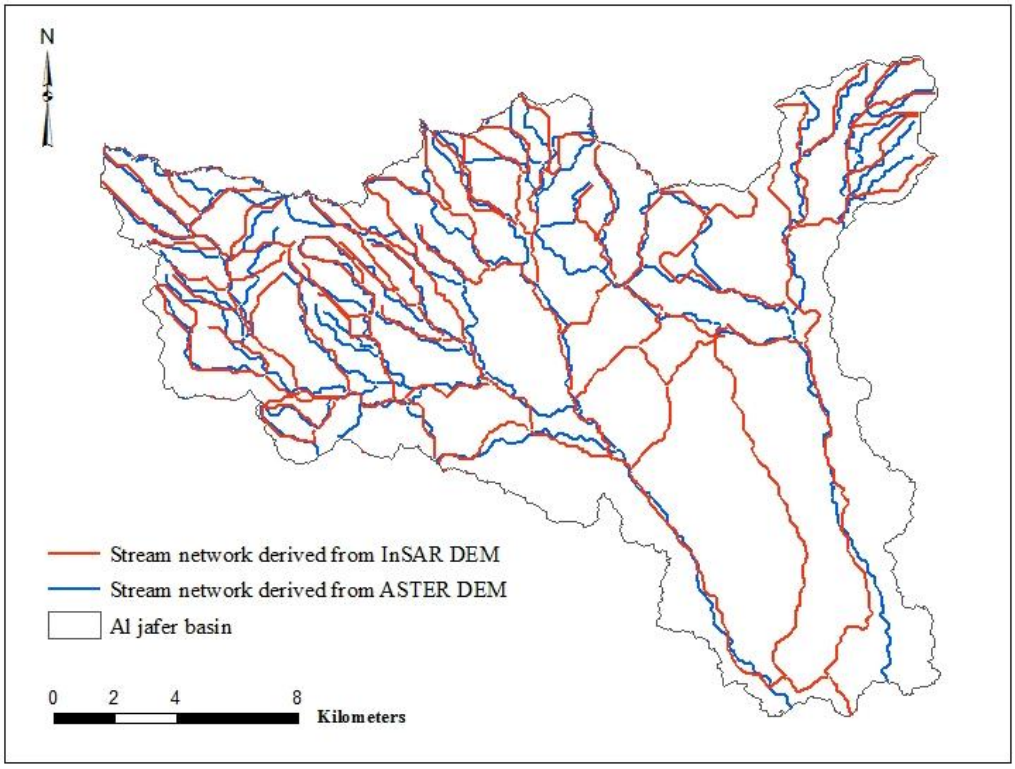

Figure 6.16: Accumulated stream network comparison from InSAR and ASTER sources using DIGEM software.

6.6 Distribution of Elevation Difference with Elevation and Slope

Topography has the greatest effect on DEM accuracy quantity. The effect of topography on the spatial distribution of elevation difference was assessed by comparing the elevation difference with elevation and slope. To evaluate the accuracy of the InSAR DEMs in relation to topographic features, terrain slopes was computed with a 3x3 window. Figure 6.17 shows the variation of the mean elevation difference with elevation and slope. It can be noticed that there is no significant correlation between elevation difference and elevation derived from the InSAR DEM while there is some correlation with elevation derived from ASTER DEM, the elevation difference tends to increase as elevation increases and the highest elevation difference can be noticed only with the highest elevations. This may be due to the concentration of the largest error in the ASTER DEM being in a high elevation area caused by mismatching during the processing steps. In addition, the spatial resolution of the ASTER image (15 m) can cause more variability in the surface, which can affect the slope value clearly with the area of increasing elevation. In addition, the higher elevation area normally

suffers from a lacke of number of precise locating GCPs and TPs which cause dissimilarity between the two images leading to matching failures. However, the elevation difference tends to increase with an increase in the slope derived from the InSAR data. Furthermore, with the highest slope, only positive difference elevations are present.

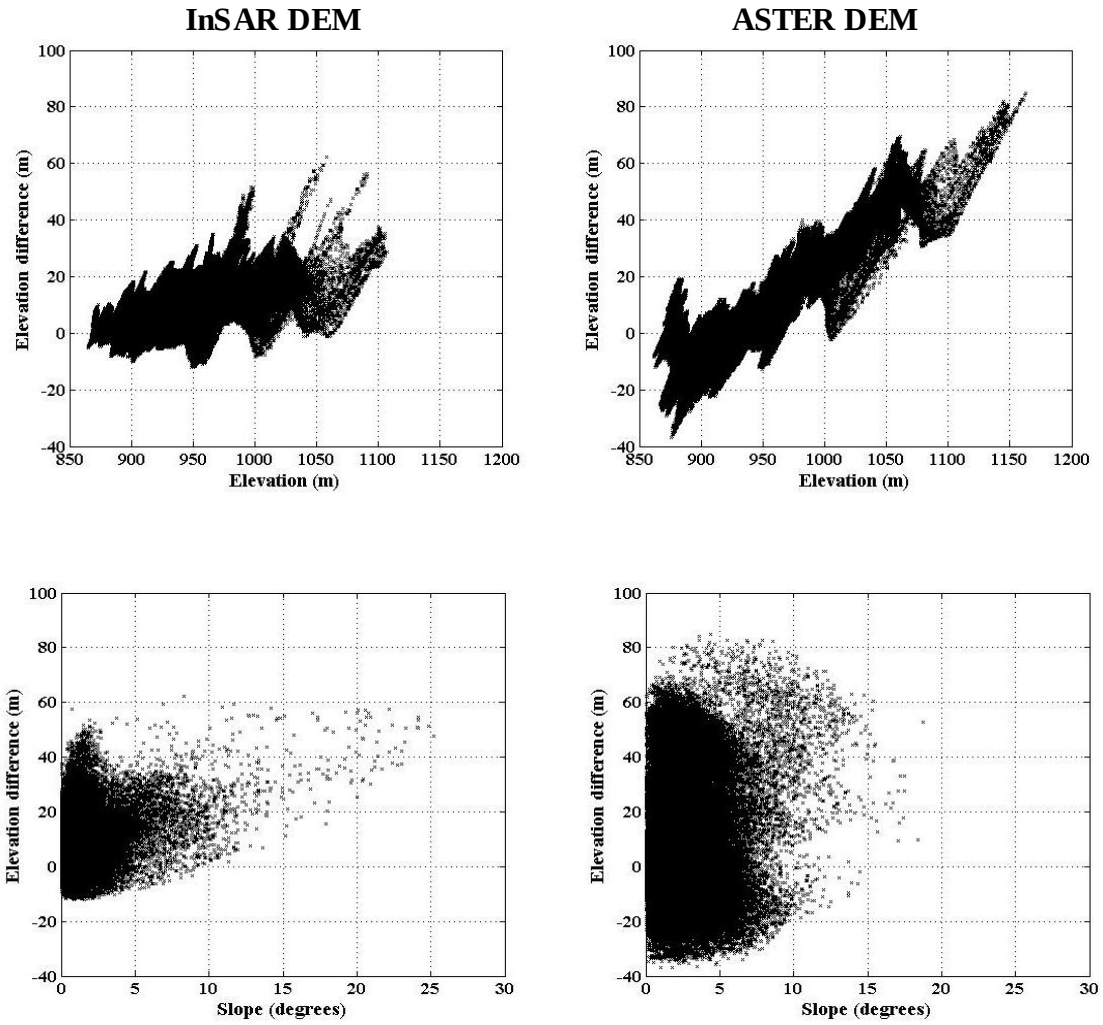

Figure 6.17: Elevation difference of the study area versus elevation and slope for DEMs derived from InSAR and ASTER data.

6.7 Effects of DEM Error on Surface Flow Analysis

The accuracy assessment in the previous sections has shown that elevations recorded within DEMs contain errors which can greatly affect derivative products of DEM (Holmes *et al.*, 2000). This can potentially have a significant impact on the application of DEMs in GIS where derivatives of elevation are frequently used (Darnell *et al.*, 2008). This section of study focuses on the effect of vertical error on surface flow derived from DEM. This can be done using simulation modelling in which numerous realisations of an error surface that are created from the difference between points with high accuracy, such as DGPS points or highly accurate DEM, and the DEM to be analysed. Some of the earliest works in this area were carried out by Veregin (1997), who examined the effects of vertical error in DEMs on the determination of flow path direction. Results of this study suggest that extreme caution should be exercised when employing flow path derived from DEM, especially if there is reason to suspect that vertical error is large or positively correlated with terrain slope. Fisher (1998) used geostatistical concepts to improve modelling of elevation error. He compares the results of using different methods of error modelling and their effects on viewshed analysis.

Kyriakidis *et al.* (1999) performed stochastic conditional simulation for generating alternative, equally probable images (numerical models) of the unknown reference elevation surface using both hard and soft data. He created elevation error surfaces using a difference between two DEMs, one used as soft data that was to be examined and samples of points interpolated from another DEM used as hard data. Holmes *et al.* (2000) presented a coherent study of DEM error propagation analysis for the first time. They did semivariogram modelling of USGS DEM error based on reference data from GPS, and created 50 realisations of the error model using Monte Carlo simulation. A number of surface derivatives including slope, aspect, plan and profile curvature, and flow accumulation were considered. It was also shown that using the original USGS DEM grossly underestimates potential landslide hazard areas emphasising the effect of DEM error on hillslope failure prediction. Wechsler (2000) implemented an analysis of DEM error propagation in commercial GIS software using the Monte Carlo method, as a part of a doctoral thesis. The effects of uncertainty on elevation and derived

topographic parameters, DEMs of different scale, and in flat and rough terrain were also focused upon as part of this study.

6.7.1 Modelling error

Analytical error models and (conditional and unconditional) stochastic simulation are the two approaches to error modelling (Fisher and Tate, 2006). Hunter and Goodchild (1995) developed an analytical model of error, based on simple probability theory and the RMSE of the DEM, which is frequently cited. This technique doesn't require the comparison of DEM data with higher accuracy data, there are the limitations with using a global accuracy measure (Wise, 2000). Stochastic simulation of random functions is used in unconditioned error simulation models. They are informed by properties of the error distribution. However, they do not honour any actual estimates of error (Fisher and Tate, 2006). Geostatistics can also be used to model the actual distribution of error with reference to a dataset with higher accuracy. Fisher (1998) considers conditional stochastic simulation to be the best method for error modelling. In stochastic imaging, the spatial uncertainty is modelled through alternative numerical representations (maps) of the same reality (Journel, 1996).

Error propagation can be demonstrated using multiple versions of the derived products from these realisations (Fisher, 1998). Kyriakidis *et al.* (1999) describe the mathematical details of the process of stochastic simulation. Conditioning the simulation model allows consideration of spatial autocorrelation by preserving sample observations of error. After modelling the error there are a number of methods for tracing the propagation of quantitative error from source to surface derivatives. The Monte Carlo method is considered to be the best method for determining the influence of error on DEM derivatives (Veregin, 1997). In Monte Carlo simulation, estimates of 'true' outcomes of stochastic processes are produced by simply running many iterations of the model process and comparing the outcomes. The method is widely recommended, though the numerical load is high as the process is repeated for typically 50–2000 simulation runs (Heuvelink, 1998).

IDRISI software has been used in the error surface modeling. It provides an extensive set of surface modeling tools. These include interpolation procedures such as inverse distance weighting, thiessen polygons, trend surface mapping and kriging. Given a digital elevation model (DEM), surface characteristics such as slope gradient, aspect, and curvature can easily be calculated. In addition, special tools are provided for mapping watersheds, viewsheds, and surface flow patterns (runoff). Geostatistical functionality within IDRISI has been employed to create error model. Figure 6.18 shows the flow chart for the processing steps of the elevation error modeling using conditional Gaussian simulation. In Gaussian simulation algorithms, a simulated value at a single location is randomly selected from the normal distribution function defined by the Kriging mean and variance based on neighbouring values. The simulated value at the new randomly visited point value is dependent upon both the original data and previously simulated values. This process is repeated until all points are simulated. The number of input nearest sample points used in interpolation was 24 points. Here, it is assumed that the error follows a normal distribution with 0-mean and a standard deviation equal to the RMSE, as it is commonly assumed in geostatistical analysis (Fisher, 1998; Hunter and Goodchild, 1995).

The first step to define the error model is calculating the error in a given DEM dataset by subtracting DEM elevation from the true elevation (DGPS elevation) at a specific location. DGPS points were delivered in ESRI shape file format. The attributes of these points included a single field containing elevation measurements and two additional fields were created to store the coordinates of the points. The effect of correlated gridded DEM error was then investigated using stochastic conditional simulation to generate multiple equally likely representations of an actual terrain surface. A raster error surface was then produced for each of the 50 simulations. All of the simulated error surfaces reproduce the measured error values at their locations. Each of these 50 realisations would have approximately the same histogram. Propagation of data uncertainty to the slope derivative and the impact on the surface flow were finally assessed.

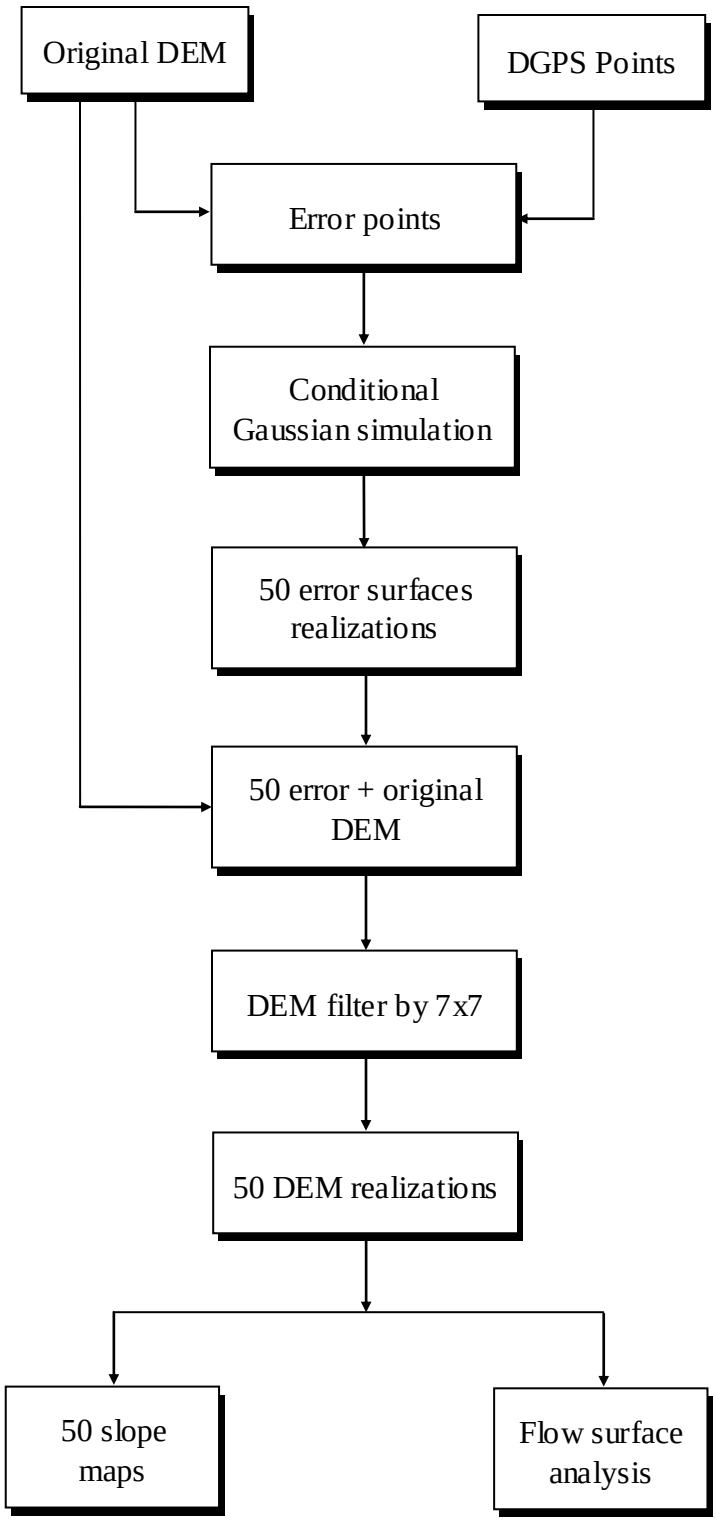

Figure 6.18: Flow chart showing processing steps of elevation error modelling using conditional Gaussian simulation.

Figures 6.19 a-d shows the maps of four randomly selected realisations. From these maps, it can be seen that the underestimation elevation area were concentrated in low elevation area. Also, from the comparison of error surfaces with the elevation surfaces, it can be noticed that the most of large errors appear in low elevation sites in south of the study area with small areas in high elevation sites in north of the study area. The final step in the simulation procedure was to add the simulated error realisations to the original ASTER DEM. This created 50 different versions of the DEM, each of which is theoretically a more accurate representation of topography than the original ASTER DEM due to the fact that they inherit the accuracy of the 680 DGPS points. These elevation surfaces, as shown in Figure 6.19 contained noise. To remove this noise, they were smoothed using a 7x7 mean filter. Figure 6.20 shows the final results for the four randomly selected realisations of elevation after adding surface errors realisations.

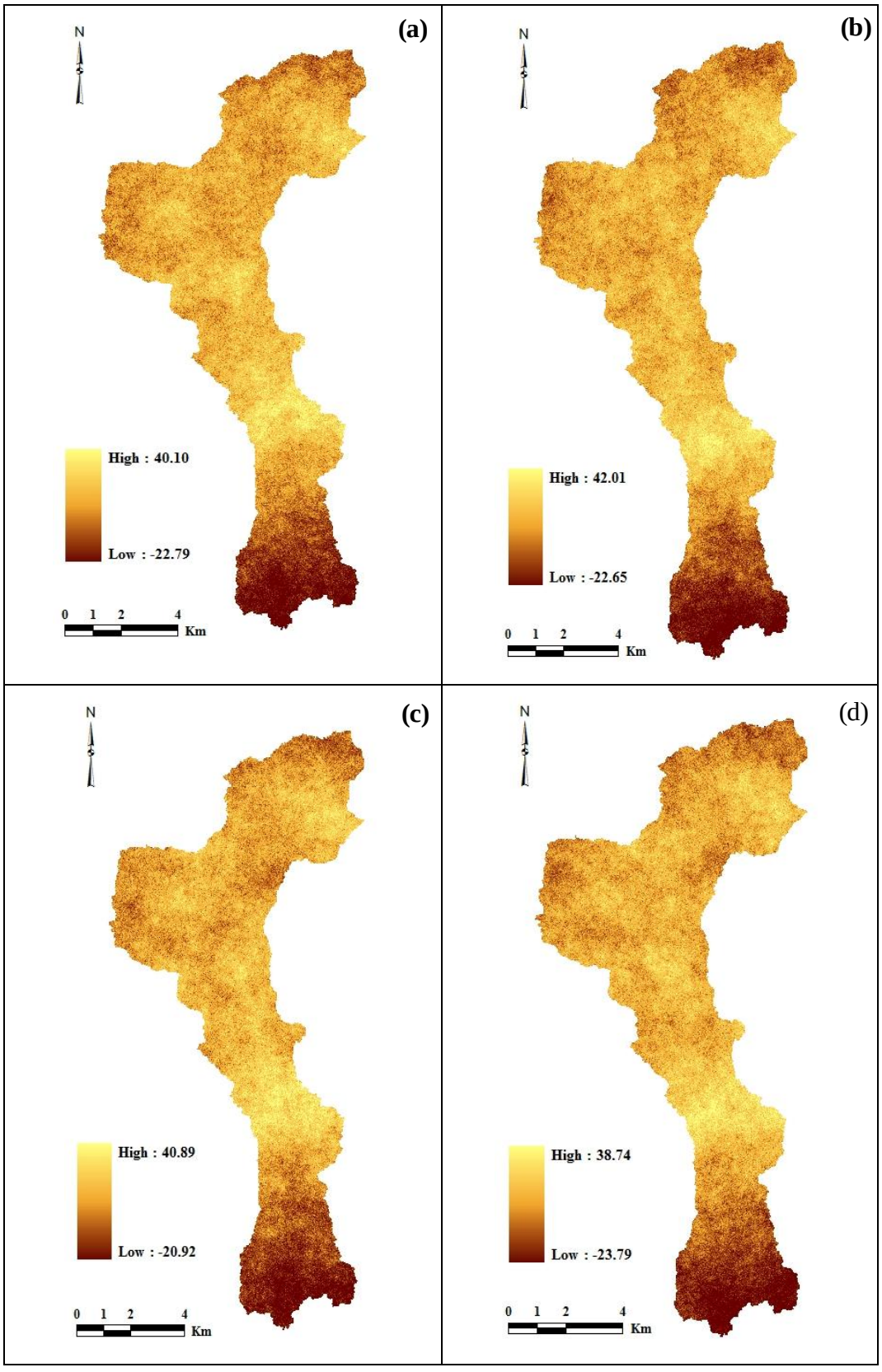

Figure 6.19: Maps of four randomly selected simulated error surfaces.

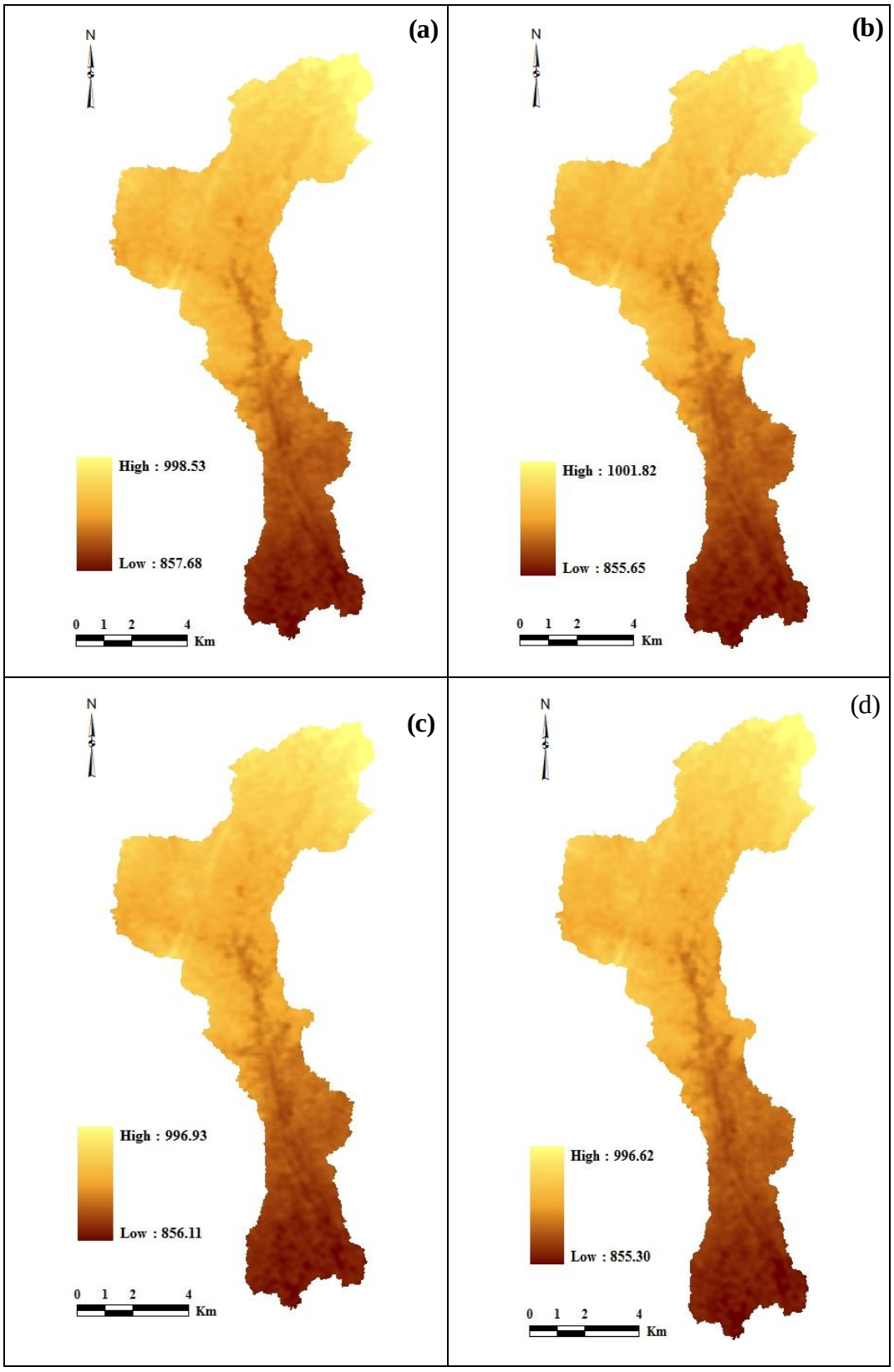

Figure 6.20: Maps of four randomly selected simulated elevation surfaces.

6.7.2 Error propagation

To demonstrate the propagation of error to slope, slope derived from each DEM realization. Then values of slope directly derived from original DEM (Figure 6.21a) were compared to the mean values of the slope realizations (Figure 6.21b) by subtracting from each other. This resulted in slope difference surface which provided an indication of how slope estimation would differ in that was derived directly from the ordinal DEM or from the multiple equally likely realizations as can be seen in Figure 6.22.

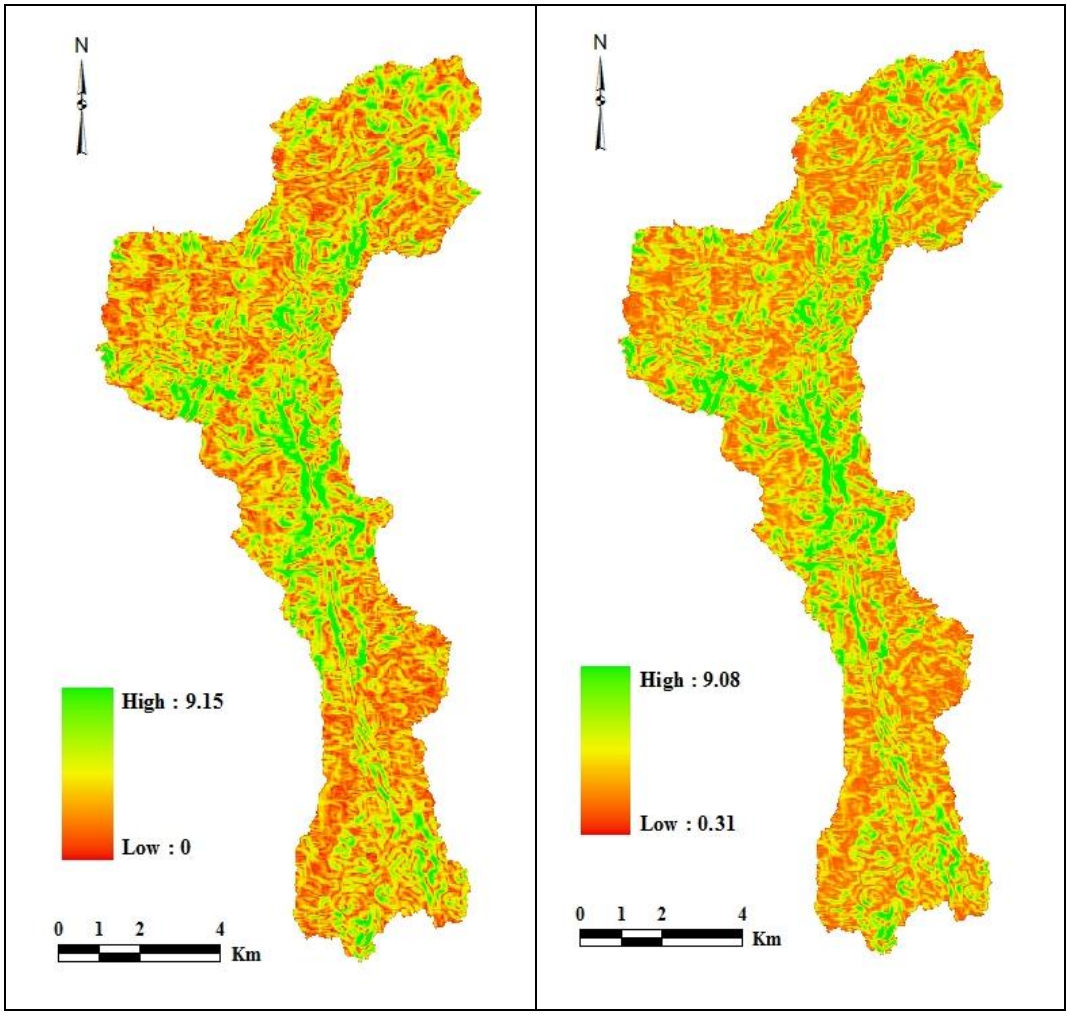

(a) (b)

Figure 6.21: (a) Slope derived from original DEM and (b) slope derived from simulated DEM.

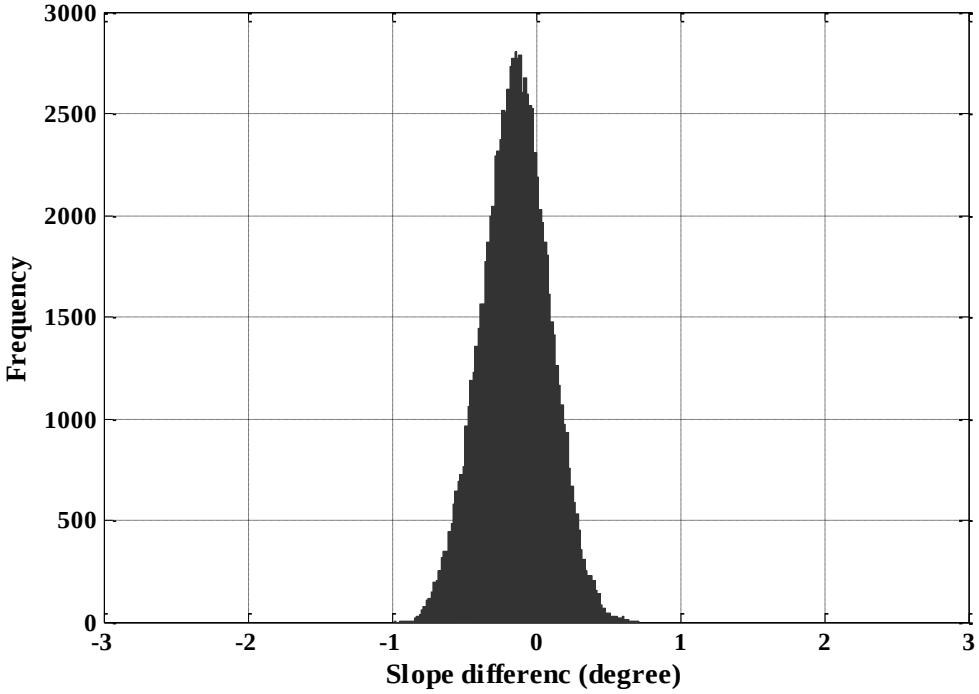

Figure 6.22: Histogram of slope difference between slopes derived from original DEM and slope derived from simulated DEM.

Slope is an important component for the determination of surface flow direction (Veregin, 1997). For this reason, the error in slope affects on other DEM derivatives such as flow direction and flow accumulation which will affect the stream network. Flow direction generation from each realization of DEM using ArcGIS® 9.2. Three statistics of properties were computed that included agreement, variability and dominance to demonstrate of error propagation on the flow direction that will affect other hydrological parameters (Veregin, 1997). Agreement determines the level of agreement between flow directions derived from original DEM and flow direction computed from all realizations. This statistic is computed by comparing flow direction values derived from original and the mode of flow direction values derived from all realizations DEMs on a cell by cell.

Variability measures the amount of variation in flow direction over all realizations. Based in D8 algorithm, the flow direction can flow in steepest direction of eight adjacent cells in the window 3x3 as described in Section 2.5.2. The flow direction for each cell in DEM over all realization calculated. For each direction of eight directions,

there are number of frequency through fifty realizations. The largest number of realizations flow in the same direction (mode) among the all 50 realization was assumed as a flow direction for that cell. For the rest of realizations, the number of realizations flow in each of other seven directions multiplied by the deviation (degree) from the flow direction cell as can be seen in Figure 6.23. The results are then summed. The variability computed for each cell in the DEM and expressed as a percentage of the maximum variability. Maximum variability occurs when the sum of the products of the number of realizations and the deviations in degrees is at a maximum. Another statistic measurement is dominance. Dominance defines the percentage of realizations for which the computed flow directions are the same from the total of realizations. The maximum value of 100% means that all realization gives the same result. A low value means that only small number of realizations has the same direction.

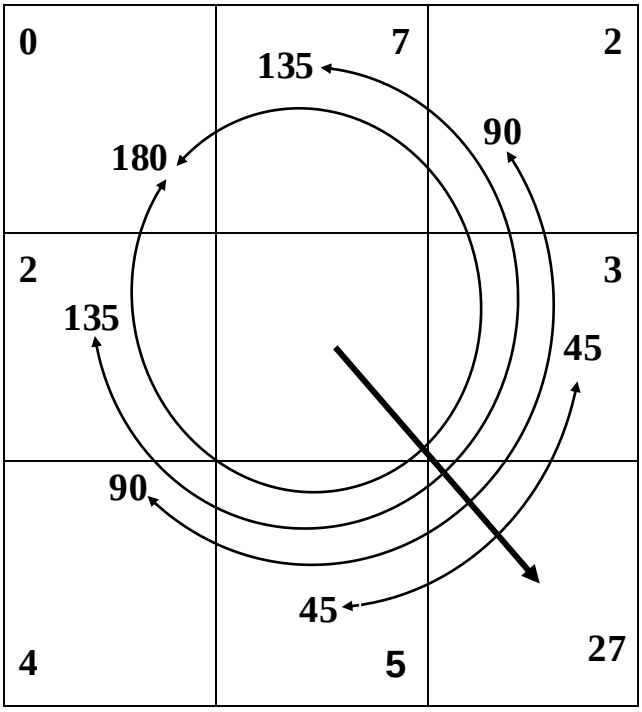

Figure 6.23: Diagram illustrating computation of variability and dominance of flow direction over 50 DEM realizations. Source: Veregin (1997:73).

The agreement between flow direction derived from the original DEM and flow direction derived from 50 realizations of DEM as given in Figure 6.24 represented a high level of agreement for 74% of the values. The variability mean is equal to about 29%, which indicates a high level of agreement. Low variability means that the probability of flow direction goes in the same direction for most of the realization and the effect of error is decreased. Figure 6.25 shows the variability between flows directions derived from DEM realizations.

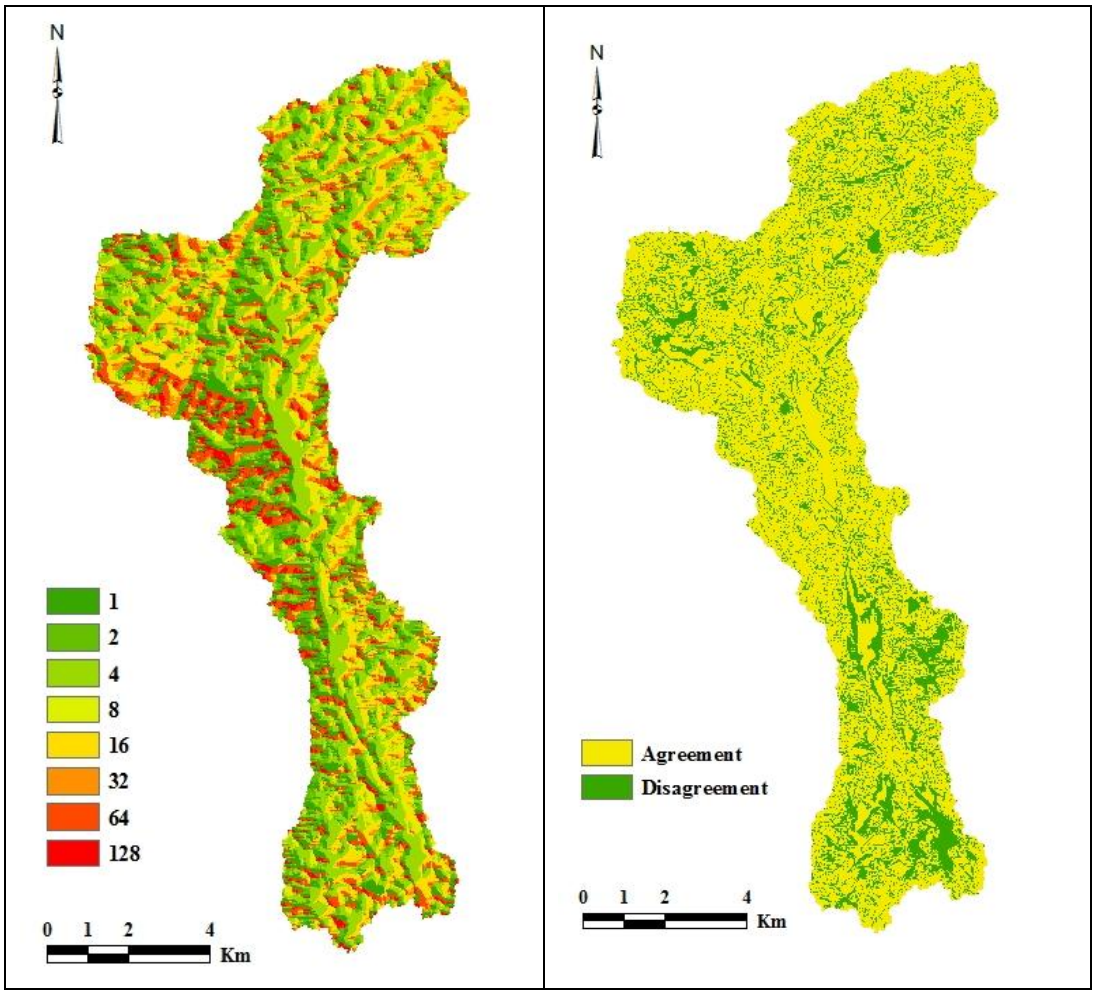

(a) (b)

Figure 6.24: (a) Maps of flow direction (mode) calculated from 50 DEM realizations and (b) agreement between flow direction model and flow direction derived from original DEM.

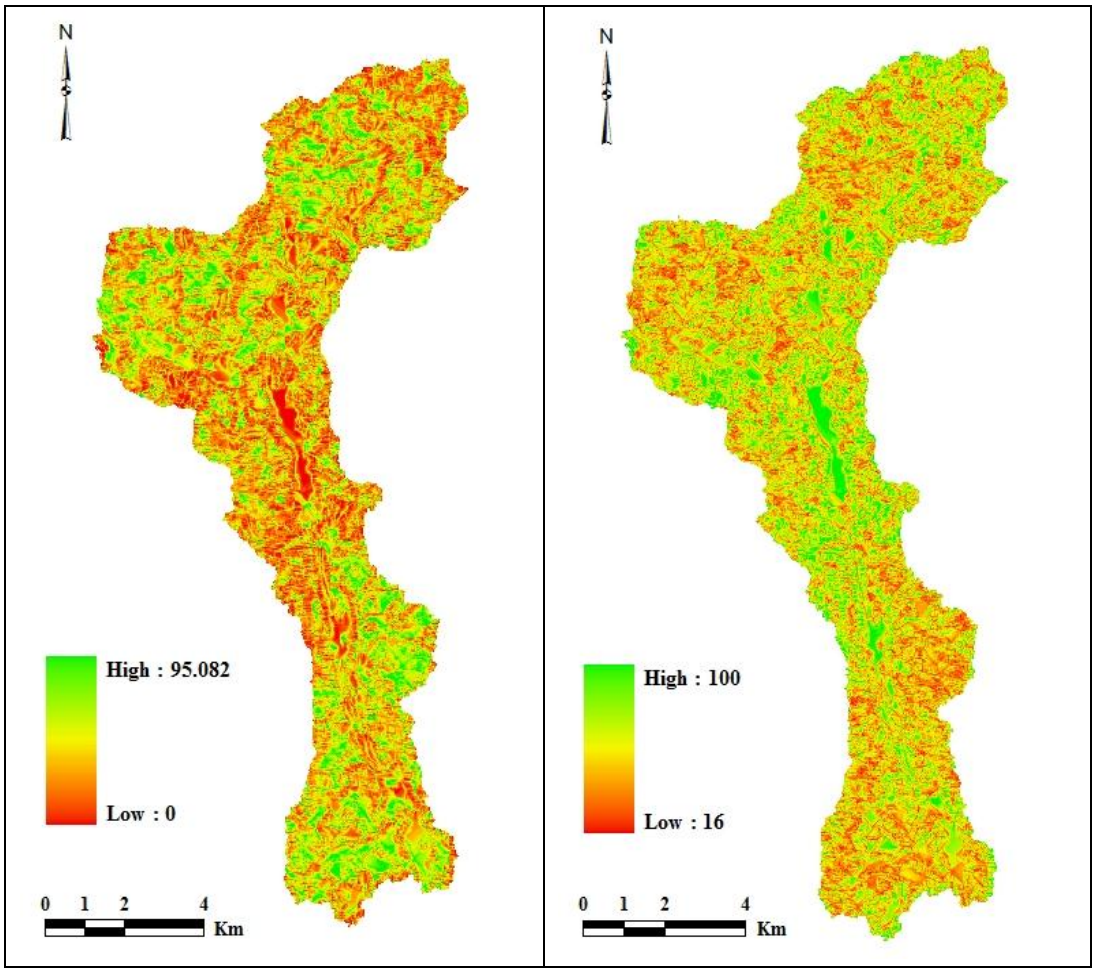

(a) (b)

Figure 6.25: (a) Maps of variability and (b) dominance computed over 50 DEM realizations.

From the scatter plot between slope and variability values shown in Figure 6.26 it can be seen that the variability is inversely correlated to the slope, which means that the high variability accrues in the low slope area as a result of the large difference in flow direction in realizations. In addition, the propagation of error in flow accumulation is calculated using the mean value for all flow accumulation derived from 50 realizations of DEMs. Figure 6.27 shows clearly how the accumulated area is sensitive to error in elevation flows. In some parts of the area, the stream lines are strongly concentrated while in the other areas, the average accumulated area leads to diffuse drainage.

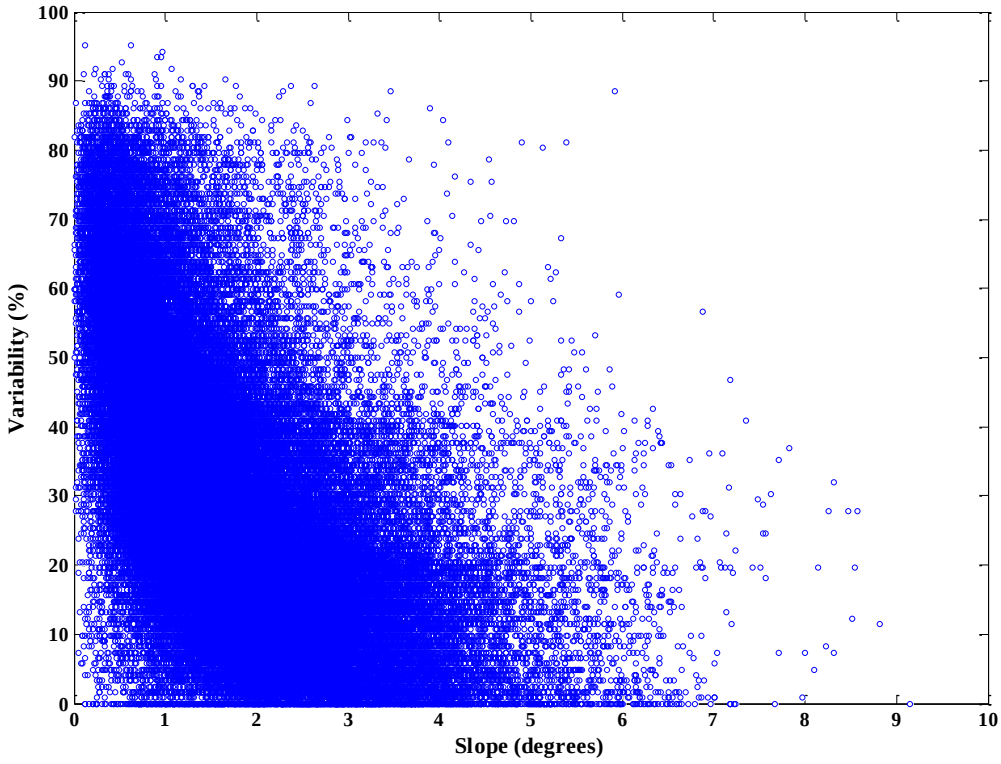

Figure 6.26: Correlation between variability and slope.

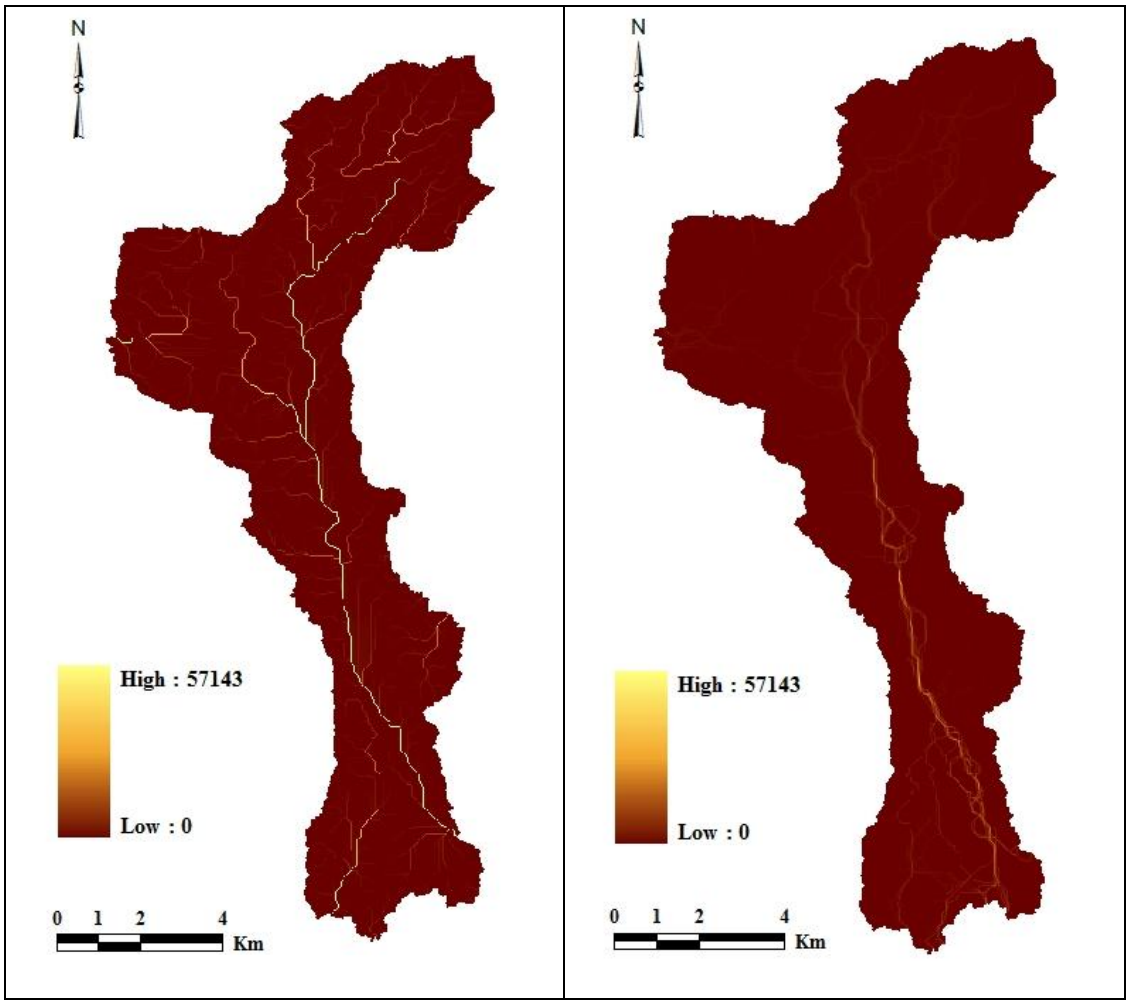

(a) (b)

Figure 6.27: (a) Maps of flow accumulated area derived from original DEM and (b) mean flow accumulated area derived from 50 DEM realizations.

6.7 Effects of DEM Resolution on Topographic Parameters

The utility of DEMs is evident from the widespread availability of digital topographic data as well as the variety of uses for and products from DEM. Slope, aspect, curvature, upslope area, flow length, and the topographic index are some of the common terrain attributes that are computed from a DEM (Thompson *et al.*, 2001). The DEM resolution and the horizontal spacing of points in the elevation grid influence the scale of terrain features represented by a DEM (Theobald, 1989). Many studies are based on the topographic parameters derived from different sources of DEMs with different horizontal resolutions. They show that as resolution decreases, slope decreases, and both upslope area and topographic index increase (Chang and Tsai, 1991; Wolock and Price, 1994; Zhang and Montgomery, 1994; Thompson *et al.*, 2001). With the decrease in DEM resolution, there was a decrease in the total flow lengths and the drainage density (Thieken *et al.*, 1999; Wang and Yin, 1998; Yin and Wang, 1999).

The disappearance of short, steep slopes and micro topographic features tends to lengthen the flow paths, thus increasing the size of catchment areas (Wilson and Gallant, 2000). A fine-resolution DEM can sometimes pick out excessive topographic detail, and can deflect stream flows from their natural courses by assumed or artefact barriers (MacMillan *et al.*, 2004). The effects of DEM resolution on a set of important topographic derivatives including slope, upslope contributing area, flow length and watershed area are examined by Simon *et al.* (2008). He studied the sensitivity of each of the derivatives to the resolution uncertainty by considering the effects of overall terrain gradient and bias from resampling. The effects of DEM resolution on a set of topographic parameters which included slope, flow accumulated area; flow length and catchment area were examined in this section. DEMs used in this study need to resampling to different resolution to achieve this goal.

Three common resampling methods are nearest neighbour interpolation, bilinear interpolation and cubic convolution which were applied in this study and only the resampling methods that available in ArcGIS® 9.2. The nearest neighbour method

performs by giving a value for each cell of the new image from the closest cell from the original image. The nearest neighbour method is computationally efficient and the fastest of the interpolation methods. The bilinear interpolation determines the new value of a cell based on a weighted distance average of the four nearest input cell centres. It is useful for continuous data and will cause some smoothing of the data. The cubic convolution, determines the new value of a cell based on a weighted distance average of the 16 nearest input cell centres. Cubic convolution tends to produce a smoother output surface than bilinear interpolation but required a longer processing time. It is appropriate for continuous data, although it may result in the output raster containing values outside the range of the input raster. It is geometrically less distorted than the raster achieved by running the nearest neighbour resampling algorithm. In some cases, it can result in output cell values outside the range of input cell values (Esri, 2006). The 20 m of ASTER and InSAR DEMs were used as the base resolution and resampled to five DEMs of 40, 60, 80, and 100 m resolutions using each of the three resampling methods. Four topographic derivatives are generated with base DEMs and all the resampled DEMs which included slope, flow accumulation, flow length and catchment area.

6.7.1 Slope

The mean slope of the test site decreased as the grid cell size increased for both DEMs. The mean slope was highest at the smallest grid cell size (20 m) for both DEMs because no smoothing was applied and the lowest was at the largest grid cell size (100 m) because of the higher level of smoothing (Figure 6.28). The mean slope of the InSAR DEM was flattened by 28% as the grid cell size was increased from 20 to 60, and by 10% as grid-cell size was increased from 60 to 100 respectively in each resampling methods, nearest neighbour, bilinear interpolation and cubic convolution. However, the mean slope of the ASTER DEM was flattened by 38, 41, and 38% as the grid-cell size was increased from 20 to 60 and by 37, 40, and 36% with the increase from 60 to 100. The Figures for both DEMs show that the resampling can cause considerable reduction of the slope angles.

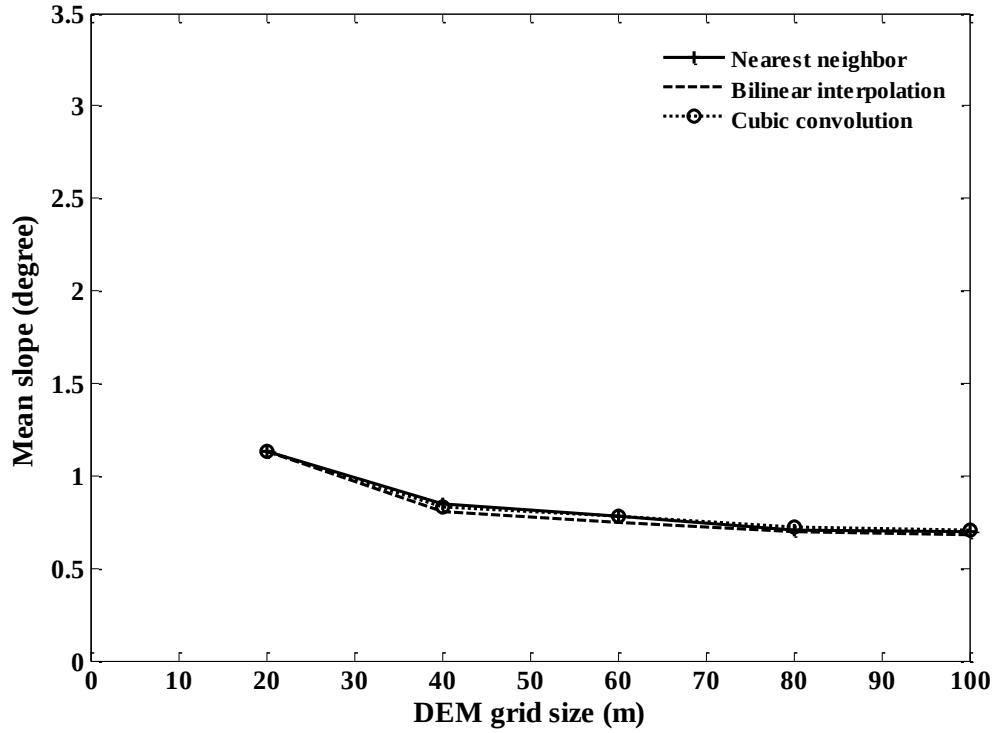

(a)

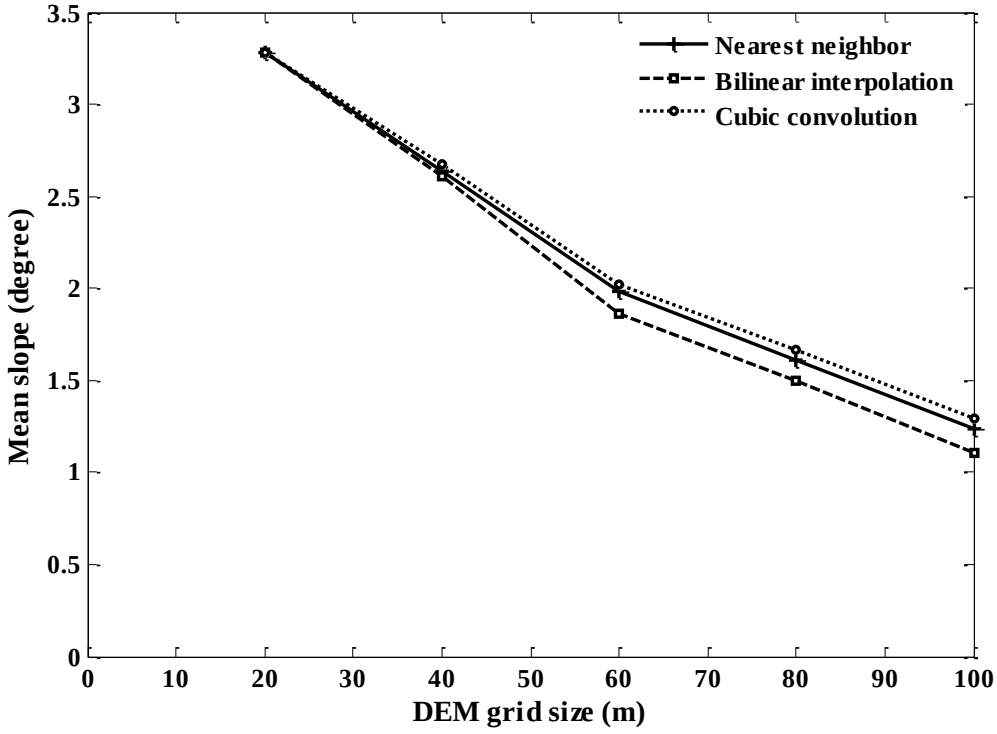

(b)

Figure 6.28: The relationship between slopes extracted from (a) InSAR and (b) ASTER DEMs and grid cell size.

6.6.2 Flow accumulation area

Figure 9.29 shows the variation of the mean of accumulated area derived from InSAR and ASTER DEMs with grid size for all resampling methods. It can be noticed that the accumulated area gradually increased in both DEMs. For InSAR DEM, the mean value of the accumulated area at 20m resolution is 248,672 m², and the value becomes 388,464 m² for the 40m using nearest neighbour. For ASTER DEM the mean value of the accumulated area at 20m resolution is 187,712 m², and the value becomes 329,552 m² for the 40m using nearest neighbour. The mean value of accumulated area increased linearly with increasing in resolution which means that flow accumulated area is very sensitive to DEM resolution.

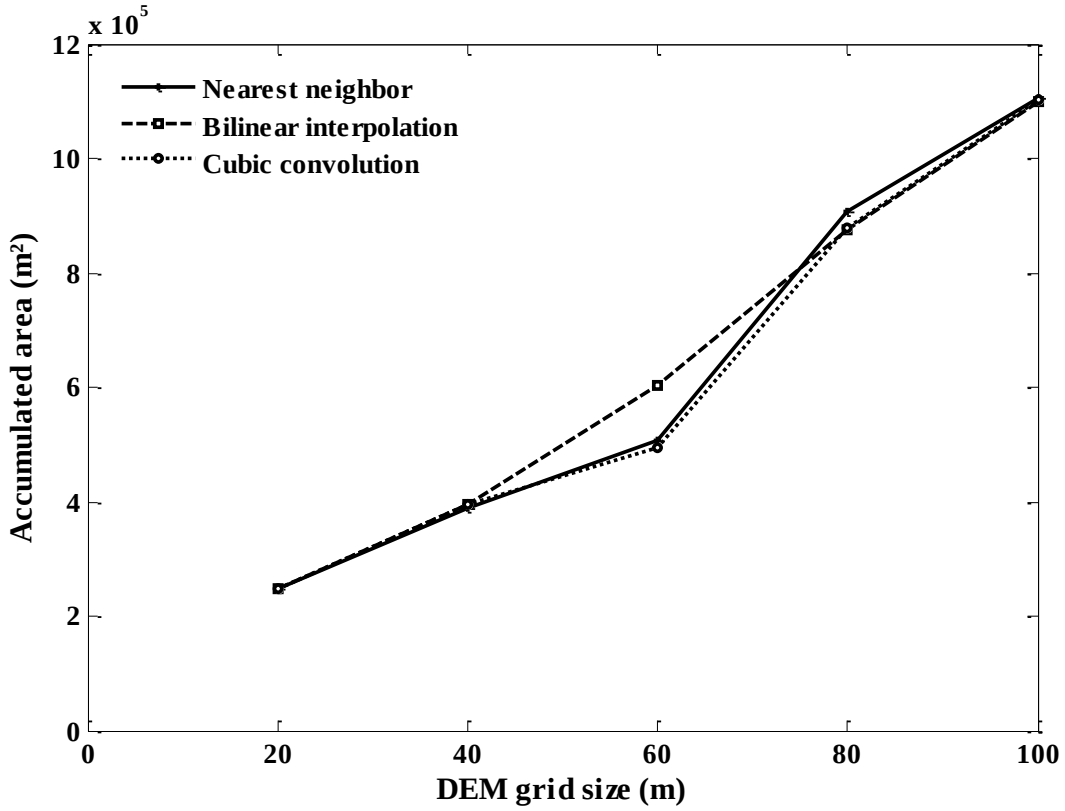

(a)

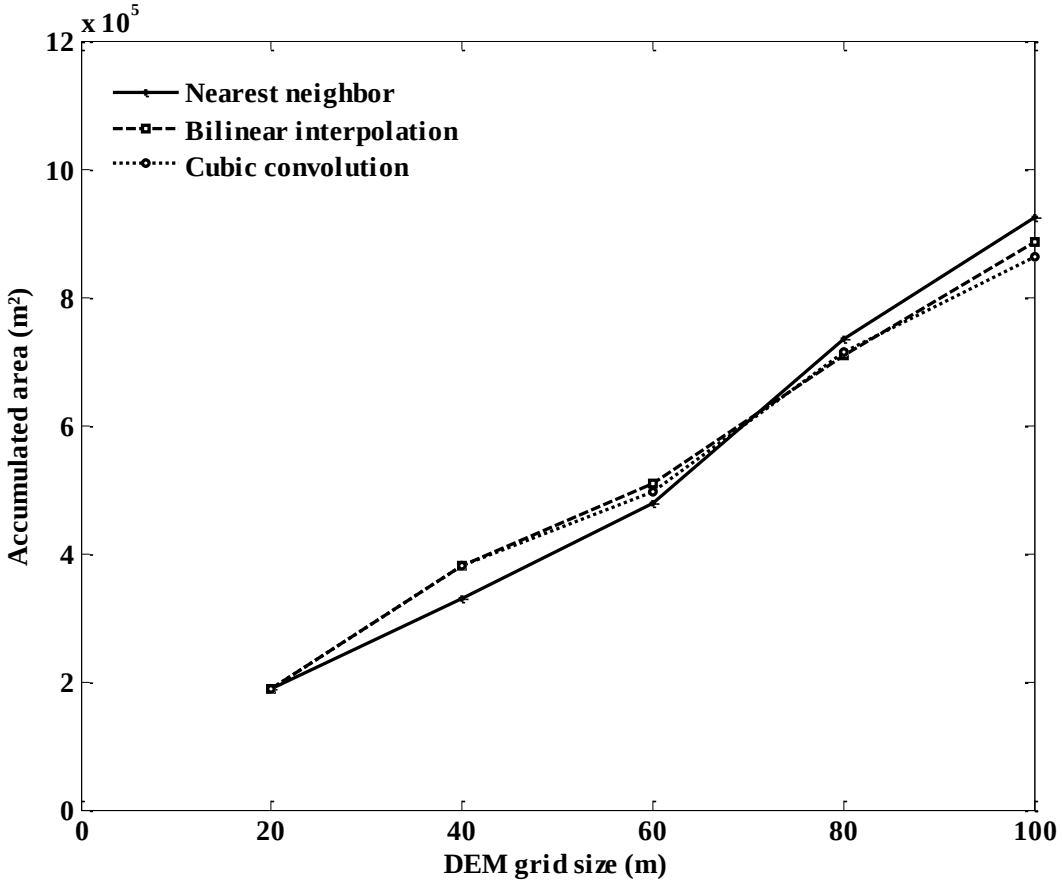

(b)

Figure 6.29: The relationship between accumulated areas extracted from InSAR (a), ASTER and (b) DEMs and grid cell size.

6.6.3 Flow length

The flow length is the distance a long a flow path from any point in the watershed to the watershed outlet. In a GIS, the flow length of an arbitrary cell is determined by summing the incremental distance from centre to centre of each cell along the flow path from selected cell to the outlet cell. The flow length assigned to the outlet cell is zero. The concept of flow lengths is important to hydrologists. When it rains, a drop of water landing somewhere in the basin must first travel some distance before reaching the outlet. Assuming constant flow velocities, the cell with greatest flow length to outlet represents the hydrologic ally most remote cell. The smallest flow lengths occur in the proximity of the watershed outlet and generally increase away from outlet. From Figure 6.30, it can be noticed that the mean flow length increased gradually with

increasing resolution for both DEMs in all resampling methods. Also, it can be seen from figure that the variation between resampling methods was very small.

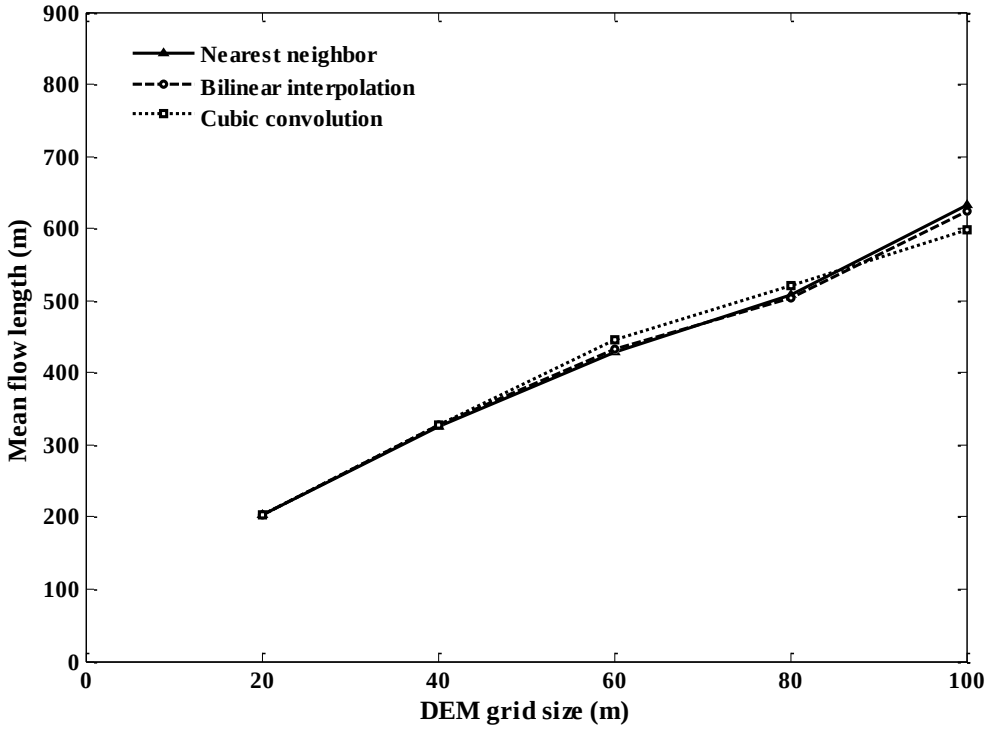

(a)

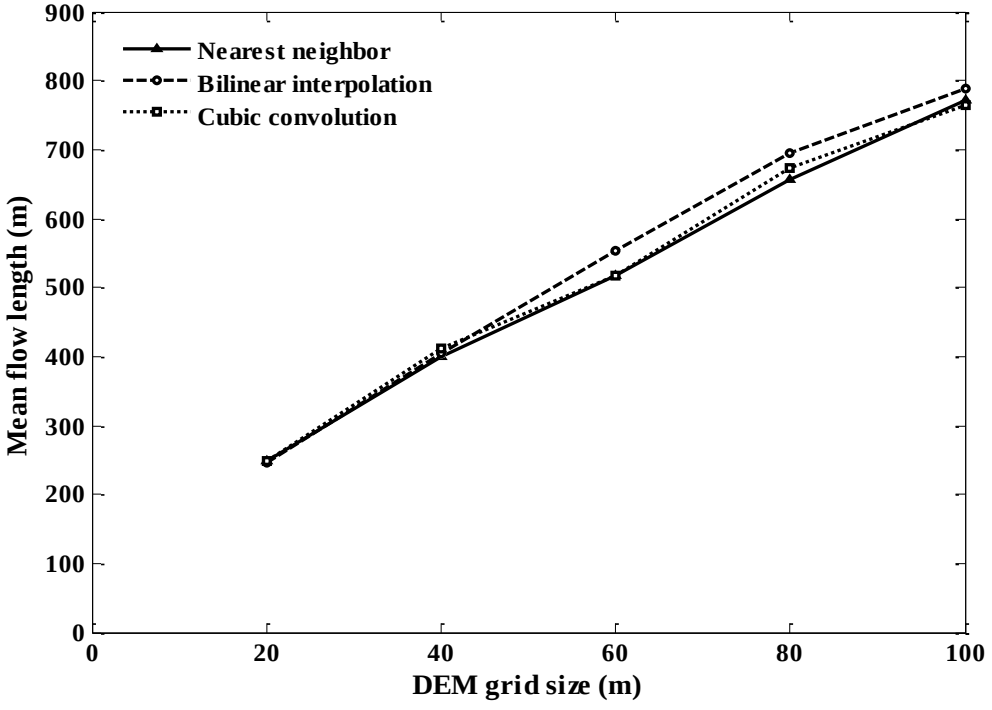

(b)

Figure 6.30: The relationship between mean flow lengths extracted from (a) InSAR, (b) InSAR DEMs and grid cell size.

6.7.4 Catchment area

Catchment area is normally defined as the total geographic area of land that drains water to a shared destination. Other common terms for a catchment area are basin, watershed, or contributing area. The variation of calculated areas for both DEMs resampling in this study is shown in Figure 6.31. While the overall variation for both DEMs appear to be a minor increase throughout the DEM resampling range, the catchment area derived from the InSAR DEM increased by 4.7, 5.0, and 4.7 % as the grid-cell size was increased from 20 to 100m respectively in each resampling method. This is similar to the effect observed for ASTER DEM, 2.7, 5.9 and 5.4 % respectively. The variation of the catchment area is due to the irregularity of resample DEM boundaries, i.e., the boundaries are becoming more and more jagged with grid size increase.

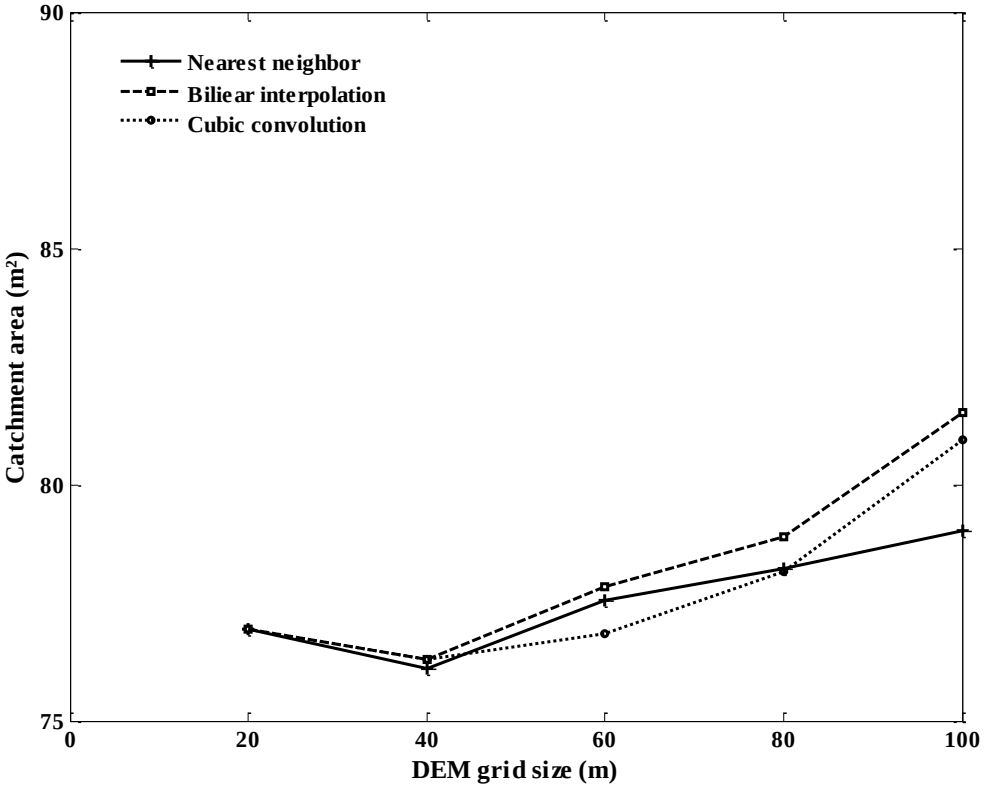

(a)

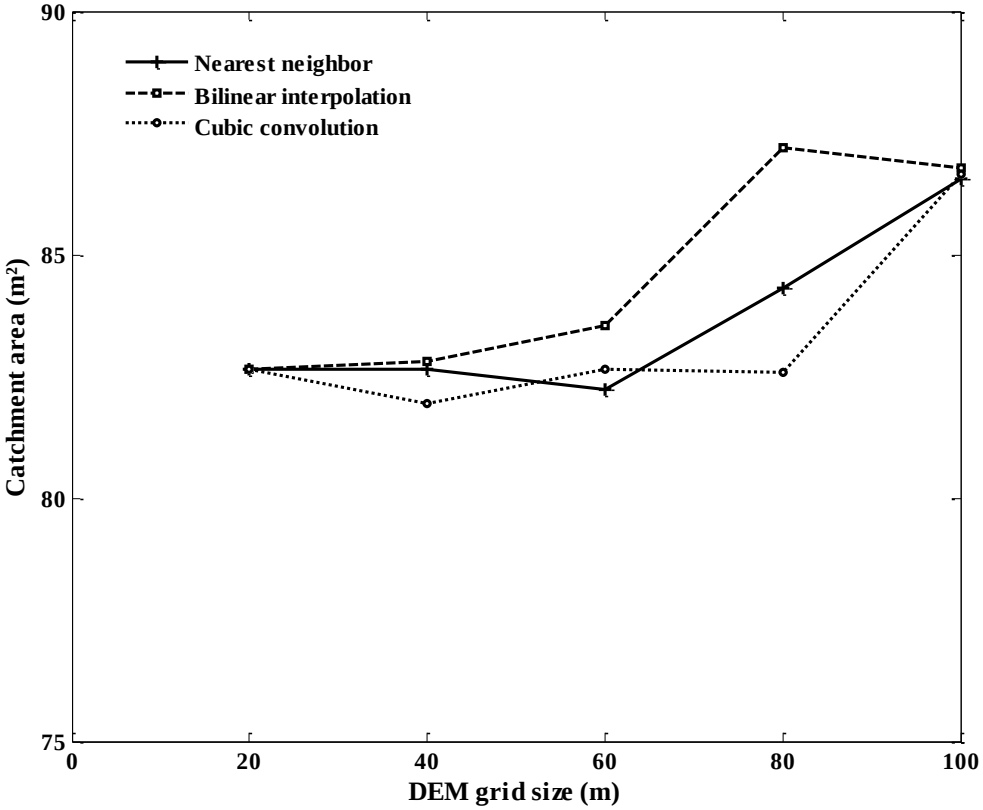

(b)

Figure 6.31: The relationship between catchment area extracted from (a) InSAR, and (b) ASTER DEM and grid cell size.

6.9 Discussion

Whether elevation data were collected by InSAR or photogrammetry techniques, the suitability of these data for a particular application is based on three issues, specifically, the degree of accuracy with which these data represent the surface, the spatial resolution of the DEM and the error propagation that will be inherited by the surface derivatives. All these issues have been addressed and assessed in previous sections. Accuracy is the most important factor to be considered when a DEM is used. The most common practice to assess the accuracy of a DEM is to generate statistical measures, such as RMSE, mean error and standard deviation. This assessment is carried out by verification of the DEM against a number of independent check points (ICPs) collected using differential GPS. This approach is a common method of accuracy assessment in many applications. ICPs indicate the degree of accuracy by applying statistical parameters based on the locations of sampling points, but not show the spatial variation of errors. Furthermore, in this study, the DEM generated from a topographic map was used to compare the DEMs generated from InSAR and ASTER data. GIS tools were utilized to generate elevation difference images to show the spatial variation of difference elevation two surfaces pixel by pixel.

Three aspects affected the accuracy of the DEM extracted from the InSAR data: the surface stability, the availability of accurate GCPs and the type of terrain. The interval time between the two acquisitions was one day for the InSAR data and the surface already was stable in this region. This stability of the surface led to good coherence (the mean coherence was about 80). Eighteen GCPs were used in InSAR processing to produce a highly accurate DEM. The GCPs were used to convert the DEM in relative height to a DEM with absolute height and to correct the baseline between the two passes. GCPs are important steps in the generation of an InSAR DEM, but present a difficult task in the processing steps as a result of the difficult identification of these points in the interferogram image. Therefore, GCPs must be selected that are highly visible to the radar and are easily geo-located or surveyed. For example, roadways are generally visible in SAR images and road intersections can be used as GCPs. The quality of the extracted DEM is based on both the accuracy of GCPs and their number, which should be at least ten points, as the greater the number of points, the more

accurate the DEM (Tsay and Chen, 2001). According to previous studies on the evaluation of DEM generated by InSAR, a vertical accuracy of approximately 10 m (Zebker *et al.*, 1994; Herland, 1997) 14 m (Sansosti *et al.*, 1999) 23 m (Rong and Hsu Chen, 2001) can be achieved. In this research, the accuracy assessment of the InSAR DEM was achieved by comparing the extracted DEM with the reference DGPS points. The RMSE of the InSAR DEM was about 7 m, which means that the accuracy was quite good for the whole area at least in terms of the requirements of small to medium scale topographic mapping. The InSAR DEM accuracy decreased only in the valley and very low relief areas.

This was also the case for the ASTER DEM regarding the overall accuracies of the generated DEMs, taking into account the quality of the GCPs used and also the type of terrain. The availability, spatial distribution, and accuracy of the GCPs, which can be precisely located on the ASTER scene, are the main factors limiting the accuracy of ASTER DEMs. The error range and its spatial distribution are highly sensitive to the distribution GCPs, as they need to be uniformly spread in the x, y and z directions. Toutin (2004) stated that GCPs should preferably cover the full range of terrain (lowest and highest elevations). Although it is well known that, theoretically, four GCPs would be enough to compute a stereo model (Toutin 2002), studies have been done by different researchers using between four and sixty GCPs (Welch *et al.* 1998; Toutin 2001, 2002; Toutin and Cheng 2002; Hirano *et al.* 2003; and San and Süzen, 2005). The use of overestimation GCPs means error propagation in the modelling can be avoided, as noted by Toutin (2002), and accuracy of the order of one pixel per 15m can be maintained (San and Süzen, 2005). The elevation error contributed by each GCP is displayed during processing of the InSAR and ASTER extracted DEMs and this information can be used to decide if a GCP is to be accepted or deleted and located again with a correct position. Repeating the GCPs' input step several times is recommended to look for consistency in the height error estimated.

In addition, the number of GCPs plays a very important role in the final accuracy of the DEM. Quantitative analysis of different DEMs generated using different numbers of GCPs indicates that the RMSE decreased from 8.39 to 6.95 m after an increase in

the number of GCPs from 10 to 18 and from 14.39 to 13.28 m after an increase in the number of GCPs from 15 to 75 for InSAR and ASTER DEMs respectively. A small decrease in the RMSE in DEM generation from the ASTER data was noticed; this may be due to the impact of error associated with locating GCPs on the image during the process of generating the DEM. Collecting most GCPs in flat or low altitude areas and far fewer in high altitude areas can create a very good DEM. An important issue in DEM accuracy is the effect of manual and automatic tie points (TPs) collection. Identifying TPs needs to have experience in surface landforms and land covers. Number of ASTER DEMs generated by using different number of TPs, the results show that TPs do not have huge impact on the accuracy of DEMs. In this study, 25 TPs were used as a constant after being identified accurately in a stereo ASTER image. 25 points is a default number of TPs used in processing steps.

To evaluate the absolute accuracy of DEMs derived from InSAR and ASTER data, the elevation difference calculated between them and the DEM derived from 1:50,000 topographic maps. Using basic map algebra, the respective DEMs were subtracted and their absolute value calculated, to determine the residual error. The results of these calculations indicate that the RMSE values were 11.66 m and 15.29 m for InSAR and ASTER DEM respectively. This method would help understand the spatial variation terrain pixel by pixel and their interaction with InSAR signals or ASTER images. The DEM derived from the topographic maps are usually influenced by the subjectivity, the interpolation method and the experience of the operator. DGPSs were used to validate DEMs derived from topographic maps and the result shows that the RMSE is 10. The correlation computed between them shows a very high correlation of about 0.996 between the TopoMap DEM elevation and DGPS elevation.

Furthermore, understanding the spatial distribution of the elevation error is important in assessing the accuracy of InSAR DEMs in order to avoid any misrepresentation of the potential and limitations of the technique. Cumulative RMSE and AMED values were plotted against the percentage of pixels for InSAR DEM comparisons with ICPs or DEMs generated from topographic maps. The cumulative graph (Figure 6.8) shows that 90% of the difference in the image for ASTER and TopoMap DEMs has an

RMSE of less than 10 m and 95% has an AMED of about 9 m. It can also be noticed that until these percentages the difference image of ASTER and TopoMap DEMs underestimated for InSAR and TopoMap DEMs. On the one hand, this indicates that a small high relief area that contains a large error in the ASTER DEM would affect the result for the whole area. On the other hand, it also indicates the success of the ASTER data in low to medium relief sites, which will encourage the use of this sort of data for hydrological modelling. In this study, the DEM accuracy is strongly related to the topographic characteristics. It was found that InSAR DEM accuracy was quite good in medium to high relief sites and decreased in low relief sites and valleys. However, the ASTER DEM was accurate in low relief sites and flat areas while in the high relief area, the accuracy was reduced.

Characterization of error in geographical data and its propagation thorough topographic modelling have been become a critical topic in GIS applications. GIS users have to understand not only the error that occurs in geographic data but also the effect of this error that will help to determine the suitability of DEM for particular application. The study examined the effects of error in two DEMs on topographic parameters which slope, flow direction and flow accumulation. These topographic parameters are used extensively in hydrological modelling applications and are derived directly from the DEM. The routing of water over a surface is closely tied to surface form. Maps of each of these parameters were created. Comparison of the DEM derivative maps with the original DEM shows the magnitude of the agreement and variability between them. The results suggest that there effect of elevation error on flow direction which propagates this error to flow accumulation and the stream network delineation especially in low relief sites.

There are number of algorithms for determine flow direction that have been explained in 2.4.2. All these flow direction algorithms produce some level of errors, which are related to the morphology of the surface (Zhou and Liu, 2002). Also, the flow direction can be largely influenced by the errors inherent in the DEM itself, so that the errors produced by the algorithm could be masked by the DEM error (Zhou and Liu, 2002). The technique used in this study is the D8 algorithm which let the water to route from

a cell to its steepest downhill neighbour. This algorithm has been criticised for only allowing flow to travel in one of eight directions, tending to yield parallel flow path on uniform slopes and only allowing convergent, not divergent, flow (Burrough and McDonnell, 1998; Fairfield and Leymarie, 1991; Tribe, 1992). Despite these significant drawbacks the algorithm is implemented in a number of GIS software packages, including ArcGIS and IDRESI. This is required to take this into account for surface flow model. In addition, ArcGIS software use a sink filling approach based on the D8 single flow direction flow routing method first described by Jenson and Domingue (1988) and Jenson (1991). This sink filling approach raises the sink elevation to that which enables flow linkage. This approach has the disadvantage of assuming that all depressions are due to an underestimation of elevation in the sink, rather than the overestimation of surrounding cells. While there was no significant difference between elevation from filled and unfilled DEMs, a significant bias was observed in the slope parameter. The sink filling procedure raised the elevation of cells where sinks were found, increasing elevations in these areas, resulting in a larger positive bias for elevation. Raising these elevations in turn decreased slope estimators in these areas, leading to negative bias for slope (Wechsler, 2007).

Another important issue that affects the DEM suitability for a particular application is resolution. This study has shown the impact of resolution in topographic parameters derived from DEMs. These topographic parameters were slope, accumulated area, flow length and catchment area. The result indicates that these parameters are very sensitive to the spatial resolution of DEMs. The mean slope of the InSAR and ASTER DEMs was reduced by 28 and 38% as the resolution was increased from 20 to 100 m. This is a result of the cutting of hills and the filling-in of valleys at larger resolutions by an aggregation scheme. The total channel lengths are shortened at a larger resolution. In addition, the mean value of the accumulated area increased linearly with the increase in resolution, which means that the flow accumulated area is very sensitive to DEM resolution. Due to the poor contrast on the flatter areas within the DEM, much of the resulting flow accumulation values were small. Most of these values less than threshold (1000 cells) chosen which caused increasing in zero flow accumulated area. The results indicate that the catchment area also increased as the resolution was

increased. In theory, the DEM resolution should be selected as a function of the size of the land surface features that are to be resolved, the scale of the processes that are modelled, and the numerical model used to model the processes. In practice, however, the selection of the DEM resolution for a particular application is often driven by the data availability, test applications, experience and cost.

6.10 Summary

The most common practice to assess the accuracy of DEMs is to generate statistical measures such as RMSE. RMSE is a measure of vertical accuracy commonly used for assessing the error of digital elevation model, it is an overall error indicator that takes into accounts both systematic and random errors introduced during data generation process. The RMSE expresses the degree to which DEM values differ from these true values. True elevations are the most probable elevations, and do not always reflect actual elevations. These test points are obtained usually from GPS field surveys. The major drawback of RMSE statistic is the fact it does not show the spatial distribution of the error. Although it provides useful information about the overall accuracy of a DEM, it is insufficient to characterize error which fluctuates spatially across a surface (Wood et al, 1993). The elevation RMSE can illustrate that in flat areas a slight DEM error can have a relatively high effect on the derived slope value which will lead to effect on flow networks. This because elevation RMSE is based on the accuracy of a single cell, while gradient RMSE is based on the accuracies of a cell and its eight neighbours. Additionally, the RMSE is based on the assumption that errors are both random and normally distributed, which may not always be the case.

This assessment is carried out by verification of the DEM against a number of check points (CPs) collected independently from GCPs and acquired using differential GPS. The results show that the RMSE of InSAR DEM can reach 7 m while for ASTER DEM 13.26 m. Also, accurate DEM generated from a topographic map are used in comparison with DEM generated from InSAR and ASTER data. It was found that the bias between ASTER DEM and TopoMap DEM is less than between InSAR DEM and TopoMap DEM in most parts of study area. Elevation difference images show the spatial variation in difference between two surfaces pixel by pixel. In determining the

relationship between DEM error and terrain character, the correlation between elevation difference and terrain parameters have been measured. In addition, the effect of error propagation in DEMs on topographic parameter was addressed in this chapter. The effect of DEM resolution on topographic parameters was assessed. Slope, accumulated area, flow length and catchment area were mapped at various DEM resolutions. It was found that understanding the accuracy of DEMs at specific resolutions plays an important role in mapping topographic structures. Furthermore, the effect of error propagation in DEMs on topographic parameter was addressed in thischapter.

Chapter 7: Conclusions

DEM data have become a vital source of topographical data for scientific investigations, such as hydrological and geomorphology studies. For many applications, the generation of DEMs from traditional sources, such as digitizing topographic maps and ground surveys, have some limitations. These limitations include availability, coverage area, cost and suitability for a particular application. In this study, a number of investigations were carried out to generate DEMs using two different approaches. The first utilised the interferometric technique using data collected from ERS-1/2 tandem images, whilst in the other, DEMs were generated based on the digital photogrammetric technique using optical remote sensing data collected by ASTER images.

The InSAR and conventional photogrammetry techniques for topographic mapping are similar in principle. In stereoscopy, the parallax obtained from the displacement of imaging positions, of a pair of images of the terrain, allows the retrieval of topography, as targets at different heights are displaced relative to each other in the two images by an amount related to their altitudes. For InSAR, the parallax measurements between images are obtained by measuring the phase difference between the signals received by the two InSAR antennas. The angle of a target relative to the baseline of the InSAR is determined directly from this phase difference. The major difference between the two is the accuracy. The accuracy of the InSAR parallax measurement is a fraction of the SAR wavelength, usually several millimetres to centimetres, whereas the parallax measurement accuracy of the stereoscopic approach is several meters or more, depending on the resolution of the imagery.

7.1 Findings: Objective 1

Evaluate the suitability of DEMs derived from interferometric synthetic aperture radar (InSAR) data from ERS-1 and ERS-2 SAR and ASTER in a semi arid region.

Overall, the results from the generation of DEMs show that remote sensing data can be used as a main source to extract DEMs that can be suitable for topographic analysis applications. The advantages of this method include its cost effectiveness, the accessibility of any site and the coverage that can be obtained from remote sensing data like InSAR and ASTER images. InSAR and stereo photogrammetry techniques, using ERS-1/2 and ASTER tandem images respectively, can achieve much greater ground coverage in a relatively short time. The generation of DEMs from InSAR and ASTER data is a very suitable method compared to other methods, like digitizing topographic maps or ground surveys, particularly for environment and land resources applications. This study proved that InSAR and ASTER data can be used to derive DEMs of acceptable accuracy for many applications in semi arid regions which give advantage particularly to InSAR data with respect to temporal decorrelation and include spread vegetation. The orbital data quality of ERS-1/2 and cloud free that need for optical made it possible to conduct good result for the extraction digital elevation model. However, it is difficult to achieve this over forest canopies and other densely vegetated area. SRTM data is limited in terms of grid size (90 m) to carry out the needed data analysis.

The InSAR technique is mainly influenced by baseline length, coherence and temporal decorrelation. In this study, different methods of estimating baseline values and the fringe rate were evaluated. The fringe rate was used to estimate the perpendicular component of the baseline, and the co-registration offsets were used to estimate the parallel component of the baseline value providing a more accurate baseline estimation when compared to other methods discussed in this study. In this study, the coherence between two SAR SLC images for the Al-Jafer site was very high. This led to successful phase unwrapping, which resulted in highly accurate DEM. In this study, the impact of temporal decorrelation was not assessed because the condition of the test

site was stable. This condition was a very important advantage in such a site as it facilitated successful DEM generation in a semi arid region.

The stereo photogrammetry technique depends on many factors including base-height ratio and image matching procedures. The second source of errors is related to errors of matching in the parts of the ASTER scene that have a low contrast. The image matching technique used in this study was the cross-correlation approach, because it is faster to process and easier to implement. The study addressed the experiences of automatic DEM generation with ENVI® Software using ASTER stereopair images, the strategy used to determine the optimal extraction parameters. This study has demonstrated the capability of ENVI® software to generate accurate DEMs, an essential requirement of any digital photogrammetric technique. It has also shown that the strategy parameters are highly sensitive, and significant gains in accuracy can be made by altering their values. Furthermore, the strategy for optimizing the DEM-extracted parameters was outlined, which subsequently resulted in significant improvements with respect to accuracy and a decreased level of interpolation.

7.2 Findings: Objective 2

Evaluate the accuracy of DEMs derived from interferometric synthetic aperture radar (InSAR) data from ERS-1 and ERS-2 SAR and ASTER of stereoimage using DGPS measurements.

Accuracy is the critical factor for many applications. This study shows the results evaluated through the comparison with highly accurate independent check points collected using DGPS. The results discussed in Chapter 6 clearly show that it is possible to produce a highly accurate DEM (with an RMSE of about 7 m) using repeat-pass InSAR from ERS–tandem pairs. These results suggest that high resolution InSAR can meet the requirements of many applications in low relief areas since it can capture small variations in relatively flat-relief and bare-earth fields. In addition, this study shows that, although it is not as accurate as the InSAR elevation model, an ASTER DEM is still accurate in reflecting topographic surface details. Given accurate

and well-distributed GCPs, an RMSE of about 13 m can be achieved using ASTER stereo images with a reasonable number of GCPs. The DEMs are very accurate in nearly flat regions and on smooth slopes with errors generally within 10 m. Larger errors appear in areas with a high variation of elevation areas, and deep valleys with extreme errors of a few tens of metres. The plot of cumulative absolute mean error and RMSE of InSAR and ASTER DEMs against the percentage of pixels resulting from the difference in images between InSAR and ASTER DEMs and the TopoMap DEM shows that the DEM derived from ASTER has a lower degree of error at most percentages of pixels. The underestimation error was located in the low relief area and valleys, while the overestimation error was located in the high relief area. The effect of vegetation may cause the high variation of elevation in valleys.

GCPs are one of the main factors that affect the accuracy of DEMs. Both techniques require high quality GCPs to derive absolute elevation measurements. GCPs are used during the generation of DEMs from InSAR data to calibrate the unwrapped phase to ground height. Identifying or selecting ground control points on the InSAR image was a difficult task because of the large amount of noise in the image, and these points could be shifted from their rightful place by a cell or two cells or more. Following the careful identification of these points, this study conducted a sensitivity experiment to ascertain the implications of the points being in slightly wrong location, using three types of windows on the assumption that the true location of the point is the middle cell in each window. After height estimation, the DEM remains in the slant range coordinate system. The spatial distribution and accuracy of GCPs, which can be precisely located on the ASTER scene, are the main factors limiting the accuracy of ASTER DEMs.

7.3 Findings: Objective 3

Evaluate the accuracy of DEMs derived from interferometric synthetic aperture radar (InSAR) data from ERS-1 and ERS-2 SAR and ASTER of stereoimage using DEM generated from topographic maps.

Another part of the accuracy assessment was done by comparing the accuracy of these DEMs with a DEM created from the 1:50,000 topographic maps. Before comparing the TopoMap DEM with the derived DEMs, its validation against highly accurate elevation data (DGPS) was done. Different assessment techniques were used in this part of the analyses of the accuracy of InSAR and ASTER DEMs, which included spatial correlation between DEMs image difference and spatial profiling of elevation. The results showed that the RMSE for the TopoMap DEM equalled about 10 m. Statistical measures and difference maps were created based on the comparisons of the TopoMap DEM with the InSAR and ASTER DEMs. The results for InSAR showed the elevation difference to be 9.2 m. The results for ASTER showed the elevation difference to be 3.8 m. From comparison of the TopoMap DEM with derived DEMs, the spatial distribution of error can be understood, and it can be correlated with influencing factors, such as slope.

Both InSAR and ASTER DEMs are able to map topographic structures, for example, small scale of high features, ridges and breaklines compared to tendency to lose these features in TopoMap DEM due to interpolation technique as noticed in comparison of DEMs profiles in Sction 6.4.3. In addition, in both DEMs, there is a loss of topographic features in flat areas with increasing grid size as can be seen in section 6.8. The ASTER DEM was more successful than the InSAR DEM in low relief areas like valleys. The probable reason for that is that the valley area was vegetated and the data gathering time coincided with peak of growing time, so the correlation was low between the InSAR data pair. This led to severe phase unwrapping errors, and the accuracy of the DEM was affected. However, the InSAR DEM was more accurate in the high relief area than was the ASTER DEM.

7.4 Findings: Objective 4

Understanding the error and resolution implications of DEMs in surface flow.

Understanding DEM accuracy is of crucial importance, as errors in its derived products will be propagated through spatial GIS analysis (Tagaki and Shibasaki, 1996;

Hunter and Goodchild, 1997). The quality of DEM-derived hydrological features is sensitive to DEM accuracy. In hydrologic modelling, for example, one might be interested in assessing DEM accuracy over areas of relatively flat terrain, since small variations in these areas affect surface run-off routes (Burrough and McDonnell 1998). Elevation error can greatly affect DEM-derivative products, such as slope, flow direction, and flow accumulation, and subsequently all interpretations dependent on these calculations. This study examined the effect of ASTER DEM error on surface flow using high accuracy GPS data with sequential Gaussian simulation. The results suggest that extreme caution should be taken during the analysis of the surface flow derived from DEMs, particularly in low relief sites, since small errors in the estimation of the elevation values can change the direction of the flow.

Slope, flow accumulated area, flow path and catchment area are the four important topographic parameters determining watershed delineation and surface runoff profile in hydrologic modelling with DEMs. The impact of DEM resolution on these parameters was examined across five different DEM grid sizes. It was found that, as the resolution increases from 20 m to 100 m for all the DEMs, the slope gradient flattens, while the accumulated area, the flow length and the catchment area increase. The results indicate the resolution of DEM is important for the analysis of hydrological parameters, since the increase in resolution can smooth features, leading to some changes in elevation. The findings suggest that a profound understanding of these topographic parameters is essential to the application of hydrological modelling with DEMs. This understanding would ensure that uncertainty in a hydrologic model is assessed in terms of spatial data resolution and would give an integral insight into the association between catchment topography and hydrologic processes.

7.5 Limitations

The limitations of the research are related to the availability of reference DEM of higher order accuracy. It would have been appropriate to have reference DEM created using highly accurate techniques such as photograph images which allow more evaluation of the potential and limitations of the technique. Also, large-scale

topographic maps do not exist for Al-Jafer basin which affects the accuracy of DEMs created using topographic maps. It was not possible to conduct GPS surveys for all the sites of the study area because some areas comprised farming fields and inaccessible army area. Also, some areas with steep and rugged terrain were inaccessible and therefore not represented by the GCPs. The survey was based mainly in the existing road network of the area, primarily roads without asphalt, which contributed to the limitation of the distribution of GCPs, and a decrease in the accuracy of the DEM.

7.6 Future Work

The aim of this research was to understand accuracies and uncertainties associated with digital elevation models derived from spaceborne remotely-sensed data and the implications of their use to understanding hydrological processes in a closed basin system in central Jordan. In answering this aim through a set of objectives, the following topics have been identified for further work.

1. More investigation is needed to study the effect of the number, distribution and identification of GCPs on DEMs. This can help to improve the results, particularly the ASTER DEM.

2. More study is needed into geomorphological and land cover analysis which can help to understand the combined of effect of these factors and the nature of error in the DEMs.

References

Abrams, M., 2000. The Advanced Spaceborne Thermal Emission and Reflection Radiometer (ASTER): data products for the high spatial resolution imager on NASA's Terra platform. International Journal of Remote Sensing, 21(5): 847-859.

Aguilar, F.J., Aguilar, M.A. and Agüera, F., 2007. Accuracy assessment of digital elevation models using a non-parametric approach. International Journal of Geographical Information Science, 21(6): 667 - 686.

Al-Harbi, S. and Tansey, K., 2007. The accuracy of a DEM derived from ASTER data using differential GPS measurements, ISPRS High-Resolution Earth Imaging for Geospatial Information Workshop, Hannover, Germany.

Al-Harbi, S. and Tansey, K., 2008a. Accuracy assessment of an ASTER derived DEM over a sparsely vegetated closed basin system in Jordan, The 7th International Symposium & Exhibition on Geoinformation (ISG 2008) at the Putra World Trade Centre (PWTC), Kuala Lumpur, Malaysia.

Al-Harbi, S. and Tansey, K., 2008b. Accuracy assessment of an InSAR derived DEM over a sparsely vegetated closed basin system in Jordan, Remote Sensing and Photogrammetric Society Annual Conference, Falmouth, UK.

Al-Rousan, N.M. and Petrie, G., 1998. System Calibration, Geometric Accuracy Testing and Validation of DEM and Orthoimage Data Extracted from Spot Stereo-pairs Using Commercially Available Image Processing Systems, University of Glasgow.

Al-Zu'bi, Y.A. and Al-Kharabsheh, A., 2003. Multicriteria analysis for water productivity in the Jordan Valley. Water International, 28(4): 501-511.

Altmaier, A. and Kany, C., 2002. Digital surface model generation from CORONA satellite images. ISPRS Journal of Photogrammetry and Remote Sensing, 56(4): 221-235.

Aronoff, S., 1989. Geographic information systems: a management perspective. Geocarto International, 4(4): 58-58.

Arrell, K., Wise, S., Wood, J. and Donoghue, D., 2008. Spectral filtering as a method of visualising and removing striped artefacts in digital elevation data. Earth Surface Processes and Landforms, 33(6): 943-961.

Aspinall, R.J. and Pearson, D.M., 1993. Data quality and spatial analysis: analytical use of GIS for ecological modeling, Proceeding of the 2nd International Conference on Environmental Modeling and Geographic Information Systems, Breckenridge, Colorado.

Band, L.E., 1986. Topographic partition of watersheds with digital elevation models. Water Resources Research, 22(1): 15-24.

Barber, C.P. and Shortrudge, A.M., 2004. Light Detection and Ranging (LiDAR)-derived elevation data for surface hydrology applications. Institute of Water Research, Michigan State University.

Bolstad, P.V. and Stowe, T., 1994. An evaluation of DEM accuracy: elevation, slope, and aspect. Photogrammetric engineering and remote sensing, 60(11): 1327-1332.

Burrough, P.A., 1986. Principles of geographical information systems for land resources assessment. Clarendon Press, Oxford. US, 194 pp.

Burrough, P.A., 1993. Soil variability: a late 20th century view. Soils and Fertilizers, 56(5): 529-562.

Burrough, P.A., McDonnell, R.A. and McDonnell, R., 1998. Principles of geographical information systems. Oxford University Press, New York, 333 pp.

Büyüksalih, G., Kocak, M.G., Oruc, M., Akcin, H. and Jacobsen, K., 2003. Handling of IKONOS-images from Orientation up to DEM Generation. Joint Workshop "High Resolution Mapping from Space 2003", Hannover. Accessed on 22/04/2007http://www.ipi.unihannover.de/fileadmin/institut/pdf/bueyuek_Ikon.pdf

Carrara, A., Bitelli, G. and Carla, R., 1997. Comparison of techniques for generating digital terrain models from contour lines. International Journal of Geographical Information Science, 11(5): 451-473.

Carter, J., 1990. Some effects of spatial resolution in the calculation of slope using the spatial derivative. Paper presented at ASPRS-ACSM Annual Convention-Technical Papers, 1990.

Carter, J.R., 1988. Digital representations of topographic surfaces. Photogrammetric Engineering and Remote Sensing, 54(11): 1577-1580.

Chang, K. and Tsai, B., 1991. The effect of DEM resolution on slope and aspect mapping. Cartography and Geographic Information Science, 18(1): 69-77.

Cheng, H.H., 2000. Photogrammetric digital data processing of Tsau-Lin big landslide. Accessed on 24/06/2007 http://www.gisdevelopment.net/aars/acrs/2000/ps1/ps102.asp

Cheng, P. and Chaapel, C., 2006. DEM Generation Using QuickBird St Using Tie Points. Accessed on 14/05/2007 http://www.pcigeomatics.com/pdfs/P36-38_GI_02_2006.pdf

Cheng, P., Gómez, F., Weber, M. and Flingelli, C., 2008. Correcting the Data Mapping of IKONOS Images. Accessed on 10/01/2009 http://www.pcigeomatics.com/pdfs/Ikonos.pdf

Chrisman, N.R. (Editor), 1991. The error component in spatial data. In Maguire D.J., Goodchild, M.F. and Rhind, D.W. (Eds). Geographical Information Sys-tems, 165-174 pp.

Cooper, M.A.R. (Editor), 1998. Datums, coordinates and differences. In Lane, S., Richards, K. and Chandler, J., editors, Landform monitoring, modelling and analysis, 21–36 pp.

Cooper, M.A.R. and Cross, P.A., 1988. Statistical concepts and their application in photogrammetry and surveying. The Photogrammetric Record, 12(71): 637-663.

Cuartero, A., Felicisimo, A.M. and Ariza, F.J., 2005. Accuracy, reliability, and depuration of SPOT HRV and Terra ASTER digital elevation models. IEEE Transactions on Geoscience and Remote Sensing, 43(2): 404-407.

Darnell, A.R., Tate, N.J. and Brunsdon, C., 2008. Improving user assessment of error implications in digital elevation models. Computers, Environment and Urban Systems, 32(4): 268-277.

Davis, T.J. and Keller, C.P., 1997. Modelling uncertainty in natural resource analysis using fuzzy sets and Monte Carlo simulation: slope stability prediction. International Journal of Geographical Information Science, 11(5): 409-434.

Desmet, P.J.J., 1997. Effects of interpolation errors on the analysis of DEMs. Earth Surface Processes and Landforms, 22(6): 563-580.

DeWitt, B.A. and Wolf, P.R., 2000. Elements of Photogrammetry with Applications in GIS.

Doucette, P. and Beard, K., 2000. Exploring the capability of some GIS surface interpolators for DEM gap fill. Photogrammetric engineering and remote sensing, 66(7): 881-888.

Dunn, M. and Hickey, R., 1998. The effect of slope algorithms on slope estimates within a GIS. Cartography, 27(1): 9-15.

Eastman, J.R., 1992. IDRISI 4.0 Technical Reference. User's Guide, Clark University, Graduate School of Geography, 213 pp.

Eckert, S., Kellenberger, T. and Itten, K., 2005. Accuracy assessment of automatically derived digital elevation models from aster data in mountainous terrain. International Journal of Remote Sensing, 26(9): 1943-1957.

Ehlschlaeger, C.R. and Goodchild, M.F., 1994. Dealing with uncertainty in categorical coverage maps: Defining, visualizing, and managing errors, Proceedings of the Second ACM Workshop on Advances in Geographic Information Systems, pp. 86-91.

El-Rabbany, A., 2002. Introduction to GPS: The Global Positioning System. Boston, MA: Artech House, 176 pp.

El-Sheimy, N., Valeo, C. and Habib, A., 2005. Digital terrain modeling: acquisition, manipulation, and applications. Boston, MA: Artech House, 257 pp.

Endreny, T.A., Wood, E.F. and Lettenmaier, D.P., 2000. Satellite-derived digital elevation model accuracy: hydrological modelling requirements. Hydrological Processes, 14(2): 177-194.

ENVI, 2008. DEM Extraction Module User's Guide. Accessed on 18/11/2008 http://www.ittvis.com/portals/0/pdfs/envi/DEM_Extraction_Module.pdf

ESA, 2008. InSAR processing: a practical approach. (European Space Agency). Accessed on 22/09/2007 http://www.esa.int/esapub/tm/tm19/TM-19_ptB.pdf

Euroimage, 2002. The world'shighest resolution commercial satellite. Accessed on 22/05/2008 http://www.eurimage.it/products/docs/quickbird.pdf

Eyton, R.J., 1991. Rate-of-change maps. Cartography and Geographic Information Science, 18(2): 87-103.

Falorni, G., Teles, V., Vivoni, E.R., Bras, R.L. and Amaratunga, K.S., 2005. Analysis and characterization of the vertical accuracy of digital elevation models from the Shuttle Radar Topography Mission. Journal of Geophysical Research, 110(F2).

FGDC, 1998. Geospatial Positioning Accuracy Standards Part 3: National Standard for Spatial Data Accuracy" (Reston, VA: US Federal Geographic Data Committee). Accessed on 10/09/2007 htpp://www.fgdc.gov/FGDC-standards projects/accuracy/part3/chapter3

Fisher, P., 1998. Improved modeling of elevation error with geostatistics. GeoInformatica, 2(3): 215-233.

Fisher, P.F. and Tate, N.J., 2006. Causes and consequences of error in digital elevation models. Progress in Physical Geography, 30(4): 467.

Florinsky, I.V., 1998a. Accuracy of local topographic variables derived from digital elevation models. International Journal of Geographical Information Science, 12(1): 47-62.

Florinsky, I.V., 1998b. Combined analysis of digital terrain models and remotely sensed data in landscape investigations. Progress in Physical Geography, 22(1): 33-60.

Fornaro, G., Franceschetti, G. and Lanari, R., 1996a. Interferometric SAR phase unwrapping using Green's formulation. IEEE Transactions on Geoscience and Remote Sensing, 34(3): 720-727.

Fornaro, G., Franceschetti, G. and Lanari, R., 1996b. Interferometric SAR phase unwrapping using Green's formulation. IEEE Transactions on Geoscience and Remote Sensing, 34(3): 720-727.

Franceschetti, G. and Lanari, R., 1999. Synthetic aperture radar processing. CRC press, Boca Raton, 305 pp.

Gamba, P., Dell Acqua, F. and Houshmand, B., 2002. SRTM data characterization in urban areas. International Archives of Photogrammetry Remote Sensing and Spatial Information Sciences, 34(3/B): 55-58.

Gao, J., 1997. Resolution and accuracy of terrain representation by grid DEMs at a micro-scale. International Journal of Geographical Information Science, 11(2): 199-212.

Garbrecht, J. and Martz, L., 1994. Grid size dependency of parameters extracted from digital elevation models. Computers & Geosciences, 20(1): 85-87.

Garbrecht, J. and Martz, L.W., 1997. The assignment of drainage direction over flat surfaces in raster digital elevation models. Journal of Hydrology, 193(1-4): 204-213.

Garbrecht, J. and Martz, L.W., 1999. Digital Elevation Model Issues In Water Resources Modelling, Proceedings the 19th ESRI International User Conference, Environmental Systems Research Institute, Sna Diego, California

Garrote, L. and Bras, R.L., 1995. A distributed model for real-time flood forecasting using digital elevation models. Journal of Hydrology, 167(1-4): 279-306.

Gelautz, M., Paillou, P., Chen, C.W. and Zebker, H.A., 2003. Radar stereo-and interferometry-derived digital elevation models: comparison and combination using Radarsat and ERS-2 imagery. International Journal of Remote Sensing, 24(24): 5243-5264.

Gens, R., 1999. SAR interferometry: Software, data format, and data quality. Photogrammetric engineering and remote sensing, 65(12): 1375-1378.

Gens, R. and Van Genderen, J.L., 1996. Review Article SAR interferometry—issues, techniques, applications. International Journal of Remote Sensing, 17(10): 1803-1835.

Goldenstein, R.M., Zebker, H.A. and Werner, C.L., 1988. Satellite radar interferometry: two-dimensional phase unwrapping. Radio Science, 23(4): 713–720.

Gong, J., Li, Z., Zhu, Q., Sui, H. and Zhou, Y., 2000. Effects of various factors on the accuracy of DEMs: an intensive experimental investigation. Photogrammetric Engineering and Remote Sensing, 66(9): 1113-1117.

Gooch, M.J., Chandler, J.H. and Stojic, M., 1999. Accuracy Assessment of Digital Elevation Models Generated Using the Erdas Imagine Orthomax Digital Photogrammetric System. The Photogrammetric Record, 16(93): 519-531.

Gorokhovich, Y. and Voustianiouk, A., 2006. Accuracy assessment of the processed SRTM-based elevation data by CGIAR using field data from USA and Thailand and its relation to the terrain characteristics. Remote Sensing of Environment, 104(4): 409-415.

Graham, L.C., 1974. Synthetic interferometer radar for topographic mapping. Proceedings of the IEEE, 62(6): 763-768.

Griffin, M.W., 1991. Military applications of digital terrain models. In Petri, G., and Kennie, T.J.M. (eds.), Terrain Modelling in Surveying and Civil Engineering McGraw-Hill, New York, 227-289 pp.

Griffith, D.A., 1996. Some guidelines for specifying the geographic weights matrix contained in spatial statistical models. In Arlinghaus, S. L. (ed.), Practical handbook of spatial statistics. CRC Press, Boca Raton, 65-82 pp.

Guo-an, T., Yang-he, H., Strobl, J. and Wang-qing, L., 2001. The impact of resolution on the accuracy of hydrologic data derived from DEMs. Journal of Geographical Sciences, 11(4): 393-401.

Guth, P.L. (Editor), 1995. Slope and aspect calculations on gridded digital elevation models: examples from a geomorphometric toolbox for personal computers. Zeitschrift fur Geomorphologie Supplementband, 31-52 pp.

Hagberg, J.O. and Ulander, L.M.H., 1993. On the optimization of interferometric SAR for topographic mapping. IEEE Transactions on Geoscience and Remote Sensing, 31(1): 303-306.

Hancock, G.R., 2005. The use of digital elevation models in the identification and characterization of catchments over different grid scales. Hydrological Processes, 19(9): 1727-1749.

Haneberg, W.C., 2006. Effects of digital elevation model errors on spatially distributed seismic slope stability calculations: an example from Seattle, Washington. Environmental and Engineering Geoscience, 12(3): 247-260.

Hanssen, R.F., 2001. Radar interferometry data interpretation and error analysis Remote sensing and digital image processing. Kluwer Academic, Dordrecht, The Netherlans, 308 pp.

Herland, E.A., 1996. Operational use of SAR interferometry for DEM generation and land use mapping, Proceedings of the Fringe 96 Workshop, held in Zurich, Switzerland. Accessed on 04/10/2007 http://earth.esa.int/workshops/fringe_1996/herland/

Heuvelink, G.B.M., 1998. Error propagation in environmental modelling with GIS. Taylor & Francis, 127 pp.

Hickey, R., 2000. Slope angle and slope length solutions for GIS. Cartography, 29(1): 1-8.

Hirano, A., Welch, R. and Lang, H., 2003. Mapping from ASTER stereo image data: DEM validation and accuracy assessment. ISPRS Journal of Photogrammetry and Remote Sensing, 57(5-6): 356-370.

Hodgson, M.E., 1995. What cell size does the computed slope/ aspect angle represent?. Photogrammetric Engineering and Remote Sensing, 71(7): 817-823.

Hodgson, M.E. et al., 2005. An evaluation of lidar-derived elevation and terrain slope in leaf-off conditions. Photogrammetric Engineering and Remote Sensing, 71(7): 817-823.

Hodgson, M.E., Jensen, J.R., Schmidt, L., Schill, S. and Davis, B., 2003. An evaluation of LIDAR- and IFSAR-derived digital elevation models in leaf- on conditions with USGS Level 1 and Level 2 DEMs. Remote Sensing of Environment, 84(2): 295-308.

Hogg, J., McCormack, J.E., Roberts, S.A., Gahegan, M.N. and Hoyle, B.S. (Editors), 1993. Automated derivation of stream-channel networks and selected catchment characteristics from digital elevation models. In Mather, P. M. (Ed)Geographical information handling—research and applications. John Wiley & Sons Ltd., New York, 207-235 pp.

Holmes, K.W., Chadwick, O.A. and Kyriakidis, P.C., 2000. Error in a USGS 30-meter digital elevation model and its impact on terrain modeling. Journal of Hydrology, 233(1-4): 154-173.

Horn, B.K.P., 1981. Hill shading and the reflectance map. Proceedings of the IEEE, 69(1): 14-47.

Huang, Y. and Van Genderen, J.L., 1994. Comparison of Several Multi-Look Processing Procedures in InSAR Processing for ERS-1&2 Tandem Mode, Proceedings of the Fringe 96 Workshop, held in Zurich, Switzerland.

Hunter, G.J. and Goodchild, M.F., 1995. Dealing with error in a spatial database: A simple case study. Photogrammetric Engineering and Remote Sensing, 61(5): 529-537.

Hunter, G.J. and Goodchild, M.F., 1997. Modeling the uncertainty of slope and aspect estimates derived from spatial databases. Geographical Analysis, 29(1): 35-49.

Jaan, R. and Hung-Hsu, C., 2001. DEM Generation in Taiwan by using INSAR and ERS Data, Paper presented at the 22nd Asian conference on remote sensing, Singapore, pp. 5-9.

Jacobsen, K., 2002. Mapping with IKONOS images, EARSeL, Prag 2002 "Geoinformation for European-wide Integration". Mill press.

Jenson, S.K. and Domingue, J.O., 1988. Extracting topographic structure from digital elevation data for geographic information system analysis. Photogrammetric Engineering and Remote Sensing, 54(11): 1593-1600.

Kennie, T.J.M. and Petrie, G. (Editors), 1991. Introduction to terrain modelling - application fields and ter¬minology. In Petrie G and TJM Kennie (eds). Terrain Modelling in Surveying and Civil Engi-neering. McGraw-Hill, New York.

Kenward, T., Lettenmaier, D.P., Wood, E.F. and Fielding, E., 2000. Effects of Digital Elevation Model Accuracy on Hydrologic Predictions. Remote Sensing of Environment, 74(3): 432-444.

Kervyn, F., 2001. Modelling topography with SAR interferometry: illustrations of a favourable and less favourable environment. Computers and Geosciences, 27(9): 1039-1050.

Kervyn, M., Goossens, R., Jacobs, P. and Ernst, G.G.J., 2008. Mapping volcano topography with remote sensing: ASTER vs SRTM. International Journal of Remote Sensing, 29(22): 6515-6538.

Kyaruzi, J.K., 2005. Quality assessment of DEM from radargrammetry data: Quality assessment from the user perspective, Enschede, the Netherlands.

Kyriakidis, P.C., Shortridge, A.M. and Goodchild, M.F., 1999. Geostatistics for conflation and accuracy assessment of digital elevation models. International Journal of Geographical Information Science, 13(7): 677-707.

Lacroix, M.P., Martz, L.W., Kite, G.W. and Garbrecht, J., 2002. Using digital terrain analysis modeling techniques for the parameterization of a hydrologic model. Environmental Modelling and Software, 17(2): 125-134.

Lang, H.R. and Welch, J., 1999. ATBD-AST-08 Algorithm theoretical basis document for aster digital elevation models standard product AST 14 version 3.0, University of Georgia, USA.

Leberl, F.W., 1990. Radargrammetric image processing. Artech House, Norwood, USA, 595 pp.

Li, F.K. and Goldstein, R.M., 1990a. Studies of multibaseline spaceborne interferometric syntheticaperture radars. IEEE Transactions on Geoscience and Remote Sensing, 28(1): 88-97.

Li, F.K. and Goldstein, R.M., 1990b. Studies of multibaseline spaceborne interferometric syntheticaperture radars. IEEE Transactions on Geoscience and Remote Sensing, , 28(1): 88-97.

Li, Z., 1992. Variation of the Accuracy of Digital Terrain Models with Sampling Interval. The Photogrammetric Record, 14(79): 113-128.

Li, Z., 2006. A study on the applicability of repeat-pass SAR interferometry for generating DEMs over several Indian test sites. International Journal of Remote Sensing, 27(3): 595-616.

Li, Z. and Chen, J. (Editors), 1999. Assessment of the accuracy of digital terrain models (DTMs): theory and practice. In Shi, W., Goodchild, M.F. and Fisher, P.F., (eds), Proceedings of the International Symposium on Spatial Data Quality 1999, Hong Kong, Hong Kong Polytechnic University.

Li, Z. and Zhu, Q., 2005. Digital terrain modeling: principles and methodology. CRC Press, Boca Raton, 323 pp.

Lillesand, T.M., Kiefer, R.W. and Chipman, J.W., 2004. Remote sensing and image interpretation. John Wiley & Sons Ltd Chichester, UK, 763 pp.

Lo, C.P. and Albert, K.W. (Editors), 2007. Concepts and Techniques of Geographic Information Systems, 2nd edition. Pearson, Prentice Hall, University of Georgia, 532 pp.

Lo, C.P. and Yeung, A.K.W., 2006. Concepts and Techniques of Geographic Information Systems (Ph Series in Geographic Information Science). Prentice-Hall, Inc. Upper Saddle River, NJ, USA.

Ludwig, R. and Schneider, P., 2006. Validation of digital elevation models from SRTM X-SAR for applications in hydrologic modeling. ISPRS Journal of Photogrammetry and Remote Sensing, 60(5): 339-358.

Lunetta, R.S.a.L., J.G., 2004. Remote Sensing and GIS Accuracy. CRC Press, Boca Raton, FL, USA.

Ma, R., 2005. DEM Generation and building detection from Lidar data. Photogrammetric engineering and remote sensing, 71(7): 847-854.

MacMillan, R.A., Jones, R.K. and McNabb, D.H., 2004. Defining a hierarchy of spatial entities for environmental analysis and modeling using digital elevation models (DEMs). Computers, Environment and Urban Systems, 28(3): 175-200.

Martz, L.W. and Garbrecht, J., 1993. Automated extraction of drainage network and watershed data from digital elevation models. Journal of the American Water Resources Association, 29(6): 901-908.

Martz, L.W. and Garbrecht, J., 1998. The treatment of at areas and depressions in automated drainage analysis of raster digital elevation models. Hydrological Processes, 12(6): 843-855.

Martz, L.W. and Garbrecht, J., 1999. An outlet breaching algorithm for the treatment of closed depressions in a raster DEM. Computers and Geosciences, 25(7): 835-844.

Masini, N. and Lasaponara, R., 2007. Investigating the spectral capability of QuickBird data to detect archaeological remains buried under vegetated and not vegetated areas. Journal of Cultural Heritage, 8(1): 53-60.

Maune, D.F., 2001. Digital elevation model technologies and applications: the DEM user's manual. The American Society for Photogrammetry and Remote Sensing. Bethesda, Maryland, 539 pp.

McCormack, J.E. and Hogg, J., 1997. Virtual-memory tiling for spatial data handling in GIS. Computers and Geosciences, 23(6): 659-669.

Meijerink, A.M.J., Brouwer, H.A.M., Mannaerts, C.M. and Valenzuela, C.R., 1994. Introduction to the use of geographic information systems for practical hydrology. ITC publication 23, Enschede, The Netherlands.

Miller, C.L. and Laflamme, R.A., 1958. The digital terrain model-theory and application. Photogrammetric Engineering and Remote Sensing, 24: 433-442.

Monckton, C., 1994. An Investigation into the spatial structure of error in digital elevation data. Innovations in GIS: Selected papers from the First National Conference on GIS Research UK, pp. 201–211.

Moore, I.D., Grayson, R.B. and Ladson, A.R., 1991. Digital terrain modelling: a review of hydrological, geomorphological, and biological applications. Hydrological Processes, 5(1): 3-30.

Moussa, R., 1997. Geomorphological transfer function calculated from digital elevation models for distributed hydrological modelling. Hydrological Processes, 11(5): 429-449.

National Mapping, D. and Survey, G., 1992. Standards for Digital Elevation Models. US Geological Survey.

Nikolakopoulos, K.G., Kamaratakis, E.K. and Chrysoulakis, N., 2006. SRTM vs ASTER elevation products. Comparison for two regions in Crete, Greece. International Journal of Remote Sensing, 27(21): 4819-4838.

Noguchi, M., Fraser, C.S., Nakamura, T., Shimono, T. and Oki, S., 2004. Accuracy assessment of QuickBird stereo imagery. The Photogrammetric Record, 19(106): 128-137.

Nonin, P. and Piccard, S., 2003. Performance analysis of DEM automatic extraction from SPOT5 sensors, Proceeding IEEE International Geoscience and Remote Sensing Symposium, Toulouse.

O'Callaghan, J.F. and Mark, D.M., 1984. The extraction of drainage networks from digital elevation data. Computer vision, graphics, and image processing, 28(3): 323-344.

Oksanen, J. and Sarjakoski, T., 2005. Error propagation of DEM-based surface derivatives. Computers and Geosciences, 31(8): 1015-1027.

Petrie, G. and Kennie, T.J.M., 1990. Terrain modelling in surveying and civil engineering. Computer-Aided Design, 19(4): 171-187.

Peucker, T.K., Fowler, R.J., Little, J.J. and Mark, D.M., 1978. The triangulated irregular network, Proceeding of the DTM Symposium American Society of Photogrammetry American Congress on Survey and Mapping, St. Louise, Missouri, U.S.A, pp. 24-31.

Poidomani, C.G., Costantini, D., Pasquali, P. and Jaeger, P., 2000. National-Scale Dem Generation Using ERS Tandem Data In Alpine Regions, Accessed 07/08/2008 http://www.sarmap.ch/goteborg_dem.pdf

Polidori, L., 1997. Cartographie radar. Gordon and Breach, Amsterdam, The Netherlands, 287 pp.

Poon, J., Fraser, C.S., Chunsun, Z., Li, Z. and Gruen, A., 2005. Quality Assessment Of Digital Surface Models Generated From IKONOS Imagery. The Photogrammetric Record, 20(110): 162-171.

Quinn, P., Beven, K., Chevallier, P. and Planchon, O., 1991. The prediction of hillslope flow paths for distributed hydrological modelling using digital terrain models. Hydrological Processes, 5(1): 59-79.

Raaflaub, L.D. and Collins, M.J., 2006. The effect of error in gridded digital elevation models on the estimation of topographic parameters. Environmental Modelling and Software, 21(5): 710-732.

Rao, K.S. et al., 2006. A study on the applicability of repeat-pass SAR interferometry for generating DEMs over several Indian test sites. International Journal of Remote Sensing, 27(3): 595-616.

Ravibabu, M.V. and Jain, K., 2008. Digital Elevation Model Accuracy Aspects. Journal of Applied Sciences, 8(1): 134-139.

Ren, K., Prinet, V., Shi, X. and Wang, F., 2003. Comparison of satellite baseline estimation methods for interferometry applications, Proceedings of the IGARSS 2003 IEEE-Remote Sensing for a Sustainable Future, Beijing, China, pp. 342-344.

Rosen, P.A. et al., 2000. Synthetic aperture radar interferometry. Proceedings of the IEEE, 88(3): 333-382.

Rufino, G., Moccia, A. and Esposito, S., 1998. DEM generation by means of ERS tandem data. IEEE Transactions on Geoscience and Remote Sensing, 36(6): 1905-1912.

San, B.T. and Süzen, M.L., 2005. Digital elevation model (DEM) generation and accuracy assessment from ASTER stereo data. International Journal of Remote Sensing, 26(22): 5013-5027.

Sansosti, E. et al., 1999. Digital elevation model generation using ascending and descending ERS-1/ERS-2 tandem data. International Journal of Remote Sensing, 20(8): 1527-1547.

Saraf, A.K., Mishra, B.P., Choudhury, S. and Ghosh, P., 2005. Digital elevation model (DEM) generation from NOAA–AVHRR night-time data and its comparison with USGS-DEM. International Journal of Remote Sensing, 26(18): 3879-3887.

Sasowsky, K.C., Petersen, G.W. and Evans, B.M., 1992. Accuracy of SPOT digital elevation model and derivatives: utility for Alaska's north slope. Photogrammetric Engineering and Remote Sensing, 58(6): 815-824.

Schmid-Mcgibbon, G. and Eyton, J.R., 1996. Frequency-based contextual landform classification. Geomatica, 50(3): 287-299.

Schoorl, J.M., Sonneveld, M.P.W. and Veldkamp, A., 2000. Three-dimensional landscape process modelling: the effect of DEM resolution. Earth Surface Processes and Landforms, 25(9): 1025-1034.

Shearer, J.W., 1990. The accuracy of digital terrain models. In Petrie, G. and Kennie, T. J. M., (Eds) Terrain modelling in surveying and civil engineering: 315-336.

Shears, J. and Allan, J., 1996. Softcopy Photogrammetry and its uses in GIS. International Archives of Photogrammetry and Remote Sensing: 70-73.

Shortridge, A., 2001. Characterizing uncertainty in digital elevation models. Spatial Uncertainty in Ecology: Implications for Remote Sensing and GIS Applications: 238–257.

Silveira, M.T., Feitosa, R.Q., Jacobsen , K., Brito, J.L.N.S. and Heckel, Y., 2008. A hybrid method for stereo image matching, The International Archives of the Photogrammetry, Remote Sensing and Spatial Information Sciences Beijing, China.

Skidmore, A.K., 1989. A comparison of techniques for calculating gradient and aspect from a gridded digital elevation model. International Journal of Geographical Information Science, 3(4): 323-334.

Slama, C.C., Theurer, C. and Henriksen, S.W., 1980. Manual of photogrammetry. American Society of Photogrammetry, Falls Church, Virginia.

Small, D., Pasquali, P. and Fuglistaler, S., 1996. A comparison of phase to height conversion methods for SARinterferometry. Geoscience and Remote Sensing Symposium, 1996. IGARSS'96.'Remote Sensing for a Sustainable Future.', International, 1.

Small, D., Werner, C. and Nuesch, D., 1993. Baseline modelling for ERS-1 SAR interferometry, Proceedings of the IGARSS 93, pp. 1204-1206.

Srinivasan, R. and Engel, B.A., 1991. Effect of slope prediction methods on slope and erosion estimates. Applied Engineering in Agriculture, 7(6): 779-783.

Stebler, O., Meier, E. and Nüesch, D., 2002. Multi-baseline polarimetric SAR interferometry—first experimental spaceborne and airborne results. ISPRS Journal of Photogrammetry and Remote Sensing, 56(3): 149-166.

Stevens, N.F., Garbeil, H. and Mouginis-Mark, P.J., 2004. NASA EOS Terra ASTER: Volcanic topographic mapping and capability. Remote Sensing of Environment, 90(3): 405-414.

Stocks, A.M. and Heywood, D.I. (Editors), 1994. Terrain modelling for mountains. In Price, M. F. and Heywood, D. I. (Eds) Mountain Environments and Geographic Information Systems. London: Taylor & Francis, pp. 25-40.

Strahler, A.N., 1964. Quantitative geomorphology of drainage basins and channel networks. Handbook of Applied Hydrology.

Sui, D.Z. and Maggio, R.C., 1999. Integrating GIS with hydrological modeling: practices, problems, and prospects. Computers, Environment and Urban Systems, 23(1): 33-51.

Sulebak, J.R., 2000. Applications of Digital Elevation Models, Department of Geographic Information Technology, SINTEF Applied Mathematics Oslo, Norway.

Survey, O., 1999. Land-Form PROFILE User Guide, Version 3.0 Data, Accessed 04/07/2007 http://www.ordsvy.gov.uk/downloads/height/profile/profil_w.pdf

Survey, U.G., 1997. Standards for digital elevation models: part 3–quality control, National mapping programme, Technical instruction, National Mapping Division, Accessed on 04/12/2007 http://rockyweb.cr.usgs.gov/nmpstds/acrodocs/dem/3DEM0897.PDF

Survey, U.G., 1998. SUSGS Geospatial Data Clearinghouse, National Mapping and Remotely Sensed Data: Digital Elevation Models (DEMs), Technical instruction, National Mapping Division, Accessed on 22/12/2007 http://edcwww.cr.usgs.gov/nsdi/gendem.htm

Takagi, M. and Shibasaki, R., 1996. An interpolation method for continental DEM generation using small scale contour maps. International Archives of Photogrammetry and Remote Sensing, 31: 847-852.

Tarboton, D.G., 1997. A new method for the determination of flow directions and upslope areas in grid digital elevation models. Water Resources Research, 33(2): 309-319.

Tarboton, D.G., Bras, R.L. and Rodriguez-Iturbe, I., 1991. On the extraction of channel networks from digital elevation data. Hydrological Processes, 5(1): 81-100.

Theobald, D.M. (Editor), 1989. Accuracy and bias issues in surface representation. In Goodchild, M.F., Gopal, S. (Eds.), Accuracy of Spatial Databases, Francis, New York, pp. 99-106.

Thieken, A.H., Lucke, A., Diekkruger, B. and Richter, O., 1999. Scaling input data by GIS for hydrological modelling. Hydrological Processes, 13(4): 611-630.

Thompson, J.A., Bell, J.C. and Butler, C.A., 2001. Digital elevation model resolution: effects on terrain attribute calculation and quantitative soil-landscape modeling. Geoderma, 100(1-2): 67-89.

Toutin, T., 2001. Elevation modelling from satellite visible and infrared (VIR) data. International Journal of Remote Sensing, 22(6): 1097-1125.

Toutin, T., 2002. Elevation modelling from satellite visible and infrared (VIR) data: a review. IEEE Transactions on Geoscience and Remote Sensing, 40(10): 2241-2247.

Toutin, T., 2004. Review article: Geometric processing of remote sensing images: models, algorithms and methods. International Journal of Remote Sensing, 25(10): 1893-1924.

Toutin, T., 2008. ASTER DEMs for geomatic and geoscientific applications: a review. International Journal of Remote Sensing, 29(7): 1855-1875.

Toutin, T. and Cheng, P., 2002. Comparison of automated digital elevation model extraction results using along-track ASTER and across-track SPOT stereo images. Optical Engineering, 41: 2102-2106.

Toutin, T. and Gray, L., 2000. State-of-the-art of elevation extraction from satellite SAR data. ISPRS Journal of Photogrammetry and Remote Sensing, 55(1): 13-33.

Tsay, J.R. and Chen, H.H., 2001. DEM generation in Taiwan by using InSAR and ERS data, Paper presented at the 22nd Asian conference on remote sensing, National University of Singapore, Singapore Institute of surveyors and valuers (SISV); Asian Association on Remote Sensing (AARS).

Tsui, J.B. and Wiley, J., 2000. Fundamentals of Global Positioning System Receivers: A Software Approach. John Wiley & Sons.

Tucker, G.E., Catani, F., Rinaldo, A. and Bras, R.L., 2001. Statistical analysis of drainage density from digital terrain data. Geomorphology, 36(3-4): 187-202.

Turcotte, R., Fortin, J.P., Rousseau, A.N., Massicotte, S. and Villeneuve, J.P., 2001. Determination of the drainage structure of a watershed using a digital elevation model and a digital river and lake network. Journal of Hydrology, 240(3-4): 225-242.

Usery, E.L. et al., 2004. Geospatial data resampling and resolution effects on watershed modeling: A case study using the agricultural non-point source pollution model. Journal of Geographical Systems, 6(3): 289-306.

Valeo, C. and Moin, S.M.A., 2000. Grid-resolution effects on a model for integrating urban and rural areas. Hydrological Processes, 14(14): 2505-2525.

Valorge, C., 2003. 3D Restitution and rendering through high resolution imagery: State of the art and new challenges.

Veregin, H., 1997. The effects of vertical error in digital elevation models on the determination of flow-path direction. Cartography and Geographic Information Science, 24(2): 67-79.

Wang, K. and Lo, C.P., 1999. An Assessment of the Accuracy of Triangulated Irregular Networks (TINs) and Lattices in ARC/INFO. Transactions in GIS, 3(2): 161-174.

Wang, X. and Yin, Z.Y., 1998. A comparison of drainage networks derived from digital elevation models at two scales. Journal of Hydrology, 210(1-4): 221-241.

Wechsler, S.P., 2000. Effect of Digital Elevation Model (DEM) Uncertainty on Topographic Parameters, DEM Scale and Terrain Evaluation, State University of New York, College of Environmental Science and Forestry, New York.

.

Wechsler, S.P., 2007. Uncertainties associated with digital elevation models for hydrologic applications: a review. Hydrology and Earth System Sciences, 11(4): 1481-1500.

Wegmuller, U., Werner, C. and Strozzi, T., 1998. SAR interferometric and differential interferometric processing chain, Proceedings IEEE International Geoscience and Remote Sensing Symposium , 1998. IGARSS'98. Bern, Switzerland.

Weibel, R. and Heller, M., 1991. Digital terrain modelling, In Maguire DJ, MF Goodchild & DW Rhind (eds). Geographical Information Sysytems - Volume 1: Principles (Longman Scientific and Technical: Avon, UK) Oxford Univ. Press.

Welch, R., Jordan, T., Lang, H. and Murakami, H., 1998. ASTER as a source for topographic data in the late 1990s. IEEE Transactions on Geoscience and Remote Sensing, 36(4): 1282-1289.

Weydahl, D.J., Sagstuen, J., Dick, Ø. and Rønning, H., 2007. SRTM DEM accuracy assessment over vegetated areas in Norway. International Journal of Remote Sensing, 28(16): 3513-3527.

Wharton, G., 1994. Progress in the use of drainage network indices for rainfall-runoff modelling and runoff prediction. Progress in Physical Geography, 18(4): 539-557.

Wilson, J.P. and Gallant, J.C., 2000. Terrain analysis: principles and applications. New York: John Wiley and Sons.

Wise, S., 1998. The effect of GIS interpolation errors on the use of digital elevation models in geomorphology, In Lane, S. N, Richards, K. S. and Chandler, J. H. (eds). Landform Monitoring, Modelling and Analysis. John Wiley and Sons: Chichester, UK, pp. 139–164.

Wise, S., 2000. Assessing the quality for hydrological applications of digital elevation models derived from contours. Hydrological Processes, 14(11): 1909-1929.

Wolf, P.R. and Dewitt, D.B., 2000. Elements of photogrammetry with applications in GIS. New York: McGraw-Hill, 340 pp.

Wolock, D.M. and Price, C.V., 1994. Effects of digital elevation model map scale and data resolution on a topography-based watershed model. Water Resources Research, 30(11): 3041-3052.

Wood, J., 1996. The Geomorphological Characterisation of Digital Elevation Models, Ph.D. Thesis, Department of Geography, University of Leicester, Leicester, UK.

Wood, J.D. and Fisher, P.F., 1993. Assessing interpolation accuracy in elevation models. IEEE Computer Graphics and Applications, 13(2): 48-56.

Wu, S., Li, J. and Huang, G.H., 2008. A study on DEM-derived primary topographic attributes for hydrologic applications: Sensitivity to elevation data resolution. Applied Geography, 28(3): 210-223.

Yamaguchi, Y., Kahle, A.B., Tsu, H., Kawakami, T. and Pniel, M., 1998. Overview of Advanced Spaceborne Thermal Emission and ReflectionRadiometer (ASTER). IEEE Transactions on Geoscience and Remote Sensing, , 36(4): 1062-1071.

Yin, Z.Y. and Wang, X., 1999. A cross-scale comparison of drainage basin characteristics derived from digital elevation models. Earth Surface Processes and Landforms, 24(6): 557-562.

Zebker, H., Werner, C., Rosen, P. and Hensley, S., 1993. Accuracy of topographic maps derived from ERS-1 interferometric radar.

Zebker, H.A. and Goldstein, R.M., 1986. Topographic mapping from interferometer synthetic aperture radar observations. Journal of Geophysical Research, 91(B5): 4993-4999.

Zebker, H.A. and Rosen, P., 1994. On the derivation of coseismic displacement fields usingdifferential radar interferometry: The Landers earthquake. Journal of Geophysical Research, 99(B10): 19617-19634.

Zebker, H.A., Rosen, P. and Earth, J., 1997. Atmospheric artifacts in interferometric SAR surface deformation and topographic maps. J. Geophys. Res. Solid Earth, 102(B4): 7547–7563.

Zebker, H.A., Werner, C.L., Rosen, P.A. and Hensley, S., 1994. Accuracy of topographic maps derived from ERS-1 interferometric radar. IEEE Transactions on Geoscience and Remote Sensing, 32(4): 823-836.

Zevenbergen, L.W. and Thorne, C.R., 1987. Quantitative analysis of land surface topography. Earth Surface Processes and Landforms, 12(1): 47-56.

Zhang, J. and Goodchild, M.F., 2002. Uncertainty in geographical information. London: Taylor and Francis, 266 pp.

Zhang, W. and Montgomery, D.R., 1994. Digital elevation model grid size, landscape representation, and hydrologic simulations. Water Resources Research, 30(4): 1019-1028.

Zhou, Q. and Liu, X., 2002. Error assessment of grid-based flow routing algorithms used in hydrological models. International Journal of Geographical Information Science, 16(8): 819-842.

Zhou, Q. and Liu, X., 2004a. Error analysis on grid-based slope and aspect algorithms. Photogrammetric Engineering and Remote Sensing, 70(8): 957-962.

Zhou, Q. and Liu, X., 2004b. Analysis of errors of derived slope and aspect related to DEM data properties. Computers and Geosciences, 30(4): 369-378.

Appendix

Appendix A: DEM extraction from InSAR images

(1) Gamma Interferometric SAR Processor (ISP) c-shell script

Set the directories

```
if ($#argv < 2) then
  echo " "
  echo "***  PROCESS JORDAN DATA  ***"
  echo "***  Copyright 2004, Gamma Remote Sensing, v1.4 18-May-2004 ts/uw/clw
***"
  echo " "
  echo "run_ISP_Jordan : To run interferometric processing sequence for Jordan"
  echo "                 and estimate the heights (DEM)."
  echo " "
  echo "usage: run_ISP_Jordan <slc1 dir> <slc2 dir>"
  echo "       slc1_dir      (input) data directory for slc1"
  echo "       slc2_dir      (input) data directory for slc2"
  echo " "
  exit
  endif

set slc1 = "$1"
set slc2 = "$2"
set no_range_looks = 1                  # enter 1 or 2 here
set no_azimuth_looks = 5       # enter 5 or 10 here
set insardir = $1_$2_$no_range_looks\x$no_azimuth_looks
set flipping = 1                  # 1: normal, -1: mirror image
# Do not forget to enter the interferogram width here
set interf_width = 4903

if( (-e "$insardir" == 0 ) ) mkdir $insardir
cd $insardir
```

Prepare slc data and processing parameter files

```
if (0) then
  if (-e "$1.slc.par") rm -f $1.slc.par
  par_ESA_ERS /home/sda8/jordan/$1/SCENE1/LEA_01.001 $1.slc.par
/home/sda8/jordan/$1/SCENE1/DAT_01.001 $1.slc
```

```
  if (-e "$2.slc.par") rm -f $2.slc.par
  par_ESA_ERS /home/sda8/jordan/$2/SCENE1/LEA_01.001 $2.slc.par
/home/sda8/jordan/$2/SCENE1/DAT_01.001 $2.slc
#  chmod 666 *
  endif
```

Offset estimation of the SLC images

```
if (0) then
  if (-e "$1\_$2.off") rm -f $1\_$2.off
  create_offset $1.slc.par $2.slc.par $1\_$2.off 1
  init_offset_orbit $1.slc.par $2.slc.par $1\_$2.off
  init_offset $1.slc $2.slc $1.slc.par $2.slc.par $1\_$2.off 2 10
  init_offset $1.slc $2.slc $1.slc.par $2.slc.par $1\_$2.off 1 1
  endif

# if (0) then  # Not used in preference to the command below
  # estimation of the registration polynomial using offset_pwr with few
  # (8x8) large (256x256 pixels) search windows
  # offset_pwr 05721.slc_esa 25394.slc_esa 05721.slc_esa.par 25394.slc_esa.par
05721_25394.off offs snr 128 128 offsets 1 8 8 7.
  # offset_fit offs snr 05721_25394.off coffs coffsets 7.0 3 0
  # rm -f offs snr offsets coffs coffsets
# endif

if (0) then
  # precision estimation of the registration polynomial using offset_SLC with many
  # (24x24) small search windows (32x32 pixel chips, 4x4 pixel search window, 2x
oversampling)
  if (-e "$1\_$2.offs ") rm -f $1\_$2.offs
  if (-e "$1\_$2.snr ") rm -f $1\_$2.snr
  if (-e "$1\_$2.offsets ") rm -f $1\_$2.offsets
  if (-e "$1\_$2.coffs ") rm -f $1\_$2.coffs
  if (-e "$1\_$2.coffsets ") rm -f $1\_$2.coffsets
  offset_SLC $1.slc $2.slc $1.slc.par $2.slc.par $1\_$2.off $1\_$2.offs $1\_$2.snr 4 4
$1\_$2.offsets 2 24 24 3.0
  offset_fit $1\_$2.offs $1\_$2.snr $1\_$2.off $1\_$2.coff $1\_$2.coffsets 3.0 4 0
  endif
```

Compute interferogram with 1x5 multilooks

```
if (0) then
  if (-e "$1\_$2.int ") rm -f $1\_$2.int
  if (-e "$1.pwr ") rm -f $1.pwr
  if (-e "$2.pwr ") rm -f $2.pwr
```

```
  interf_SLC $1.slc $2.slc $1.slc.par $2.slc.par $1\_$2.off $1.pwr $2.pwr $1\_$2.int
$no_range_looks $no_azimuth_looks
  endif

if (0) then
  if (-e "$1\_$2.mag_phase.bmp") rm -f $1\_$2.mag_phase.bmp
  rasmph $1\_$2.int $interf_width 1 0 1 1 1. 0.35 $flipping $1\_$2.mag_phase.bmp
  if (-e "$1\_$2.mag_phase_pwr.bmp") rm -f $1\_$2.mag_phase_pwr.bmp
  rasmph_pwr $1\_$2.int $1.pwr $interf_width 1 1 0 1 1 1.0 0.35 $flipping
$1\_$2.mag_phase_pwr.bmp
  if (-e "$1.pwr.bmp") rm -f $1.pwr.bmp
  if (-e "$2.pwr.bmp") rm -f $2.pwr.bmp
  raspwr $1.pwr $interf_width 1 0 1 1 1.0 0.35 $flipping $1.pwr.bmp
  raspwr $2.pwr $interf_width 1 0 1 1 1.0 0.35 $flipping $2.pwr.bmp
  endif
```

Baseline estimation

```
if (0) then   # generate baseline file (first remove an eventual first estimate)
  if (-e "$1\_$2.base") rm -f $1\_$2.base
#  base_init $1.slc.par $2.slc.par - - $1\_$2.base 0 1024 1024
#  base_init $1.slc.par $2.slc.par $1\_$2.off - $1\_$2.base 1 1024 1024
  base_init $1.slc.par $2.slc.par $1\_$2.off $1\_$2.int $1\_$2.base 2 1024 1024
#  base_init $1.slc.par $2.slc.par $1\_$2.off $1\_$2.int $1\_$2.base 3 1024 1024
#  base_init $1.slc.par - $1\_$2.off $1\_$2.int $1\_$2.base 4 1024 1024
  endif

if (0) then   # curved Earth phase trend removal ("flattening") and filter
  if (-e "$1\_$2.flt") rm -f $1\_$2.flt
  ph_slope_base $1\_$2.int $1.slc.par $1\_$2.off $1\_$2.base $1\_$2.flt
  if (-e "$1\_$2.flt_mag_phase.bmp") rm -f $1\_$2.flt_mag_phase.bmp
  rasmph $1\_$2.flt $interf_width 1 0 1 1 1. 0.35 $flipping $1\_$2.flt_mag_phase.bmp
  if (-e "$1\_$2.flt_mag_phase_pwr.bmp") rm -f $1\_$2.flt_mag_phase_pwr.bmp
  rasmph_pwr $1\_$2.flt $1.pwr $interf_width 1 1 0 1 1 1.0 0.35 $flipping
$1\_$2.flt_mag_phase_pwr.bmp
  endif
if (0) then   # coherence estimation and generation of SUN rasterfile
  if (-e "$1\_$2.cc") rm -f $1\_$2.cc
  cc_wave $1\_$2.flt $1.pwr $2.pwr $1\_$2.cc $interf_width
  if (-e "$1\_$2.cc.bmp") rm -f $1\_$2.cc.bmp
  ras_linear $1\_$2.cc $interf_width 1 0 1 1 0.0 1.0 -1 $1\_$2.cc.bmp
  if (-e "$1\_$2.cc_pwr.bmp") rm -f $1\_$2.cc_pwr.bmp
  rascc $1\_$2.cc $1.pwr $interf_width 1 1 0 1 1 0.1 0.9 1.0 0.35 $flipping
$1\_$2.cc_pwr.bmp
  endif
```

```
if (0) then   # adaptive interferogram filtering and generation of SUN rasterfile
  if (-e "$1\_$2.cc_filt") rm -f $1\_$2.cc_filt
  if (-e "$1\_$2.flt_filt") rm -f $1\_$2.flt_filt
  adf $1\_$2.flt  $1\_$2.flt_filt $1\_$2.cc_filt $interf_width .5
  if (-e "$1\_$2.flt_filt_mag_phase_pwr.bmp") rm -f
$1\_$2.flt_filt_mag_phase_pwr.bmp
  rasmph_pwr $1\_$2.flt_filt $1.pwr $interf_width 1 1 0 1 1 1.0 0.35 $flipping
$1\_$2.flt_filt_mag_phase_pwr.bmp
  endif
```

Phase unwrapping

```
if (0) then   # phase unwrapping (first remove an eventual first estimate)
  if (-e "$1\_$2.flag") rm -f $1\_$2.flag
  if (-e "$1\_$2.flt_filt.unw") rm -f $1\_$2.flt_filt.unw
  corr_flag $1\_$2.cc_filt $1\_$2.flag $interf_width 0.3
  neutron $1.pwr $1\_$2.flag $interf_width
  residue $1\_$2.flt_filt $1\_$2.flag $interf_width
  tree_cc $1\_$2.flag $interf_width
  grasses $1\_$2.flt_filt $1\_$2.flag $1\_$2.unw $interf_width
  if (-e "$1\_$2.unw.bmp") rm -f $1\_$2.unw.bmp
  rasrmg $1\_$2.unw $1.pwr $interf_width 1 1 0 1 1 .5 1. .35 0.0 $flipping $1\_$2.unw.bmp
  endif
```

Height model generation and geocoding

```
if (0) then    # Least square estimation of interferometric baseline
  if (-e "$1\_$2.gcp_ph") rm -f $1\_$2.gcp_ph
  if (-e "$1\_$2.base") rm -f $1\_$2.base
  gcp_phase $1\_$2.unw $1\_$2.off $1\_$2.gcp $1\_$2.gcp_ph
  base_ls $1.slc.par $1\_$2.off $1\_$2.gcp_ph $1\_$2.base 1 1 1 1 1 1
  endif

if (0) then    # Interferometric estimation of heights and ground ranges (use disras to
display output bmp)
  if (-e "$1\_$2.hgt") rm -f $1\_$2.hgt
  if (-e "$1\_$2.hgt.bmp") rm -f $1\_$2.hgt.bmp
  if (-e "$1\_$2.grd") rm -f $1\_$2.grd
  hgt_map $1\_$2.unw $1.slc.par $1\_$2.off $1\_$2.base $1\_$2.hgt $1\_$2.grd
  rashgt $1\_$2.hgt $1.pwr $interf_width 1 1 0 1 1 160.0 1. .35 $flipping
$1\_$2.hgt.bmp
  endif

if (1) then    # Resample interferometric height map to orthonormal coordinates (use
disras)
  if (0) then
    if (-e "$1\_$2.rhgt") rm -f $1\_$2.rhgt
```

```
    if (-e "$1\_$2.rpwr") rm -f $1\_$2.rpwr
    res_map $1\_$2.hgt $1\_$2.grd $1.pwr $1.slc.par  $1\_$2.off $1\_$2.rhgt $1.rpwr 7
7 20
    endif
  if (1) then
    set resampled_width = 4982
    if (-e "$1\_$2.rhgt.bmp") rm -f $1\_$2.rhgt.bmp
    rashgt $1\_$2.rhgt $1.rpwr $resampled_width 1 1 0 1 1 160.0 1. .35 $flipping
$1\_$2.rhgt.bmp
    endif
  endif
cd .
```

(2) Interferogram and Image Offset Parameter File

```
title:     19960501_19960502
initial_range_offset:                  7
initial_azimuth_offset:                808
slc1_starting_range_pixel:             0
number_of_slc_range_pixels:            4903
offset_estimation_starting_range:      48
offset_estimation_ending_range:        4855
offset_estimation_range_samples:       24
offset_estimation_range_spacing:       209
offset_estimation_starting_azimuth:    48
offset_estimation_ending_azimuth:      26534
offset_estimation_azimuth_samples:     24
offset_estimation_azimuth_spacing:     1151
offset_estimation_window_width:        4
offset_estimation_window_height:       4
offset_estimation_threshhold:          3.00
range_offset_polynomial:               5.95791   2.7456e-04   1.7408e-06  -8.5690e-11
azimuth_offset_polynomial:             807.69118  -3.9442e-05 7.0908e-06  -1.7916e-10
slc1_starting_azimuth_line:            0
interferogram_azimuth_lines:           5154
interferogram_width:                   4903
first_nonzero_range_pixel:             0
number_of_nonzero_range_pixels:        4891
interferogram_range_looks:             1
interferogram_azimuth_looks:           5
interferogram_range_pixel_spacing: 7.904890    m
interferogram_azimuth_pixel_spacing:    19.922385    m
```

resampled_range_pixel_spacing: 20.000000 m
resampled_azimuth_pixel_spacing: 20.000000 m
resampled_starting_ground_range: 246459.32031 m
resampled_pixels_per_line: 4984
resampled_number_of_lines: 5133

Appendix B: Program interface to calculate Dominance and variability

- Create shapefile which has attribute table contains 50 field each of them represent one flow direction realization.

- Export this table to text file and read it using this program to calculate Dominance and variability.